Publicação Especial Nº 01/99

Asteróides: Um Estudo de Suas Propriedades Físico-Químicas

Marcos Antonio Florczak

Tese de Doutorado
Rio de Janeiro, Dezembro de 1998

CONSELHO NACIONAL DE DESENVOLVIMENTO CIENTÍFICO E TECNOLÓGICO
OBSERVATÓRIO NACIONAL

ASTERÓIDES: UM ESTUDO DE SUAS PROPRIEDADES FÍSICO-QUÍMICAS

- TESE DE DOUTORADO -

Aluno: Marcos Antonio Florczak
Orientadora: Daniela Lazzaro

Apresentada como requisito para a obtenção do grau de
Doutor em Astrofísica pelo CNPq/ON.

Rio de Janeiro - Dezembro de 1998

Aos meus sobrinhos: Lucas e Beatriz

Agradecimentos

Em primeiro lugar a Daniela Lazzaro, não apenas pela orientação constante que tornou este trabalho possível, como pela amizade e pela paciência!

A Antonella Barucci pela acolhida e pelo acompanhamento atencioso durante minha estadia em Meudon.

Aos amigos do departamento de física do CEFET-Pr que concordaram com minha licença para a realização deste doutorado.

Aos amigos do departamento de astrofísica que proporcionaram momentos agradáveis na sala do café.

A CAPES e CNPq pelo apoio financeiro.

A Sara, Arandi, Sandra C, Sandra R, Cláudia, Pierre, Alain, Stella, Dora, Simone, Paulo, Cris, aos colegas da pós-graduação do ON e de Meudon pela amizade. A minha irmã, minha mãe, meus queridos sobrinhos. Enfim, a todos que participaram da minha vida nestes últimos anos.

Resumo

O objetivo deste trabalho é analisar do ponto de vista físico-químico algumas amostras selecionadas de asteróides visando uma melhor compreensão destes objetos. Para isto foram realizadas observações, tanto em fotometria como em espectroscopia. A finalidade das observações espectroscópicas é a determinação da possível composição mineralógica, enquanto as fotométricas devem caracterizar o estado rotacional. Foram realizadas também observações do cometa Chiron com o objetivo de analisar e monitorar sua atividade durante sua aproximação ao periélio.

Para a análise espectroscópica foram selecionadas 3 famílias de asteróides (Eos, Themis e Flora), alguns objetos próximos à órbita da Terra, asteróides do tipo C e candidatos a missão espacial Rosetta. Para os membros das famílias observadas encontramos um comportamento espectral similar, sugerindo uma origem comum de seus membros. Encontramos indícios de um processo de alteração aquosa nos membros da família de Themis e um processo de "envelhecimento" superficial nos de Flora. Os resultados de Eos e Themis nos levam a concluir que os corpos originais destas famílias deveriam ser parcialmente diferenciados. Quanto aos asteróides do tipo taxonômico C, foi encontrado que a maior parte dos observados apresenta indícios de um processo de alteração aquosa.

Dos estudos fotométricos foram obtidas curvas de luz para 25 asteróides, sendo que determinamos para 19 destes seu período rotacional. As observações de Chiron revelaram que apesar de estar nas proximidades de seu periélio, este objeto se mantém num mínimo de brilho.

Abstract

The aim of the present work is to analyze the physical-chemical properties of a selected sample of asteroids in order to better understand these objects. Photometric and spectroscopic observations were, therefore, realized. The former aiming the determination of the possible mineralogical composition and the latter the characterization of the rotational state of the objects. Photometric observations of comet Chiron were also performed in order to analyze and monitor its activity as it approached perihelion.

The spectroscopic study was performed on three families (Eos, Flora and Themis), on some objects with orbit near the Earth, on a sample of C-type asteroids and on possible targets of the Rosseta spatial mission. We found a similar spectral trend in each of the families indicating a probable common origin. Indication of a process of aqueous alteration was found in some of the members of Themis and of space weathering on those of Flora. The obtained results for Eos and Themis lead us to conclude that the parent-bodies of these families should have been partially differentiated. For the C-type asteroids, the presence of aqueous alteration was detected in most of the objects of our sample.

From the photometric study the lightcurves of 25 asteroids were obtained. For 19 of these was possible to determine a rotational period. Chiron's observations revealed that it is currently at a minimum of brightness, although being at perihelion.

Índice

Capítulo 1

Introdução

Acredita-se que o Sol e seu sistema planetário se formaram, a cerca de 4,6 bilhões de anos, a partir de uma nuvem de gás e poeira em rotação. Esta nuvem teria colapsado pela própria auto-gravidade formando, na região central, um objeto estelar, chamado proto-sol, e um disco de gás e poeira do qual todo o sistema planetário se originou. Este disco foi chamado por Pierre Simon de Laplace de nebulosa solar em 1796. Este modelo, inicialmente proposto por Emmanuel Kant em 1755 e posteriormente por Laplace, se tornou a base dos atuais modelos de formação do Sistema Solar, sendo conhecido como a cosmogonia de Kant-Laplace.

A partir da cosmogonia de Kant-Laplace torna-se necessário explicar a origem dos planetas, asteróides e cometas a partir da nebulosa solar, sendo que o modelo atualmente mais aceito para explicar este processo é chamado de "modelo padrão". Neste modelo considera-se a agregação física ou química ("coagulação") de grãos de poeira (micrométricos) em corpos de 0,1 a 10 km de diâmetro, chamados planetesimais, e a subsequente acumulação destes formando finalmente os planetas. Este modelo embora remonte a 1794 com Chladni, 1898 com Proctor e 1904 com Chamberlin, tem sua versão atual devida aos trabalhos de Safronov (1969) e da "Escola de Kyoto" com Hayashi e colaboradores (1985).

Na formação dos planetas, segundo o modelo padrão, supõe-se que a força gravitacional da estrela seja dominante sobre os planetesimais, enquanto que outras forças podem ser tratadas apenas como perturbações em suas órbitas keplerianas. As maiores perturbações em suas trajetórias heliocêntricas seriam resultado de interações gravitacionais

com outros planetesimais e protoplanetas, enquanto que as forças não-gravitacionais seriam colisões inelásticas mútuas, dissipação devida ao gás presente na nebulosa solar e pressão de radiação (Lissauer, 1993). Estas perturbações podem levar a pequenas mudanças na inclinação e excentricidade fazendo com que os planetesimais cruzem a órbita de seus vizinhos ocasionando eventuais colisões. As baixas inclinação e excentricidade podem ser consideradas como uma velocidade relativa entre os corpos em um sistema de referência local, que gira com velocidade kepleriana circular. Quando dois corpos colidem inelasticamente com uma velocidade relativa menor que duas vezes a velocidade de escape, estes se fundem tornando-se um corpo maior, caso contrário tem-se um processo de fragmentação.

Simulações numéricas deste modelo levam a dois tipos de soluções. A primeira seria a de um crescimento ordenado onde obtem-se corpos grandes, de tamanhos similares, seguidos por pequenos, cuja distribuição seguiria uma lei de potência. A segunda seria o crescimento *runaway*, onde um corpo cresceria mais rápido do que seus vizinhos, capturando todos os planetesimais dentro de uma certa região.

Soluções do tipo *runaway* têm obtido bons resultados para explicar a formação de planetas terrestres, principalmente a Terra e Vênus. Entretanto, apresentam problemas com a formação dos planetas gigantes pois a escala de tempo para a formação destes é muito grande, incompatível com a hipótese que tenham se formado antes dos terrestres. Além do mais, como os planetas gigantes apresentam uma fração significativa de H_2 e He, seria necessário um crescimento rápido de seus núcleos para ocorrer uma captura gravitacional do gás da nebulosa solar.

Quanto à origem dos asteróides, devemos considerá-la como parte de um problema mais geral que é a origem dos planetas. Segundo a hipótese de Olbers, sugerida logo após sua descoberta de Pallas, os asteróides seriam oriundos da fragmentação de um planeta. Esta hipótese é entretanto contraditória com a variação da composição química dos asteróides em relação a suas distâncias heliocêntricas e com a distribuição de suas órbitas, o que demostra que estas seriam o resultado de eventos diversos.

Não foram obtidas, ainda, soluções do tipo *runaway* aceitáveis para asteróides, pois levam à formação de corpos muito maiores do que os maiores asteróides encontrados.

Para obter melhores soluções é necessário refinar o modelo com a inclusão de outros efeitos presentes na época da formação do Sistema Solar como, por exemplo, a hipótese de que Júpiter tenha se formado antes dos planetas terrestres e dos asteróides. Esta hipótese implica que a forte perturbação gravitacional de Júpiter pode ter sido responsável pela interrupção do processo de acumulação dos planetesimais na região asteroidal, impedindo a formação de um novo planeta.

Com relação à origem dos cometas, Oort (1950) propôs que estes seriam os planetesimais que se encontravam na região asteroidal e que devido a fortes perturbações gravitacionais dos planetas gigantes, seriam lançados em órbitas quase parabólicas, tendo em seguida um aumento do periélio pela passagem de uma estrela vizinha, formando a região atualmente conhecida como nuvem de Oort.

Os grandes afélios e a vasta distribuição das inclinações dos cometas de longo período (superior a 200 anos) são os mais fortes indícios da existência desta grande nuvem esférica. Estes cometas, por sua vez, poderiam ser lançados desta nuvem para o interior do Sistema Solar através de perturbações ocasionadas pela passagem de estrelas próximas e/ou pela passagem de uma nuvem molecular gigante. Por outro lado, os cometas de curto período (inferior a 200 anos), devido às suas baixas inclinações, viriam da região conhecida como cinturão de Kuiper ($\sim$ 40 - 500 UA) (Fernández, 1980). Com as recentes descobertas de objetos transneptunianos (Jewitt e Luu, 1995), temos finalmente evidências observacionais da existência deste cinturão.

Quanto à origem da nuvem de Oort existem várias hipóteses, como a formulada por Oort, onde esta seria um remanescente da formação planetária (Fernández e Brunini, 1998). Há ainda as hipóteses de uma formação independente dos planetas, ou uma captura gravitacional de uma nuvem de uma estrela vizinha em formação. Quanto ao cinturão de Kuiper, este poderia ser o remanescente dos planetesimais que se encontravam na região além de Netuno e que devido à baixa densidade não conseguiram se aglutinar em mais um planeta (Festou et al., 1993).

É necessário se obter mais informações sobre os processos pelo quais o Sistema Solar passou, não apenas para refinar o modelo padrão, mas também para servir como

um teste de seus resultados. Os asteróides e os cometas podem ser esta fonte de informações, pois seu pequeno tamanho e consequentemente sua limitada atividade geológica, indicam que sejam corpos primordiais em comparação com os planetas. Estes provavelmente guardam as informações da história química e mineralógica e dos processos predominantes na nebulosa solar, sendo portanto possível que algums dos materiais presentes no cinturão de asteróides sejam fósseis residuais dos planetas terrestres no início de sua formação.

Atualmente temos mais de 9500 asteróides numerados em um total de mais de 25000 observados (Tholen, 1998). Estes objetos não são exclusivos da região entre Marte e Júpiter, chamada de cinturão principal, mas são também encontrados no Sistema Solar interior sendo conhecidos como objetos próximos da Terra (NEO, ou *Near Earth Objects*), ou no sistema solar exterior, cruzando a órbita de planetas gigantes e denominados de *Centauros*. Há também os objetos recém descobertos além da órbita de Netuno, os *Transnetunianos*.

A distribuição de asteróides no cinturão principal nos revela uma estrutura resultante de uma série de fenômenos físicos significativos. Observamos uma série de lacunas e acúmulos de objetos em determinadas regiões determinados por ressonâncias com Júpiter. Outras concentrações seriam resultados de colisões catastróficas de corpos maiores, sendo chamadas de *famílias* para diferenciá-las de outros agrupamentos de origem essencialmente gravitacional, como os *Troianos* e os *Hildas*, que estão em ressonância *1:1* e *3:2* com Júpiter. A figura 1.1 mostra a distribuição heliocêntrica de semi-eixo maior para aproximadamente 4000 asteróides numerados.

O objetivo deste trabalho é analisar do ponto de vista físico-químico algumas amostras destes pequenos corpos considerados entre os mais primitivos do Sistema Solar. Para isto realizamos várias missões de observação, tanto em fotometria como em espectroscopia. As observações espectroscópicas com a finalidade de determinar a possível composição mineralógica de asteróides, e as fotométricas a de caracterizar o estado rotacional destes objetos. No caso específico de Chiron, objeto possivelmente em transição entre o

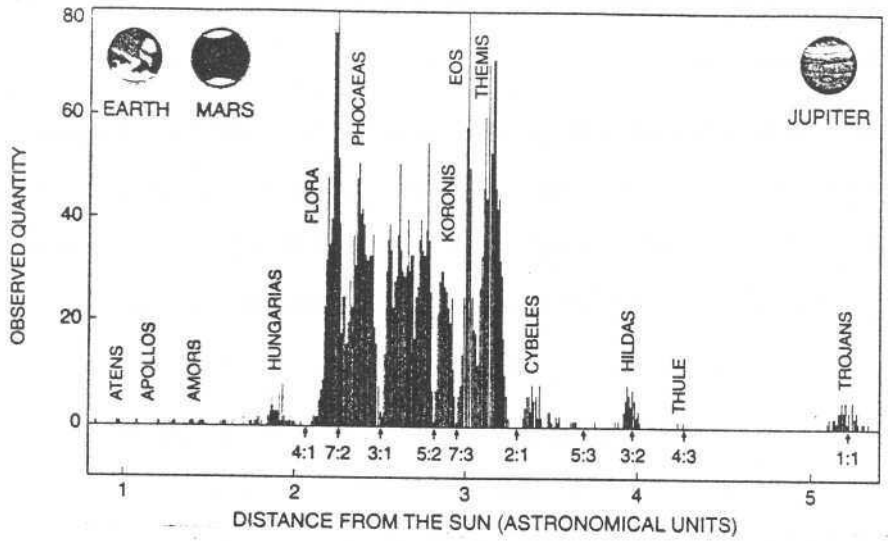

Figura (1.1) *Distribuição heliocêntrica de semi-eixo maior para aproximadamente 4000 asteróides numerados (Binzel et. al, 1991). Notamos uma série de agrupamentos, como as famílias de asteródes Eos, Themis, Koronis e Flora, e agrupamentos de origem essencialmente gravitacional como os Hildas e os Troianos.*

Cinturão de Kuiper e o Sistema Solar interior, o objetivo foi o de analisar e monitorar a sua atividade cometária, visando um melhor entendimento de sua evolução.

As amostras escolhidas para a análise espectroscópica foram principalmente de famílias de asteróides, visando a confirmação ou não de uma origem comum de seus membros, assim como o conhecimento da composição mineralógica atual destes objetos

e, conseqüentemente, um entendimento da possível composição do corpo original. Isto poderia fornecer indícios sobre gradientes físico-químicos e térmicos ocorridos na região do cinturão, já que suas formações devem ter sido originadas em regiões distintas. Também escolhemos objetos próximos à órbita da Terra, pois estes podem fornecer informações importantes sobre a origem de meteoritos. Os asteróides do tipo taxonômico C foram também analisados, pois nos remetem ao problema da alteração aquosa em asteróides e aos eventos térmicos ocorridos.

Estudamos também o estado rotacional de asteróides do cinturão principal, dando ênfase aos pequenos objetos. O interesse principal deste estudo é a caracterização da evolução colisional sofrida por estes objetos. Nosso objetivo foi principalmente o de aumentar a amostra estatística dos períodos de rotação e amplitudes de curvas de luz conhecidos.

Com respeito a Chiron, a finalidade foi de analisar e monitorar seu comportamento, visando uma melhor compreensão deste tipo de objeto. Chiron, desde a sua descoberta, apresentou um comportamento atípico, e sua primeira aproximação ao periélio se caracterizava portanto como um momento muito propício para observação.

O presente trabalho está organizado em quatro partes, iniciando com uma breve revisão histórica sobre a descoberta dos asteróides. Os resultados das observações espectroscópicas são apresentados no capítulo 3. As observações fotométricas de asteróides são descritas no capítulo 4, enquanto as de Chiron no capítulo 5. Por fim, apresentamos as conclusões e algumas perspectivas futuras.

Capítulo 2

A Descoberta dos Asteróides

A existência de um planeta na região que chamamos de cinturão de asteróides foi sugerida por Johannes Kepler quando escreveu: "*Inter Jovem et Martem Interpossui Planetam*". Kepler deve ter utilizado sua crença em um universo ajustado de forma ordenada para fazer esta afirmação, já que a distância entre Marte e Júpiter era muito maior comparada às distâncias entre os outros planetas já conhecidos (fig. 2.1). Apesar desta afirmação este *planeta* não fazia parte de seu modelo cosmológico.

Em 1766, Titius von Wittenburg, professor em Wittenberg, desenvolve uma fórmula empírica para as distâncias planetárias (Cunningham, 1988a). Titius definiu a distância do Sol a Saturno como sendo de 100 unidades, logo Mercúrio estaria a 4 unidades do Sol, Vênus a 4+3=7, a Terra a 4+6=10, e finalmente Marte a 4+12=16. Entretanto, existe uma falha nesta progressão regular: no espaço 4+24=28 unidades não é encontrado nenhum planeta. "*Podemos acreditar que o Criador do mundo tenha deixado este espaço vazio? Certamente, não!*" Disse Titius, provavelmente influenciado pela mesma crença em um universo ordenado que Kepler possuía. Seguindo com a lei teríamos Júpiter a 4+48=52 e, finalmente, Saturno a 4+96=100 unidades. Esta fórmula pode ser escrita como:

$$Y = 0,4 + 0,3(2^{n-1}), \qquad n = 0, 1, 2.... \tag{2.1}$$

Para $n = 0$, $Y = 0,4$ que corresponde à órbita de Mercúrio em unidades astronômicas.

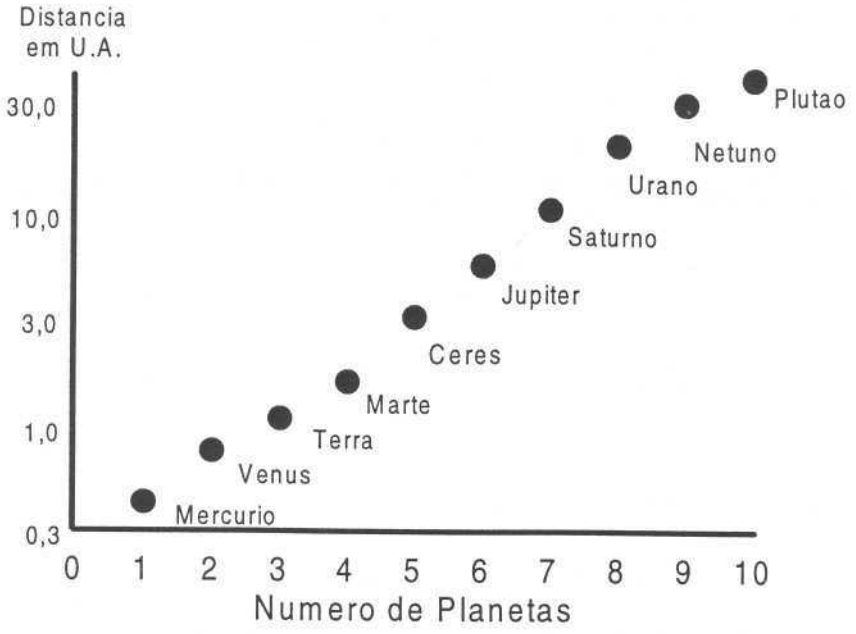

Figura (2.1) *Distâncias planetárias*

Na segunda edição do livro de Johann Elert Bode *, "Introdução ao Conhecimento do Céu Estrelado", publicado em Hamburgo em 1772 (Shapley e Howarth, 1929), ele fala da provável existência de outros planetas no Sistema Solar. Em 1781, William Herschel descobre Urano. Bode se vale desta descoberta para divulgar esta fórmula, onde ao aplicá-la para Urano obtém-se 4+192=196 unidades, valor este em acordo com as observações.

Devido à utilização por Bode da fórmula de Titius para promover o problema do *planeta ausente* (entre Marte e Júpiter), esta é normalmente conhecida como Lei de Titius-Bode (fig. 2.2). Uma das características desta "lei" é a de ser puramente empírica, baseada apenas nas observações, como adverte Bode, que faz o seguinte comentário em relação a esta lei: *...ela indica a ordem harmoniosa que reina em todo lugar, no grande*

* *Johann Elert Bode (1747 - 1826), astrônomo alemão, diretor do Observatório de Berlin, fundador da revista Astronomisches Jahrbuch*

		Mean distance
Mercury	387 units	387
Venus	387 + 293 = 680	723
The Earth	387 + 2 × 293 = 973	1,000
Mars	387 + 4 × 293 = 1,559	1,524
Probable planet between Mars and Jupiter	387 + 8 × 293 = 2,731	
Jupiter	387 + 16 × 293 = 5,075	5,203
Saturn	387 + 32 × 293 = 9,763	9,541
Uranus	387 + 64 × 293 = 19,139	19,082

Figura (2.2) *Lei de Titius-Bode. Publicado por Bode com o professor Wurm na Astronom. Jahrb. em 1790, p. 168. A distância média de Mercúrio ao Sol é de 387 (a distância da Terra = 1000) (Shapley e Howart, 1929).*

trabalho da Natureza.

Neste momento histórico, onde a comunidade astrônomica anseia pela descoberta do *planeta ausente,* surge a figura do Barão Franz Xaver von Zach (1754 - 1832). Zach, nascido em Pest, hoje parte de Budapeste, muda-se para Londres em 1783 onde torna-se amigo de William Herschel e Count Moritz von Brühl, embaixador da Saxônia. Em 1785, ele acompanha Brühl a uma visita a Ernst II, Duque de Saxe-Gotha, que expressa o interesse em construir um observatório próximo a Gotha (na antiga Alemanha Oriental). Brühl se oferece para adquirir um telescópio de Herschel e sugere que Zach seja o diretor. Logo em 1788, Gotha possui o "Observatório Seeberg", contendo finos refratores, sextantes e cronômetros, tornando-se um dos mais bem equipados da Europa.

Quando o Observatório Seeberg estava pronto, Zach deu atenção à pesquisa astronômica, já que se dedicava anteriormente à geodésia. Crente na "lei de Titius-Bode", ele tenta encontrar o planeta entre Marte e Júpiter. Mas, sem sucesso, logo conclui que um esforço mais organizado seria necessário.

Para conseguir a ajuda da comunidade astronômica, Zach começou em 1798 a editar a revista astronômica "Geographical Ephemeris" e organizou o primeiro congresso

astronômico. Por 10 dias, 14 astrônomos discutiram sobre diversos temas, como o significado do tempo, a adoção do sistema métrico e a demarcação de novas constelações. O jornal logo se torna um veículo importante de disseminação de pesquisas. Seu primeiro volume contém 18 observações do eclipse solar de 24 de junho de 1797. Zach deve ser apreciado pelo rigoroso critério científico na escolha dos artigos (Shapley e Howart, 1929).

Em 1800 Zach funda um jornal menos formal, o Monthly Correspondence, e cede a editoração do Geographical Ephemeris a outros. Com isto sobra mais tempo para a procura do planeta ausente e então Zach estabelece uma companhia fechada de 24 astrônomos para a procura deste suposto planeta. Schröter foi selecionado como presidente da "polícia celeste" e Zach seu secretário. Para cada membro foi designada uma área de 15° de largura por 7° a 8° de altura em relação à eclítica para efetuar a procura sistemática (Cunningham, 1988b).

Mas coube ao acaso a descoberta do "planeta ausente" por um astronômo siciliano, Giuseppe Piazzi, que foi o primeiro diretor do Observatório Real de Palermo, responsável por um dos mais importantes catálogos de estrelas do seu tempo. Durante a primeira noite de 1801, Piazzi viu uma "estrela" fraca não catalogada na constelação de Touro. Em 24 de janeiro de 1801, época da invasão da Itália por Napoleão, Piazzi escreve uma carta em seu dialeto siciliano a uma amiga em Milão:

"Devido a circustâncias políticas, temos interrompido todas as nossas correspondências, eu me aventuro a lhe escrever, impaciente por contar-lhe as novidades. No primeiro dia de janeiro eu observei uma estrela de oitava magnitude em Touro, a qual na noite seguinte avançou aproximadamente 3'30" para o norte e 4' para Áries. Verificando minhas observações do 3.° e 4.° dias de janeiro eu encontrei mais ou menos o mesmo movimento. No 5.°, 6.°, 7.°, 8.° e 9.° dias de janeiro o céu estava nublado. Eu ainda vi a estrela em janeiro no 10.° e 11.° dias subseqüentes e 13.° ... 23.° de janeiro. Sua ascenção reta na primeira observação era 51° 47' *com uma declinação de* 16° 8' 19" *dos dias 10 ao 11, de um movimento retrógrado tornou-se direto. E no 23.° dia de janeiro eu observei uma ascenção reta de* 51° 46' *com uma declinação de* 17° 8'. *Eu tinha anunciado esta estrela como um cometa. Mas o fato de a estrela não estar acompanhada de nebulosidade*

e seu movimento ser muito lento e um tanto uniforme, tem me causado muitas vezes considerações que talvez este seja mais que um cometa. Entretanto eu serei muito cuidadoso antes de fazer conjecturas públicas. Quando eu coletar um grande número de observações, eu calcularei seus elementos. Neste meio tempo seria muito bom se você o observasse, informando-me de seus resultados.

No dia seguinte ele escreve uma carta similar a Bode em Berlim, onde no final da carta diz *"...Eu peço ajuda para saber se outros astrônomos já o observaram; neste caso me salvaria de computar sua órbita."* Bode não teve dúvida de que o objeto descoberto por Piazzi era o oitavo planeta do Sistema Solar. A descoberta foi anunciada no Monthly Correspondence. Em honra a deusa protetora da Sicília, Piazzi deu o nome de *Ceres* a este novo objeto. Logo após sua descoberta Piazzi recebe uma carta, enviada por Zach antes deste fato, convidando-o a participar da "polícia celeste".

O novo objeto foi observado durante 41 noites quando então, devido a uma doença de Piazzi, as observações foram interrompidas. Quando ele retomou as observações, Ceres já tinha se deslocado bastante no céu e era tão difícil achá-lo quanto na época de sua descoberta. Era necessário um novo método de determinação de órbita com poucos pontos astrométricos. Surge então Carl Friedrich Gauss (1777 - 1855), matemático alemão e diretor do Observatório de Göttingen, que resolveu o problema, aplicando o método dos mínimos quadrados à teoria de órbitas. Como ele mesmo diz: *" uma ótima oportunidade de testar os valores práticos de meus conceitos é empregá-los para a determinação da órbita do planeta Ceres"* (Shapley e Howarth, 1929). Em outubro de 1801 ele publica os elementos orbitais de Ceres: semi-eixo maior 2,77 U.A.; excentricidade 0,08; inclinação 11°.

Com as efemérides previstas por Gauss, Zach foi o primeiro a reencontrar Ceres em 7 de dezembro de 1801. Como havia quatro estrelas fracas próximas da posição prevista, ele não se sentiu apto a confirmar a redescoberta. Somente nas primeiras horas da manhã do mês de janeiro em 1802, Zach concluiu a identificação de Ceres. Independentemente, Heinrich W. M. Olbers em 1 de janeiro de 1802 também o encontra.

Mas o problema do planeta ausente não estava solucionado, pois a magnitude de Ceres era muito menor do que a de Marte e Júpiter. Os astronômos tinham previsto um

corpo bem maior, o qual apresentaria seu disco quando observado através de um telescópio, assim como os outros seis planetas conhecidos. Olbers continua a observar Ceres a fim de fornecer novos dados a Gauss para um cálculo mais preciso da órbita. Em 28 de março, ele descobre um outro objeto se movendo próximo a Ceres no céu. Um segundo planeta, que levou o nome de Pallas, tinha sido descoberto. Gauss, se referindo a Ceres e Pallas diz: *" um casal de torrão de barro o qual chamamos de planeta."*. Esta frase é um bom indicador de que estes novos objetos não foram prontamente aceitos como planetas.

No ano seguinte à descoberta de Pallas, o próprio Olbers, baseando-se em uma teoria de 1794 de Chladmi sobre a origem extra-terrestre dos meteoritos, chegou a propor que estes novos objetos seriam restos da explosão de um planeta na região entre Marte e Júpiter. Neste mesmo ano, William Herschel sugeriu o nome de "asteróides" para estes corpos, que significa em grego "quase-estrela", devido à sua aparência estelar quando vistos através de um telescópio.

Com as descobertas de Juno, feita por Harding no Observátorio Schoeter em 1.º de setembro de 1804, e Vesta, encontrado por Olbers em 19 de março de 1807, a hipótese do planeta ausente terminava. Mas a teoria que propunha que os asteróides seriam fragmentos de um planeta maior "salva" a lei de Titius-Bode. O interesse sobre os asteróides parece terminar momentaneamente, e os seguintes a serem descobertos foram Astraea (1845), Hebe (1847), Iris (1847), Flora (1847), Metis (1848) e Hygieia (1849), por diversos observadores.

E o Barão? Ele funda o seu terceiro jornal astronômico, Correspondence, publicado em francês entre 1818 e 1827, quando já não era mais diretor do Observatório de Seeberg. Ele morre na epidemia de cólera em 1832.

Sucederam-no na direção deste observatório, Bernhard von Lindenau, Joham Encke e Peter Hansen. Em 1856, o observatório foi transferido para a cidade de Gotha, e a sede antiga transformou-se em restaurante e foi finalmente destruída pelo fogo em 1901.

Na virada do século a comunidade astronômica perdeu parte do interesse pela pesquisa sobre estes pequenos planetas, chegando ao ponto de ser considerado impróprio aos grandes observatórios seu estudo (Gehrels, 1979). Somente no final da década de

70 o estudo de asteróides começou a passar por uma grande transformação, devida principalmente ao desenvolvimento de uma taxonomia e à interpretação de sua composição mineralógica, assim como às descobertas de um número muito maior destes objetos. Esperamos acrescentar, com este trabalho, um pouco mais de informação sobre estes pequenos corpos, que já chegaram a ser chamados de *vermes do céu*.

Capítulo 3

Composição Mineralógica de Asteróides

3.1 - Introdução

Acredita-se que os asteróides sejam objetos preservados de uma população de planetesimais que existia na região do Cinturão. Em outras partes do Sistema Solar, populações similares a esta se aglutinaram para formar os planetas. À medida que a matéria foi sendo acretada para formar os planetas, processos físico-químicos foram modificando os componentes originais. Os asteróides, por outro lado, devido ao seu pequeno tamanho, devem ter mantido menos alterados seus materiais originais. Mais ainda, a identificação da composição mineralógica dos asteróides pode fornecer dados sobre os possíveis gradientes de temperatura, pressão e composição da nebulosa proto-planetária. Note-se que certos materiais exigem intervalos de temperatura bem definidos para se formar. Como exemplo podemos citar certos materiais condritos, os enstatites, que requerem uma temperatura muito maior para formação do que os carbonáceos. Conseqüentemente, associar a composição mineralógica à posição heliocêntrica pode prover informações importantes para elaborar modelos de formação do Sistema Solar.

O conhecimento sobre a composição dos asteróides pode ainda ajudar a resolver alguns problemas fundamentais em planetologia (Gaffey *et al.*, 1993), tais como: *a)* a origem dos meteoritos, em especial dos condritos ordinários, que representam a maior parte dos que caem na Terra e para os quais ainda não há uma identificação precisa da população de asteróides a eles associados; *b)* os mecanismos principais de aquecimento, que podem ser discriminados através de uma caracterização detalhada dos asteróides ígneos,

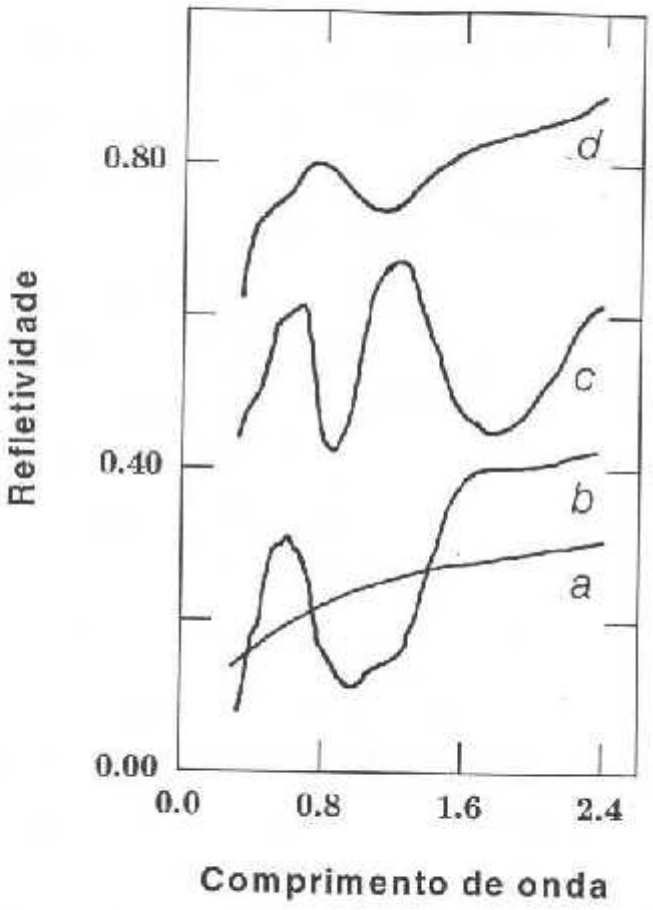

Figura (3.1) *Curvas espectrais de reflexão para 4 minerais comuns em meteoritos e possivelmente presentes em asteróides. (a) Ni-Fe; (b) olivina; (c) piroxênio e (d) feldspato (Burns, 1993).*

desenvolvidos para determinar as abundâncias relativas destes minerais através de calibrações empíricas em laboratório (Adams, 1974; McFadden e Gaffey, 1978; Cloutis *et al.*, 1986; Cloutis e Gaffey, 1991), mas todos limitados a algumas espécies de minerais.

A caracterização do material superficial pode ser dividida em 4 categorias: classificação taxonômica, forma da curva espectral, bandas de absorção e análise quantitativa

dos espectros. A classificação taxonômica usa parâmetros como índice de cor e albedo os quais devem ser representativos da composição superficial. Em geral, diferentes classes taxonômicas podem representar diferentes composições, embora o oposto não seja óbvio: os asteróides de uma mesma classe não possuem necessariamente o mesmo tipo de composição. A comparação da curva espectral de asteróides com a de meteoritos é uma forma rápida de identificar uma possível mineralogia, embora algumas classes, como as E, M e P, sejam difíceis de distinguir entre si apenas através da curva espectral. A existência de certas bandas de absorção é também um forte indício de seu tipo mineralógico; como exemplo mais comum temos as bandas que indicam um processo de alteração aquosa, típicas dos filossilicatos. Uma análise quantitativa de algumas bandas espectrais pode indicar as abundâncias relativas de certos materiais. Por exemplo, as áreas e posições do mínimo das bandas de 1 e 2 μm indicam a quantidade relativa de olivina e piroxênio, caracterizando o tipo de composição provável do piroxênio.

Embora a comparação direta entre as curvas espectrais de asteróides e os espectros de meteoritos e minerais terrestres tenha tido um sucesso limitado, tem revelado a possível composição destes objetos. Muitas das diferenças entre os espectros de asteróides e de meteoritos com composição provavelmente análoga, têm sido atribuídas a processos espaciais de "envelhecimento" da superfície asteroidal, tais como: vitrificação, choques, vento solar, etc. As conseqüências destes processos na superfície de um asteróide foram observadas pela sonda espacial *GALILEO*. Discutiremos mais detalhadamente este processo na seção 3.4.

3.1.1 - Taxonomia e Caracterizacão Mineralógica

As primeiras diferenças entre as cores dos asteróides começaram a ser percebidas logo após suas descobertas. William Herschel publicou em 1802 que a cor de Ceres era diferente daquela de Pallas. Os primeiros espectros de asteróides foram obtidos em 1929 por Bobrovnikoff, o qual igualmente constatou que o espectro de Ceres era mais azul do que o de Pallas. Entretanto, apenas na década de oitenta foi acumulada uma quantidade de dados suficiente para se elaborar uma classificação taxonômica de asteróides.

A taxonomia de asteróides é baseada na análise estatística de grandezas como cor, albedo e características espectrais no visível e infra-vermelho próximo destes objetos. Três classificações, obtidas independentemente e por diferentes métodos, são as mais utilizadas. Tholen (1984) analisou essencialmente os dados espectro-fotométricos em 7-cores do catálogo Eight Color Asteroid Survey–ECAS (Zellner *et al.*, 1985) contendo 405 asteróides. Foram propostas 8 classes principais –C, S, M, A, E, P, D, T–, 3 subclasses –B, F, G– e 3 outras classes contendo apenas um objeto por classe –V, R, Q–, ou seja, 4 Vesta, 349 Dembowska e 1862 Apollo. O método de classificação utilizado baseia-se num algoritmo chamado "árvore minimal".

Na taxonomia de Barucci (Barucci *et al.* 1987) é utilizado o método "G–Mode" (Coradini *et al.*, 1977) aplicado aos dados espectro-fotométricos de 7-cores do ECAS e aos albedos de 438 asteróides obtidos pelo Infrared Astronomical Satellite–IRAS (Matson, 1986). São obtidas 9 classes principais: B, E, G, C, M, D, S, V, A.

Finalmente, a taxonomia de Tedesco (Tedesco *et al.*, 1989) utiliza os índices de cor u–x do ECAS, os albedos do IRAS e índices de cores U–V. Através de uma análise em pares destes três parâmetros, os autores encontraram 11 classes de asteróides, embora estas não sejam suficientes para classificar todos os objetos. Três objetos: 2 Pallas, 4 Vesta e 349 Dembowska não foram classificados neste sistema.

As classificações de Barucci e de Tholen, que são as mais usadas, são coerentes entre si (Tholen e Barucci, 1989) com algumas pequenas diferenças: as classes F, T e B de Tholen estão incluídas nas classes B, D e C de Barucci, respectivamente. Os objetos Q, R e V de Tholen são classificados como V por Barucci.

Estas taxonomias são baseadas em dados obtidos essencialmente no visível, ignorando as características mineralógicas fundamentais que os asteróides possuem no infra-vermelho. Com o aumento dos dados neste intervalo de comprimento de onda, se espera que uma nova classificação taxonômica venha a ser feita a qual possa relacionar de forma mais segura uma classe com um tipo mineralógico.

Vale salientar que embora a classificação taxonômica não utilize nenhum critério mineralógico específico para a definição das classes, os parâmetros óticos utilizados nestas

classificações estão ligados à composição mineralógica superficial dos asteróides. Uma caracterização mineralógica superficial para alguns asteróides e alguns tipos de meteoritos com composição similar a uma determinada classe taxonômica, foram propostos por Gaffey (1978) e Gaffey e co-autores (1989). Os tipos mais comuns de meteoritos análogo, e uma caracterização mineralógica geral para as principais classes taxonômicas estão descritos na tabela I. Podemos notar uma variação considerável de composição entre as classes, assim como dentro de uma mesma classe. O tipo S por exemplo, varia desde os meteoritos pallasitas (rochoso-ferrosos) aos condritos ordinários (ver seção 3.1.2).

Tabela I

Principais Classes de Asteróides: Caracterização Mineralógica
e Meteoritos Análogos

Classe	Possível Composição	Meteorito Análogo
C (B, F e G)	Silicatos hidratados + Carbono Substâncias Orgânicas	Condritos CI e CM
D e P	Silicatos anidros + Carbono Material orgânico	Não tem Partícula de poeira orgânica(?)
E	Enstatite	Acondritos enstatites
M	Metal + Enstatites	Meteoritos ferrosos
S	Metal+ Olivina + Piroxênio	Pallasitas (Ferro-rochosos) Condritos CO/CV Condritos ordinários
V	Piroxênio + Feldspato	Acondritos basálticos

3.1.2 - Classificação Geral de Meteoritos

Uma classificação geral de meteoritos quanto à sua composição química os separa em 3 tipos fundamentais: rochosos, ferrosos e rochoso-ferrosos. Os ferrosos são misturas de Fe, Ni e Co, enquanto que os rochoso-ferrosos são misturas de minerais silicatos e metais. Os ferrosos representam em torno de 3 % de todos os meteoritos que caem na Terra e, de acordo com a quantidade de Ni em sua composição, eles são classificados em: hexahedrito (< 7 % Ni), octahedrito (> 7 % Ni) e ataxito ricos em Ni (16 a 60 % de Ni) (Lewis e Hutson

1993). Os rochoso-ferrosos, que são em torno de 1 % dos que caem na Terra podem ser agrupados em 2 classes: os pallasitas, onde a olivina é dominante e os mesosideritos, onde os piroxênios e feldspatos são dominantes. A tabela II mostra um esquema da taxonomia de meteoritos.

Dentro dos rochosos há uma enorme diversidade em relação às propriedades físicas e químicas, podendo esta classe ser subdividida em condritos e acondritos, baseado na presença ou não de côndrulos. Os côndrulos são pequenos grãos esféricos que variam de tamanho microscópico a alguns milímetros, usualmente compostos por ferro, alumínio ou silicatos de magnésio, sendo sua composição similar àquela encontrada na fotosfera solar (Sears e Dodd, 1988).

Tabela II

Taxonomia de Meteoritos

Rochosos: Predomínio de silicatos, sendo 96% de todos os que caem na Terra
- **Condritos** 88%
  - Primitivos, material indiferenciado, com idade de $4{,}6\times10^9$ anos
  - Abundância de elementos próximas à solar
  - Formado por côndrulos
- **Acondritos** 8%
  - Objetos ígneos (99% de silicatos e óxidos)
  - Material diferenciado de acordo com a densidade
  - Quase todo o material foi solidificado a 4,6 $\times10^9$ anos atrás

Rochoso-ferrosos: 1% de todos os que caem na Terra
- Aproximadamente 50% de misturas metálicas e 50% de silicatos

Ferrosos: 3% de todos os que caem na Terra
- Aproximadamente 99% de misturas de Fe, Ni e Co

Os meteoritos condritos não sofreram uma fundição nem uma diferenciação de seus elementos, sendo portanto considerados primitivos. Esta diferenciação separaria gravitacionalmente em camadas seus componentes, devido à diferença de densidade entre eles. Os acondritos teriam sofrido este processo de aquecimento e, conseqüentemente, uma diferenciação de seus materiais. A figura 3.2 mostra um esquema idealizado de dois tipos de

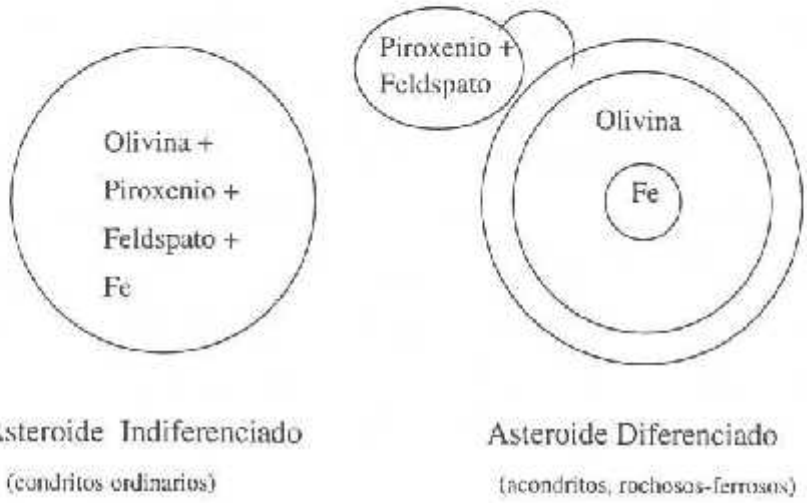

Figura (3.2) *Secções transversais de um corpo original (asteróide) idealizado de meteoritos. A primeira figura representa um asteróide indiferenciado, composto por grãos de olivina, piroxênio, feldspato e ferro misturados de forma homogênea, com composição similar aos condritos ordinários. A segunda representa um asteróide diferenciado formado pela fusão destes materiais, separados gravitacionalmente de acordo com a densidade (Feierberg et al., 1982). Este segundo modelo poderiam ser o corpo original dos meteoritos acondritos e/ou rochosos-ferrosos.*

asteróides, onde o primeiro não sofreu um processo de diferenciação de seus materiais, enquanto o segundo foi aquecido suficientemente para fundir seus elementos e separá-los em camadas. No primeiro caso, este corpo poderia ser a origem de um meteorito condrito, enquanto no segundo caso de acondritos e/ou rochoso-ferrosos. No segundo caso, se o corpo diferenciado sofresse uma colisão catastrófica, seu núcleo metálico poderia ser o corpo original de meteoritos ferrosos.

Os meteoritos condritos, por sua vez, se dividem em 3 suclasses: os carbonáceos, os

os enstatites e os ordinários. Os condritos ordinários são a grande maioria, aproximadamente 88 % dos que caem na Terra, e possuem uma composição que é uma mistura de grãos de olivina, piroxênio, feldspato e metais. De acordo com a abundância de ferro presente em sua composição são divididos em: H, L e LL. Os meteoritos do grupo H apresentam uma alta quantidade de ferro (Fe:Si $\approx$ 0,8), os L possuem uma baixa quantidade de Fe (Fe:Si $\approx$ 0,6) e os LL uma quantidade ainda menor (Fe:Si $\approx$ 0,5). Estes meteoritos têm aproximadamente a mesma mineralogia, sendo que estas diferenças na quantidade de Fe devem refletir temperaturas distintas em sua formação, onde o ferro poderia ser mais abundante a altas temperaturas na nebulosa solar (Lewis e Hutson, 1993).

Os condritos carbonáceos representam aproximadamente 9% de todos os condritos, sendo altamente oxidados e contendo compostos orgânicos, minerais opacos, água e pouco metal livre. Estes meteoritos são freqüentemente aceitos como as amostras químicas mais primitivas do material proto-solar, embora tenham sofrido uma alteração em sua mineralogia devido a um metamorfismo térmico e/ou um processo de alteração aquosa a baixa temperatura (McSween, 1979). O metamorfismo térmico resultaria em uma mudança de Fe/Mg entre os côndrulos e os grãos de olivina e piroxênio, enquanto que num processo de alteração aquosa a baixa temperatura (< 320 K) a água agiria como solvente produzindo materiais como os filossilicatos, sulfatos, óxidos, carbonatos e hidróxidos. Os condritos carbonáceos são subdivididos nos grupos: CI, CM, CO e CV. Os CO e CV são similares aos condritos ordinários, mas possuem olivinas mais ricas em Fe. Os condritos CM e CI possuem uma variedade de silicatos hidratados. A maior parte dos meteoritos CO e CV parece ter sofrido um metamorfismo, enquanto que os CM e CI um processo de alteração aquosa.

Os condritos enstatites, que representam de 4 a 5 % de todos os condritos, possuem predominantemente metais, enstatites e vários sulfidos (Sears e Dodd 1988). Eles são divididos em 2 grupos: EH (alta quantidade de Fe e côndrulos) e EL (baixa quantidade de Fe e côndrulos).

Os meteoritos ígneos rochosos, chamados de acondritos, são aqueles que foram submetidos a altas temperaturas sendo, no mínimo, parcialmente fundidos e resultando

em uma diferenciação de seus componentes (fig 3.2). Os acondritos representam aproximadamente 8 % dos que caem na Terra, sendo divididos em 6 classes de acordo com as abundâncias de Ca, Mg e Fe: eucrites, howardites, diogenites, ureilites, acondritos enstatites e rochas lunares e marcianas.

3.1.3 - Principais Classes e suas Problemáticas

A seguir faremos uma breve descrição das principais classes de asteróides, suas prováveis composições e suas problemáticas.

a) Classe C

Os asteróides do tipo C, que são a maioria no cinturão principal (fig. 3.3), são caracterizados por baixos albedos e por um espectro de reflexão plano no visível e infravermelho próximo, além de um declive em intensidade para comprimentos de onda inferiores a 0,5 μm (fig. 3.4). Estes asteróides têm sido associados a meteoritos condritos carbonáceos CI e CM os quais, devido aos seus baixos albedos, teriam uma grande quantidade de material opaco, como o carbono (Johson e Fanale, 1973). As classes F, B e G foram descritas por Tholen como variações da classe C e teriam surgido, segundo Bell e co-autores (1989), por alteração química em um período pós-acreção. Todos os membros destas classes se encontram na mesma zona do cinturão que os objetos da classe C.

Os espectros de reflexão de muitos asteróides do tipo C mostram a banda de absorção em 3 μm, característica da presença de silicatos hidratado ou filossilicatos (Lebofsky, 1978; Feiberg *et al.*, 1985). Esta banda sugere que a superfície destes asteróides tenha sido submetida a um processo de alteração aquosa em uma mistura de silicatos anidros e gelo. Por outro lado, a ausência desta banda em muitos asteróides desta classe poderia indicar insuficiência destes silicatos hidratados implicando que: (i) o corpo original não possuía gelo, (ii) o asteróide escapou de um processo de aquecimento necessário para gerar esta alteração aquosa, (iii) o objeto foi aquecido a tal ponto de se desidratar completamente (Gaffey *et al.*, 1993).

A ausência desta banda também foi estudada por Feierberg e co-autores (1985), que propuseram que um aquecimento interno devido ao decaimento de radioisótopos (como

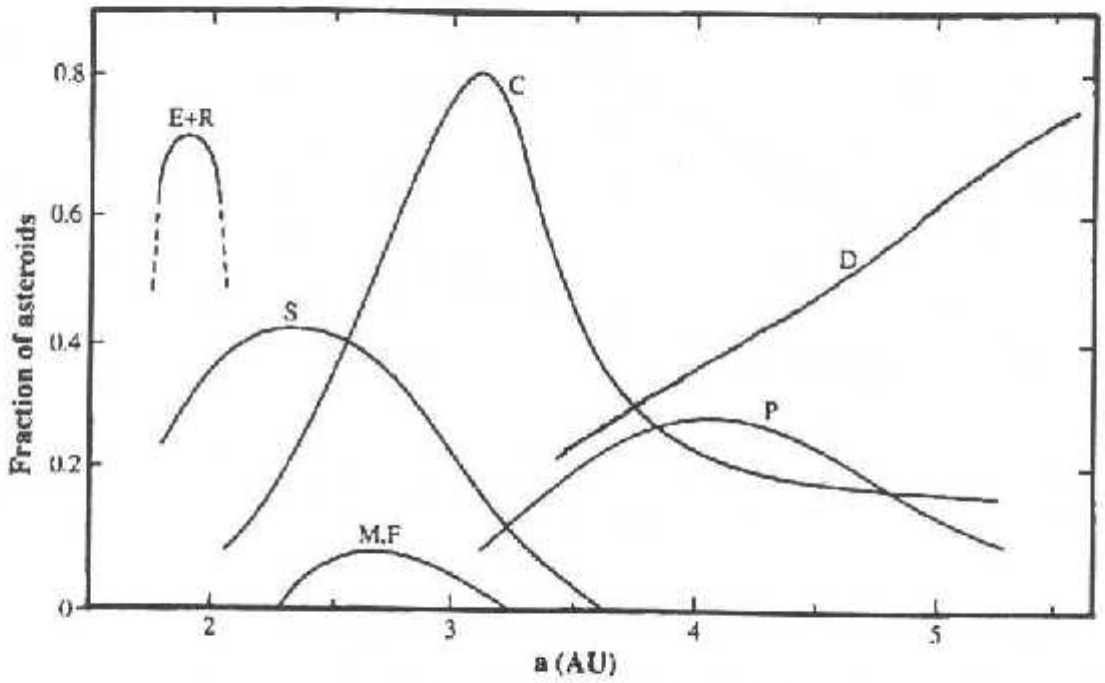

Figura (3.3) *Alguns tipos taxonômicos em função de suas distâncias heliocêntricas. Vemos que os S dominam na parte interna do cinturão, enquanto que os C na parte externa (Gradie e Tedesco, 1982).*

o ^{26}Al) levaria a água do interior para a superfície. Subseqüentes colisões revelariam então seus núcleos anidros. Sendo assim, os asteróides oriundos do material nuclear não apresentariam as bandas de absorção relativas à alteração aquosa. Evidências de um metamorfismo térmico nestes tipos de asteróides foram encontradas por Hiroi e co-autores (1993) quando compararam os espectros de três meteoritos do tipo CM - CI incomuns (apresentavam evidência de metamorfismo térmico), com os de três asteróides [1 Ceres (G), 31 Euphrosyne (C) e 704 Interamnia (F)] encontrando grandes semelhanças. Além disto, aquecendo (entre 600^oC e 1000^oC) em laboratório o meteorito Murchison, um tipo

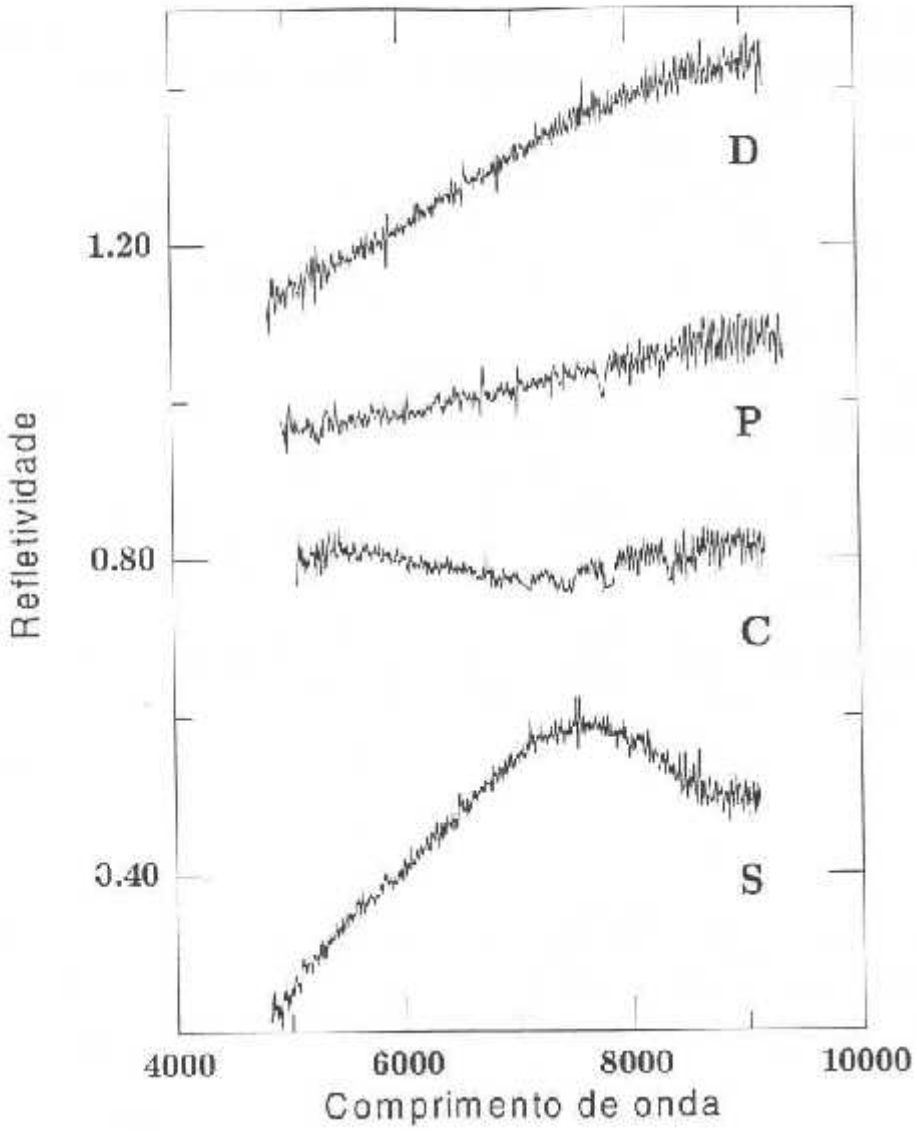

Figura (3.4) *Espectros típicos de reflexão de 4 tipos taxonômicos.*

comum de meteorito condrito carbonáceo, verificou-se que à medida que a temperatura aumentava o espectro deste objeto se tornava mais próximo dos de 5 asteróides do tipo C e 5 do tipo G. Isto levou Hiroi e co-autores a sugerir que os asteróides do tipo C, B,

G e F seriam os núcleos de objetos que sofreram uma alteração térmica, e os meteoritos condritos carbonáceos seriam uma amostra das camadas mais externas que permaneceriam inalteradas.

Uma banda de absorção em 0,7 μm, atribuída à transferência de carga $Fe^{2+} \rightarrow Fe^{3+}$ em filossilicatos, tem sido também encontrada em vários asteróides do tipo C e G (Sawyer, 1991) e em vários meteoritos condritos carbonáceos (Gaffey e McCord, 1979). Uma forte correlacão entre as bandas de 3,0 e de 0,7 μm foi posteriormente encontrada por Vilas (1994) sugerindo sua origem por processos de alteração aquosa de seus materiais superficiais, já que a banda de 3,0 μm é um indicador da presença de água. A presença desta banda em vários asteróides deste tipo contradiz a hipótese de que eles tenham sofrido um grande aquecimento, pois esta banda desaparece totalmente quando submetemos um meteorito condrito carbonáceo (do tipo Murchison) a uma temperatura próxima ou maior que $400^{o}C$ (Vilas e Sykes, 1996).

Esta aparente contradição entre os modelos para explicar a composição superficial destes asteróides talvéz possa ser explicada se considerarmos que haja uma diversidade na composição mineralógica dentro desta classe de objetos. Além disto, esta diversidade pode também ser uma indicação de diferentes processos térmicos que estes objetos sofreram.

Foi encontrado por Vilas e Sykes (1996) uma leve correlação entre o metamorfismo térmico, a alteração aquosa e o diâmetro dos asteróides do tipo C e subtipos. Exceto para a classe B, a percentagem dos asteróides que apresentam a banda de 0,7 μm diminui com o diâmetro. Isto poderia ser explicado considerando que, para uma dada distância heliocêntrica, os corpos menores seriam os fragmentos de partes distintas de corpos originais, revelando então uma maior diversidade em sua composição. Os corpos maiores, por sua vez, manteriam uma maior homogeneidade na composição. Este tipo de correlação foi também encontrado por nós nos membros da família de Themis (ver seção 4.7.3).

Muitas outras bandas de absorção relacionadas com o processo de alteração aquosa e atribuídas à transferência de cargas em minerais silicatos têm sido encontradas, tais como: 0,43, 0,60-0,65 e 0,80-0,90 μm (Vilas *et al.*, 1994). Todas estas bandas são atribuídas à presença de óxidos de ferro em filossilicatos. Vilas e co-autores (1994) propuseram a

existência de uma região no cinturão principal onde estariam os asteróides com indícios de alteração aquosa. Esta região estaria entre 2,6 e 3,5 U.A., com a exceção de uma pequena zona entre 2,8 e 3,0 U.A.. Dados obtidos por nós confirmam a existência desta região, mas não da pequena zona vazia deste tipo de asteróides (ver seção 3.2).

b) Classe S

Os asteróides do tipo S, que dominam a parte interna do cinturão de asteróides (fig.3.2), pertencem à segunda classe mais numerosa. Suas características espectrais são as bandas de absorção em 1 e 2 μm devidas à transição do ion Fe^{2+}. A razão entre as áreas das bandas de 1 e 2 μm pode ser usada para se calcular a abundância relativa de olivina e piroxênio, enquanto a posição destas bandas pode fornecer o tipo de composição do piroxênio (Cloutis *et al.*, 1986). A inclinação da curva espectral no visível é atribuída à presença de NiFe na superfície. Os asteróides do tipo S possuem um albedo moderado, entre 0,10 e 0,30. Um espectro do tipo S pode ser visto na figura 3.4.

A presença de olivina, piroxênio e NiFe na superfície deste tipo de asteróide não é suficiente para realizar uma precisa correlação com um meteorito análogo. Este tipo de composição pode estar associado tanto aos condritos ordinários, de composição indiferenciada, quanto aos acondritos e rochoso-ferrosos, de material diferenciado (fig. 3.2).

Os espectros dos asteróides do tipo S apresentam uma grande variação em seus parâmetros espectrais, e a interpretação de sua composição superficial tem sido fonte de muitas controvérsias (ver Chapman 1996 e referências). Foi comum associar este tipo de asteróide aos meteoritos condritos ordinários, pois eles são os mais abundantes entre os que caem na Terra e os asteróides do tipo S são os mais comuns na parte interna do cinturão. Entretanto, os tipos espectrais destes asteróides e meteoritos não são idênticos. Na tentativa de resolver este problema duas teorias surgiram. Uma afirma que estes asteróides seriam sim os corpos originais dos condritos ordinários e que a diferença nos espectros seria devida a um processo de alteração espacial agindo em sua superfície. Este processo agiria sobre a superfície dos asteróides tornando seus espectros mais avermelhados e as bandas de absorção mais atenuadas, além de escurecer sua superfície (fig 3.5) (Pieters

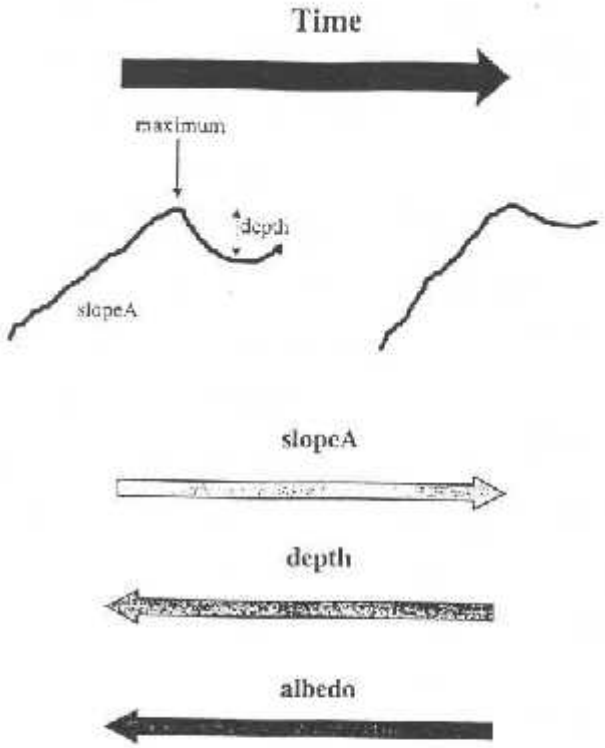

Figura (3.5) *Conseqüências sobre os parâmetros espectrais devido a um processo de alteração espacial.*

& McFadden, 1994; Chapman, 1996). Os meteoritos condritos ordinários seriam portanto os fragmentos das camadas mais internas, que não teriam sofrido alteração de composição.

Outros pesquisadores, entretanto, rejeitam a hipótese acima e associam estes asteróides a um tipo de composição diferenciada. Eles propõem que os meteoritos condritos ordinários viriam ou de um asteróide até hoje ainda não descoberto, ou de pequenos asteróides, menores do que 10 km, os quais, por estarem abaixo do limite observacional, ainda não foram detectados (Bell et al., 1989).

Determinar a natureza dos asteróides do tipo S pode nos dar importantes informações sobre as condições e processos no início do Sistema Solar. Se estes asteróides tiverem um tipo de composição indiferenciada, a parte interna do cinturão foi pouco aquecida. Por outro lado, se estes asteróides forem diferenciados, isto significa que eles sofreram um grande evento térmico (Wetherill e Chapman, 1988; Gaffey *et al.*, 1993).

Historicamente, a diversidade de características espectrais neste tipo de asteróide levou vários autores a diferentes resultados sobre sua composição. Chapman e co-autores (1973) encontraram semelhanças entre o asteróide 1985 Toro (objeto próximo a órbita da Terra) e alguns meteoritos condritos ordinários, sugerindo então a hipótese de alteração espacial na superfície deste tipo de asteróide. Feierberg e co-autores (1982), analisando os espectros de 11 asteróides num intervalo espectral de 0,3 a 2,5 μm, obtiveram as abundâncias relativas de olivina e piroxênio. Comparando estes resultados com os de minerais terrestres, concluíram que estes asteróides possuíam uma composição muito similar aos condritos ordinários. Bell (1988) definiu uma nova classe de objetos (tipo K), pertencentes à classe S, com material análogo aos meteoritos condritos carbonáceos (ver item e) Classe K). Por outro lado, Gaffey (1984) encontrou variações espectrais com a rotação em 8 Flora e concluíu que estas variações seriam incompatíveis com meteoritos indiferenciados, como os condritos ordinários. Remetemos ao artigo de Chapman (1996) para uma detalhada descrição e revisão histórica da problemática dos asteróides do tipo S.

Estas diferentes conclusões sobre a mineralogia devem refletir uma diversidade na composição deste tipo de asteróide, incluíndo uma composição indiferenciada encontrada nos condritos ordinários. Desta forma, Gaffey e co-autores (1993) analisando os espectros de 39 asteróides do tipo S propuseram 7 subtipos (designados de S(I) a S(VII)). Os tipos mineralógicos propostos seriam produto desde uma pequena até uma total diferenciação. Apenas o subtipo S(IV) poderia ser associado aos condritos ordinários. Como a percentagem sugerida pelos autores para o subtipo S(IV) é muito pequena, eles concluíram que a maior fonte dos meteoritos condritos ordinários não seria este subtipo.

Entretanto, Chapman (1996) baseado nos resultados da sonda *GALILEO* defende a hipótese de que os corpos originais dos condritos ordinários são de fato os asteróides do tipo S. Um dos resultados mais importantes obtidos por esta sonda foi o de encontrar evidências de que um processo de alteração espacial pode agir sobre um asteróide. Este efeito poderia ser responsável pela conversão de um espectro do tipo condrito ordinário em um de asteróide típico da classe S. As imagens e espectros de Ida mostram uma variação de cor em sua superfície, também observada em menor grau em Gaspra. Estes dois asteróides são do tipo S, sendo que Gaspra pertence à família de Flora e Ida à família de Koronis.

Na figura 3.6 reproduzimos uma imagem de Gaspra obtida pela sonda *GALILEO*, mostrando sua superfície coberta por crateras. As bordas das crateras, chamadas de regiões *azzurras*, se mostram mais azuis que as regiões planas. Estas bordas seriam regiões mais "jovens" pois teriam exposto sua composição mais interna. O espectro destas regiões se mostra mais próximo de um meteorito condrito ordinário do que o de regiões mais planas, ou "velhas" (Chapman, 1996).

A hipótese de alteração espacial é também corroborada analisando-se a Lua. Os espectros da superfície lunar aparecem mais lineares, mais avermelhados e com bandas de absorção mais fracas do que as rochas lunares. Uma evidência experimental deste processo foi também obtida por Moroz e co-autores (1996) por simulação em laboratório numa amostra do meteorito Elenkova (condrito ordinário L5). Foi observado que os parâmetros espectrais desta amostra de meteorito se modificavam de forma a se aproximar dos parâmetros típicos dos asteróides da classe S, quando submetidos a uma fundição e cristalização de seu material superficial através de impulsos de laser no vácuo.

c) Classes D e P

Os asteróides pertencentes às classes D e P dominam o cinturão externo, sendo caracterizados por baixos albedos e associados a uma mistura de materiais orgânicos, silicatos anidros, material opaco e gelo (Bell *et al.*, 1989; Gaffey *et al.*, 1989).

Os asteróides do tipo D são considerados os mais primitivos, tendo sido formados a baixa temperatura na nebulosa solar. Os espectros desta classe são muito vermelhos, com uma inclinação aumentando com o comprimento de onda (fig. 3.4). Os do tipo P possuem uma inclinação menor estando entre os dos tipos C e D (Lazzarin *et al.*, 1995; Fitzsimmons *et al.*, 1994). Nenhum meteorito análogo foi encontrado para estes tipos de objetos.

d) Classes E e M

A classe E possui um albedo muito alto (0,4 a 0,5), com uma composição normalmente associada aos meteoritos enstatites acondritos (aubrites). Os aubrites são fragmentos da crosta e/ou manto de corpos que sofreram um grande processo de diferenciação,

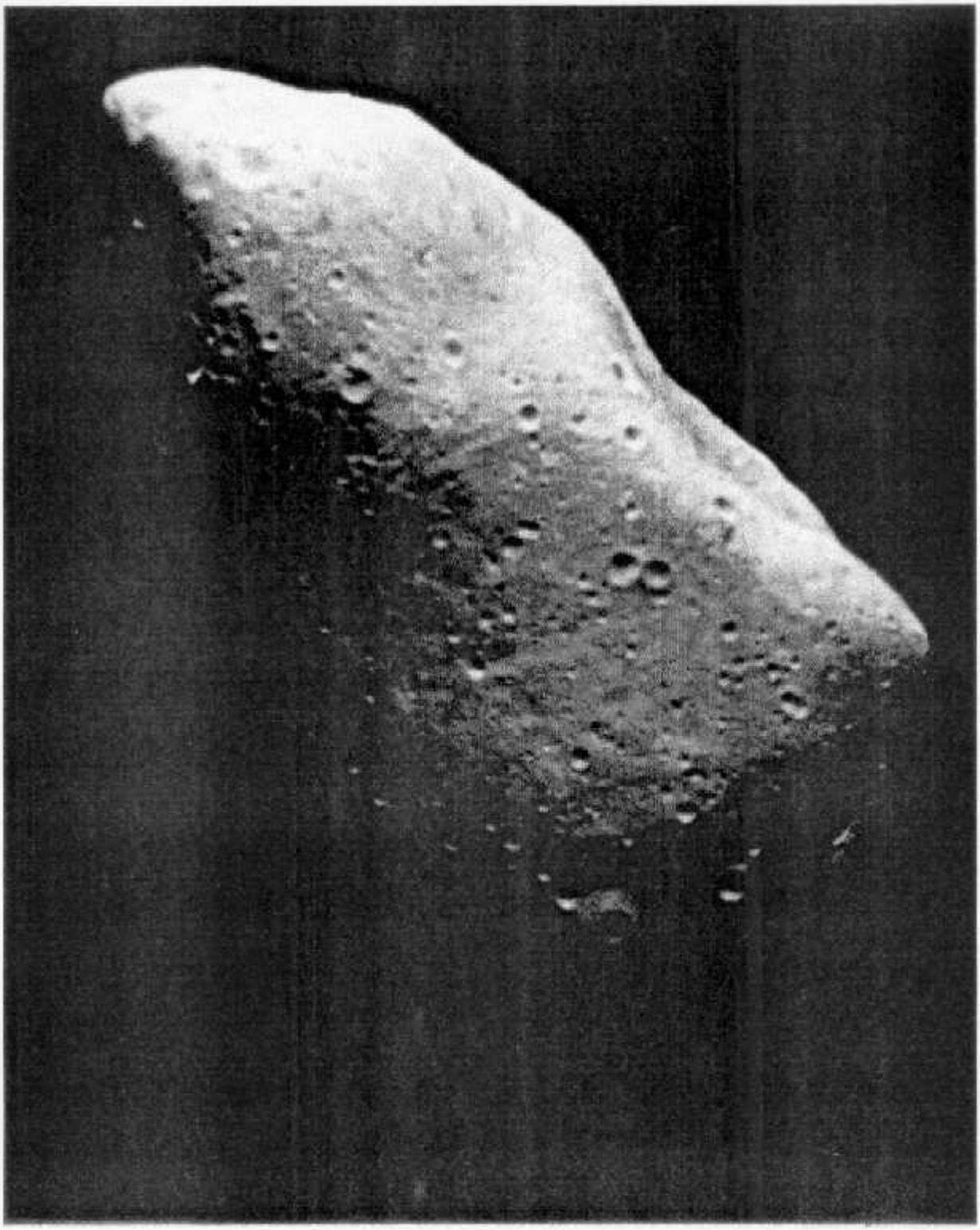

Figura (3.6) *Imagem de Gaspra obtida pela sonda espacial GALILEO.*

tendo sido submetidos a temperaturas superiores a 1500°C (Gaffey *et al.*, 1992). Na região de Hungaria encontramos a maior parte dos asteróides da classe E, com semi-eixo maior entre 1,79 e 1,98 U.A. e inclinação entre 15° e 40°.

Os asteróides do tipo M possuem um albedo moderado, entre 0,15 e 0,25, com uma característica espectral similar aos meteoritos ferrosos (diferenciados) e aos condritos enstatites (material levemente diferenciado com alta percentagem de ferro, mais do que 25%) (Moroz, 1994). Os membros de ambas as classes devem ser diferenciados e os corpos originais devem ter sido submetidos a altas temperaturas (Rivkin *et. al.*, 1995; Zellner *et al.*, 1977). São caracterizados no visível e infra-vermelho próximo por um espectro de plano a similar aos do tipo P, sendo difícil de diferenciar entre si os tipos E e M.

e) Classe K

Bell (1989) propôs esta classe baseado nos espectros de 4 membros da família de Eos. Os espectros desta classe são parecidos com os do tipo S, mas com uma fraca absorção em 1 μm e um comportamento plano entre 1,1 e 2,5 μm, ou seja, similar aos do tipo C no infra-vermelho. Estas características sugerem que os condritos carbonáceos CO e CV sejam seus meteoritos análogos. Nos espectros de 43 objetos da família de Eos foi encontrado um valor máximo de intensidade em aproximadamente 8388 $\AA$, bem diferente do valor médio dos asteróides do tipo S, que é em 7500 $\AA$ (ver seção 3.8.1). Este valor pode ser uma identidade muito forte para este tipo taxonômico.

3.2 - Observações e Reduções

Com o objetivo de estudar a composição mineralógica de asteróides realizamos observações espectroscópicas, escolhendo as famílias de asteróides como objeto principal de análise e, em segundo plano, os objetos próximos da órbita da Terra, os asteróides do tipo C e os candidatos à missão espacial *Rosetta*.

Os espectros de baixa resolução deste capítulo foram obtidos em várias missões de observação, realizadas principalmente nos anos de 1996, 1997 e 1998. As observações foram feitas essencialmente no telescópio de 1,5 m do European Southern Observatory (ESO, La Silla, Chile) usando um espectrógrafo Boller&Chivens com um detector CCD

Ford (2048×2048). A faixa espectral estudada varia de 4900 a 9200 $\AA$ com um FWHM (largura à meia altura de uma distribuição gaussiana) de 10 $\AA$.

As reduções dos dados foram feitas utilizando os pacotes IRAF (Image Reduction and Analysis Facility) e MIDAS (Munich Image Data Analysis System). Esta redução consiste preliminarmente em: - 1) Subtrair uma *imagem* de fundo (*Bias*) do CCD das *imagens* dos objetos. O *bias* é o valor constante de leitura do CCD quando o obturador está fechado - 2) Dividir todos os dados pelo *flat-field*, obtido através de uma exposição do CCD a uma luz de intensidade uniforme. Isto é feito para corrigir a diferença de ganho entre um pixel e outro. - 3) Obter um espectro unidimensional com a escala em intensidade por pixel. - 4) Calibrar a escala em pixel para comprimentos de onda do espectro obtido, através do espectro de uma lâmpada de He–Ar. - 5) Corrigir a extinção atmosférica.

Para a obtenção do espectro de reflexão do asteróide efetuamos também observações de estrelas do tipo solar (Hardorp, 1978). Lembramos que um asteróide não tem luz própria mas apenas reflete a luz do Sol, desta forma seu espectro é do tipo solar. As características mineralógicas da superfície do asteróide são obtidas através da divisão do espectro do asteróide pelo da estrela do tipo solar (fig. 3.7). Em geral observamos três estrelas por noite e fazemos a divisão entre estas para verificar se o resultado desta divisão é um espectro plano, o que indicaria que a diferença nos espectros destas estrelas não afetará os resultados. Em quase todas as missões foi realizado este teste, obtendo-se uma diferença insignificante entre as análogas solares. Nas primeiras missões também tivemos o cuidado de observar alguns asteróides com espectros bem conhecidos, para efeito de comparação, obtendo sempre bons resultados.

3.3 - Resultados

A seguir descreveremos os resultados obtidos destas observações.

3.3.1 - Alteração Aquosa

Com o objetivo de entender melhor o processo de alteração aquosa realizamos uma campanha de observação de asteróides do tipo C procurando indícios deste processo. O artigo a seguir descreve o trabalho realizado, cujos resultados podem ser resumidos em:

Figura (3.7) *Passos a serem efetuados para a obtenção de um espectro de reflexão asteroidal.*

- observamos 29 objetos, sendo que em 70 % deles encontramos características de alteração aquosa;
- destes 29 objetos, 13 apresentavam a banda de 0,7 μm, e 7 as bandas entre 0,60-0,65 e 0,8-0,9 μm;
- confirmamos a existência, no cinturão principal, da região onde são encontrados os asteróides com indicação de hidratação;

- a região em questão não apresenta limites muito precisos, contrariando o proposto por Vilas e co-autores (1994);
- foram encontrados alguns asteróides com indícios de alteração aquosa entre 2,8 e 3,0 U.A., excluíndo assim a existência de uma lacuna onde não haveria ocorrência deste processo.

ICARUS 132, 388–396 (1998)
ARTICLE NO. IS985889

Search for Aqueously Altered Materials on Asteroids[1]

M. A. Barucci, A. Doressoundiram, and M. Fulchignoni

Observatoire de Paris, 92195 Meudon Principal Cedex, France
E-mail: barucci@obspm.fr

M. Florczak

ON/CNPq, Dep. Astrofisica, 20921 Rio de Janeiro, Brazil, and CEFET, Dep. Fisica, 8000 Curitiba, Brazil

M. Lazzarin

Dipartimento di Astronomia, Vicolo dell'Osservatorio 5, 35122 Padova (Italy)

and

C. Angeli and D. Lazzaro

ON/CNPq, Dep. Astrofisica, 20921 Rio de Janeiro, Brazil

Received July 9, 1997; revised December 3, 1997

The analysis of visible and near-infrared reflectance spectra of C-class objects has revealed the presence of features that appear to indicate a history of aqueous alteration on their surfaces. This result can provide constraints on our understanding of the early Solar System. We have recorded spectra covering 0.48–0.92 μm for 29 C-class objects with orbital semimajor axes between 2.3 and 3.6 AU. About 70% of the observed objects show features produced as the result of aqueous alteration processes. © 1998 Academic Press

1. INTRODUCTION

The thermal metamorphism of asteroids is still intriguing and debated. To contribute to this discussion, we have investigated the problem of aqueous alteration of asteroid surfaces. The detection of aqueous alteration materials on dark asteroids can give important constraints on the understanding of the formation and evolution of solid bodies in the early Solar System.

The asteroid belt shows a compositional structure that varies with heliocentric distance and with thermal history (Gradie *et al.* 1989; Barucci *et al.* 1987). Asteroid compositions reflect a trend from silicaceous objects (S-types) in the inner part of the belt, through bodies of carbonaceous type, to more primitive ones in the outer part (the D-type asteroids). This trend may indicate that solid materials experienced different thermal histories in the different zones of the asteroid belt during their primordial evolution. The high-albedo objects (S-type) seem to have undergone heating and differentiation during their evolution. Near 2.5 AU the belt becomes dominated by low-albedo objects belonging to the classes C, P, and D. C objects dominate the region up to 3 AU. Their spectra are similar to those of carbonaceous chondrite meteorites (Hiroi and Vilas, 1995), indicating a primitive composition that probably experienced less dramatic changes than the materials in the S type asteroids. Beyond 3 AU the asteroid population is essentially composed of P and D type asteroids. These more distant objects are believed to have undergone even less thermal and geological evolution. The surfaces of these objects are assumed to be darkened by the presence of a significant amount of carbon-rich organic compounds.

The C class, originally defined by Chapman *et al.* (1975), is strictly linked to some homogeneous subgroups: the F, B, and G class asteroids. Hiroi *et al.* (1993, 1996) studied the thermal metamorphism of the C, F, B, and G class asteroids. They compared the spectra of these asteroids with spectra of carbonaceous chondrites, including thermally metamorphosed CI/CM meteorites. They gave constraints on the heating temperatures of some asteroids. They conclude that hydrous materials cannot survive at temperatures higher than 400°C. Materials become increasingly anhydrous between 400 and 600°C and com-

[1] Based on observations carried out at the European Southern Observatory (ESO) of La Silla, Chile, some under the agreement with the CNPq, Observatório National (Brazil).

0019-1035/98 $25.00

TABLE I
Observational Circumstances

Asteroids	UT Date	Exp.	R(AU)	Δ (AU)	α	m_v	Solar analog
47 Aglaja	06/01/97	2	3.222	2.783	16.9	13.5	HD 44594
70 Panopaea	20–22/05/96	2	2.633	1.970	19.4	12.7	HD 144585
85 Io	03/02/97	2	3.146	2.390	13.2	12.8	HD 44594
105 Artemis	02/01/97	2	2.684	2.598	21.4	13.9	HD 44594
156 Xanthippe	17/10/96	2	3.152	2.263	9.6	13.5	HD 44594
171 Ophelia	20/06/95	2	3.109	2.154	7.7	13.0	HD 1835
173 Ino	03/01/97	2	2.634	1.678	6.3	11.5	HD 44594
175 Andromache	20–21/05/96	2	3.907	3.635	14.9	14.9	HD 144585
194 Prokne	03/01/97	2	3.235	2.558	14.3	13.1	HD 44594
238 Hypatia	20–21/05/96	2	3.131	2.717	18.2	13.8	HD 144585
266 Aline	20/06/95	1	3.096	2.172	9.4	13.6	HD 1835
350 Ornamenta	03/01/97	2	2.706	2.514	21.3	13.6	HD 44594
	21/06/95	1	3.440	2.509	7.9	13.6	HD 1835
373 Melusina	22/05/96	1	3.368	2.457	8.8	14.3	HD 144585
375 Ursula	21/05/96	1	3.380	2.808	16.3	13.1	HD 144585
379 Huenna	27/03/96	1	2.992	2.461	17.9	13.2	HD 144585
404 Arsinoe	17/10/96	2	3.004	2.144	11.4	13.8	HD 44594
	02/01/97	2	3.075	3.154	16.1	14.9	HD 44594
419 Aurelia	27/03/96	1	1.965	1.739	30.5	12.4	HD 144585
429 Lotis	28/03/96	1	2.894	1.905	3.3	13.9	HD 144585
469 Argentina	06/01/97	2	2.621	2.256	21.6	13.5	HD 44594
490 Veritas	26/03/96	1	3.480	2.484	1.2	13.2	HD 144585
511 Davida	03/01/97	2	2.615	1.896	17.3	10.6	HD 44594
521 Brixia	20/05/96	1	3.437	2.679	12.7	14.1	HD 144585
735 Marghanna	20/05/96	1	3.436	2.737	13.7	15.2	HD 144585
740 Cantabia	16/10/96	2	3.282	2.321	5.4	13.8	HD 44594
	03/01/97	2	3.214	2.848	17.3	14.7	HD 44594
751 Faina	15–16/10/96	5	2.165	1.222	11.3	11.5	HD 44594
909 Ulla	16/10/96	2	3.197	2.341	10.7	13.9	HD 44594
1031 Arctica	11/01/97	1	2.884	2.007	10.6	14.0	HD 44594
1445 Konkolya	20/06/95	1	3.215	2.292	9.0	16.8	HD 1835
1963 Bezovec	15–16/10/96	4	2.165	1.345	19.1	14.2	HD 44594

Note. Exp is the number of exposures, R and Δ are the heliocentric and geocentric distances respectively, α the solar phase angle, and m_v the visual magnitude.

pletely anhydrous for temperatures larger than 600°C. The thermal metamorphism of low albedo asteroids is extensively discussed by Vilas and Sykes (1996).

The proof of the presence of aqueous alteration products on C asteroids was first evidenced by observations near 3 μm by Lebofsky (1980) and by Jones *et al.* (1990), showing the strong water of hydration absorption feature centered in that wavelength region. They suggested that selective induction heating produced the observed aqueous alteration at the surface (perhaps in the interior) originating both the carbonaceous chondrite parent bodies and the material characterizing the present C-type objects.

In the visible range, the presence of aqueous alteration products was discovered by Vilas and Gaffey (1989) and discussed later by Vilas (1994) and Vilas *et al.* (1994).

Vilas *et al.* (1994) proposed that a particular zone of the outer main belt seems characterized by objects which have undergone some kind of aqueous alteration process, that is, a low temperature chemical alteration of materials by liquid water which produces materials such as phyllosilicates, sulfates, oxides, carbonates, and hydroxides. This region has been localized between 2.6 and 3.5 AU and the asteroids that have shown the presence of aqueously altered materials (hydrated silicates or clays) are essentially of the C type. This might indicate the presence of water ice in the original asteroids that were heated sufficiently during the primordial phases of our Sun to provide water for chemical alteration.

Some Cs do not show aqueously altered features. Even if some of these could be originally anhydrous, others could be unaffected by heating and may preserve interior ices, along with the Ps and Ds (Barucci *et al.*, 1996). The P and D classes are expected to preserve nearly unaltered primitive solid and volatile mixtures.

TABLE II
Presence of Hydration Bands on the Observed Asteroids

Asteroid	Semi-major axis AU	Diameter[a] Km	Hydration	Band depth %
47 Aglaja[3]	2.880	127	yes	2.0
70 Panopaea[1]	2.614	122	yes	2.9
85 Io[2]	2.654	155	yes	1.3
105 Artemis[3]	2.373	119	yes	4.4
156 Xanthippe	2.730	121	yes	2.2
171 Ophelia[2,3]	3.132	117	yes	1.3
173 Ino	2.744	154	no	—
175 Andromache	3.186	101	no	—
194 Prokne[1]	2.617	168	yes	3.2
238 Hypatia[1]	2.905	148	yes	2.0
266 Aline[2]	2.806	109	yes	2.2
350 Ornamenta[1]	3.116	118	yes	5.0
373 Melusina[1]	3.115	96	yes	3.0
375 Ursula	3.126	190	no	—
379 Huenna	3.130	92	no	—
404 Arsinoe[1]	2.593	98	yes	5.7
419 Aurelia	2.592	129	no	—
429 Lotis	2.608	70	no	—
469 Argentina[3]	3.157	126	yes	1.3
490 Veritas[1]	3.168	116	yes	2.5
511 Davida[3]	3.172	326	yes	1.3
521 Brixia[1]	2.742	116	yes	2.5
735 Marghanna[1]	2.726	74	yes	2.3
740 Cantabia	3.050	91	no	—
751 Faina[1]	2.551	110	yes	3.1
909 Ulla	3.539	116	no	—
1031 Arctica[1]	3.045	75	yes	3.4
1445 Konkolya	3.118	25	no	—
1963 Bezovec[1]	2.422	45	yes	4.4

Note. The depth of the deepest absorption is reported in the last column. [1] Absorption band around 0.7 μm; [2] absorption band around 0.6–0.65 μm; [3] absorption band around 0.8–0.9 μm.

[a] The diameters are determined by IRAS except for 375 Ursula and 1445 Konkolya, for which the IRAS albedo value is not available and an estimate for the diameter has been computed assuming albedo 0.05.

To better define and understand the nature of the "alteration zone," we have performed a CCD spectroscopic survey of C-type asteroids to obtain homogeneous and high S/N spectra to search for the presence of features due to aqueous alteration products.

2. OBSERVATIONS AND DATA REDUCTION

The observations were performed during several runs during the last four years at the European Southern Observatory of La Silla (Chile) using the 1.5 m telescope with a Boller & Chivens spectrograph and a CCD (2048 × 2048 pixels). The grating is 225 gr/mm with a dispersion of 0.033 μm/mm at the first order. The CCD has a 15 μm square pixel, giving a dispersion of about 5 Å/pixel in the wavelength direction. The spectral range is about $0.48 < \lambda < 0.92$ μm with a FWHM of 10 Å.

Each spectrum was recorded through a slit oriented in the East–West direction with an airmass near 1. The circumstances of the observations are listed in Table I, in which the heliocentric and geocentric distances, the solar phase angle, and the visual magnitude are reported.

Following ordinary data reduction procedures we also recorded bias, flat field, calibration lamp, and spectrophotometric standard star spectra at different intervals throughout the night. The final step of the reduction procedure, which consists of the determination of the reflectivity of the asteroids, was performed by recording spectra of solar analog stars (Hardorp, 1978). In Table I, we give the solar analogs used for each asteroid.

The spectra were reduced using the software packages Midas and IRAF. All asteroid spectra are normalized at 1 around 0.55 μm.

3. RESULTS

The reflectivity spectra of the 29 observed asteroids are reproduced in the Appendix. Most of the objects have been observed several times as reported in Table I. All the spectra have been fitted with a polynomial of order ten and a straight line continuum defined by a linear least-squares fit to the data has been removed to reveal traces of aqueous alteration.

About 70% of the observed objects show features associated with aqueous alteration processes. The band depth, which gives an indication to the degree of hydration, has been computed for the hydrated asteroid and reported in Table II. Thirteen of them (Fig. 1) show a broad absorption band around 0.7 μm with a depth relative to the continuum ranging from 3 to 6%. The 0.7 μm absorption feature is believed to arise from $Fe^{2+} \rightarrow Fe^{3+}$ charge transfer absorptions in phyllosilicate minerals (Vilas and Gaffey, 1989, Vilas *et al.* 1993). This band accompanies an evident UV absorption shorter than 0.5 μm in most of the 13 objects. The UV band is due to a strong ferric oxide intervalence charge transfer transition (Vilas *et al.*, 1994). Other weaker features (depth about 1 to 2%) have been found around 0.6–0.65 μm, 0.8–0.9 μm on seven asteroids (Fig. 2). These bands are the results of the action of aqueous alteration on iron-bearing silicates. As well described by R. G. Burns (1970), the 0.6–0.65 μm feature corresponds to the $^6A_1 \rightarrow {}^4T_2(G)Fe^{3+}$ charge transfer transition in iron oxides, and the 0.8–0.9 μm feature corresponds to $^6A_1 \rightarrow {}^4T_1(G)Fe^{3+}$ charge transfer transition in iron oxides. Vilas *et al.* (1994) show a comparison between asteroid spectra and hematite, goethite, and jarosite spectra (aqueously altered products of anhydrous silicates) which show absorption bands centered around 0.86, 0.93, 0.94 μm.

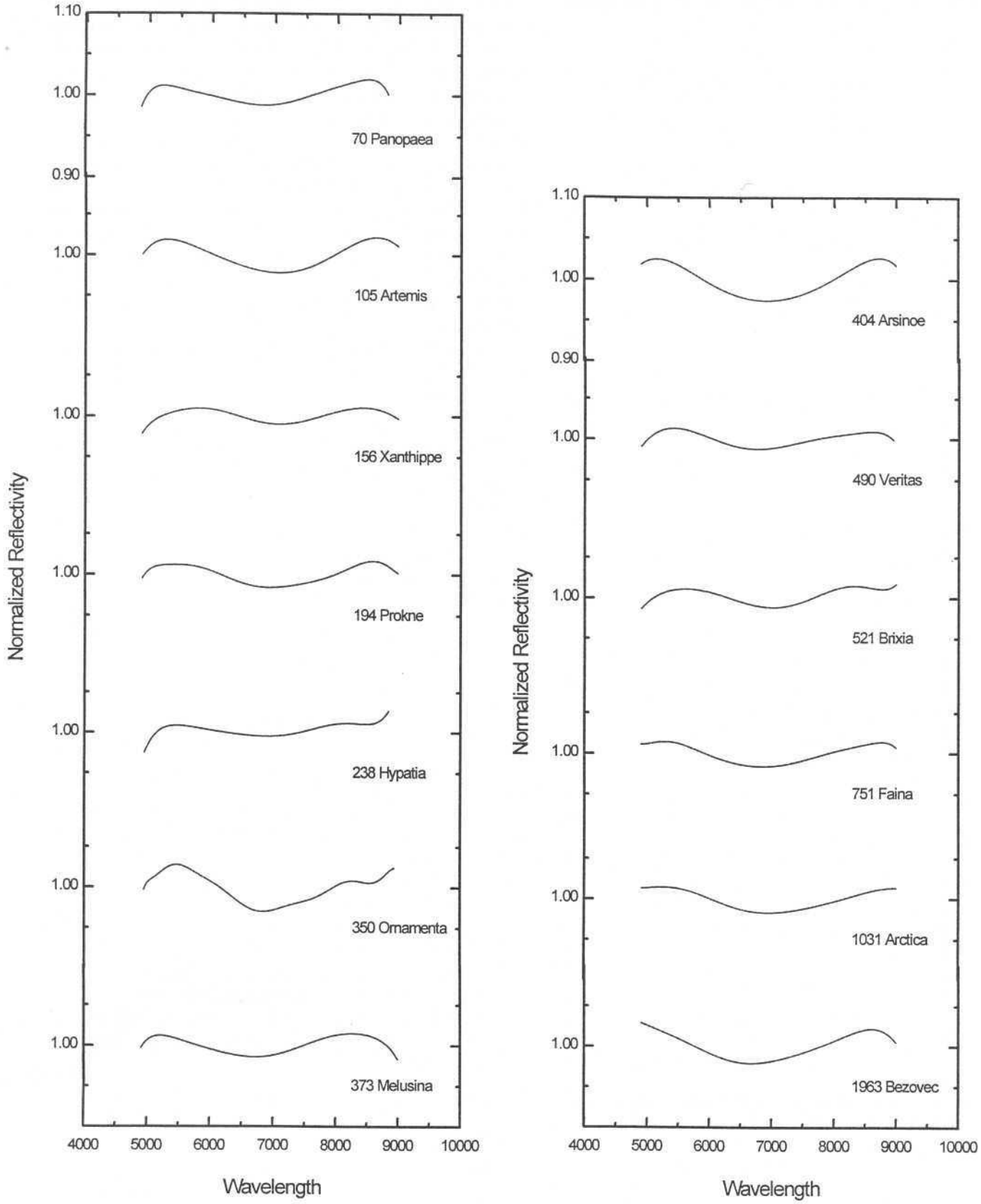

FIG. 1. Spectra of 13 of the observed asteroids which show a broad absorption band around 0.7 μm. The spectra were fitted with a polynomial; a linear continuum has been removed.

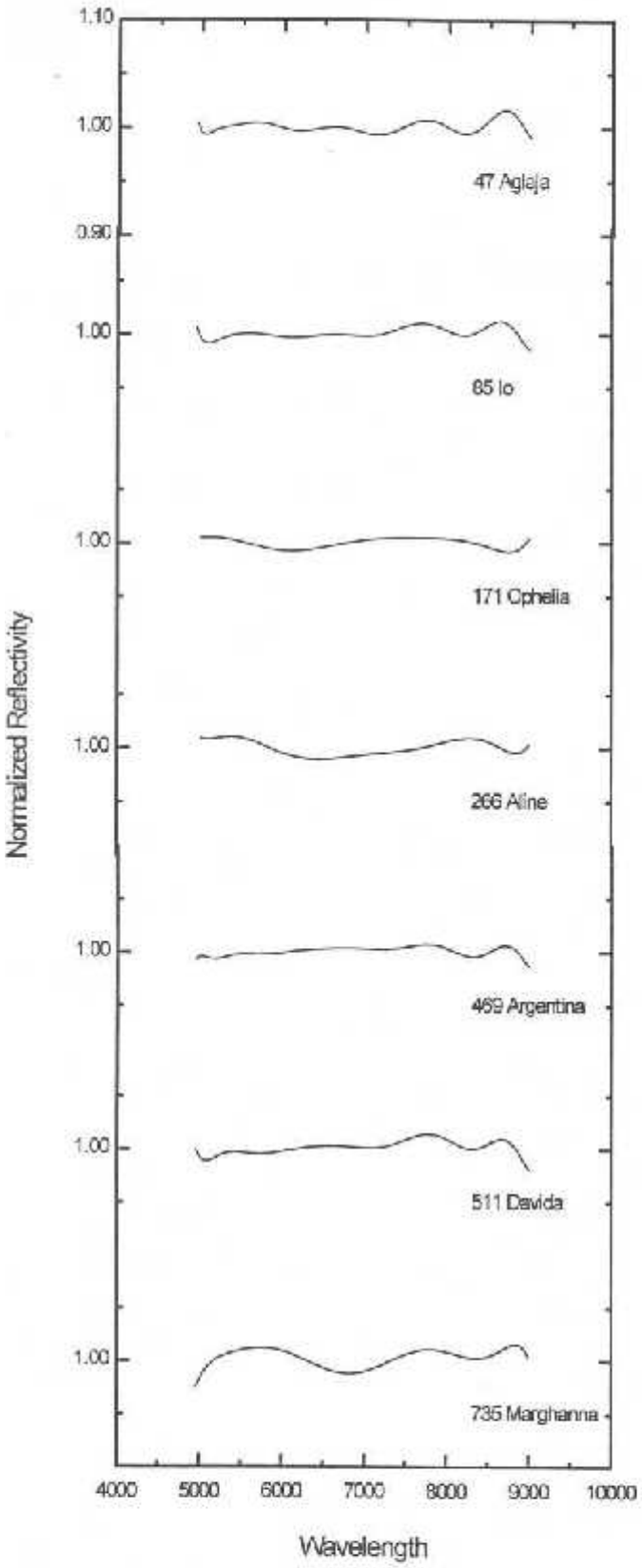

The observed asteroids have been selected from C class asteroids and in the region of the belt ranging between 2.37 AU and 3.54 AU as shown in the histogram reported in Fig. 3. Vilas *et al.* (1994) defined an "aqueous alteration zone" from 2.6 to 3.5 AU with an exception of a small zone from 2.8 to 3.0 AU. From this analysis: (i) we confirm the existence of the aqueous alteration zone, (ii) we found hydration features on four asteroids located closer to the sun than 2.6 AU, probably indicating that the boundaries of the "alteration zone" are not so tight, and (iii) we found some asteroids showing hydration features between 2.8 AU and 3 AU, excluding the existence of a gap in the "aqueous alteration zone," which, on the other hand, it would be very difficult to explain. No evidence of a correlation between the asteroid sizes and hydration (Table II) has been found in our sample, but the analyzed sample may suffer from an observational bias.

In 1997, Merényi *et al.* made a prediction of water in asteroids using an artificial neural net tool analyzing data for 80 asteroids belonging to almost all the taxonomic classes. Their analysis includes 23 C type asteroids, four of which are included in our sample: 70 Panopaea, 349 Dembowska, 429 Lotis, and 511 Davida. We confirm the prediction for three of them while for the asteroid 375 Ursula we found no trace of aqueous alteration, while they defined it as "wet?"

4. CONCLUSION

We carried out observations of 29 C class asteroids, searching for low-temperature minerals on the surfaces, and 70% of our sample showed the presence of hydrated silicated materials, thus supporting the existence of a mild aqueous alteration episode in the early Solar System. Our observations seem to indicate that "the aqueous alteration zone" may have less precise boundaries than those defined in the literature; moreover, we do not find evidence for a gap between 2.8 AU and 3.0 AU.

The region of aqueous alteration seems to mark the separation between the inner asteroid belt, dominated by a more evolved mineralogy, from the more distant asteroids, characterized by an unaltered mixture of low-temperature materials.

FIG. 2. Spectra of seven of the observed asteroids which show weaker features around 0.6–0.65, 0.7, and/or 0.8–0.9 μm. The spectra were fitted with a polynomial; a linear continuum has been removed.

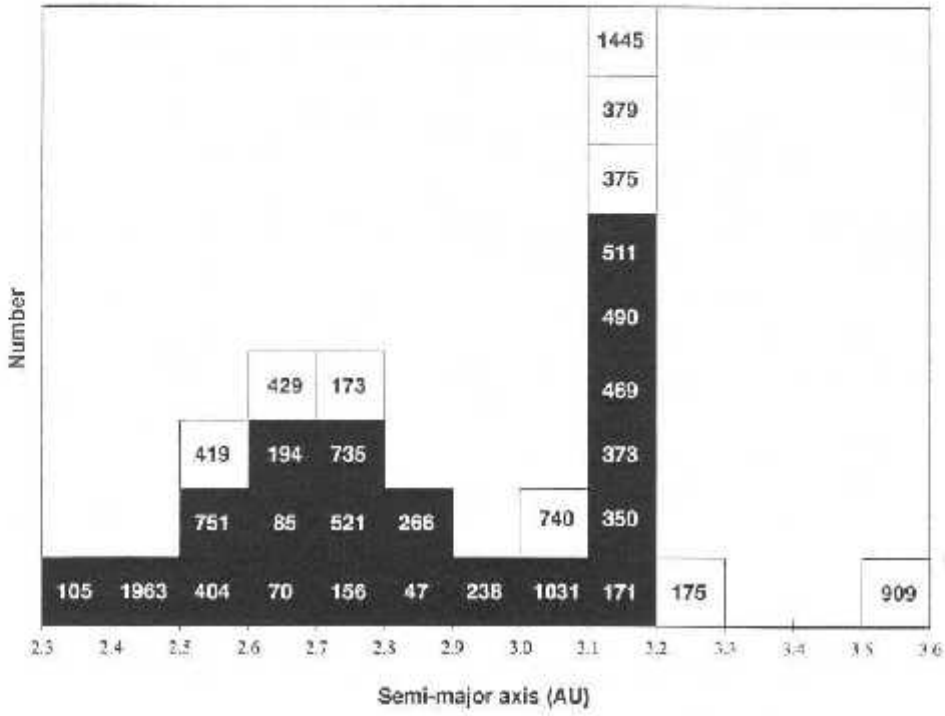

FIG. 3. Spatial distribution of the 29 observed asteroids. The objects which show trace of aqueous alterations are reported in the black cells.

APPENDIX

Relative Reflectivity for 29 Asteroids

The spectra are presented by increasing asteroid number. They are normalized around 0.55 μm in order of convention.

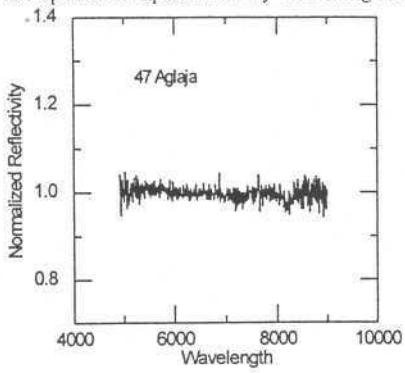

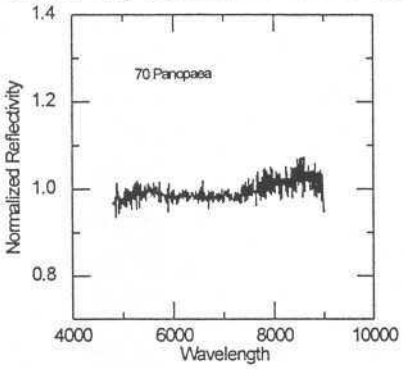

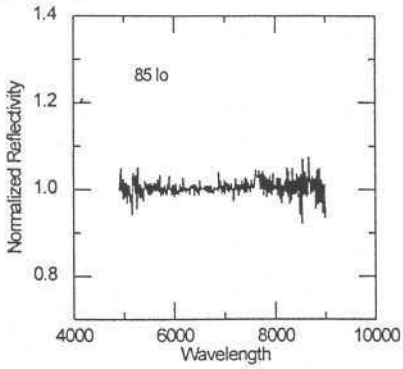

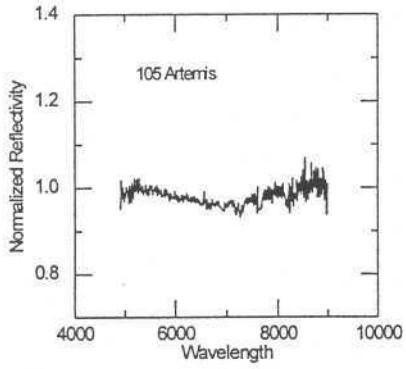

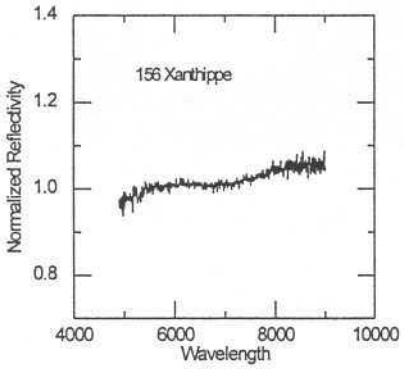

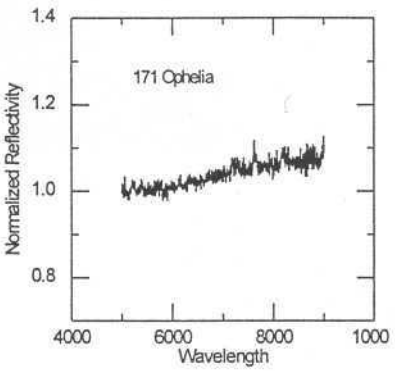

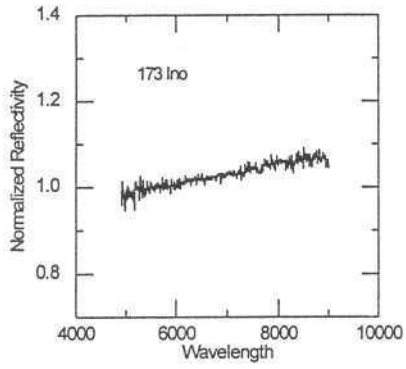

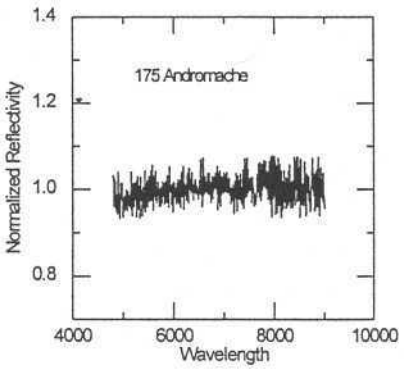

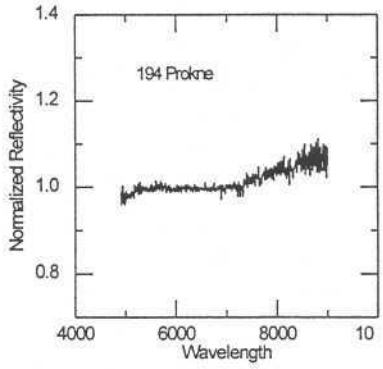

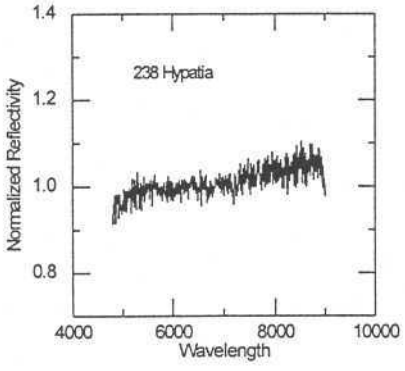

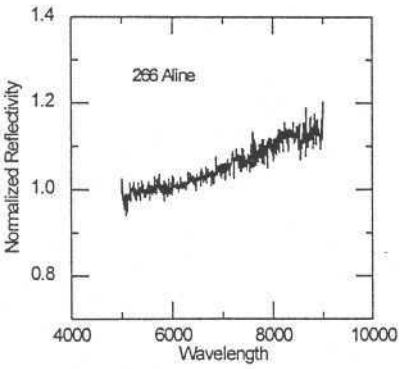

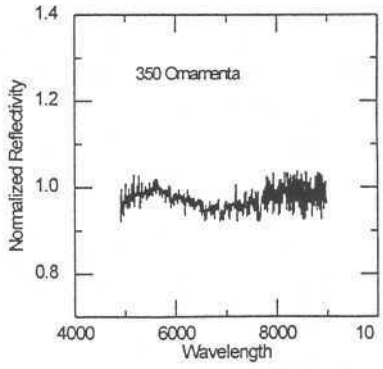

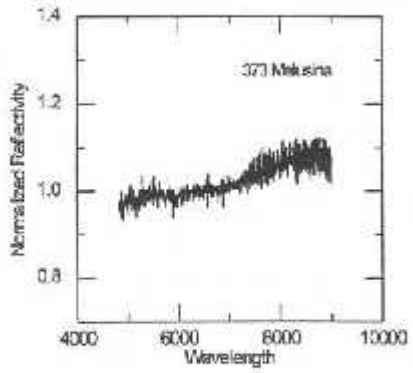
373 Melusina
Normalized Reflectivity
Wavelength

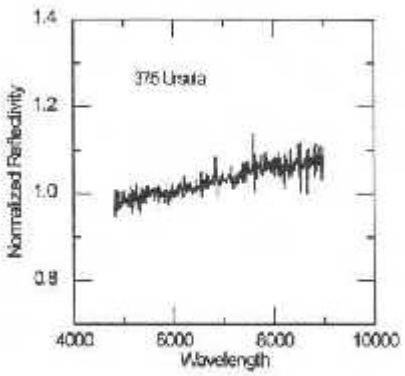
375 Ursula
Normalized Reflectivity
Wavelength

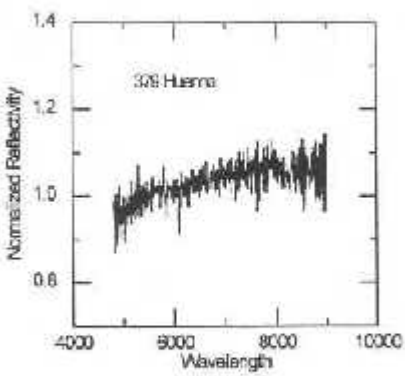
378 Huenna
Normalized Reflectivity
Wavelength

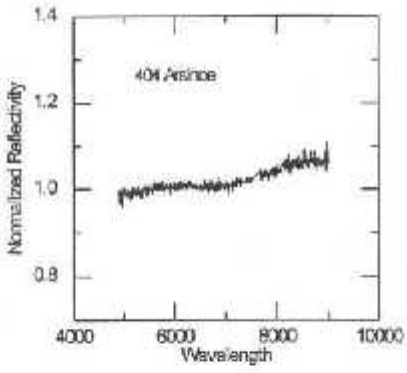
404 Arsinoe
Normalized Reflectivity
Wavelength

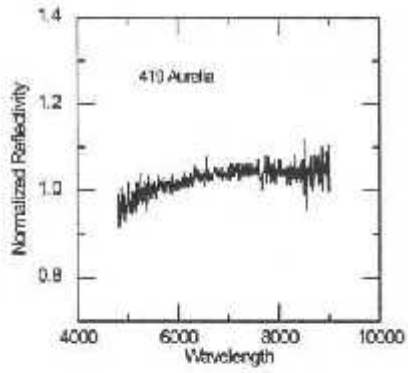
410 Aurelia
Normalized Reflectivity
Wavelength

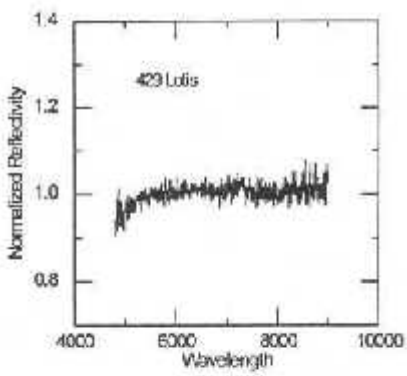
423 Lotis
Normalized Reflectivity
Wavelength

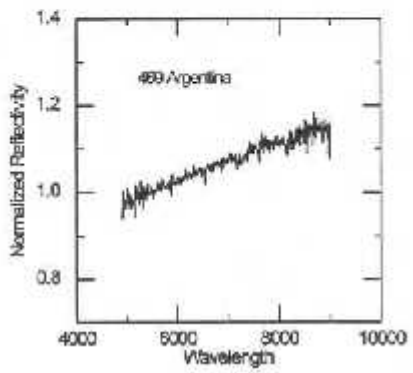
469 Argentina
Normalized Reflectivity
Wavelength

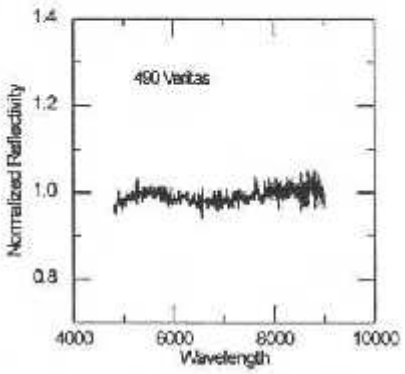
490 Veritas
Normalized Reflectivity
Wavelength

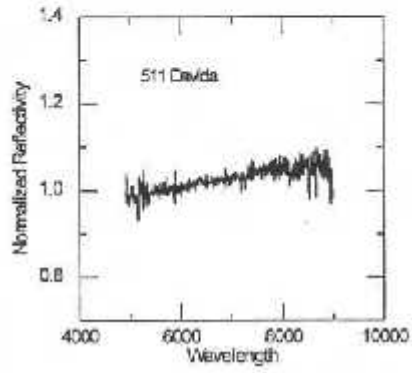
511 Davida
Normalized Reflectivity
Wavelength

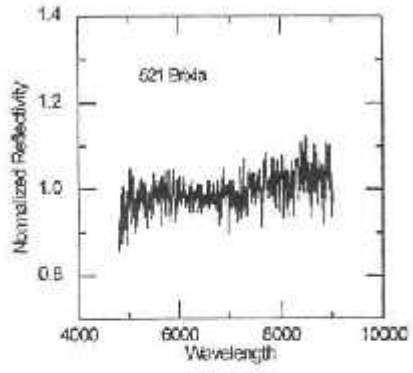
521 Brixia
Normalized Reflectivity
Wavelength

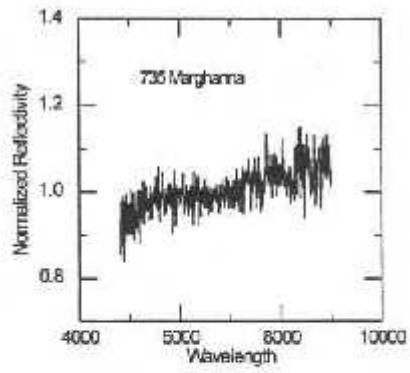
735 Marghanna
Normalized Reflectivity
Wavelength

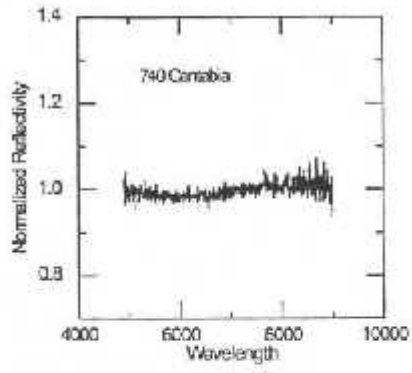
740 Cantabia
Normalized Reflectivity
Wavelength

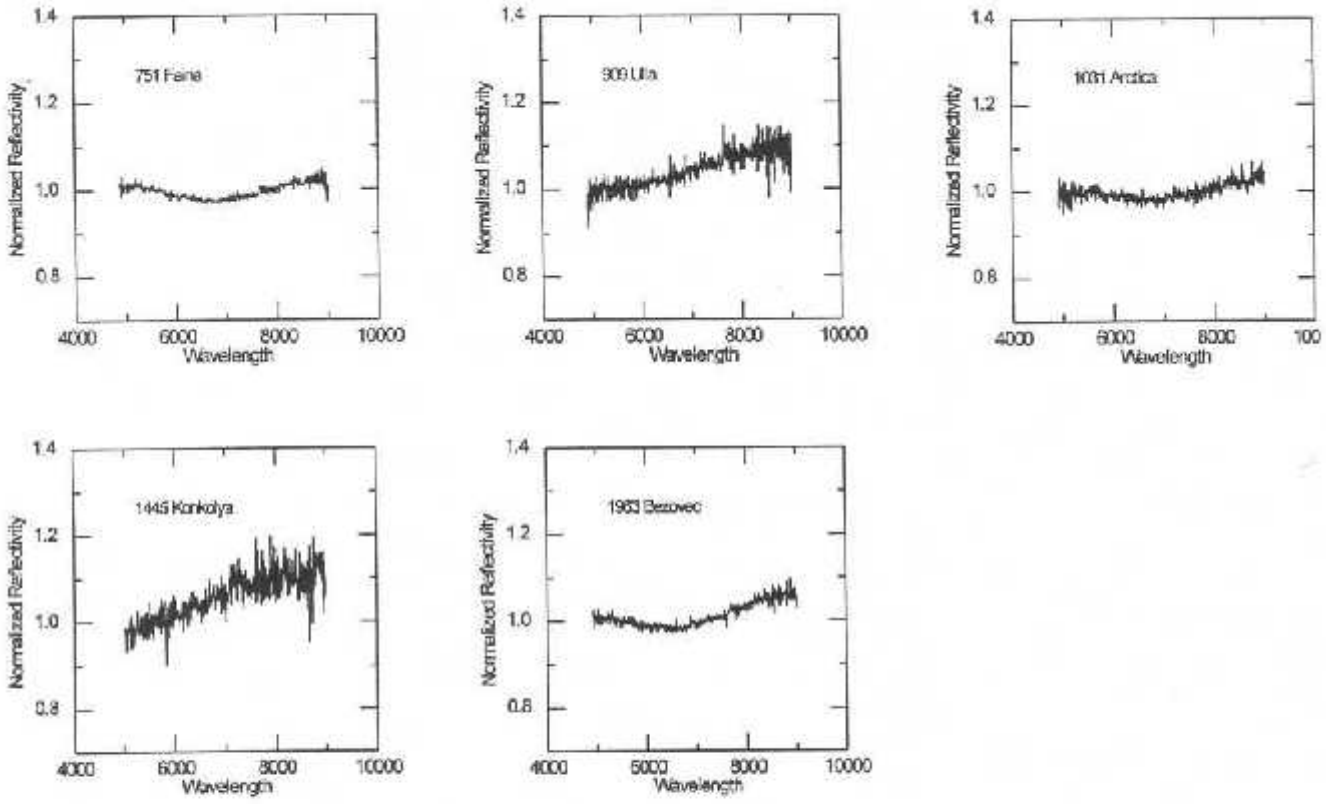

ACKNOWLEDGMENTS

We are very grateful to Toby Owen for helpful comments and discussions. We thank Lucy McFadden and Takahiro Hiroi for their constructive review of the paper. C. Angeli and M. Florczak acknowledge CNPq, which allowed them to have fellowships.

REFERENCES

Barucci, M. A., M. T. Capria, A. Coradini, and M. Fulchignoni 1987. Classification of asteroids using G-mode analysis. *Icarus* **72,** 304–324.

Barucci, M. A., M. Fulchignoni, and M. Lazzarin 1996. Water ice in primitive asteroids? *Planet. Space Sci.* **44,** 1047–1049.

Burns, R. G. 1993. *Mineralogical Applications of Crystal Field Theory.* Cambridge: Cambridge Univ. Press.

Chapman, C. R., D. Morrison, and B. Zellner 1975. Surface properties of asteroids: A synthesis of polarimetry, radiometry, and spectrophotometry. *Icarus* **25,** 104–130.

Gradie, J. C., C. R. Chapman, and E. F. Tedesco 1989. Distribution of taxonomic classes and the compositional structure of the asteroid belt. In *Asteroids II* (R. P. Binzel, T. Gehrels, and M. S. Matthews, Eds.), pp. 316–335. Univ. of Arizona Press, Tucson.

Hardorp, J. 1978. The Sun among the stars. *Astron. Astrophys.* **63,** 383–390.

Hiroi, T., and F. Vilas 1995. Characterization of absorption bands (0.6–0.9 μm) in reflectance spectra of primitive asteroids. *Lunar Planet. Sci.* **26,** 611–612.

Hiroi, T., C. M. Pieters, M. E. Zolensky, and M. E. Lipschutz 1993. Evidence of thermal metamorphism on the C, G, B, and F asteroids. *Science* **261,** 1016–1018.

Hiroi, T., M. E. Zolensky, C. M. Pieters, and M. E. Lipschutz 1996. Thermal metamorphism of the C, G, B and F asteroids seen from the 0.7 μm, 3 μm and UV absorption strength in comparison with carbonaceous meteorites. *Meteorit. Planet. Sci.* **31,** 321–327.

Jones, T. D., L. A. Lebofsky, J. S. Lewis, and M. S. Marley 1990. The composition and the origin of the C, P and D asteroids: Water as a tracer of thermal evolution in the outer belt. *Icarus* **88,** 172–192.

Lebofsky, L. A. 1980. Infrared reflectance spectra of asteroids: A search for water of hydration. *Astron. J.* **85,** 573–585.

Merényi, E., E. S. Howell, A. S. Rivkin, and L. A. Lebofsky 1997. Prediction of water in asteroids from spectral data shortward of 3 microns. *Icarus* **129,** 421–439.

Vilas, F. 1994. A cheaper, faster, better way to detect water of hydration in Solar System bodies. *Icarus* **111,** 456–467.

Vilas, F., and M. J. Gaffey 1989. Phyllosilicate absorption features in main-belt and outer-belt asteroid reflectance spectra. *Science* **246,** 790–792.

Vilas, F., and M. V. Sykes 1996. Are low albedo asteroids thermally metamorphosed? *Icarus* **124,** 483–489.

Vilas, F., S. M. Larson, E. C. Hatch, and K. S. Jarvis 1993. CCD reflectance spectra of selected asteroids. II. Low albedo asteroids spectra and data extraction techniques. *Icarus* **105,** 67–79.

Vilas, F., K. S. Jarvis, and M. J. Gaffey 1994. Iron alteration minerals in the visible and near infrared spectra of low albedo asteroids. *Icarus* **109,** 274–283.

3.3.2 - Objetos Próximos da Terra (NEA *)

A população de objetos próximos da órbita da Terra é constituída em geral por pequenos corpos, com tamanhos da ordem de poucos quilômetros ou menos. Objetos deste tamanho no cinturão principal não são acessíveis à observação, mas o podem ser na população dos NEA, já que estes podem alcançar distâncias de até 0,01–0,02 U.A. da Terra. Estes objetos não devem representar uma população original, pois suas órbitas são instáveis devido ao fato de cruzarem as dos planetas interiores. Provavelmente são fragmentos de colisões catastróficas ocorridas no cinturão principal, "transportados" até esta região.

Esta população é convencionalmente classificada em 3 grupos: Aten, Apollo e Amor (Shoemaker *et al.*, 1979). Os asteróides Aten possuem órbitas interiores à da Terra, com semi-eixo maior inferior a 1 U.A. e distância afélica superior ou igual a 0,983 U.A. (0,983 U.A. representa a distância periélica da Terra). Os Apollo são definidos como objetos que possuem semi-eixo maior superior a 1 U.A. e distância periélica menor ou igual a 1,017 U.A. (1,017 U.A. representa a distância afélica da Terra). Desta forma, os asteróides dos grupos de Aten e Apollo são cruzadores da órbita da Terra. O grupo Amor é definido pelos objetos que possuem semi-eixo maior superior a 1 U.A. e distância periélica entre 1,017 U.A. e 1,300 U.A.. Os objetos do grupo Amor não cruzam a órbita da Terra mas se aproximam dela.

Esta população possui uma grande diversidade em suas propriedades físicas, onde a maior parte dos tipos taxonômicos estão representados, tendo sido encontrado, inclusive, um asteróide do grupo Amor com albedo típico do tipo D (3552 Don Quixote). Cerca da metade destes objetos são classificados como do tipo S, enquanto que no cinturão principal os asteróides de baixo albedo (C e subtipos, B, F e G) predominam.

Várias observações espectroscópicas têm sido realizadas com o objetivo de relacionar estes objetos a algum tipo de meteorito. O asteróide 1862 Apollo tem propriedades espectrais muito próximas dos meteoritos condritos ordinários, sendo classificado por Bell

* *Near Earth Asteroids*

e co-autores (1989) como do tipo Q, classe proposta por eles para resolver o problema da origem destes meteoritos. Binzel e co-autores (1996) encontram 6 objetos desta população com espectros muito similares aos dos meteoritos condritos ordinários e 29 com propriedades espectrais intermediárias entre asteróides do tipo S e estes meteortos. Devido à distribuição ser contínua e não haver nenhuma distinção evidente entre os objetos similares aos condritos ordinários (possíveis candidatos aos objetos do tipo Q, segundo Bell e co-autores) e os outros com espectros do tipo S, os autores sugerem que os asteróides do tipo Q não seriam um grupo realmente distinto. Uma das explicações para a semelhança de alguns asteróides com meteoritos condritos ordinários seria a de que estes objetos seriam fragmentos mais jovens que não teriam sofrido ainda um processo de envelhecimento espacial de sua superfície. A distribuição dos espectros de forma contínua revelaria esta tendência de envelhecimento, também observada em objetos da família de Flora (ver seção 3.3.3).

Com o objetivo de melhor compreender a distribuição de composição dos asteróides próximos da Terra e a origem dos meteoritos condritos ordinários obtivemos espectros de 8 asteróides desta população num intervalo entre 0,5 e 1,0 μm, aproximadamente. O artigo a seguir descreve o trabalho realizado, cujos principais resultados podem ser resumidos em:

- foram encontrados quatro objetos com características similares aos condritos ordinários, um com espectro do tipo C e três do tipo S mas sem um meteorito análogo;
- sugerimos que a diferença de espectros entre os objetos do tipo S seja devida ao processo de envelhecimento espacial descrito acima;
- foi encontrada uma banda de absorção em 0,6 μm no espectro do asteróide 5836 1993 MF, típica de um processo de alteração aquosa, incomum nos asteróides do tipo S.

Astron. Astrophys. 327, 388–391 (1997)

ASTRONOMY AND ASTROPHYSICS

Compositional properties of Near-Earth Asteroids: spectroscopic comparison with Ordinary Chondrite Meteorites

M. Lazzarin[1], M. Di Martino[2], M.A. Barucci[3], A. Doressoundiram[3], and M. Florczak[3,4]

[1] Dip. di Astronomia, Vic. Osservatorio 5, I-35122 Padova, Italy (lazzarin@astrpd.pd.astro.it)
[2] Oss. Astronomico di Torino, I-10025 Pino Torinese, Italy (dimartino@to.astro.it)
[3] Obs. de Paris, F-92195 Meudon Principal Cedex, France (barucci@obspm.fr, Alain.Doressoundiram@obspm.fr)
[4] ON/CNPq, Dep. Astrofisica, 20921 Rio de Janeiro, Brazil (Florczak@obsn.on.br)

Received 7 March 1997 / Accepted 5 May 1997

Abstract. Some years ago we started a spectroscopic survey, in the visible region, of Earth-approaching asteroids to investigate their compositional nature in order to improve the comprehension of their origin. To date we have obtained low-resolution spectra, in the range 0.5-1.0 μm, of 1 Aten (3753 *1986 TO*), 4 Apollo (1864 *Daedalus*, 5786 *Talos*, *1989 JA*, 2063 *Bacchus*), and 3 Amor (3352 *McAuliffe*, 4954 *Eric*, 5836 *1993 MF*). Most of them show spectra similar to those of the S taxonomic class; Bacchus only has a spectrum which resembles those of more primitive objects (C-type).

It has not been possible to definitively distinguish to which S-subclass the observed objects belong because the spectra we obtained do not cover the necessary spectral range to make this investigation as described by Gaffey et al. (1993). Nevertheless four of the observed objects have visible spectra similar to those of ordinary chondrites meteorites suggesting a strong relation between the two classes of objects.

Moreover 5836 *1993 MF* shows an absorption feature near 6000 Å probably due to the presence of aqueous altered materials.

Key words: asteroids – meteroids

1. Introduction

Near-Earth Asteroids (NEA) represent one of the most peculiar classes of objects in the Solar System. Their orbits can approach or even intersect the terrestrial one. More than 360 NEAs have been discovered to date. The largest object of this population has a diameter of 38 km, two others are about 20 km in size, the remaining have diameters less than 10 km, and about 3/4 of them are smaller than 3 km. According to the more recent estimate (Rabinowitz et al., 1994; Muinonen et al., 1995), NEAs with diameter $\geq$1 km are about 2000, and at present we know the orbits of only about 7% of them.

The population of NEA is extremely heterogeneous in all the aspects of their physical properties. Available data show that shapes, rotation rates and albedos of NEAs are on the average practically the same as those of main-belt objects. However, among NEAs there are objects with unusual shapes (very elongated, dumb-bell like and possibly binary), with very complex non-principal axis rotation (*tumbling* asteroids) and with peculiar mineralogical compositions. Recent radar observations allow to assume that a substantial part of NEAs could be binary systems. In the NEA population all the taxonomic types have been identified, except the B and the P classes, even though the most numerous classes observed are S and C respectively.

The discovery of the very dark (albedo about 0.03) and reddish D-type Amor asteroid 3552 *Don Quixote* has been rather unexpected because most of the asteroids belonging to this class are located in the outermost parts of the main belt (Trojan and Hilda groups) and they represent the most primitive objects among asteroids. The variety of taxonomic classes discovered among NEAs indicates that this population is heterogeneous in origin and composition.

The importance to study NEAs is connected to several reasons:

a) the impacts by these objects are the principal cause of the craterization of the Earth and the Moon, at least in the last 3.8 Gyr (Wetherill and Shoemaker, 1982). The discovery of the majority of the possible "dangerous" objects and the knowledge of their physical properties are two of the main research lines to be followed in order to solve the problem of "asteroid hazard".

b) They could be the sources of chondritic and achondritic meteorites (Wetherill, 1976; Di Martino et al., 1995);

c) It is likely that a good number of these objects represent the final evolutionary state of comets, that is a devolatilized nucleus.

d) They could be potential sources of metals and other raw materials in the neighbourhood of the Earth space. At present we know two M-type asteroids (3554 *Amun* and 6178 *1986 DA*) and the results of radar observations leave no doubts about the

Send offprint requests to: Monica Lazzarin

metallic nature of them (Tedesco and Gradie, 1987; Ostro et al., 1991).

Anyway, one of the most interesting aspects in the study of NEA is to understand their origin. In fact, their dynamical lifetimes are shorter than the age of the Solar System. Moreover, owing to the constant craterization of the inner Solar System bodies from their formation, it is believed that the population of NEA is practically constant in number. So, it has to be continuously supplied by some sources and/or mechanisms which have been identified in: (i) the dynamical evolution of the fragments coming from catastrophic collisions in the main belt (Greenberg and Nolan, 1989), and in (ii) extinct or dormant comet nuclei (Weissmann et al., 1989; Binzel et al., 1992).

An example of the latest case is comet P/Encke, a low active comet on an Apollo-like orbit. On the other hand, some NEA have been discovered on cometary-like orbits as 2201 *Oljato* (McFadden et al., 1993, Lazzarin et al., 1996) or dynamically connected with meteor streams, that are believed to be cometary in origin (Asher et al., 1994).

The most striking evidence of this connection is the Apollo object 4015 *1979 VA*, discovered as an asteroid and then recognized as the non active comet Wilson-Harrington.

Another important aspect of NEAs is that they are very likely the principal sources for meteorites, in particular for ordinary chondrite (OC) meteorites. The OC are considered the remnants of the primitive solar nebula: they have been scarcely thermally processed during the evolutionary stages of the Solar System.

Binzel et al. (1996) have recently found a quite clear relationship between OC and some NEAs. If the idea that part of NEAs could be the parent bodies of OC is confirmed, it would help to understand the origin of part of these objects: they would have been injected into near-Earth orbits from the main-belt reservoir.

In order to try to answer to all these open questions we started a long term spectroscopic survey of NEAs, which preliminary results we present in this paper.

2. Observations and data reduction

The low-resolution spectra we present in this paper have been obtained during different observing runs between 1993 and 1996 (Table 1). The observations have been performed at the European Southern Observatory (ESO, La Silla, Chile) and at the Asiago Observatory (Italy). At La Silla we used the 1.5 m telescope equipped with a Boller & Chivens spectrograph and a type Ford CCD (2048×2048 pixels) detector. The grating used was a 225 gr/mm with a dispersion of 330 Å/mm in the first order. The CCD has a 15 μm square pixel, yielding a dispersion of 5 Å/pixel in the wavelength direction. The spectral range covered is about $0.5 < \lambda < 1$ μm with an instrumental FWHM of 10 Å.

At the Asiago Observatory we used the 1.82 m telescope equipped with a Boller & Chivens spectrograph and a Thomson CCD (430×600 pixels) as detector. The grating was a 150 gr/mm with a dispersion of 340 Å/mm in the first order. The CCD has 23 μm square pixels giving a dispersion of about 7.8 Å/pixel in the wavelength direction. The spectral coverage is about $0.5 < \lambda < 1$ μm with an instrumental FWHM of 15.6 Å.

The reduction of the spectra has been performed using standard procedures of data reduction using the softwares MIDAS, IRAF and IDL. In order to calibrate the observational data, bias, flat-field, calibration lamp, spectrophotometric standard star and solar analog (Hardorp, 1978) spectra were secured at different intervals throughout each night. After bias subtraction, flat-field correction, cosmic-rays removal, wavelength calibration, airmass correction, flux calibration, division by the solar analog spectrum, we obtained the reflectivity spectra of the objects. The standard stars and the solar analogs were observed at airmasses similar to those of the asteroids with differences less than 0.2 in each case. In Table 1 we report the circumstances of the observations.

3. Results

The reflectance spectra of the eight asteroids, normalized at 1 around 5500 Å, are shown in Fig. 1 to Fig. 3. The objects we observed are: 1 Aten (3753 *1986 TO*), 4 Apollo (1864 *Daedalus*, 5786 *Talos*, *1989 JA*, 2063 *Bacchus*), and 3 Amor (3352 *McAuliffe*, 4954 *Eric*, 5836 *1993 MF*).

For each object an indication of the diameter is given (Tholen, 1995). Some of the spectra show some shallow spurious features which are probably due to the division by the solar analog spectrum, that is a non perfect elimination of the solar features, or also to a non perfect cancellation of the atmospheric O_2 bands at 7612 Å and 6880 Å.

3753 *1986 TO*

This is the only Aten object we have observed and no spectral information was available before for this asteroid. The spectrum we obtained (Fig. 1) shows the typical trend of the objects belonging to the S-class, but it is different from the spectra of OC assemblages.

The estimated diameter of this asteroid is about 5 km and its rotational period $P_{syn.} = 18^h.14$ (Hoffmann et al., 1993).

4954 *Eric*

This rather large asteroid, with a diameter of about 12 km, has a rotational period of about 11 hours (Wisniewski et al., 1996). Barucci et al. (1994) obtained the near infrared spectrum of this object (1.0-2.5 μm) and the coupling with that obtained in the visible (Fig. 1) suggests the belonging of this object to the S taxonomical class. No similarity with ordinary chondrite spectra has been identified.

1989 JA

This Apollo asteroid has an estimated diameter of about 1.5 km. Also the spectrum of this object shows the typical S-type trend, but again different from the ordinary chondrite ones (Fig. 1).

Table 1. Observational characteristics of the NEAs.

Asteroid	Date [UT]	Observ.	Tel.	r [AU]	Δ [AU]	m_v	Solar Analog
1864 Daedalus	1994/04/17	ESO	1.50m	1.596	0.638	15.8	HD 44594
2063 Bacchus	1996/05/20	ESO	1.50m	1.279	0.374	16.3	HD144585
3352 McAuliffe	1994/04/18	ESO	1.50m	1.579	0.584	16.0	HD 44594
3753 1986 TO	1993/09/25	ESO	1.50m	1.341	0.578	15.5	Hyades 64
4954 Eric	1994/04/18	ESO	1.50m	2.100	1.396	16.0	HD 44594
5786 Talos	1996/10/16	ESO	1.50m	1.123	0.309	16.6	HD 28099
5836 1993 MF	1993/09/14	Asiago	1.82m	1.251	0.308	13.8	16 Cyg B
1989 JA	1996/10/17	ESO	1.50m	1.272	0.377	16.9	HD 28099

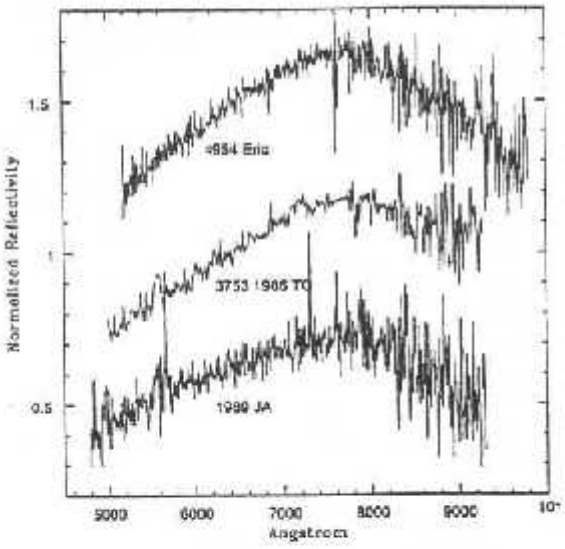

Fig. 1. Reflectance spectra of the near-Earth Asteroids *1989 JA*, 3753 *1986 TO*, 4954 *Eric*. The spectra have the typical trend of the S-types.

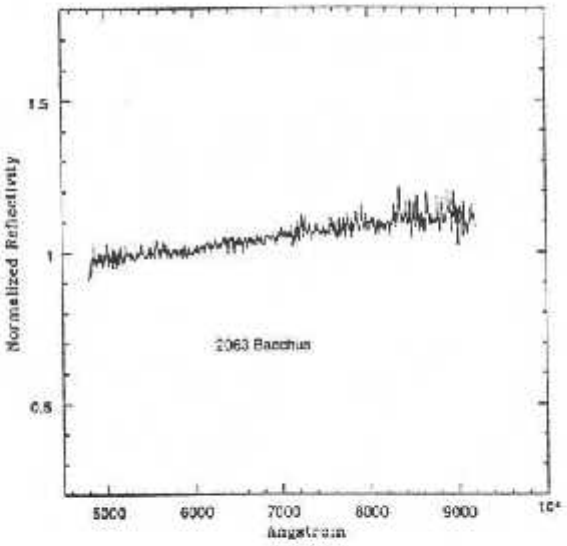

Fig. 2. Reflectance spectrum of the near-Earth object 2063 *Bacchus*.

2063 Bacchus

This Apollo object has an estimated diameter of about 2 km. It shows a spectrum (Fig. 2) different from all the other near-Earth objects here presented. It is redder than the solar spectrum and resembles that of the more primitive C-type asteroids. Its reflectance slope is 3.7±0.1 %/10^3 Å in the spectral range 5000÷7500 Å, which is consistent with the reflectance slopes of C-type objects more than with those of D-types (lower limit of the reflectance slopes of D objects is about 7%/10^3 Å).

1864 *Daedalus*

This Apollo asteroid has been classified as an SQ-type by Tholen (1989). Its rotational period, P_{syn} = 8.57 hours, has been determined by Gehrels et al. (1971) and this object shows a large amplitude (0.85 mag) of the lightcurve, which implies a very elongated shape. The estimated diameter is about 3 km. No previous spectral information is available on this asteroid and the spectrum we obtained (Fig. 3) shows a trend similar to that of S-type asteroids. Anyway, in this case, as reported in Fig. 3, there is a good match between the spectrum obtained and the laboratory spectra of L4-type OC.

5786 *Talos*

This Apollo asteroid has an estimated diameter of 1.7 km. Also the optical spectrum of Talos is similar to that of OC, in particular to H6-type (Fig. 3).

3352 *McAuliffe*

No physical information was available on this Amor asteroid, except the diameter, that has been estimated in about 3 km. The S-type spectrum obtained (Fig. 3) is very similar to that of H4-type OC.

5836 *1993 MF*

This object, with an estimated diameter of about 6 km, has a rotational period of 4.959 hours (Mottola et al., 1995 and Wisniewski et al. 1996). The spectrum of this asteroid that we obtained (Fig. 3) shows an absorption feature centered around

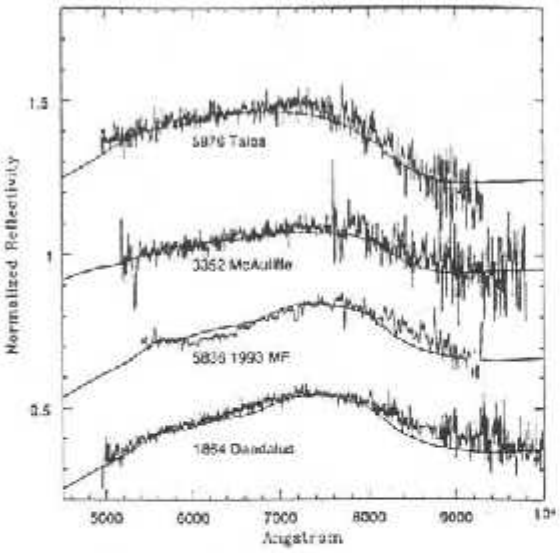

Fig. 3. Spectra of near-Earth asteroids compared with laboratory spectra of ordinary chondrites assemblages. Averaged L4-subtype OC spectrum is superimposed to 1864 *Daedalus* and 5836 *1993 MF*; averaged H4-subtype OC spectrum is compared with 3352 *McAuliffe* and averaged H6-subtype OC spectrum is superimposed to the spectrum of 5876 *Talos*.

6000 Å which is suggestive of the presence of aqueous altered materials and found in some C and S asteroids also by Vilas et al. (1992, 1994) and Hiroi et al. (1996). This feature is even more evident when we compare the spectrum of 1993 MF with that of L4-type OC (Fig. 3): there is a good match between the two except around 6000 Å where there is the absorption band.

4. Discussion and conclusion

A better investigation of the spectra obtained and a consequent clearer classification of the objects here presented would require near-infrared data. In fact, this could allow a more detailed comparison with the spectra of OC and also a comparison with the S-subclasses as designed by Gaffey et al. (1993). Nevertheless, the results obtained are suggestive of some conclusions.

Among the eight observed objects, only one, 1864 *Daedalus*, had been previously classified as an SQ-type and we confirm the belonging to the S class. All the others show the typical trend of S-type objects, except 2063 *Bacchus* which spectrum has the typical behaviour of C-type objects. Four of the observed objects (1864 *Daedalus*, 5836 *1993 MF*, 3352 *McAuliffe* and 5876 *Talos*) show a spectrum that, within the errors, match quite consistently the laboratory spectra of OC. So these objects are potential parent bodies for these meteorites and this could suggest: a main-belt origin and a surface formed by undifferentiated mineral assemblages. The differences between the four objects similar to the OC and the other three typical S type asteroids could be due to space weathering effects: different ages of the objects are probably responsible of different surface reflectance characteristics (Chapman, 1996). The asteroids which composition is closer to OC would be those with "younger" surfaces (Binzel et al. 1996).

The asteroid 5836 *1993 MF*, besides its similarity to OC assemblages, shows also an absorption band centered around 6000 Å suggestive of the presence of aqueous altered materials.

References

Asher, D.J., Clube, S.V.M., Napier, W.M., and D.I. Steel, 1994, Vistas in Astronomy 38, 1
Barucci, M.A., Lazzarin, M., Owen, T., Barbieri, C., and M. Fulchignoni, 1994, Icarus 110, 287
Binzel, R.P., Xu, S., Bus, S.J., and E. Bowell, 1992, Science 257, 779
Binzel, R.P., Bus, S.J., Burbine, T.H., and J.M. Sunshine, 1996, Science 273, 946
Chapman, C.R., 1996, Meteoritics and Planetary Science 31, 699
Di Martino, M., Manara, A., and F. Migliorini, 1995, A & A 302, 609
Dunlap, J.L., 1974, AJ 79, 324
Gaffey, M.J., Bell, J.F., Brown, R.H., Piatek, J.L., Reed, K.L., and D.A Chaky, 1993, Icarus 106, 573
Gehrels, T., Roemer, E., and B.G. Marsden, 1971, ApJ 76, 607
Greenberg, R., and M.C. Nolan, 1989, in Asteroids II, eds. R.P. Binzel, T. Gehrels, and M.S. Matthews, Univ. of Arizona Press, Tucson, p.778
Hardorp, J., 1978, A & A 63, 383
Hiroi, T., Vilas, F., Sushine, J.M., 1996, Icarus 119, 202
Hoffmann, M., Rebahn, H., Neukum, G., and E.H. Geyer, 1993, Acta Astronomica 43, 61
Lazzarin, M., Barucci, M.A., and Doressoundiram, A., 1996, Icarus 122, 122
McFadden, L.A., Cochran, A.L., Barker, E.S., Cruikshank, D.P., and A.W.K. Hartmann, 1993, Journ. Geophys. Res. 98, 3031
Mottola, S., De Angelis, G., Di Martino, M., Erikson, A., Hahn, G., and G. Neukum, 1995, Icarus 117, 62
Muinonen, K.,Bowell, E., and K. Lumme, 1995, A & A 293, 948
Ostro, S.J., Campbell, D.B., and J.F. Chandler, 1991, Science 252, 1399
Rabinowitz, D.L., Bowell, E., Shoemaker, E., and K. Muinonen, 1994, in: Hazard Due to Comets and Asteroids, ed. T. Gehrels, Univ. of Arizona Press, Tucson, p. 285
Tedesco E. F., and J. Gradie, 1987, AJ 93, 738
Tholen, D. J., 1989, in Asteroids II, eds. R.P. Binzel, T. Gehrels, and M.S. Matthews, Univ. of Arizona Press, Tucson, p. 1139
Tholen, D.J. 1995, Ephemerides program EPHEM, (vers. 1.0) Celstech
Vilas, F., and L.A. McFadden, 1992, Icarus 100, 85
Vilas, F., Jarvis, K.S., and M.J. Gaffey, 1994, Icarus 109, 274
Weissman, P.R., A'Hearn, M.F., McFadden, L.A., and H. Rickman, 1989, in Asteroids II, eds. R.P. Binzel, T. Gehrels, and M.S. Matthews, Univ. of Arizona Press, Tucson, p. 880
Wetherill, G.W., 1976, Geochim. Cosmochim. Acta 40, 1297
Wetherill, G.W., and E.M. Shoemaker, 1982, in Geological Implications of Impacts of Large Asteroids and Comets on the Earth, eds. L.T. Silver and P.H. Silver, Geological Soc. of America, Boulder, p.1
Wisniewski, W.Z., Michalowski, T.M., Harris A.W. and McMillan R.S., 1997, Icarus 126, 395

This article was processed by the author using Springer-Verlag LaTeX A&A style file *L-AA* version 3.

3.3.3 - Famílias de Asteróides

Do ponto de vista dinâmico, as famílias são agrupamentos de asteróides cujos elementos próprios a', e', i' (semi-eixo maior, excentricidade e inclinação, respectivamente) são muito similares entre si. O primeiro a reconhecer estes agrupamentos foi Hirayama em 1918, que os denominou "famílias" sugerindo uma origem comum destes objetos. Hirayama (1918) identificou inicialmente as famílias de Eos, Themis e Koronis (fig. 3.8). Em 1922, e em artigos posteriores, ele identificou as famílias de Maria, Phocaea, Flora e Pallas (Kozai, 1994).

Atualmente todos os modelos de formação de famílias propõem que sua origem se deve a colisões catastróficas de um ou mais corpos. Assim, o estudo das famílias de asteróides pode nos dar a oportunidade de observar a estrutura interna de corpos de vários quilômetros de diâmetro. Se o corpo original tiver sido de composição homogênea, encontraremos características espectrais similares em todos os seus membros, salvo quando os objetos oriundos desta colisão sofreram um processo físico-químico de alteração de sua composição superficial, ou "envelhecimento espacial". Entretanto, se o corpo original era diferenciado poderemos encontrar características espectroscópicas diferentes entre seus membros, dependendo de que parte deste corpo originou cada fragmento. Como exemplo, temos que um asteróide do tipo M poderia ser parte de um núcleo metálico, enquanto um do tipo V poderia ser proveniente de uma crosta basáltica.

O estudo das famílias pode também nos dar informações sobre a origem dos meteoritos pois, como resultado do impacto da colisão que formaria uma família, teríamos a injeção de fragmentos em regiões instáveis, como em ressonâncias com Júpiter ou ressonâncias seculares, e estes seriam lançados em regiões internas do Sistema Solar. Por exemplo, a existência de meteoritos eucrites e alguns NEO com características basálticas, estaria ligada à família de Vesta (Binzel e Xu, 1993).

Podemos também usar as famílias de asteróides como um teste de modelos de colisões catastróficas de grandes dimensões, já que os experimentos em laboratório são 10^6 vezes menores. Da mesma forma, podemos estudar a evolução colisional por que passou

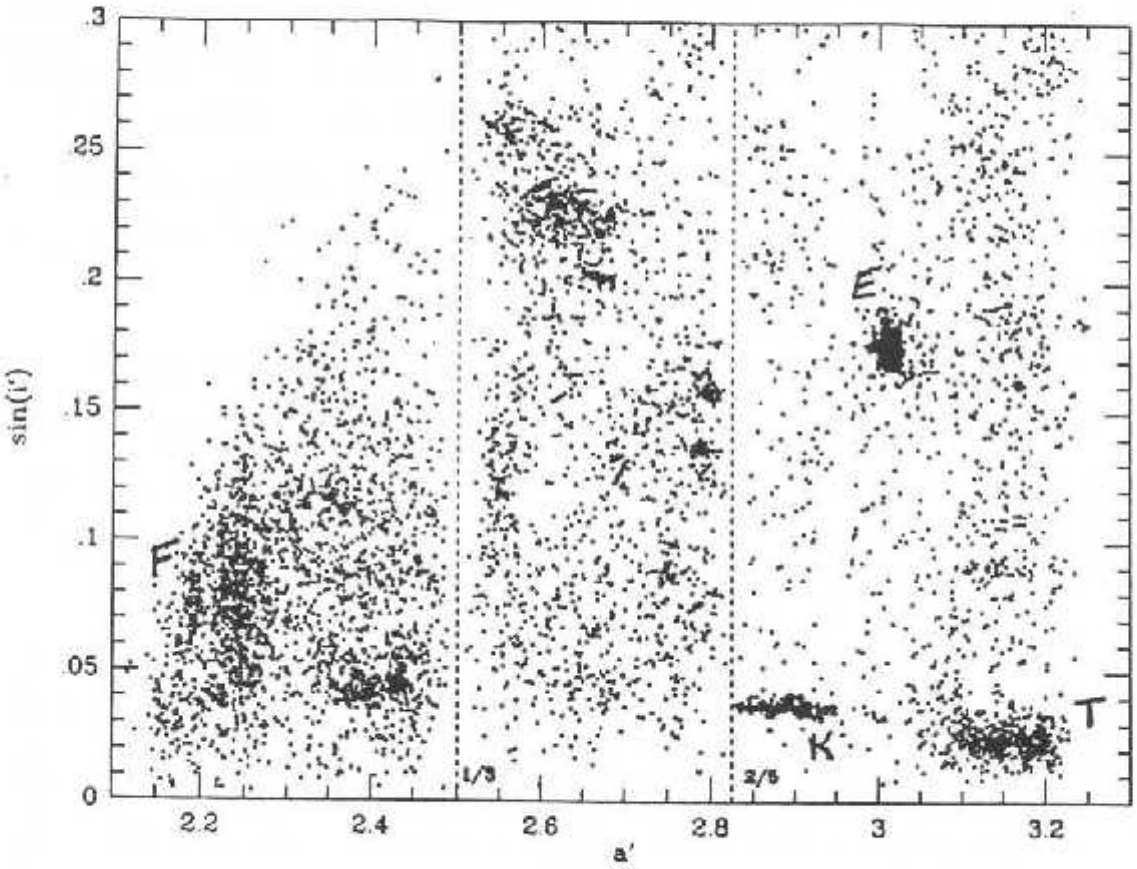

Figura (3.8) *Distribuição de asteróides em relação ao semi-eixo maior próprio e ao seno da inclinação própria (Zappalà et. al, 1994). Os símbolos E, K, T e F se referem às famílias de Eos, Koronis, Themis e Flora, respectivamente.*

o cinturão desde a sua formação, já que os modelos de evolução colisional para o cinturão não devem diferir muito dos que descrevem a evolução em uma família.

Os elementos osculadores dos asteróides variam com o tempo devido a perturbações

planetárias. Desta forma, estes elementos não são apropriados para a identificação de famílias e os elementos próprios são então usados para este propósito. Estes elementos são os parâmetros orbitais dos quais foram retirados os efeitos devidos às perturbações planetárias, e são obtidos através de sofisticadas técnicas de médias (Knežević e Milani, 1994).

Duas técnicas estatísticas diferentes têm sido usadas para a identificação de famílias: *hierarchical clustering* (Zappalà *et al.*, 1995, 1994 e 1990) e *wavelet analysis* (Bendjoya, 1993). Os resultados mostram-se de bom acordo, usando as duas técnicas (Zappalà *et al.*, 1995), quando aplicados a 12.487 asteróides com os elementos próprios calculados por Milani e Knežević (1994).

A fim de caracterizar do ponto de vista mineralógico algumas famílias de asteróides realizamos estudos espectroscópicos em membros das famílias de Eos, Flora e Themis, as quais podem ser vistos na figura 3.8. Os resultados estão descritos nas próximas seções.

a) Família de Eos

A família de Eos foi uma das primeiras a serem identificadas e é uma das mais numerosas, contando com mais de 450 membros segundo o trabalho de Zappalà e co-autores (1995). O asteróide 221 Eos é o maior de seus membros com 110 km de diâmetro. Os objetos desta família possuem um semi-eixo maior entre 2,96 e 3,10 U.A.. A ressonância 9/4 (a $\approx$ 3,03 U.A.) separa a família entre uma região densamente e outra fracamente povoada.

Embora seja uma família bem identificada, sua origem ainda não é explicada. Os modelos colisionais para esta família têm tido dificuldades em explicar a fraca dispersão em semi-eixo maior em relação as dispersões em excentricidade e inclinação (Marzari *et al.*, 1995). As idades sugeridas para esta família variam desde 100 milhões de anos (Morbidelli *et al.*, 1995) até a idade do Sistema Solar (Binzel, 1988).

Nas taxonomias de Tholen e de Barucci a maior parte dos objetos desta família que possuem classificação são do tipo S. Entretanto Bell (1989), analisando os espectros de alguns membros, encontrou diferenças com os espectros típicos dos S no infravermelho

próximo, se aproximando mais dos espectros do tipo C. Além dos espectros, os albedos também sugerem uma classe diferente, que Bell denominou de K. Também encontrou semelhanças destes espectros com os dos meteoritos condritos CO e CV. Mais recentemente, Xu e co-autores (1995a) observaram uma ligeira heterogeneidade nos espectros de 6 membros desta família.

A fim de analisar e melhor entender a distribuição de composição dos objetos da família de Eos observamos 45 membros, representando cerca de 10% do total. A seguir descreveremos alguns dos resultados obtidos, os quais são detalhados no artigo apresentado na próxima seção. As tabelas e figuras citadas nesta seção são referentes ao artigo.

Obtivemos espectros no intervalo espectral entre 4800 e 9200 $\AA$. Nossos resultados mostram um comportamento espectral comum aos asteróides desta família, exceto para 1910 Mikkailov e 4455 Ruriko (discutiremos mais tarde estes dois objetos). A figura 1 mostra um ajuste polinomial de todos os espectros normalizados em 5500 $\AA$. Encontramos um gradiente de refletividade *, no intervalo espectral de 5500 a 7500 $\AA$, de 6,3 $\%/10^3$ $\AA$ a 15,3 $\%/10^3$ $\AA$ (com exceção dos dois asteróides citados acima). Os máximos dos espectros estão situados entre 8000 a 8500 $\AA$. Não encontramos nenhuma relação entre a distribuição espectral e o ângulo de fase, análoga solar, albedo ou diâmetro.

Apesar de ser considerado que os asteróides do tipo K seriam indistinguíveis dos do tipo S em nosso intervalo espectral, detectamos uma significativa diferença na localização do máximo dos espectros quando comparamos nossa amostra de Eos com a de asteróides do tipo S na vizinhança desta família. O máximo dos espectros destes objetos está localizado em torno de 7500 $\AA$ (fig. 2), valor bem inferior ao dos objetos de Eos, 8388 $\AA$. Este pode ser um parâmetro importante para detectar um objeto da família de Eos que tenha escapado de sua localização inicial. De fato, Zappalà e co-autores (1996) observaram alguns membros da família de Eos dentro da ressonância 9/4 calculando que estes estão a ponto de ser ejetados da região. Estes objetos foram chamados de "fugitivos de Eos".

---

* *Gradiente de refletividade é o coeficiente angular da reta em ajuste linear do espectro num determinado intervalo de comprimento de onda.*

Os objetos 1910 Mikkailov e 4455 Ruriko possuem espectros do tipo C. Sugerimos que este objetos seriam de fundo, ou seja, asteróides que já se encontravam na região de Eos na época da colisão e que lá permaneceram sem serem membros da família (fig. 3).

Para uma análise mais completa da mineralogia destes asteróides seria necessário identificar a profundidade da banda de 1 μm o que não é possível devido à região analisada. Mas alguns parâmetros de nossos espectros podem ser extraídos, como a posição do máximo (que se revelou peculiar para os membros de Eos), o gradiente de refletividade entre 5000 e 7500 $\AA$ e 8000 e 8500 $\AA$ (chamaremos de gradiente de refletividade A e B) e um valor de profundidade aparente medido como a razão da intensidade em 7500 e em 9000 $\AA$. Todos estes valores estão listados na tabela 2. Lembramos que na hipótese de alteração espacial da superfície de um asteróide o gradiente de refletividade A estaria relacionado à profundidade aparente da banda, o que não ocorre no caso em questão (ver figura 4).

Três hipóteses podem explicar a diversidade observada na distribuição espectral da família de Eos:

1- o asteróide original de Eos era parcialmente diferenciado e os fragmentos oriundos da colisão que gerou esta família vieram de partes diferentes do corpo original;

2- o corpo original da família era homogêneo, mas sofreu um processo de alteração espacial de sua superfície, sendo que os fragmentos podem ter vindo da superfície alterada quimicamente ou do interior, com a composição preservada;

3- o corpo original era homogêneo gerando fragmentos também homogêneos, mas as superfícies foram alteradas quimicamente com o tempo. Colisões secundárias em alguns dos membros revelariam em parte ou totalmente a composição interna, assim os objetos cujos espectros situam-se na parte inferior da distribuição seriam mais "jovens" (composição original) e os da parte superior da distribuição seriam mais "velhos" (composição mais alterada quimicamente).

A primeira hipótese é pouco provável pois implicaria na existência de duas populações bem distintas na família de Eos, o que não é verificado já que a distribuição espectral é contínua (fig. 1).

Na análise dos parâmetros espectrais dos objetos desta família não encontramos qualquer relação entre eles, exceto para um grupo de apenas 5 objetos (fig 5), onde o gradiente de refletividade A e a profundidade aparente estão bem correlacionados. Desta forma, não podemos descartar totalmente a segunda hipótese, concluindo que o corpo original da família de Eos deve ter sido parcialmente diferenciado e que um processo de alteração espacial está agindo sobre alguns membros da família.

Analisando os espectros de meteoritos obtidos por Gaffey (1976) encontramos três, do tipo CO e CV (fig. 6), que se ajustam à parte inferior de nossa distribuição, como previsto para os asteróides do tipo K. Encontramos também um meteorito mesosiderite que se ajusta à nossa distribuição, mas como este meteorito exige uma temperatura de formação muito mais alta do que os condritos CO e CV, não pode ser representativo dos membros desta família.

ICARUS 131, 15–31 (1998)
ARTICLE NO. IS975857

Eos Family: A Spectroscopic Study[1]

A. Doressoundiram and M. A. Barucci

Observatoire de Paris, 92195 Meudon Principal Cedex, France
E-mail: alaind@mesioq.obspm.fr

M. Fulchignoni

Université Paris VII

and

M. Florczak

Observatoire de Paris, 92195 Meudon Principal Cedex, France; Dep. Astrofísica, ON/CNPq, 20921 Rio de Janeiro, Brazil; and Dep. Física, CEFET, 80000 Curitiba, Brazil

Received February 24, 1997; revised August 20, 1997

The Eos family detected by Hirayama in 1918 has been always considered to be compositionally homogeneous. To investigate the composition and the homogeneity of the members of this family, we started a spectroscopic survey at the European Southern Observatory (ESO) with wavelength coverage ranging from 4800 to 9200 Å. We observed 45 Eos asteroid members, which constitutes the first large survey of this family. Our results reveal the Eos objects have spectral signature characterizing the whole family: a maximum at $\lambda \sim 8000$–8500 Å and a reflectivity gradient spanning a continuous range. Only two of the 45 investigated objects seem to be interlopers. While the lower range of this spectral distribution has been easily connected with CO–CV chondrites, we have found no satisfactory meteorite counterpart to the upper range. We have interpreted the spread out of Eos spectra to be the results of compositional variation among the Eos members, implying that the Eos parent body was partially differentiated. Moreover, a space weathering effect has been proven to be present, but with a minor role played in the diversity of Eos family, the major role being the compositional variation.

Key Words: asteroids composition; spectroscopy; meteorites.

1. INTRODUCTION

Near the beginning of the century, Hirayama (1918) was the first to detect statistically significant clusterings of asteroid orbits, called families, because he believed that the members within each group were related by a common origin. He speculated that families originated from the self-disruption of asteroids in a manner that perhaps was similar to the spontaneous disruption of cometary nuclei. Kuiper (1950) rejected this theory because of the lack of a suitable mechanism and proposed that the dominating process acting in the asteroid belt was mutual collisions. The Hirayama families were suggested to be the results of the collisional disruption of large parent bodies. The essential role played by catastrophic events in determining many of the most important physical properties of asteroids is widely recognized and it is now well accepted that asteroid families are the remnants of the energetic inter-asteroid collisions. Numerous studies have shown the importance of collisional processes on the evolution of the asteroid belt. The dynamical family memberships have been determined with high reliability in recent years, thanks to the development of refined perturbation theories for the long-term evolution of asteroid orbits (Milani and Knežević 1990, 1992, 1994, Knezevic and Milani 1994). Several authors with various techniques tried to reanalyze the asteroid population to better define families (Bendjoya *et al.* 1991, Lindblad 1994, Zappala *et al.* 1990, 1995).

The Eos family was one of the first four families with Koronis, Themis, and Maria, discovered by Hirayama. They were later confirmed by Carusi and Valsecchi (1982). Eos is also the third most populous family after Koronis and Themis. According to the latest results of Zappala *et al.* (1995) who applied two different methods of clustering, the numbers of recognized members is now more than 450.

[1] Based on observations carried out at the European Southern Observatory (ESO) of La Silla, Chile.

0019-1035/98 $25.00

The Eos family is the result of a total breakup of a parent body where 221 EOS (110-km-diameter) is the largest fragment. The Eos family members have their proper semimajor axis spanning from about 2.96 to 3.10 AU, where the 9/4 resonance ($a \approx 3.03$ AU) abruptly cut the distribution of asteroids into a high density part and a low density part (Morbidelli *et al.* 1995, Fig. 8). According to Morbidelli *et al.* (1995), this resonance is responsible for the depletion of about 50 to 75% of the original members. Binzel (1988) found that the rotation rates of Eos family members are significantly faster than others, estimating a modeled age of the Eos family comparable to that of the Solar System, 4.6 billion years. However, Morbidelli *et al.* (1995) suggested an age of 100 Myr, but they were not certain if this was the age of the whole Eos family or the age of a secondary breakup event. Also, Marzari *et al.* (1995) tried to estimate the family age by means of a collisional evolution model. However, they found some difficulties in explaining the very low dispersion of Eos family in semimajor axis, compared to the dispersion in eccentricity and inclination. Even if this family has been early identified, its origin remains unexplained. In fact, more generally, our poor understanding of the values of breakup and collisional evolution parameters lead to the present uncertainties. Collisional experiments as well as large survey are necessary to constrain the model parameters and lead to more precise estimates of the asteroid family ages.

Dynamically well identified, Eos family's members were also long recognized to be spectroscopically well separated from the background. However, on the other hand, the classification of Eos asteroids has often posed a difficult problem. Starting in 1977, Gradie and Zellner, in one of the first asteroid classifications based on the UBV colors, classified the Eos objects between C, S, and U. Gradie (1978) assumed this spread in albedos and colors to be the effect of compositional differences among family members. A recent similar spread in JHK colors for the Eos family was shown by Veeder *et al.* (1995). Tholen, in 1984, as well as Zellner *et al.* (1985) put almost all the Eos family objects into the S class. However, according to Gaffey *et al.* (1993), this does not constitute a proof of homogeneity. The S class is the most spectrally diverse asteroid taxonomic type, with a range of different mineralogies and meteoritic analogs. Barucci *et al.* (1987) also classified 15 of 16 Eos asteroid members into the same S class and mainly into the S0 subdivision (13 S0, 1 S1, 1S3). Finally, to characterize properly the uniqueness of the Eos family properties, Bell (1989) proposed a new asteroid type called K. This new suggestion was based on the first IR spectra of four members of the Eos family (Bell *et al.* 1987) that differ from S-type spectra and show similarities with CO and CV chondrites. Tedesco *et al.* (1989) also defined a K class, but did not definitely state whether the Ks are end members of the Ss or are slightly separated. More recently, Xu *et al.* (1995) on the base of the SMASS survey, have shown a modest degree of heterogeneity within their sample of six Eos family asteroids.

The data from previous work summarized above appear to favor a heterogeneous parent body. To understand better the composition of the Eos family, we observed a large sample of objects to have homogeneous data and to reduce selection effects. We obtained reflectance spectra of 45 Eos asteroids (with diameter range between 15 and 50 km), which constitutes more than 10% of the whole numbered population. In Section 2 we present the observational circumstances and the reduction techniques used. The general results are given in Section 3 and discussed in Section 4. A comparison of our objects with meteorites is done in Section 5 and finally, Section 6 concludes this study.

2. OBSERVATIONS AND DATA REDUCTION

The observations were performed at the European Southern Observatory at La Silla (Chile) using the 1.5-m telescope with a Boller & Chivens spectrograph and Loral CCD (2048 × 2048 pixels). We used the 225 g/mm grating with a dispersion of 330 Å/mm in the first order. The CCD has square 15-μm pixels, giving a dispersion of about 5 Å/pixel in the wavelength direction. The spectral range is about $4800 < \lambda < 9200$ Å with a FWHM of 10 Å. The spectra were taken through a 2- to 8-arcsec slit (depending on the sky conditions and the airmass value during the observations) oriented in the east–west direction. Particular care has been taken on the choice of the slit's width to mitigate the consequences of atmospheric differential refraction (Filipenko 1982). This problem, important in spectroscopy, is critical in our case. Indeed, the possible loss of light at both ends of the spectrum could lead to erroneous classification of asteroid type and false computation of spectral slope. The objects were observed near the meridian, with airmass lower than 1.2. We observed the asteroids during three observing runs in March 25–27, May 19–22, and October 17, 1996. One more asteroid, 3328 1985 QD1, was obtained in a previous observation, as possible alternative candidate to the Rosetta mission (Barucci *et al.* 1997). The weather conditions were good during all the observational time.

Particular care was taken to ensure proper calibration of the asteroid spectra. Many bias images were obtained each night to monitor the readout noise of the CCD, as well as flat field images to get the pixel to pixel variation in sensitivity. In fact, to better minimize this effect, we were cautious to place each spectrum along the same CCD columns. Wavelength calibration frames were performed regularly during the night with light from a helium–argon lamp. The production of reflectance spectra from the wavelength calibrated spectra is achieved through the division

TABLE I

Observational Circumstances as Date of Observations, Solar Phase Angle (α), Distances to the Sun (r) and the Earth (Δ), Visual Magnitude (m), Solar Analog, and Slitwidth Are Listed for the Eos Observed Asteroids

Asteroids	date	α (°)	r (A.U)	Δ (A.U)	m_v	Solar analog	Slit width
450 Brigitta	26/03/96	2.5	3.320	2.330	15.0	HD76151	2"
513 Centesima	21/05/96	4.5	3.248	2.259	14.5	HD144585	8"
633 Zelima	22/05/96	15.0	3.098	2.397	14.9	HD144585	8"
669 Kypria	21/05/96	18.6	2.852	2.298	15.3	HD144585	8"
766 Moguntia	20/05/96	16.0	3.257	2.666	15.7	HD144585	8"
1112 Polonia	20/05/96	17.9	3.031	2.494	15.4	HD144585	8"
1129 Neujmina	20/05/96	3.0	3.276	2.273	14.9	HD144585	8"
1148 Rarahu	21/05/96	15.1	3.156	2.455	15.4	HD144585	8"
1186 Turnera	26/03/96	3.8	3.284	2.303	13.9	HD76151	2"
1207 Ostenia	27/03/96	7.3	3.081	2.138	15.6	HD144585	2"
1364 Safara	21/05/96	12.1	2.803	1.916	15.0	HD144585	8"
1388 Aphrodite	27/03/96	4.4	3.152	2.174	15.4	HD144585	2"
1413 Roucarie	21/05/96	4.8	3.139	2.151	15.5	HD144585	8"
1416 Renauxa	22/05/96	5.1	3.345	2.364	15.3	HD144585	8"
1434 Margot	17/10/96	8.5	3.070	2.156	15.1	HD44594	5"
1552 Bessel	22/05/96	11.7	3.306	2.480	16.3	HD144585	8"
1711 Sandrine	17/10/96	9.8	2.700	1.777	15.1	HD44594	5"
1732 Heike	21/05/96	8.8	3.274	2.356	16.1	HD144585	8"
1844 Susilva	22/05/96	9.1	2.939	2.001	15.5	HD144585	8"
1910 Mikkailov	19/05/96	15.6	2.944	2.203	15.6	HD144585	8"
1957 Angara	28/03/96	6.9	2.936	1.980	15.7	HD144585	2"
2180 Marjaleena	27/03/96	8.2	3.118	2.192	15.7	HD144585	2"
2191 Uppsala	27/03/96	5.3	3.105	2.136	15.8	HD144585	2"
2315 Czechoslovakia	27/03/96	3.8	3.302	2.321	15.5	HD144585	2"
2358 Bahner	22/05/96	4.2	3.272	2.280	15.7	HD144585	8"
2443 Tomeileen	20/05/96	11.7	2.944	2.065	14.8	HD144585	8"
3028 Zhangguoxi	26/03/96	12.8	2.952	2.124	15.4	HD76151	2"
3062 Wren	21/05/96	9.3	3.152	2.236	15.7	HD144585	8"
3318 Blixen	21/05/96	7.0	3.013	2.047	15.5	HD144585	8"
3328 1985 QD1	21/06/95	15.3	2.747	1.936	16.2	HR6060	2"
3469 Bulgakov	21/05/96	8.0	2.798	1.836	15.2	HD144585	8"
3713 Pieters	22/05/96	8.0	3.009	2.058	15.8	HD144585	8"
3736 Roskoke	22/05/96	7.9	2.887	1.928	15.4	HD144585	8"
3772 Piaf	22/05/96	7.5	2.873	1.908	15.4	HD144585	8"
3914 Kotogahama	22/05/96	12.0	2.894	2.018	16.3	HD144585	8"
3955 Bruckner	20/05/96	6.3	3.142	2.171	15.9	HD144585	8"
4058 Cecilgreen	27/03/96	4.1	3.170	2.190	15.9	HD144585	2"
4059 Balder	20/05/96	9.7	2.882	1.953	16.1	HD144585	8"
4077 Asuka	22/05/96	1.4	2.916	1.905	15.2	HD144585	8"
4102 1988 TE3	28/03/96	1.9	2.969	1.974	15.6	HD144585	2"
4115 Peternorton	21/05/96	6.2	3.013	2.037	16.1	HD144585	8"
4455 Ruriko	20/05/96	2.5	3.098	2.092	15.3	HD144585	8"
4493 1988 TG1	21/05/96	15.8	3.190	2.552	16.4	HD144585	8"
4498 Shinkoyama	22/05/96	3.0	3.068	2.064	15.6	HD144585	8"
4537 Valgrisrap	22/05/96	1.8	2.991	1.981	15.3	HD144585	8"

by the spectrum of a solar analog star. For this purpose, HD44594, HD76151, and HD144585 (Hardorp 1978) were observed during each night. The stars were observed at airmass similar to those of the objects. The observational circumstances are listed in Table I, which shows the observed V magnitude, distances to the Sun (r) and the Earth (Δ), the solar phase angle (α), the solar analog used, and the slitwidth in arcseconds. At the end, we obtained 45 spectra, which constitutes the first large survey of the Eos family.

The data reduction was performed with the MIDAS package developed at ESO. Although we notice no significant change in bias and flatfield frames from one night to another, we use for each night a separate bias and flatfield. Cosmic rays were identified individually and removed manually. Using the context *long* of MIDAS, the following steps were performed successively to acquire the final spectra of each asteroid:

—bias substraction of each frame

—flatfielding each frame by dividing each bias corrected frame by a normalized bias corrected flatfield

—sky substraction using the sky area on each side of the spectrum

—the two dimensional spectrum was collapsed to one dimension

—wavelength calibration was performed using the helium–argon lamp frames

—spectra were corrected from airmass by using the mean extinction curve of La Silla (Tüg 1977)

—division with the solar spectra treated in the same way as the asteroid spectrum

—normalization to unit flux at 5500 Å by convention.

We have checked the extinction correction by comparing the same solar analog taken at different airmass. The differences were found to be insignificant. We have also investigated the possibility of systematic errors in the asteroid spectrum introduced by the use of different solar analogs. The differences were found to be small ($\leq 1\%/10^3$ Å).

3. RESULTS

The reflectivity spectra of the objects, normalized around 5500 Å, are reported in the Appendix. Due to incomplete removal of the solar spectrum and atmospheric bands, there are some residuals left in the spectra. The largest residuals are from a prominent atmospheric O_2A band at 7619 Å and O_2B band at 6882 Å and a solar absorption line at 6563 Å (H_α). Some false absorptions are also present in the red part of the spectra due to telluric H_2O bands (see, for example, the spectra of 766 Moguntia and 4059 Balder). The spectra are discussed below. Table II contains the reflectance gradient slopeA, which is a linear fit to the spectrum between 5000 and 7500 Å in $\%/10^3$ Å. This is an indicator of the spectral slope (redness) of the spectrum as introduced by Luu and Jewitt (1990).

This survey demonstrates a common general trend of the family spectral behavior (except 1910 Mikkailov and 4455 Ruriko, which cases will be discussed later). The spectra have a reflectivity gradient (slopeA) ranging from $6.3\%/10^3$ Å for 4115 Peternorton to $15.3\%/10^3$ Å for 1552 Bessel in the spectral range 5500–7500 Å. The maximum of the spectra is typically located around 8000–8500 Å with a median value of 8388 Å (Fig. 1). For further discussions, we may introduce two parts at both ends of the spectral range. Based on the values of reflectivity gradients, we refer to a lower asteroid range, i.e., the object whose spectra have a gradient around $6–9\%/10^3$ Å, and an upper asteroid range, i.e., those having spectra spanning around $12–15\%/10^3$ Å.

We wonder whether this wide range of slope is connected with some observational circumstances. No correlations have been found with phase angle (linear correlation coefficient, 0.3) or with the solar analog or slit used. We have also investigated the effect of the diameter. The IRAS albedo, average diameter, and its 1σ uncertainty are given in Table II (Tedesco *et al.* 1992). For the asteroids not observed by IRAS, the diameters have been estimated assuming the average albedo of Eos family (0.1524) and the absolute magnitudes listed in the last column of Table II. We have found no spectral slope-size relation as the one yielding in the Hilda family (Dahlgren *et al.* 1997). The correlation coefficient r of slopeA with asteroid size is $r = 0.09$.

The Eos asteroids observed by ECAS display quite a similar reflectivity gradient range. In SMASS survey, five of the six asteroids observed have their spectra within this span while 2091 Sampo's spectra, similar to a C type is below the lower limit of our span. Three of our asteroids have been included in the ECAS survey (Tholen 1984), two of which belonging to the lower range (1434 Margot and 1711 Sandrine) are well fitted by our data spectra, while in the case of 1148 Rarahu (intermediate between lower and upper range), the fit is less good. 513 Centesima, which spectra is intermediate, was observed by the 25 color survey (Chapman and Gaffey 1979) and presents a good agreement with our data.

The wide range of slope displayed by Eos objects is typical of S type objects. Nevertheless, many Eos members have been found to be of K type, based upon infrared spectral observations (Granahan *et al.* 1993, Clark *et al.* 1994). A K type asteroid, as described by Bell *et al.* (1988) is one which has S type visible spectral characteristics and C type infrared spectral characteristics; e.g., K type spectra contain a shallow pyroxene band near 1 μm which is not seen in C type asteroids, but does not exibit the expected second pyroxene band near 2 μm which is typically seen in S type asteroids. There are a few K type objects which are not Eos members. The Ecas data available have shown that we could not distinguish Eos K type objects from non-Eos K type objects. However, on the other hand, if S type objects are indistinguishable from Eos objects based on their spectral range, we have nevertheless detected a significant difference in the location of the maximum of the spectra. We have compared in Fig. 2 our data with the S

TABLE II
List of the Spectral Parameters Discussed in the Text

Asteroids	Max (Å) ± 10 Å	SlopeA (%/10^3Å) ± 0.2	SlopeB (%/10^3Å) ± 4-5	band depth ± 0.05	Albedo %	D (km)	σ_D (km)	H (mag)
450 Brigitta	7641	6.6	-6.3	0.93	0.1229	33.3[b]	1.3	10.28
513 Centesima	8593	10.8	-1.4	1.02	0.0885	50.2[b]	1.8	9.75
633 Zelima	8090	7.2	-11.2	0.95	0.1918	34.4[b]	1.4	9.73
669 Kypria	8583	14.0	-5.4	1.00	0.1405	31.8[b]	1.3	10.24
766 Moguntia	8344	14.6	-5.7	0.97	0.1572	31.3[b]	2.3	10.15
1112 Polonia	8368	09.2	-1.1	1.02	0.1319	35.8[b]	1.6	10.05
1129 Neujmina	8202	07.1	-6.4	0.98	0.1216	34.8[b]	1.4	10.20
1148 Rarahu	8509	13.9	-9.7	1.01	0.1393	33.2[b]	2.9	10.15
1186 Turnera	8529	9.4	-1.5	1.01	0.2919	35.6[b]	2.0	9.20
1207 Ostenia	8195	10.7	-9.0	0.97	0.1338	22.9[b]	1.3	11.0
1364 Safara	8626	13.5	-4.1	1.2	-	26.2		10.6
1388 Aphrodite	8244	10.3	-7.8	0.98	0.1317	25.2[b]	2.8	10.81
1413 Roucarie	8754	12.8	-0.6	1.14	0.1677	21.5[b]	2.5	10.9
1416 Renauxa	8402	11.2	-7.4	1.01	0.1459	29.0[b]	2.7	10.40
1434 Margot	8312	8.9	-5.8	1.00	0.1353	29.7[b]	1.4	10.43
1552 Bessel	8569	15.3	-3.9	1.06	0.2042	18.6[b]	1.8	11.0
1711 Sandrine	8263	7.4	-5.2	1.00	-	21.7		11.01
1732 Heike	8421	9.8	-8.7	0.99	0.1108	24.1[b]	4.2	11.1
1844 Susilva	8212	10.8	-13.4	0.97	-	21.8		11.0
1910 Mikkailov *	-	2.0	-2.9	-	-	25.0		10.7
1957 Angara	[a]	6.6	0.8	1.04	-	18.5		11.36
2180 Marjaleena	8703	13.2	-2.6	1.02	-	21.8		11.0
2191 Uppsala	7956	7.2	-9.7	0.96	0.1734	17.5[b]	1.3	11.3
2315 Czechoslovakia	8381	12.5	-5.3	0.98	0.1686	23.5[b]	1.1	10.7
2358 Bahner	8212	6.7	-8.2	0.99	-	21.8		11.0
2443 Tomeileen	8510	8.1	-4.5	1.00	0.1540	30.9[b]	1.6	10.2
3028 Zhangguoxi	8593	11.8	-2.2	1.04	0.1417	25.6[b]	1.4	10.7
3062 Wren	8602	13.6	-1.7	1.00	0.1357	25.0[b]	1.5	10.8
3318 Blixen	8671	11.6	7.2	1.06	-	21.8		11.0
3328 1985 QD1	8401	10.5	-1.7	1.03	-	25.0		11.7
3469 Bulgakov	8642	10.9	-2.0	1.08	-	20.8		11.1
3713 Pieters	8329	9.1	-13.7	0.96	-	19.0		11.3
3736 Roskoke	8124	8.5	-11.5	0.96	-	20.8		11.1
3772 Piaf	8501	12.6	-8.1	1.03	-	19.9		11.2
3914 Kotogahama	8295	10.3	-10.4	1.00	-	15.8		11.7
3955 Bruckner	8510	10.4	-7.9	1.04	-	19.0		11.3
4058 Cecilgreen	8366	8.2	-9.7	0.99	-	19.0		11.3
4059 Balder	8388	8.6	-5.1	0.95	-	15.8		11.7
4077 Asuka	8246	8.7	-10.3	1.00	-	19.0		11.3
4102 1988 TE3	[a]	7.9	6.5	1.03	-	17.3		11.5
4115 Peternorton	8328	6.3	-6.5	0.94	-	15.8		11.7
4455 Ruriko *	-	2.4	-3.2	-	-	21.8		11.0
4493 1988 TG1	8217	10.2	-1.38	0.97	0.1636	20.7[b]	1.1	11.0
4498 Shinkoyama	8462	12.2	-7.3	0.98	-	19.0		11.3
4537 Valgrisrap	8388	8.8	-11.1	1.01	-	19.9		11.2

* Eos asteroids which have been considered to be interlopers.
[a] Objects which do not exhibit a maximum of flux (see text).
[b] Iras diameters and the corrresponding σ error.

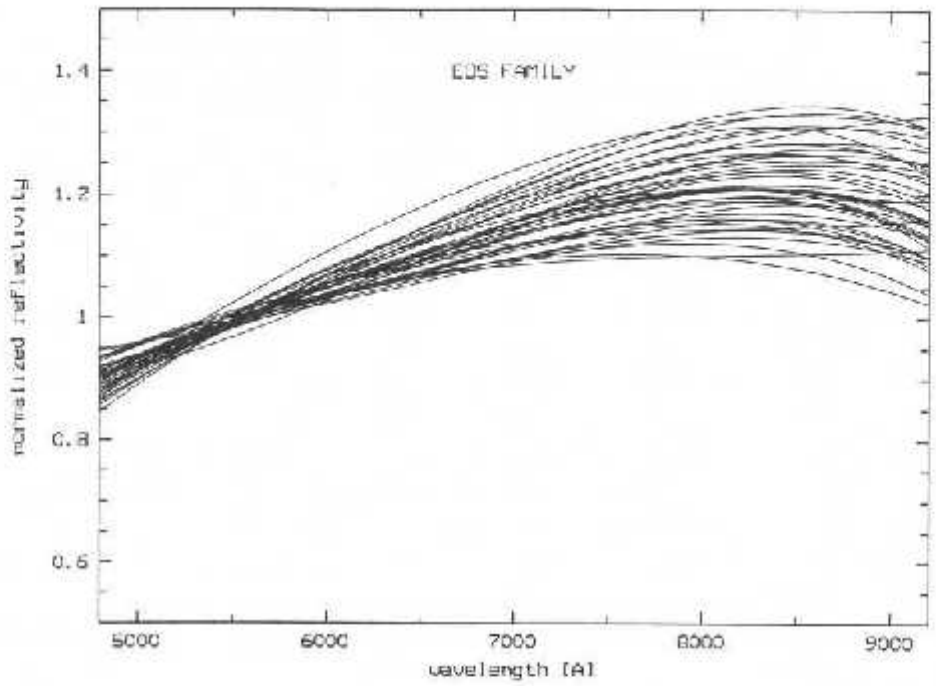

FIG. 1. Spectra of the observed Eos family asteroids except the two interlopers (1910 Mikkailov and 4455 Ruriko). All the spectra were fitted by a smooth polynomial for clarity. There appears to be a continuous spread out of the family's spectral behavior and a maximum of the spectra located around 8000–8500 Å.

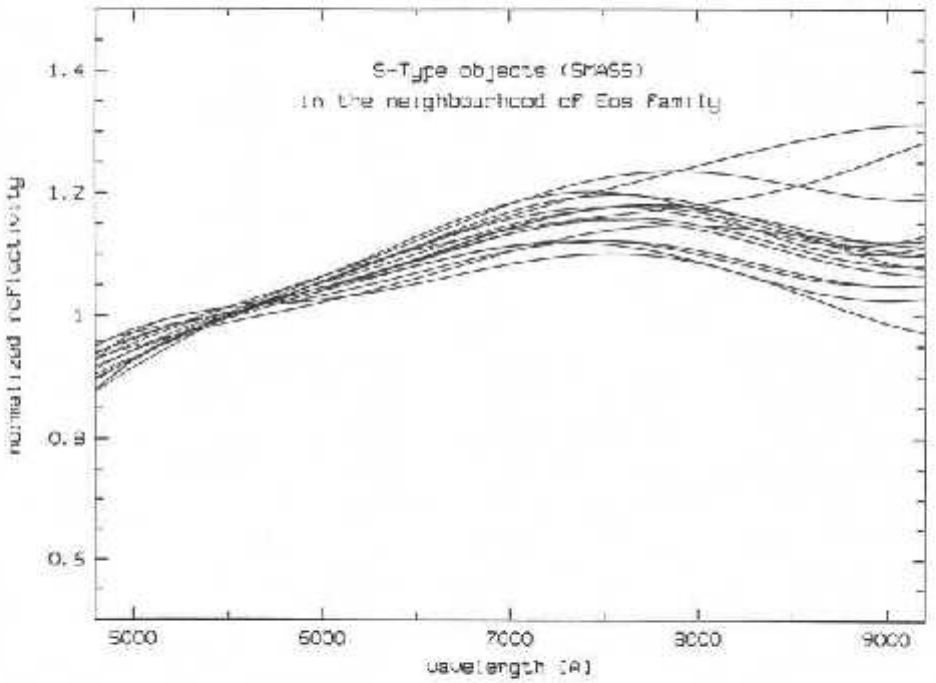

FIG. 2. Spectra of S-type objects located in the neighborhood of Eos family ($2.8 < a < 3.2$ AU). The data are taken from SMASS. The spectra were fitted by a smooth polynomial for clarity. The maximum is clearly located around 7500 Å, which is significantly below the maximum median value found for the Eos family. This implies that the Eos population is distinct from the S-type one in regard to this feature.

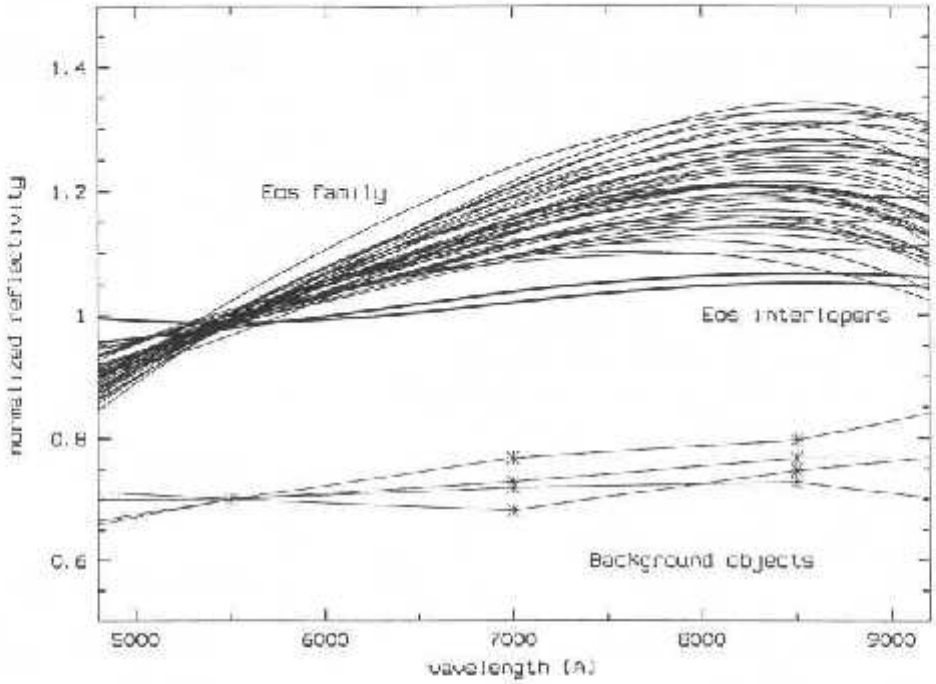

FIG. 3. The Eos family (top) is compared to its interlopers (center, bold line) and the background objects with $2.9 < a < 3.1$; $0.03 < e < 0.11$; $7° < i < 13°$ (bottom). It can be seen that the spectra of background objects (C-type) are very similar to the ones of the interlopers.

objects taken from SMASS (Binzel 1995). We have chosen these asteroids in the neighborhood of Eos family ($2.8 < a < 3.2$ AU). The maximum is clearly located around 7500 Å which is significantly below the maximum median value found for Eos family. This may constitute a finger print to the Eos family, allowing to identify any original Eos member that escaped its original location. Zappala *et al.* (1996) have observed such Eos asteroids, which they called Eos fugitives, while leaving their original location. By recovering the history of their travel to Earth, in the form of a CV/CO chondrite, we should shed a light on the complex resonance's mechanisms that provide meteorites and near earth asteroids

In the wide similar spectral behavior of the Eos family members, we find two anomalous members: 1910 Mikkailov and 4455 Ruriko spectrally similar to C type asteroids (see Fig. 3). We think that they are interlopers, i.e, background objects. According to Gradie *et al.* (1989), the Eos family is located in a region dominated by C type objects. Trying to add more information to this problem, we have plotted in Fig. 3 the eight-color spectra of background objects ($2.9 < a < 3.1$; $0.03 < e < 0.11$; $7° < i < 13°$). As expected, the spectra look C type, very similar to the ones of interlopers.

4. DISCUSSION

The wide observed range of slopes can be explained by three hypotheses:

1. The Eos parent body was partially differentiated, and the impact exposed fragments coming from different layers inside the target.

2. Eos parent body was homogeneous but fragments coming from the parent body surface have been aged by a space weathering process. As reported in Section 1, the age of the collision that formed the Eos family is not well determined. One can assume that this original breakup occurred at a time sufficient for space weathering to alter Eos parent's surface. Therefore fragments coming from the surface should have been significantly reddened compared to the interior of the parent body.

3. The third possible scenario for the explanation of the wide range of slope involves also space weathering. Space weathering processes have aged all the Eos members since the initial formation of the family, when on the other hand, some secondary collisions have rejuvenated some part of the family. Thus, the surfaces of the upper range asteroids are older than those of the lower range objects.

The two later hypotheses invoke the so-called space weathering process that alters the asteroid surfaces with time. The space weathering process is supposed to alter the asteroid regolith, which, exposed to the interplanetary environment, progressively changes color with time. The asteroid surface appears darker and its reflectance spectrum is redder (with much weaker absorptions bands) than does the spectrum of its constituent rocks. It has been known that such processes are responsible for altering the

lunar regolith and, to a less extent, asteroid regolith (Pieters and McFadden 1994). One can argue that this phenomenon can easily be "dished up in every shape," but in fact, recently, data analyses from Galileo's Ida encounter have provided convincing evidence that the space-weathering process is operating on Ida (Chapman 1996). Space weathering is not simply a working hypothesis and should be a valid option, as well as a differentiated parent body.

The second hypothesis alone could hardly be valid because it implies two well separated populations, one old and one young, whereas the Eos family is characterized by a continuous slope range. The third hypothesis also is difficult to rely on because of the paradox of 221 Eos, the largest member, which appears to have a relatively fresh surface (SMASS data imply 221 Eos is in the lower range of spectral slopes). On the other hand, these arguments do not exclude the possibility that two or the three hypotheses may work together. The goal of the following analysis will be to estimate which one is dominant.

We can analyse the whole Eos family with a few spectral parameters. When we look at the Eos spectra (but with a few exceptions we will discuss later), we can distinguish two approximately linear segments, the first from about 5000 to 7500 Å (segment A) and a second segment from about 8500 to 9200 Å (segment B). Between the two segments occur a bend in the spectral reflectance. In this bend is located the maximum of the reflectance curve. Then the spectral parameters characterizing the spectra could be the slopes of both segment A and segment B (namely, slopeA and slopeB) and the maximum of the reflectance curve, Max.

Most of Eos objects spectra exhibit the broad shallow absorption feature longward of 8000 Å. This feature is the most diagnostic one in our spectral interval for surface mineralogy. Asteroid surface material characterization is based upon the interpretation of observable diagnostic properties to determine the presence, abundance, and/or composition of one or more minerals or chemical species on the surface of that object (Gaffey *et al.* 1989). The feature longward of 8000 Å is due to the presence of an olivine–pyroxene mixture band around 1 μm. Several diagnostic and potentially diagnostic spectral parameters can be extracted from asteroid spectrum for olivine–pyroxene mixtures (Cloutis *et al.* 1986). For example, the 1-μm band position parameter is correlated with the Ca^{2-} content of pyroxene, as well as the olivine–pyroxene abundance ratio. For mineralogical significance of spectral parameter, see Gaffey *et al.* (1993).

In our survey, unfortunately, the spectral coverage does not allow deep investigation of mineralogy. However, we can argue that the parameter Max is directly related to the position of the 1-μm absorption band and thus is correlated with the surface mineralogy. The values of slope B computed in the interval 8500–9200 Å using a least mean square linear interpolation are reported in Table II. Large error bars are due to the noisy data in this interval. Negative values are diagnostic of a 1-μm absorption feature. The slopeB values range from -13.8 to $-1.4\%/10^3$ Å. Most of the values of Max range between 8000 and 8500 Å. This might argue for a compositional variation in the olivine–pyroxene mixture and thus for a true compositional variation among the Eos members.

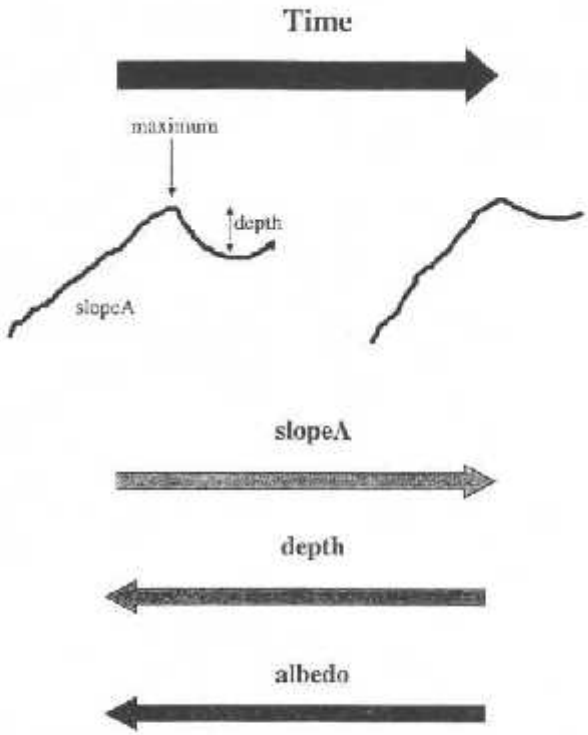

FIG. 4. Behavior of space weathering and spectral parameters.

Only a few Eos objects (1112 Polonia, 1143 Roucarie, 4102 1988 TE3, 1957 Angara) do not have a negative slopeB value diagnostic of the 1-μm feature. This is easily explained for the first three asteroids for which computation of slopeB gives erroneous results due to noisy data and incomplete removal of telluric H_2O bands. On the other hand, the positive slope B of 1957 Angara seems real but we cannot rule out that the telescopic data was erroneous.

4.1. Investigating the Space Weathering Hypotheses

We have shown that there exists a true compositional variation among the Eos asteroids. However, space weathering may indeed be present. So the work below will help to evaluate and remove the role played by space weathering in the diversity within the Eos family.

The space weathering process alters the asteroids by darkening the surface. The effects on the spectra are as follows: the spectra look redder and the absorption bands

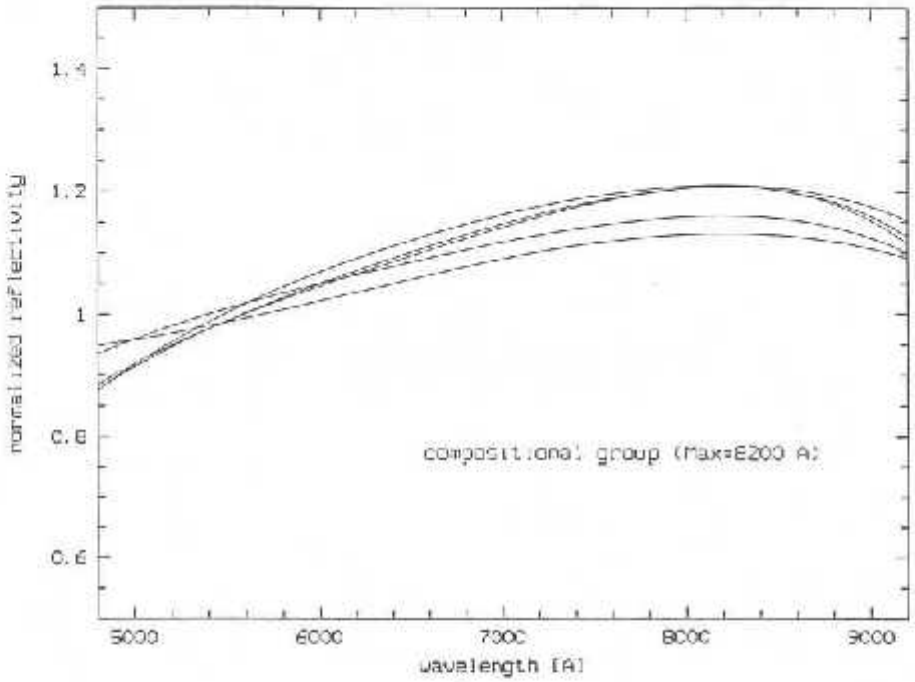

FIG. 5. A compositional group (same Max value). This plot shows that a same space weathering type behavior is present within such a compositional group.

are weakened. These traits were observed by Galileo on Ida's surface where the small fresh craters appeared bluer than other regions (Chapman 1996, and references therein), proving that Ida presents a strong case that space weathering exists. Figure 4 illustrates the relations between space weathering and spectral parameters. We have introduced another useful spectral parameter, the apparent band depth, which is sensitive to the space weathering process. The apparent band depth is computed as the relative reflectance at ~7500 Å outside the 1-μm band, divided by the relative reflectance at ~9000 Å inside the band.

First of all, when investigating the whole Eos family, no correlations have been found between spectral parameters, proving that space weathering is not the prime cause of the diversity seen within the Eos family.

The Eos family can be sorted according to the location of the maximum of the spectra (max). Such a compositional group is shown in Fig. 5 for a maximum value of around 8200 Å. It can be seen that a space weathering process is present within this compositional group. Then the spectral parameters which are sensitive to space weathering processes should be compared. Slope A and band depth were found to be very correlated ($r = -0.96$). However, the correlation with the third "space weathering" parameter (albedo) fails. We should also note that the later correlation was difficult to compute due to incomplete albedo data. In conclusion, space weathering appears to be the source of a nonnegligible part of the diversity within the Eos family.

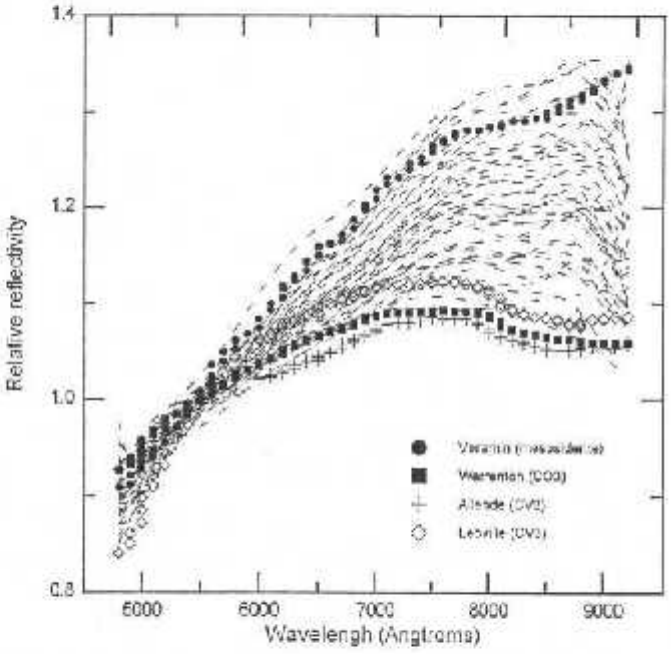

FIG. 6. Spectra of the observed Eos family asteroids except the two interlopers (1910 Mikkailov and 4455 Ruriko). All the spectra were fitted by a smooth polynomial for clarity. There appears to be a continuous but limited spread out of the family's spectral behavior. Comparison with some CO–CV and Veramin meteorites are reported. The plotted meteorite spectra are the average of several size grain meteorite spectra (30 to 300 μm).

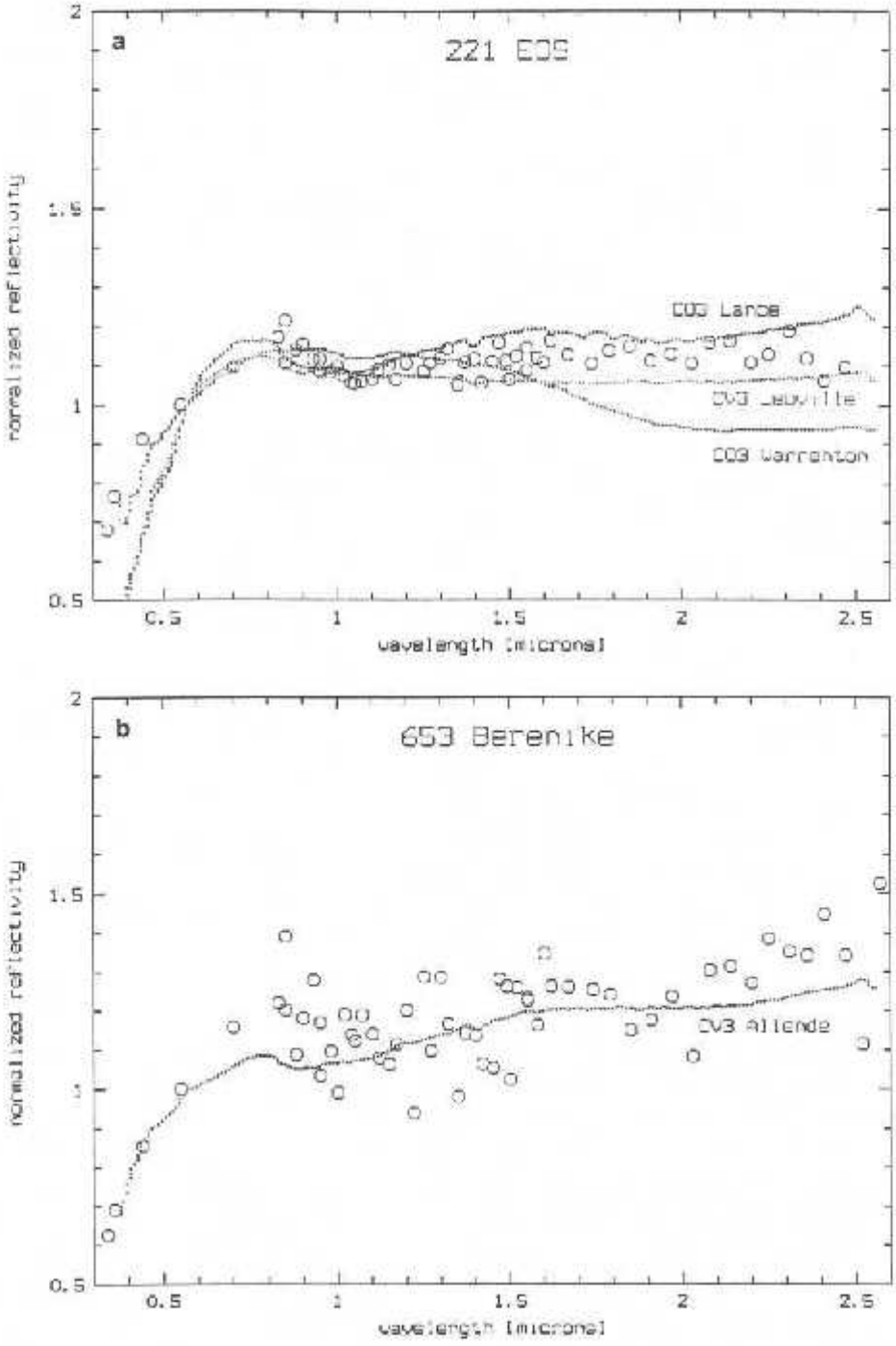

FIG. 7. (a, b, c, d) Spectra of four Eos family asteroids, observed both by ECAS and 52-color asteroid survey. They are compared with meteorite spectra in an extended wavelength range.

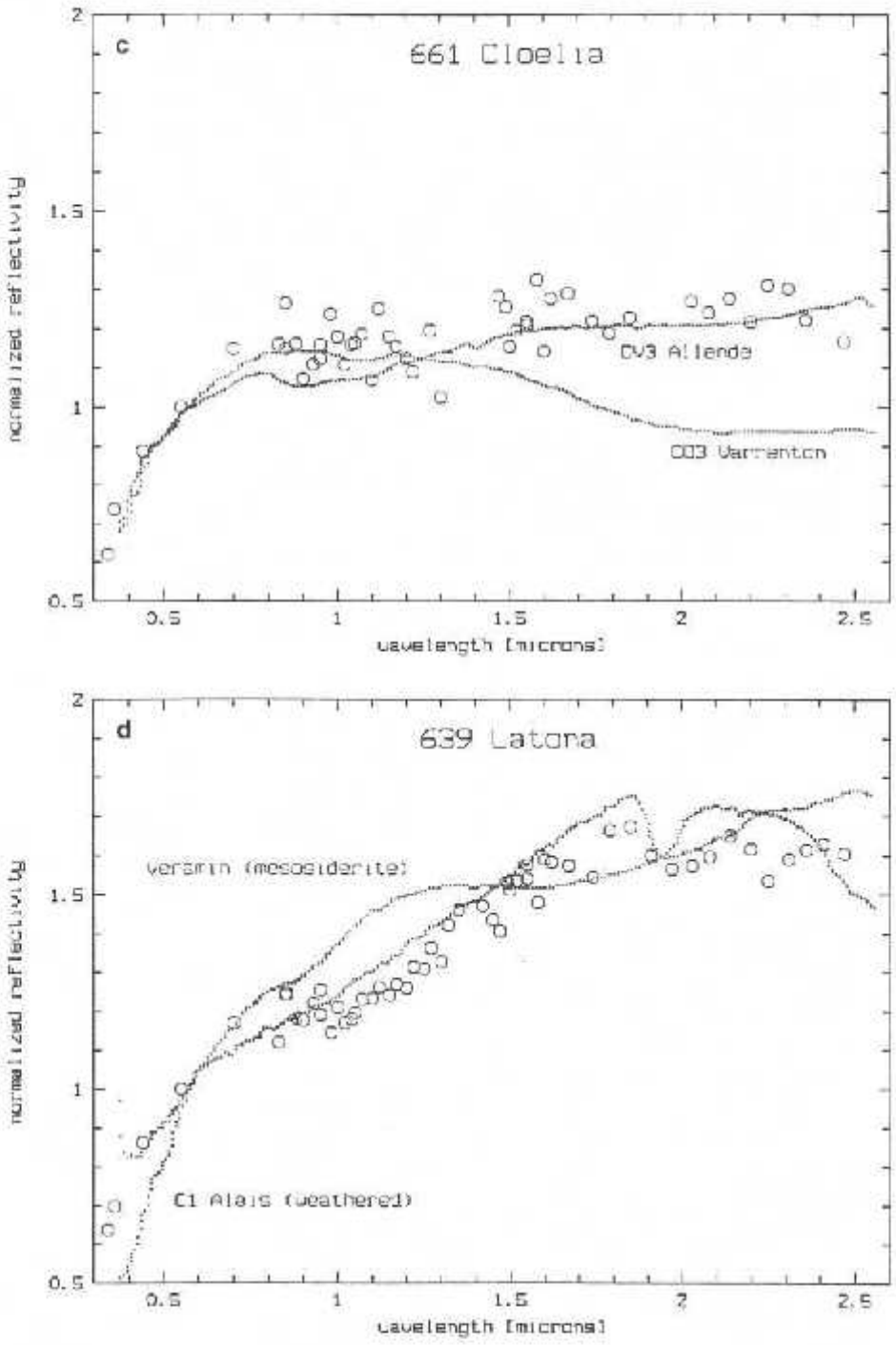

FIG. 7—*Continued*

5. COMPARISON WITH METEORITES

K type objects and consequently Eos asteroids have been, to date, generally linked to CO/CV carbonaceous chondrites (Bell *et al.* 1987, Bell 1988). The spectra of all carbonaceous chondrites types are dominated by the presence of a semiconductive opaque phase (carbon) which results in a very low albedo and weak or absent features. We carried out, in the range $4800 < \lambda < 9200$ Å, a comparison of our spectra with the spectral reflectances obtained by Gaffey (1976) for a wide collection of meteorites measured as powders of several sizes ranging from unsorted coarse (≈300 μm) to fine (≈30 μm) in the spectral coverage from 3700 to 25,000 Å. Our first result confirms that most CO/CV meteorites fit quite well our spectral reflectance curves, but for only the lower range asteroids (Fig. 6). The objects belonging to the upper range have their spectral reflectance quite similar to the one of Veramin mesosiderite. This meteorite is a stony iron meteorite, i.e., a metal–silicate mix.

Our comparison with meteorites over limited wavelength interval should be viewed with caution. Obviously, we cannot validate our interpretation without comparing in the near infrared range. The comparison in a larger range, 3700–25,000 Å, is meaningful. For instance, the differences between carbonaceous chondrites and mesosiderite meteorites, already significant in the 4800- to 9200-Å range is highly emphasized in the infrared range.

We have done a comparison between meteorites and the only four Eos family members observed by both the 52-color asteroid survey and the 8-color asteroid survey (221 EOS, 639 Latona, 653 Berenike, and 661 Cloelia). Thus, we obtained, for these asteroids, a total wavelength coverage from 3400 to 24,000 Å, which almost corresponds to the one of the Gaffey meteorite collection of diffuse reflectance (3500–25,000 Å). 221 Eos, 653 Berenike, and 661 Cloelia are very similar to CO/CV chondrites (Figs. 7a–7c). On the other hand, 639 Latona, whose spectrum is closer to the ones in the upper range of our survey, is similar to the Veramin mesosiderite (Fig. 7d), even if the comparison is not completely satisfactory, especially around 10,000 Å. However, within the limits of the noisy data, the spectrum of 639 Latona looks more like an olivine–stony iron (pallasite) or a highly metamorphosed CV/CO chondrite (Gaffey, private commun.). The spectrum of the C1 carbonaceous chondrite Alais can also be comparable to the spectrum of Latona (Fig. 7d), but this meteorite is considered by Gaffey (1976) as weathered (not well preserved).

Mesosiderite Veramin is the only meteorite (available in the Gaffey collection) spectrally similar to the upper range spectra of Eos objects but the following considerations lead to the conclusion that mesosiderite could not be linked with the upper range spectra of Eos asteroids.

1. Our data end at 9200 Å; thus, it is difficult to compare the final part of the spectra and to state if spectra will rise up as the Veramin spectrum does.

2. Among the four Eos asteroids observed by the 52-color asteroid survey, only one, 639 Latona could be comparable to Veramin meteorite, but with noticeable discrepancy around 10,000 Å. As first stated by Bell in 1989, 639 Latona may be an interloper.

3. The strong argument against deriving stony–iron and CO/CV assemblages from the same parent body arises from the origin of stony–iron meteorites. The processes required to form either a mesosiderite (at least partial melting of parent body to form a basaltic crust) or a pallasite (high degree of melting to form a core within the parent body) would sharply restrict the abundance or even preclude the presence of CV/CO assemblages in the parent body.

6. CONCLUSION

We have obtained 45 spectra of Eos family members in the spectral range 4800–9200 Å, which constitutes the first large survey of Eos family. Our survey demonstrates that the reflectance curves of the family span continuously in a range of reflectivity gradient and that the Eos family should be characterized by the maximum of the spectra typically located between 8000 and 8500 Å. By "flagging" Eos asteroids, this could help in identifying, for example, some Near Earth Asteroids, as escaped Eos asteroids. Another result of our survey is that we have found 2 C-type asteroids which should be interlopers, i.e., background objects, within the family.

Based on the analysis of spectral parameters, we have shown that the diversity seen within the Eos family is due to a true compositional variation among the Eos members and thus a partial differentiation within the Eos parent body. Within a compositional group, we have shown that space weathering is present and constitutes a nonnegligible part in the diversity of Eos objects.

To investigate the family composition and origin, we have carried out a comparison of our spectra with the Gaffey collection of meteorite spectra. It appears that the lower range of our distribution is well fitted by CO–CV meteorite spectra, whereas the upper range seems similar to a mesosiderite one. Thermal considerations suggest the exclusion of any relationship between CO–CV meteorites and mesosiderites.

APPENDIX: RELATIVE REFLECTIVITY FOR 45 EOS FAMILY ASTEROIDS

The spectra are presented by increasing asteroid number. They are normalized around 5500 Å by convention.

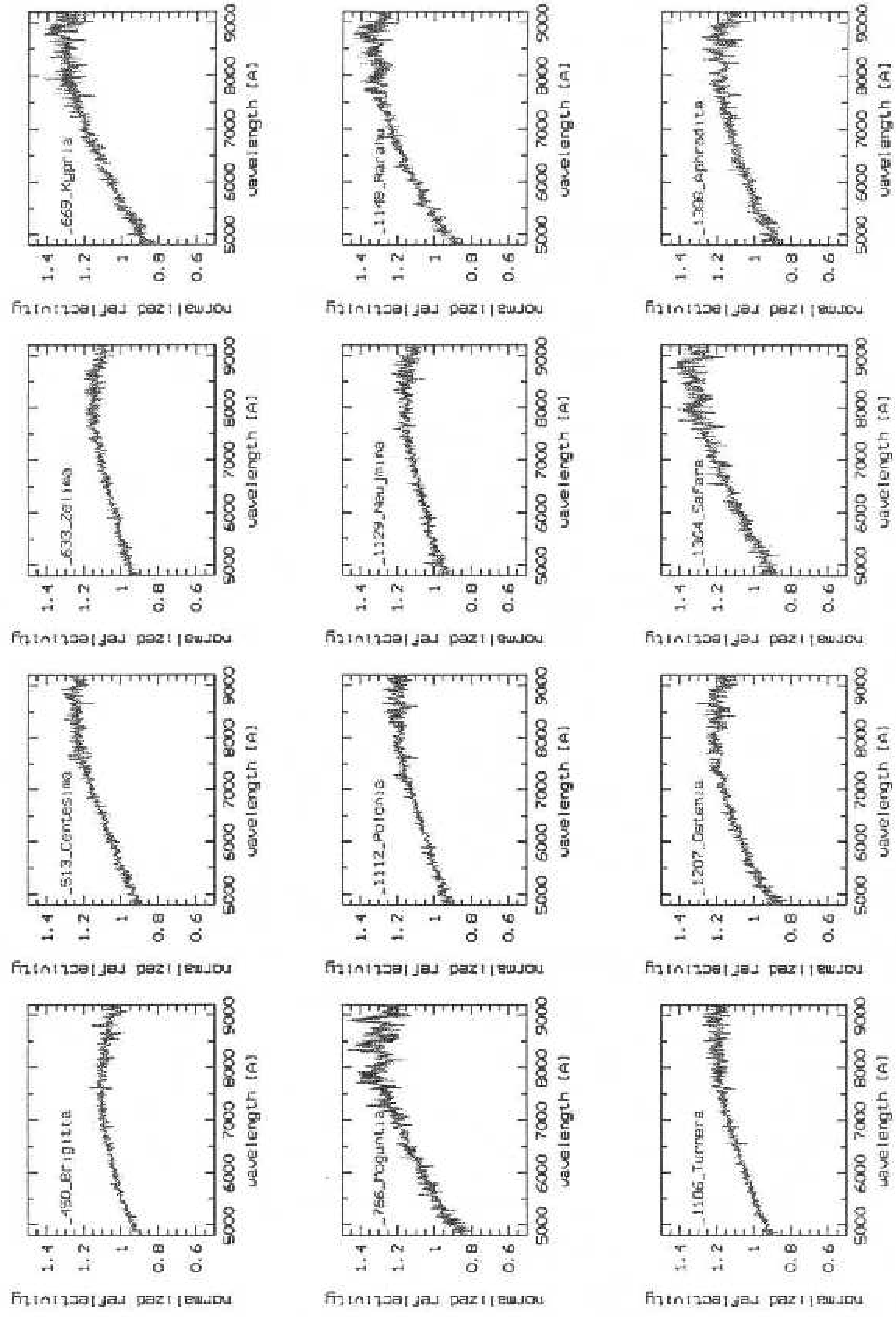

450_Brigitta
513_Centesima
633_Zelima
669_Kypria
766_Moguntia
1112_Polonia
1129_Neujmina
1148_Rarahu
1186_Turnera
1207_Ostenia
1364_Safara
normalized reflectivity
wavelength [A]

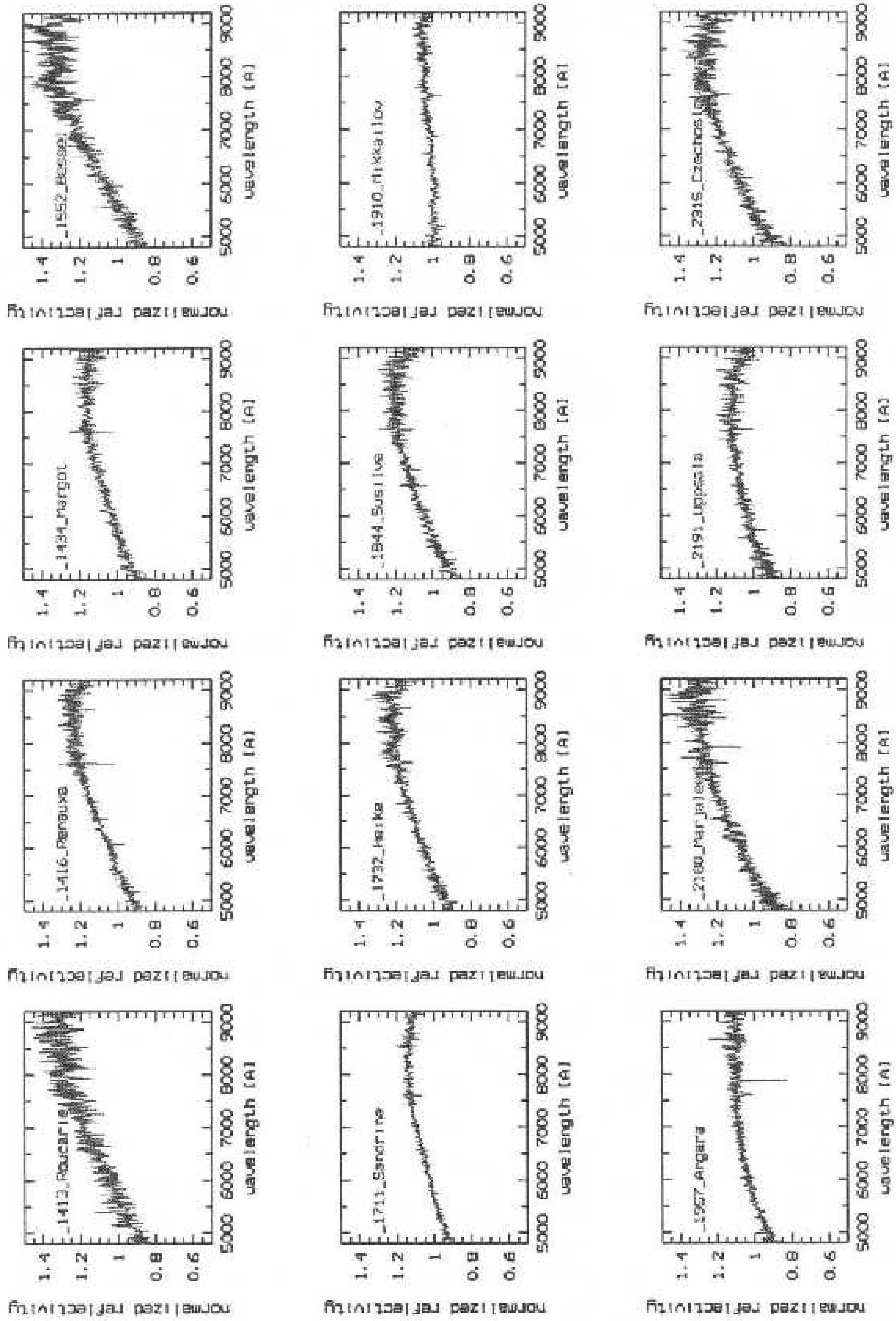
normalized reflectivity
wavelength [A]
1552_Bessel
1910_Mikhailov
1434_Margot
1844_Susilva
2191_Uppsala
1416_Renauxa
1732_Heike
1711_Sandrine

3062_Utsa
3713_Pieters
3955_Bruckner
3028_Zhangguoxi
3469_Bulgakof
2914_Kotogahama
2443_Tsvetlana
3328_1985-QD1
3772_Prof
2358_Bahner
3318_Birkeland
3735_Rostokina
normalized reflectivity
wavelength [A]

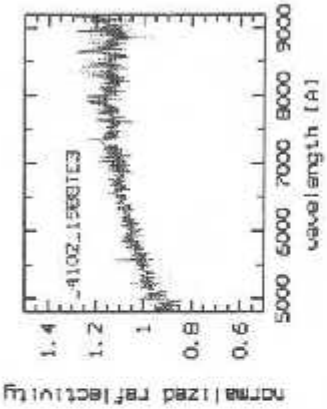
4102_1998TE3
normalized reflectivity
wavelength (A)

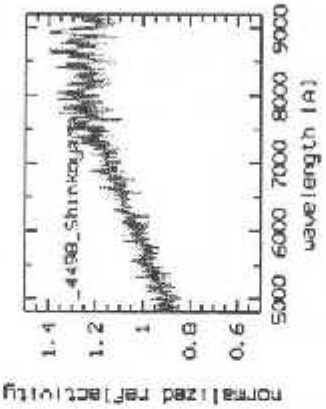
4498_Shinkoji
normalized reflectivity
wavelength (A)

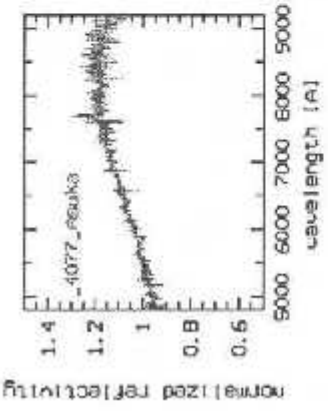
4077_Kuuka
normalized reflectivity
wavelength (A)

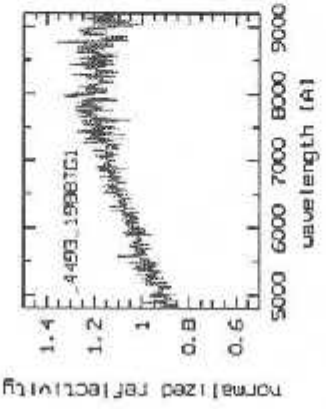
4493_1998TG1
normalized reflectivity
wavelength (A)

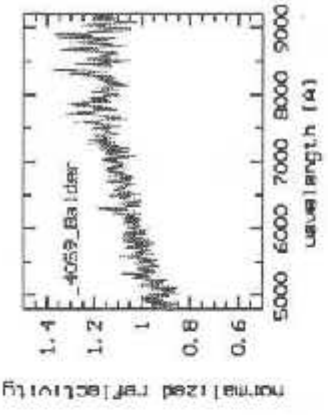
4069_Balder
normalized reflectivity
wavelength (A)

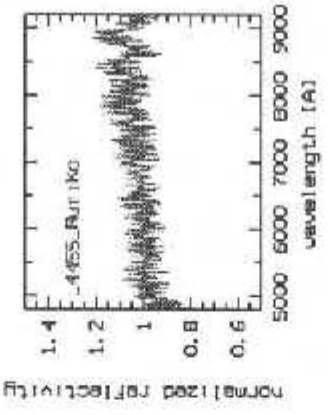
4465_Rurikо
normalized reflectivity
wavelength (A)

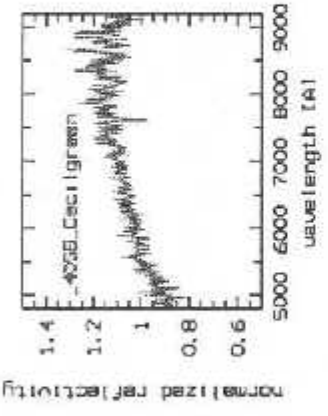
4038_Cecilgreen
normalized reflectivity
wavelength (A)

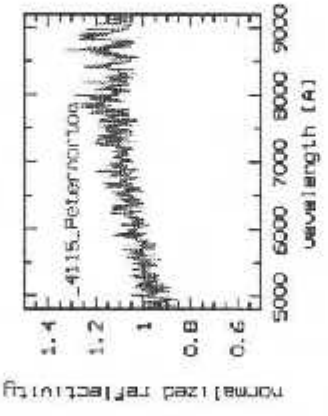
4115_Petermorton
normalized reflectivity
wavelength (A)

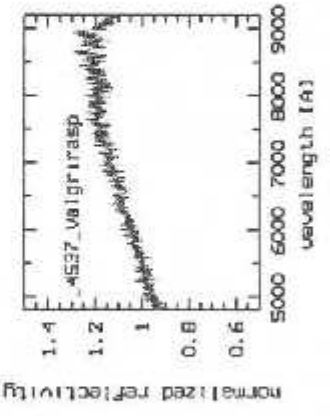
4527_Valgrimsep
normalized reflectivity
wavelength (A)

ACKNOWLEDGMENTS

We are grateful to V. Zappalà for providing a list of nominal Eos asteroids members and for valuable comments. We thank also R. P. Binzel, M. Birlan, R. H. Hewins, C. Perron, and D. J. Tholen, for discussions and helpful suggestions. We thank also the two referees, S. J. Bus and M. J. Gaffey, for their careful remarks, which greatly helped in improving this paper. The reflectance spectra of meteorites were retrieved from the PDS database, small body node. M. A. Florczak thanks CNPq for its financial support during the present research.

REFERENCES

Barucci, M. A., M. T. Capria, A. Coradini, and M. Fulchignoni 1987. Classification of asteroids using G-mode analysis. *Icarus* **72,** 304–324.

Barucci, M. A., A. Doressoundiram, M. Fulchignoni, M. Florczak, M. Lazzarin, and C. Angeli 1997. Compositional type characterization of Rosetta asteroid candidates. *Planet. Spa. Sci.*, in press.

Bell, J. F., B. R. Hawke, and P. D. Owensby 1987. Carbonaceous chondrites from S-type asteroids? *Bull. Am. Astron. Soc.* **19,** 841.

Bell, J. F. 1988. A probable asteroidal parent body for the CO or CV chondrites. *Meteoritics* **23,** 256–257.

Bell, J. F. 1989. Mineralogical clues to the origin of asteroid dynamical families. *Icarus* **78,** 426–440.

Bendjoya, Ph., E. Slezak, and C. Froeschlé 1991. The wavelet transform: A new tool for asteroid family determination. *Astron. Astrophys.* **251,** 312–330.

Binzel, R. P. 1988. Collisional evolution in the Eos and Koronis families: Observational and numerical results. *Icarus* **73,** 303–313.

Carusi, A., and G. B. Valsecchi 1982. On asteroid classification in families. *Astron. Astrophys.* **115,** 327–335.

Chapman, C. R. and M. J. Gaffey 1979. Reflectance spectra for 277 asteroids. In *Asteroids* (T. Gehrels, Ed.), pp. 655–687. Univ. of Arizona Press, Tucson.

Chapman, C. R. 1996. S-type asteroids, ordinary chondrites, and space weathering: The evidence from Galileo's fly-bys of Gaspra and Ida. *Meteoritics Planet. Sci.* **31,** 699–725.

Clark, B. E., J. F. Bell, D. J. O'Connor, and F. P. Fanale 1994. Infrared spectral observations of smaller (50 km) main belt S, K, and M type asteroids. *Proc. Lunar Planet. Sci. 25th*, 265–266.

Cloutis, E., M. J. Gaffey, T. L. Jackowski, and K. L. Reed 1986. Calibration of phase abundance, composition, and particle size distribution for olivine–orthopiroxene mixtures from reflectance spectra. *J. Geophys. Res.* **91,** 11,641–11,653.

Dahlgren, M., C.-I. Lagerkvist, A. Fitzsimmons, I. P. Williams, and M. Gordon 1997. A study of Hilda asteroids. II. Compositional implication from optical spectroscopy. *Astron. Astrophys.* **323,** 606–619.

Filippenko, A. V. 1982. The importance of atmospheric differential refraction in spectrophotometry. *Publ. Astron. Soc. Pacific* **94,** 715–721.

Gaffey, M. J. 1976. Spectral reflectance characteristics of the meteorites classes. *J. Geophys. Res.* **81,** 905–920.

Gaffey, M. J., J. F. Bell, and D. P. Cruikshank 1989. Reflectance spectroscopy and asteroid surface mineralogy. In *Asteroids II* (R. P. Binzel, T. Gehrels, and M. S. Matthews, Eds.), pp. 98–127. Univ. of Arizona Press, Tucson.

Gaffey, M. J., J. F. Bell, R. H. Brown, T. H. Burbine, J. L. Piatek, K. L. Reed, and D. A. Chaky 1993. Mineralogical variations within the S-type asteroid class. *Icarus* **106,** 573–602.

Gradie, J. C. 1978. *An Astrophysical Study of the Minor Planets in the Eos and Koronis Asteroid Families.* Ph.D. Dissertation, Univ. of Arizona, Tucson.

Gradie, J. C., and B. Zellner 1977. Asteroids families: Observational evidence for common origins. *Science* **197,** 254–255.

Gradie, J. C., C. R. Chapman, and E. F. Tedesco 1989. Distribution of taxonomic classes and the compositional structure of the asteroid belt. In *Asteroids II* (R. P. Binzel, T. Gehrels, and M. S. Matthews, Eds.), pp. 98–127. Univ. of Arizona Press, Tucson.

Granahan, J. C., G. Smith, and J. F. Bell 1993. New K type asteroids. *Proc. Lunar Planet. Sci. Conf. 14th*, 557–558.

Hardorp, J. 1978. The Sun among the stars. I. A search for solar spectral analogs. *Astron. Astrophys.* **63,** 383–390.

Hirayama, K. 1918. Groups of asteroids probably of common origin. *Astron. J.* **31,** 185–188.

Knežević, Z., and A. Milani 1994. Asteroid proper elements: The Big picture. In *Asteroids, Comets, Meteors 1993* (A. Milani, M. Di Martino, and A. Cellino, Eds.), pp. 143–158. Kluwer Academic, Dordrecht.

Kuiper, G. P. 1950. On the origin of asteroids. *Astron. J.* **55,** 164.

Lindblad, B. A. 1994. A study of asteroid dynamical families. In *75 Years of the Hirayama Asteroid Families: The Role of Collisions in the Solar System History* (Y. Kosai, R. P. Binzel, and T. Hirayama, Eds.), Astronomical Society of the Pacific Conference Series, Vol. 63, pp. 63–75. Astronomical Society of the Pacific, San Francisco.

Luu J. X., and D. C. Jewitt 1990. Charge couple device of asteroids. 1. Near-Earth and 3:1 resonance asteroids. *Astron. J.* **99,** 1985–2011.

Marzari, F., D. Davis, and V. Vanzani 1995. Collisional evolution of asteroid families. *Icarus* **113,** 168–187.

Milani, A., and Z. Knežević 1990. Secular perturbation theory and computation of asteroid proper elements. *Celest. Mech. Dynam. Astron.* **49,** 347–411.

Milani, A., and Z. Knežević 1992. Asteroid proper elements and secular resonances. *Icarus* **98,** 211–232.

Milani, A., and Knežević, Z. 1994. Asteroid proper elements and the dynamical structure of the asteroid main belt. *Icarus* **107,** 219–254.

Morbidelli, A., V. Zappalà, M. Moons, A. Cellino, and R. Gonczi 1995. Asteroid families close to mean motion resonances: Dynamical effects and physical implications. *Icarus* **118,** 132–154.

Pieters, C., and L. A. McFadden 1994. Meteorites and asteroid reflectance spectroscopy: Clues to early Solar System processes. *Annu. Rev. Earth Planet. Sci.* **22,** 457–497.

Tedesco, E. F., J. G. William, D. L. Matson, G. J. Veeder, J. C. Gradie, and L. A. Lebofsky 1989. Three-parameter asteroid taxonomy classifications. In *Asteroids II* (R. P. Binzel, T. Gehrels, and M. S. Matthews, Eds.), pp. 1151–1161. Univ. of Arizona Press, Tucson.

Tedesco, E. F., G. J. Veeder, J. W. Fowler, and J. R. Chillemi 1992. *The Iras Minor Planet Survey.* Phillips Laboratory Technical Report PL-TR-92-2049. Hanscom Air Force Base, MA.

Tholen, D. J. 1984. *Asteroids Taxonomy from Cluster Analysis of Photometry.* Ph.D. thesis, Univ. of Arizona, Tucson.

Tüg, H. 1977. Vertical extinction on La Silla. *Messenger* **11,** 7–8.

Veeder, J. G., D. L. Matson, P. D. Owensby, J. C. Gradie, J. F. Bell, and E. F. Tedesco 1995. Eos, Koronis, and Maria family asteroids: Infrared (JHK) photometry. *Icarus* **114,** 186–196.

Xu, S., R. P. Binzel, T. H. Burbine, and S. J. Bus 1995. Small main belt asteroid spectroscopic survey: Initial results. *Icarus* **115,** 1–35.

Zappalà, V., A. Cellino, P. Farinella, and Z. Knežević 1990. Asteroid families. I. Identification by hierarchical clustering and reliability assessment. *Astron. J.* **100,** 2030–2046.

Zappalà, V., P. Bendjoya, A. Cellino, P. Farinella, and C. Froeschlé 1995. Asteroids families: Search of a 12,487-asteroid sample using two different clustering techniques. *Icarus* **116,** 291–314.

Zappalà, V., A. Cellino, F. Migliorini, and M. Di Martino 1996. Eos fugitives: A plausible source of CV/CO chondrites. *Bull. Am. Astron. Soc.* **28**(3), 1100.

Zellner, B., D. J. Tholen, and E. F. Tedesco 1985. The eight-color asteroids survey: Results for 589 minor planets. *Icarus* **61,** 355–416.

b) Família de Flora

A família de Flora foi primeiramente identificada por Hirayama em 1919. Em trabalhos subseqüentes, este agrupamento foi dividido em 4 subfamílias (Brouwer, 1951; Arnold, 1969), e até em 10 famílias (Williams, 1992). A dificuldade de se estudar a região de Flora se deve a 2 razões: a proximidade da ressonância secular ν_6, que dificulta o cálculo dos elementos próprios, e a grande quantidade de objetos de fundo nesta região. Devido à dificuldade de separação entre os objetos de fundo e os reais objetos de uma família, Farinella e co-autores (1992) introduziram um novo termo, "clan", para este tipo de agrupamento. Zappalà e co-autores (1995) propõem que Flora seja um clan, com semi-eixo maior próprio entre 2,167 e 2,311 U.A. e 477 membros. Devem ser encontrados cerca de 170 objetos de fundo. O maior objeto desta família é 8 Flora com 136 km de diâmetro, seguido por 43 Ariadne com 66 km e os outros membros com diâmetro inferior a 30 km. A maior parte dos membros desta família que possuem classificação são do tipo S.

Com o objetivo de entender melhor a distribuição de composição mineralógica dos objetos e a origem do clan de Flora realizamos um "survey" espectroscópico. A seguir descreveremos os principais resultados obtidos, enquanto que o artigo descrevendo o trabalho completo é apresentado na seção seguinte. As figuras e tabelas citadas nesta seção são referentes ao artigo.

Obtivemos 47 espectros de objetos do clan de Flora, sendo que 42 apresentaram características similares (espectros do tipo S). Este resultado sugere uma origem comum, embora deva ser ressaltado que a região de Flora é predominantemente de objetos do tipo S. Os outros 5 objetos apresentaram espectros diferentes, levando-nos a propor que não pertencem ao clan. Um deles apresenta um espectro similar a 2 meteoritos eucrites, implicando numa classificação do tipo V e uma provável origem na família de Vesta (fig 2). A figura 3 mostra um ajuste polinomial de todos os espectros normalizados em 5500 Å, com exceção destes 5 objetos. Quando acrescentamos os espectros do clan de Flora obtidos pelo "survey" SMASS (Xu *et al.*, 1995a e 1995b), encontramos que, com exceção de um objeto do tipo C, a distribuição permanece inalterada (fig 1). Com estes espectros, totalizamos 60 objetos do clan de Flora com comportamento espectral similar.

O valor médio encontrado para o máximo dos espectros está em torno de 7580 $\AA$, sendo que varia entre 7250 e 7860 $\AA$, com um erro de 250 $\AA$ devido ao ruído nos espectros. Devido a esta barra de erro não podemos afirmar se a variação acima é real ou não. Se esta variação for real, indicaria uma variação na composição mineralógica, enquanto o contrário indicaria uma homogeneidade na composição destes objetos.

A profundidade da banda de 1 μm não pôde ser medida devido ao intervalo espectral analisado, mas podemos ter uma idéia desta profundidade através da razão de intensidade entre 9200 e 7500 $\AA$. Encontramos uma tendência de aumento do gradiente de refletividade A (medido entre 5000 e 7500 $\AA$) com o decréscimo desta profundidade aparente, sugerindo que um processo de alteração espacial esteja agindo na superfície destes asteróides como descrito anteriormente (ver seção 3.1.3, item b).

Em comparação com os espectros de meteoritos, encontramos 4 condritos ordinários que se ajustam à parte inferior da distribuição espectral dos objetos do clan de Flora (fig 4). Isto sugere que os objetos da parte inferior da distribuição tenham uma composição similar à de meteoritos condritos ordinários mas que, devido a um processo de alteração espacial da superfície como descrito na seção 3.4, sua real composição seja mascarada. Colisões aleatórias poderiam retirar em parte ou totalmente a crosta alterada, revelando suas camadas mais interiores.

ICARUS 133, 233–246 (1998)
ARTICLE NO. IS985928

A Visible Spectroscopic Survey of the Flora Clan[1]

Marcos Florczak

Dep. Astrofísica, ON/CNPq, 20921 Rio de Janeiro, Brazil; Observatoire de Paris, 92195 Meudon Principal Cedex, France; and Dep. Física, CEFET, 80000 Curitiba, Brazil
E-mail: florczak@on.br

M. Antonietta Barucci and Alain Doressoundiram

Observatoire de Paris, 92195 Meudon Principal Cedex, France

Daniela Lazzaro and Cláudia A. Angeli

Dep. Astrofísica, ON/CNPq, 20921 Rio de Janeiro, Brazil

and

Elisabetta Dotto

Observatoire de Paris, 92195 Meudon Principal Cedex, France; and Dip. di Fisica, Universitá di Padova, 35131 Padova, Italy

Received May 12, 1997; revised February 2, 1998

We observed 47 Flora clan members at the ESO (European Southern Observatory) in the wavelength range 4900–9200 Å. We found 42 objects with common characteristics: a maximum around $\lambda = 7500$ Å and a reflectivity gradient spanning a continuous but limited range. Only five objects show different spectral behavior (one is probably V type). Looking for meteorite analogs, we only find four ordinary chondrites that present features similar to those of the lower part of the Flora spectral distribution. This behavior is consistent as the consequence of some space-weathering process. © 1998 Academic Press

1. INTRODUCTION

In 1918 Hirayama (1918) first recognized some nonrandom concentrations in the asteroid orbital elements, and hence first introduced the concept of families identifying three of them: Koronis, Eos, and Themis. One year later he included the Flora group (Hirayama 1919) in this category. These families provide an unique opportunity to investigate the mineralogical composition of the interior of solar system bodies, since they have components that are considered as remnants of energetic interasteroidal collisions, with catastrophic disruption of a parent body.

The validity of this concept was first confirmed by Brouwer (1951), who computed the proper elements of 1537 asteroids and added a few other families. The Flora family was then split into four subfamilies. This division was supported by Arnold (1969) with a qualitative argument, but not recognized by Lindblad and Southworth (1971). Later, Carusi and Massaro (1978) claimed that there exist no such subfamilies, although they identified three subgroups in this region. They rejected this result as spurious as a consequence of their method.

The complexity in describing the Flora region comes from two distinct reasons. First, the determination of proper elements is a difficult task because of the proximity to the ν_6 and the secondary secular resonances, leading to large uncertainties in the assessment of families. Second, the high-density background and the probable multicollisional origin of the family contribute to the complexity of the region. Williams (1992), for example, broke up this region into 10 families, suggesting that many collisional events could have caused this splitting.

Farinella *et al.* (1992) introduced a new term, "clans," to represent groupings for which unequivocal membership definition and/or separation from other background groups is impossible. Thus, in the clans the expected number of interlopers can be a significant fraction of the total number. Zappalà *et al.* (1994) proposed that the Flora region could be a clan, identifying 477 members with a very high background density and estimating the presence of nearly 170

[1] Based on observations made with the 1.52 m telescope at the European Southern Observatory (La Silla, Chile) under the agreement with the CNPq/Observatório Nacional (Brazil).

0019-1035/98 $25.00

interlopers (see also Zappalà *et al.* 1995). In what follows, we will use the Zappalà *et al.* (1994) definition of members of the Flora clan.

Many hypotheses have been made concerning the origin of the Flora family or clan. Wiesel (1978) proposed that it could be the result of a collision between two asteroids of similar size, a proto-Flora and a proto-Ariadne. Tedesco (1979), using UBV colors, verified that 98% of the clan members have a homogeneous distribution of colors. The conclusion was that a common origin of Flora clan is almost certain, but the clan probably did not originate from the castastrophic disruption of a single parent body. Gaffey (1984) suggested that 8 Flora, the biggest asteroid in the clan, could be the metal-rich core of the original parent body, while the smaller members could be metal-poor fragments from its crust and mantle.

The Flora clan members have their proper semimajor axes between 2.167 and 2.311 AU (Zappalà *et al.* 1995). The largest member is 8 Flora, with a diameter of 136 km, followed by 43 Ariadne with a diameter of 66 km (Tedesco 1997). The remaining members do not exceed 31 km in diameter.

Most of the objects which have been classified belong to the S-type class (Tholen 1989 and references therein). Xu *et al.* (1995a) reported CCD spectra of 20 asteroids members of the Flora clan, of which all but one (C-type, 2259 Sofievka) were classified as S-type. It is worth noting that certain S-type objects seem to be possible sources of ordinary chondrites. Binzel *et al.* (1996) found that near-Earth asteroid spectra continuously span the range between ordinary chondrite meteorites and S-class asteroids in the 4500- to 9500-Å spectral region. Chapman (1996), based on the results of the Galileo observations of Gaspra, Ida, and Dactyl, all S-class asteroids, suggested that a "space weathering" process would operate to convert the spectrum of ordinary chondrite material to that of S-type asteroids.

Froeschlé and Scholl (1986), from numerical integrations of synthetic particles located inside the ν_5 secular resonance, found that fragments injected into this region at low inclinations become Earth-crossers within 1 Myr. Moreover, Scholl and Froeschlé (1991) proposed the Flora region as a possible mainbelt source of meteorites.

McCord and Gaffey (1974) analyzed the reflectance spectra of 8 Flora, concluding that the surface of this asteroid was composed of mixtures of metal and pyroxene. Feierberg *et al.* (1982) suggested that 8 Flora could be an ordinary chondrite candidate in the asteroid belt. However, Gaffey (1984) found that its spectrum varies with rotation, implying a spatially heterogeneous surface composition inconsistent with that of ordinary chondrites. He concluded that the surface material indicates a differentiated body.

The asteroid 43 Ariadne, on the other hand, was suggested by Johnson and Matson (1973) to be an ordinary chondrite due to its spectrum being similar to that of 1685 Toro. Gaffey (1984) found that the H and K reflectance of 43 Ariadne (Veeder *et al.* 1978) is consistent with a metal-poor, olivine-dominated assemblage.

Gaffey *et al.* (1993) defined seven subclasses of S-types (designated S(I)–S(VII)) based on their analyses of visible to near-IR spectral absorption bands. Parameters derived from analyses of these bands are directly related to the abundance of minerals present on the asteroid surfaces. In the subset of the S-types studied, Gaffey *et al.* (1993) concluded that only members of the S(IV) subclass could have compositions which might include ordinary chondrites. In their work they state that 8 Flora could be ambiguously classified as type S(III) or S(IV) while two other members of the Flora clan, 364 Isara and 43 Ariadne, are classified as S(II) and S(III), respectively. In this sense their work indicates some variation between different clan members.

The asteroid 951 Gaspra, a member of the Flora clan, has also been extensively studied using the data returned by the Galileo spacecraft instruments. The spectra obtained show color differences (Carr *et al.* 1994) that indicate a heterogeneous composition, and Granahan *et al.* (1994) suggest that 951 Gaspra is indeed a differentiated object. The same conclusion was made by Kivelson *et al.* (1993) from the study of Gaspra's magnetic moment per unit of mass, which shows that it falls into the observed range of iron meteorites and highly magnetized chondrites. On the other hand, Hood and Sonnet (1994), using magnetization intensities from a larger sample of meteorites, suggest that even if a stony-iron composition cannot be ruled out, the Galileo data are also consistent with ordinary chondrite.

In order to have a global understanding of the origin of this clan it is necessary to investigate systematically the compositional distribution of it members. For this purpose, we performed spectroscopic observations of a large sample of members of the Flora clan.

2. OBSERVATIONS AND REDUCTION

The observations were performed at the European Southern Observatory at La Silla (Chile) using a 1.5-m telescope equipped with a Boller and Chivens spectrograph and a CCD 2048 × 2048 pixels with a readout noise of ±7 electrons. We used the 225-gr/mm grating with a dispersion of 330 Å/mm in the first order. The CCD has a square 15-μm pixel, giving a dispersion of about 5 Å/pixel in the wavelength direction. The useful spectral range is about $4900 < \lambda < 9200$ Å with a FWHM of 10 Å. The spectra were taken through a 5-arcsec slit oriented in the East–West direction. The slit width has been chosen to minimize the consequences of atmospheric differential refraction and reduce the loss of light at both ends of the spectrum. This is important in the sense that a substantial loss of light

may lead to an erroneous spectral characterization of an object. Care was also taken that the observations were made as near as possible to the meridian of the asteroid.

We observed the Flora clan in January 1997, from January 1 to 8, with excellent atmospheric conditions. The observational circumstances, from the EPHEM program (Tholen 1989), are listed in Table I, which shows the distance from the Sun and from the Earth, the solar phase angle, the estimated visual magnitude, and the diameter. The given diameters are from IRAS (Tedesco 1997), whenever available, otherwise are estimated through the absolute magnitude and a visual albedo of 0.15.

The spectral data reduction was performed using the Image Reduction and Analysis Facility (IRAF) package and taking much care to ensure a proper calibration of the spectra. The bias level of each night was determined through an average of the many bias images taken in the night. This averaged bias was then subtracted from each frame and pixel-to-pixel variations were removed by dividing the resulting image by a normalized medium flat field. The IRAF apsum package was used to sum the pixel values within a specified aperture and to subtract the background level. Wavelength calibration was performed several times during each night using a He–Ar lamp, and spectra were corrected from airmass by using the mean extinction curve of La Silla (Tüg 1977). This correction was checked by comparing the same analog star taken at different airmass and the differences were negligible. Since each analog was observed several times during each night we also reduced each asteroid spectrum with the solar analog taken at the same airmass (or as near as possible). Again no difference could be observed, which confirms the quality of the data. In what follows we used the solar analog HD 44594 (Hardorp 1978) to compute reflectivities, since this is the solar analog which most closely matches the spectra of the Sun. Two other solar analogs, HD 28099 and HD1835, were also observed in order to estimate the quality of the night. The ratios between the spectra of the three solar analogs for the night of January 4th which show no substantial variation, are given in Fig. 1. Similar ratios were obtained during the other nights. The influence of different solar analogs on the resulting spectra has also been checked, showing differences less than $1\%/10^3$ Å. All asteroid spectra are normalized around 5500 Å by convention.

3. RESULTS

The obtained reflectance spectra, normalized at 5500 Å, are shown in the Appendix. ECAS data (Zellner *et al.* 1985) are also overlapped on the spectra whenever available.

In Table II are given the computed spectral parameters of the observed Flora clan members. In this table the second column, named "slope A," indicates the reflectivity gradient (linear fit) computed in the 5000–7500 Å range, which is an indicator of the redness (or spectral slope) of the spectra as introduced by Luu and Jewitt (1990). The next column contains "slope B," which indicates the reflectivity gradient computed in the range 8000–9200 Å. The position of the maximum is given in the fourth column, were the error is in part due to the proximity of the prominent atmospheric band at 7619 Å. The apparent depth of the absorption band, computed as the division of the normalized reflectivity at 7500 and at 9200 Å, is given in the next column. The albedo, whenever available, is given in the last column.

The analysis of this table readily shows some common characteristics in the spectra of the observed members of the Flora clan (except five objects that will be discussed later): a maximum between 7250 and 7860 Å, with a median value of 7580 Å, a slope A between 8.3 and 16.1 $\%/10^3$ Å, and a slope B in the range from −5.57 to −13.65 $\%/10^3$ Å. No relations were found between reflectivity gradients and asteroid diameters, but this result can be attributed more to the very limited span of diameters present in the Flora clan than to some real physical property. It must be noted that the slight variation in the location of the maximum is difficult to analyze in the face of the error bars. If this variation is real it could imply diversity in the surface composition of the members of the clan. On the other hand, if it is not real, it would confirm unique composition and the differences in the spectra would need to be explained by some other processes, such as space weathering.

It must be noted that the absorption band with the minimum around 9000–10000 Å, which is required to derive the olivine–pyroxene ratio (Cloutis *et al.* 1986), is not well defined in our spectra due to the limited spectral range coverage. The determined apparent depth is just an indication of the real depth of the absorption band, but this value can be useful in deriving some mineralogical information. We have found a trend between the slope A and the apparent depth indicating that as the first increases the second decreases. This can be an indication of a space weathering process which darkens the surface of the object, increasing its redness (and therefore the slope A) and decreasing the depth of the absorption band (Wetherill and Chapman, 1988; Pieters and McFadden 1994).

Some asteroids in our sample were also observed by other authors in a similar or even wider spectral range. Comparison in the same spectral range reveals similar trends. This is the case of 43 Ariadne, observed by Xu *et al.* (1995a, 1995b), by the ECAS (Zellner *et al.* 1985), by the 24-filter survey (Chapman and Gaffey 1979), and by the 52-color survey (Bell *et al.* 1988). Asteroids 352 Gisela and 2510 Shandong were compared only to ECAS for the same spectral range. The similarity we are referring to is that of the slopes in the ranges 5000–7500 and 7500–9200 Å, slopes A and B, respectively. In this sense, 43 Ariadne and 352 Gisela closely match the points given by

TABLE I

Observational Circumstances: Exp Is the Number of Exposures, R and Δ Are the Heliocentric and Geocentric Distances, Respectively, α Is the Solar Phase Angle, m_v Is the Visual Magnitude, and D Is the Diameter ((*) IRAS Diameter)

Asteroids	UT Date dd/mm/yy	Exp.	R(AU)	Δ (AU)	α	m_v	D (Km)
43 Ariadne	02/01/97	2	2.553	1.624	9.1	11.6	65.9*
298 Baptistina	04/01/97	2	2.164	1.395	20.0	14.4	21.9
352 Gisela	02/01/97	2	2.107	1.170	10.8	12.6	20.3*
525 Adelaide	04/01/97	1	2.027	1.226	20.8	15.5	10.9
685 Hermia	05/01/97	1	2.074	1.966	28.0	16.1	10.9*
929 Algunde	06/01/97	1	2.331	1.599	19.6	15.9	13.2
1056 Azalea	04/01/97	1	2.594	1.651	7.6	15.4	16.0
1060 Magnolia	07/01/97	2	2.579	1.655	9.4	16.4	10.1
1089 Tama	04-06/01/97	2	1.945	1.671	30.3	15.4	12.9*
1117 Reginita	03/01/97	1	2.677	1.863	14.2	16.2	15.0
1130 Skuld	04/01/97	1	2.370	1.443	10.2	15.4	13.2
1219 Britta	04/01/97	1	1.981	1.946	28.9	16.0	11.4*
1274 Delportia	08/01/97	1	2.051	1.671	28.3	15.8	15.1
1365 Henyey	05-07/01/97	2	2.528	1.855	19.1	16.0	16.0
1399 Teneriffa	05/01/97	1	2.135	1.173	7.4	16.3	6.1
1449 Virtanen	05/01/97	1	2.515	1.661	13.6	16.2	11.6
1530 Rantaseppa	04/01/97	1	2.359	1.490	14.1	16.6	8.3
1602 Indiana	09/01/97	1	2.012	1.542	28.3	16.2	12.2*
1621 Druzhba	02/01/97	2	1.965	1.420	28.3	15.1	9.5*
1798 Watts	05-06/01/97	2	1.944	1.308	27.1	16.0	9.6
1806 Derice	02/01/97	2	2.001	1.089	14.3	14.5	13.8
2019 van Albada	02/01/97	2	2.601	1.681	9.5	15.7	17.3*
2031 Bam	04/01/97	1	2.074	1.107	6.3	15.3	8.8
2093 Genichesk	06/01/97	1	2.634	1.823	14.5	16.8	10.5
2112 Ulyanov	01/01/97	1	1.946	1.690	30.3	16.7	9.6
2341 Aoluta	06/01/97	1	2.093	1.228	17.2	15.4	11.0
2478 Tokai	02/01/97	2	2.086	1.284	20.02	15.9	9.6
2510 Shandong	07/01/97	1	2.227	1.876	25.9	16.8	10.5
2780 Monnig	07/01/97	1	2.195	1.346	16.6	16.5	7.6
2815 Soma	03/01/97	1	2.351	1.402	8.1	16.3	8.0
2820 Iisalmi	08/01/97	1	2.318	1.452	14.6	16.3	9.2
2841 Puijo	05/01/97	1	2.131	1.264	16.2	15.7	10.1
2914 Glarnisch	06/01/97	1	2.075	1.203	16.5	16.6	6.0
2961 Katsurahama	02/01/97	2	2.085	1.172	13.8	15.7	8.7
2975 Spahr	04/01/97	1	2.157	1.283	15.5	15.7	10.1
3023 Heard	07/01/97	2	2.185	1.332	16.5	16.8	6.6
3033 Holbaek	04/01/97	1	2.346	1.371	4.1	15.9	8.7
3067 Akmatova	03/01/97	1	2.042	1.414	25.7	16.4	8.7
3073 Kursk	02/01/97	2	1.941	1.019	14.0	15.8	7.0
3105 Stumpff	03-04/01/97	2	2.300	1.410	12.9	16.4	8.3
3181 Ahnert	05/01/97	1	2.174	1.227	9.2	15.5	9.6
3478 Fanale	08/01/97	1	2.314	1.680	21.9	16.8	14.9*
3533 Toyota	04/01/97	1	1.960	1.215	24.0	15.6	9.6
3875 Staehle	05/01/97	1	2.623	1.699	9.1	16.7	9.6
4278 Harvey	08/01/97	1	2.059	1.174	15.8	16.5	5.5
4299 1952 QX	03/01/97	1	2.014	1.190	19.9	16.2	8.3
4422 Jarre	02/01/97	2	2.224	1.245	2.8	15.4	10.5

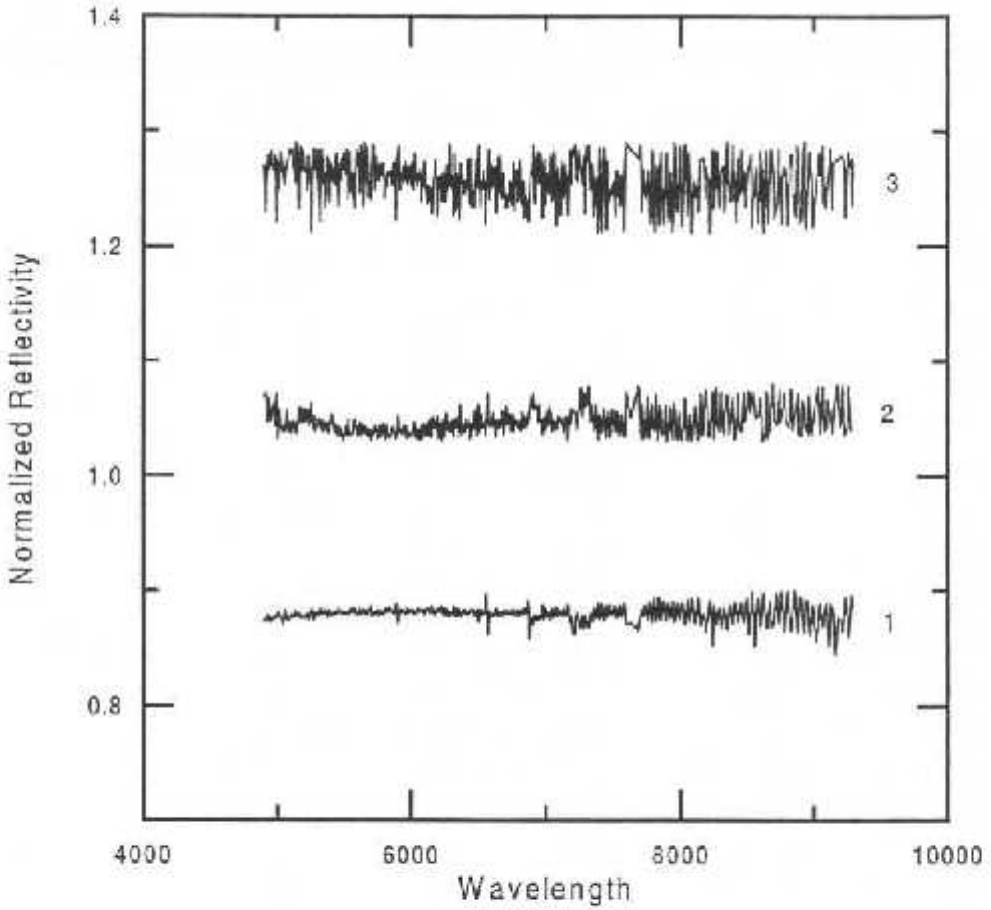

FIG. 1. The ratios between the spectra of the three solar analogs observed during the night of January 4th are presented. Spectrum 1 is the ratio between HD28099 and HD44594, Spectrum 2 is the ratio between HD28099 and HD1835, and Spectrum 3 is the ratio between HD1835 and HD44594.

ECAS. Some differences are present in the comparison of 2510 Shandong with ECAS, especially in the range 7000–9200 Å, where our spectra are quite noisy.

Five objects have spectral behavior different from that of the majority of the Flora clan and therefore we assume that they are interlopers, even though the confirmation of this assumption will need a more detailed mineralogical analysis. Asteroid 298 Baptistina has a spectrum similar to those of the E, M, or C type, 2093 Genichesk to the C type, 3533 Toyota to the M type, and 3875 Stachle to the G or B type. We found two eucrite meteorites' spectra with trends similar to 4278 Harvey's (Fig. 2), suggesting a V-type classification. This finding, if confirmed, is quite surprising due to the distance of 4278 Harvey from Vesta and the other V-type asteroids (Migliorini *et al.* 1997, and private communication). In order to assert the real importance of this discovery in an evolutionary scenario of Vesta-type asteroids more observations of 4278 Harvey are needed, along with a dynamical study, which is out of the scope of the present paper. We hope to return to this problem.

Migliorini *et al.* (1995) statistically computed the expected number of interlopers in each of the asteroid families. For the Flora clan they estimated the presence, with 95% confidence, of between 0 and 3 interlopers on nearly 24 family members, in the diameter range either of 6–10 km or of 10–50 km. Our results, suggesting the presence of two interlopers in each diameter range, are in agreement with the estimates of Migliorini *et al.* (1995). The possible V-type asteroid, 4278 Harvey, is the only object in our survey in the size range 3–6 km, and therefore no comparison can be made with the results of Migliorini *et al.* (1995). Even if our results match the expected number of interlopers, much care should be taken in making conclusions. First of all, since the family and nonfamily members in this region are expected to be S type, the classification of one object as interloper must rely on more observations and on a wider spectral coverage. On the other hand, as various authors have pointed out (Migliorini *et al.* 1995; Zappalà *et al.* 1995), the complexity of the Flora clan makes an unambiguous identification of family members difficult even with the most modern techniques.

TABLE II
List of Spectral Parameters

Asteroids	slopeA $\%/10^3$ Å $\pm$ 0.4	slopeB $\%/10^3$ Å $\pm$ 5	Max Å $\pm$ 250 Å	deph % $\pm$ 0.05	albedo
43 Ariadne	9.9	-9.36	7500	1.12	0.2740
298 Baptistina	5.1	-2.52			
352 Gisela	13.0	-7.96	7630	1.10	
525 Adelaide	11.0	-11.54	7450	1.15	
685 Hermia	10.6	-12.32	7640	1.16	0.2807
929 Algunde	12.0	-9.33	7510	1.11	
1056 Azalea	12.7	-10.01	7620	1.13	
1060 Magnolia	9.8	-11.46	7480	1.14	
1089 Tama	10.8	-10.90	7250	1.12	0.2435
1117 Reginita	9.6	-11.28	7530	1.18	
1130 Skuld	14.2	-10.53	7660	1.10	
1219 Britta	12.2	-9.29	7570	1.23	0.2267
1274 Delportia	14.5	-7.60	7820	1.10	
1365 Henyey	10.7	-10.55	7570	1.12	
1399 Teneriffa	8.3	-10.88	7470	1.16	
1449 Virtanen	13.5	-10.99	7750	1.13	
1530 Rantaseppa	11.7	-10.95	7580	1.11	
1602 Indiana	8.6	-13.18	7500	1.18	
1621 Druzhba	13.7	-13.65	7570	1.19	0.4388
1798 Watts	10.4	-12.09	7580	1.34	
1806 Derice	12.7	-10.00	7610	1.12	
2019 vanAlbada	14.6	-13.28	7610	1.10	
2031 Bam	14.2	-11.19	7510	1.13	
2093 Genichesk	1.4	-4.60			
2112 Ulyanov	13.0	-12.40	7610	1.13	
2341 Aoluta	14.8	-11.57	7570	1.15	
2478 Tokai	14.0	-8.50	7620	1.09	
2510 Shandong	10.2	-9.52	7640	1.16	
2780 Monnig	15.2	-9.20	7860	1.00	
2815 Soma	8.7	-12.33	7420	1.17	
2820 Iisalmi	12.3	-5.57	7650	1.07	
2841 Puijo	8.5	-12.36	7420	1.14	
2914 Glarnisch	11.7	-12.20	7530	1.12	
2961 Katsurahama	10.8	-10.89	7600	1.14	
2975 1970AF1	16.1	-10.13	7680	1.10	
3023 Heard	10.3	-10.12	7450	1.15	
3033 Holbaek	10.7	-9.27	7540	1.12	
3067 Akmatova	13.8	-12.08	7690	1.10	
3073 Kursk	13.2	-11.30	7600	1.14	
3105 Stumpff	11.6	-12.90	7640	1.14	
3181 Ahnert	14.8	-10.19	7680	1.16	
3478 Fanale	10.5	-8.83	7520	1.14	0.06
3533 Toyota	4.9	+9.13			
3875 Staehle	4.1	-11.30			
4278 Harvey	11.8	-25.53			
4299 1952QX	11.0	-10.23	7540	1.11	
4422 Jarre	8.9	-8.44	7750	1.15	

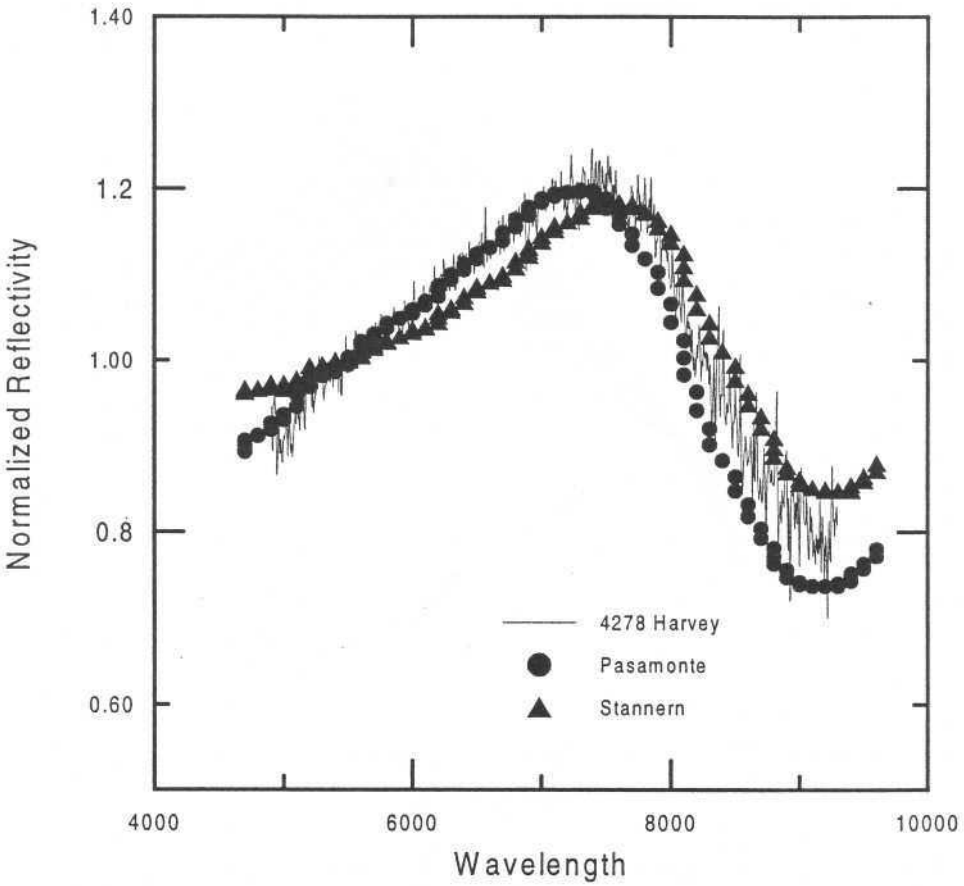

FIG. 2. Spectrum of the asteroid 4278 Harvey compared with two eucrite-type spectra. The meteorites are Pasamonte and Stannean (Gaffey, 1976).

4. COMPARISON WITH METEORITES

It is widely presumed that meteorites are fragments of asteroids, produced in the asteroid belt by collisions. If this is true, the meteorites should then provide some information about the mineralogical composition of their parent bodies. The composition of S-type asteroids is generally thought to be different combinations of pyroxene, olivine, and metallic Ni–Fe (Wetherill and Chapman 1988). Unfortunately, the presence of these materials is not sufficient to define a meteorite analog, and two different types of mineral association can be linked to S-types: undifferentiated ordinary chondrite (H, L, LL)[2] and differentiated stony iron.

Since the S-type asteroids are the most abundant in the inner belt and among the Earth-crosser population, one might expect that they are also the parent bodies of the most abundant meteorites falling on Earth, the ordinary chondrites (OC). However, the spectra of S-type asteroids do not match completely with those of OC meteorites. This has been known as the "S-type conundrum" (Wetherill and Chapman 1988; Gaffey *et al.* 1993; Chapman 1996; and references therein). Thus we have at least two possibilities: either the OC are indeed fragments of S-type asteroids and their spectra do not match due to a "space weathering" process which slightly modifies the surfaces of asteroids (Pieters and McFadden 1994; Chapman 1996); or the parent bodies of OC meteorites are small asteroids (less than 10 km in diameter) whose location favors rapid transport of fragments from the main belt to the Earth (Bell *et al.* 1989; Bell 1994).

Having this controversy in mind, a global comparison of our spectra with those of meteorite analogs is of special importance. For this purpose we fitted our spectra by a linear polynomial (least squares) in order to have a clearer graphic. We performed the same procedure on the spectra of the Flora clan obtained by SMASS[3] (Xu *et al.* 1995a,

[2] The classes H, L, and LL for high Fe, low Fe, and low Fe–low metal (Sears and Dodd 1988).

[3] The SMASS asteroids: 8, 915, 951, 1451, 1518, 1577, 1651, 1807, 1967, 2017, 2130, 2440, 2538, 3677, 4025, 4145, 4373, 4640.

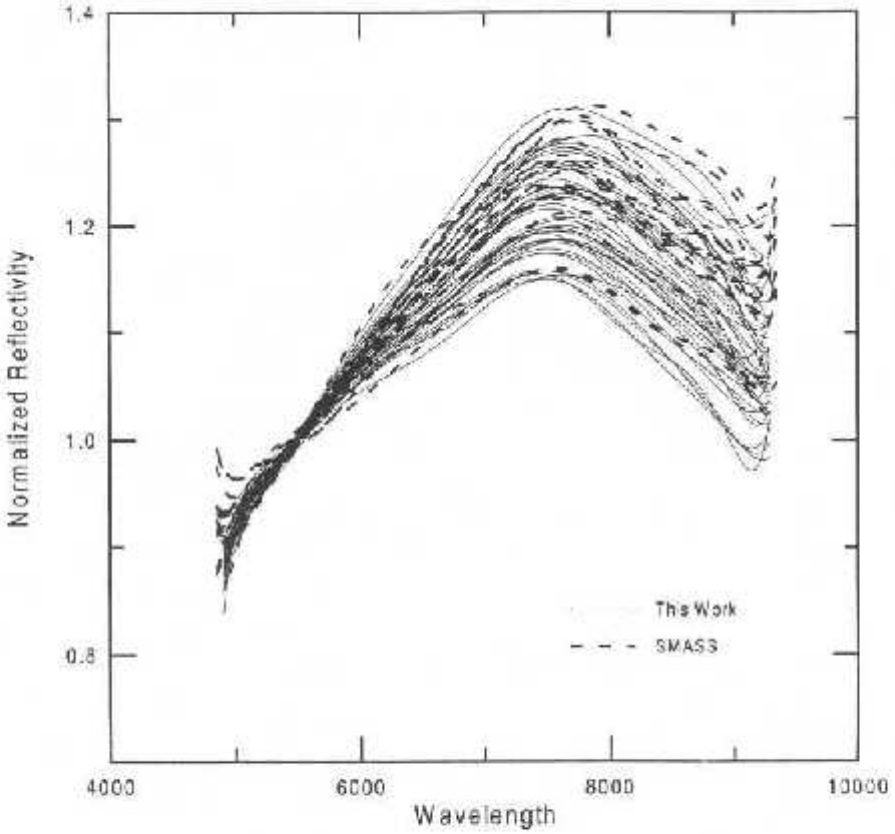

FIG. 3. Spectra of the Flora clan presented in this work without the five possible interlopers—298 Baptistina, 2093 Genichesk, 3533 Toyota, 3875 Staehle and 4278 Harvey—and the SMASS spectra of Flora clan obtained by Xu *et al.* (1995a, 1995b) (except 2259 Sofievka). All the spectra are normalized around 5500 Å and are fitted by a polynomial for clarity.

1995b). All the possible interlopers in the present work and in Xu *et al.* (1995a) were excluded. The totality of 60 spectra thus obtained shows similar behavior, as can be seen in Fig. 3. Note that all spectra span a continuous and limited range of reflectivities.

Finally, we compared our spectra to those of meteorites measured by Gaffey (1976) for the same spectral range. We find that only the spectra of ordinary chondrites (L3, L4, L5, and LL types) have trends similar to those of the lower range of the Flora spectral distribution (Fig. 4).

5. CONCLUSION

Forty-seven spectra of Flora clan asteroids were obtained. Among these, 42 spectra show similar behavior, spanning over a continuous but limited range, with reflectivity gradient ranging from 8.3 to 16.1%/10^3 Å (computed between 5000 and 7500 Å). Five asteroids were found with spectra differing substantially from the general behavior and we suggest that they might be interlopers since we do not have information on visual-albedo and/or infrared data. Nineteen spectra of SMASS were also compared to our results showing analogous behavior. No correlation was found between reflectivity gradients and asteroid diameters.

Four ordinary chondrites' spectra, one LL type and three L types have been found that show behavior similar to the lower range of the Flora clan spectra. Therefore, we propose that ordinary chondrites are a lower limit of the continuous distribution of spectra of the Flora clan.

We interpret the obtained continuous span of spectral characteristics as the result of different time-dependent space weathering. We must recall that the results of the Galileo spacecraft showed that a space weathering process can occur on an asteroid surface (Chapman 1996). This phenomenon would modify the properties of the surface material (Wetherill and Chapman 1988), the asteroid surface appears darker and its reflectance spectrum is redder than does the spectrum of its constituent rocks, with much weaker absorption bands. This is exactly the behavior shown by the observed members of the Flora clan. We take thus the continuous spectral distribution found as an indication that collisions have rejuvenated part of the clan. Therefore, the asteroid surface which spectrum is similar

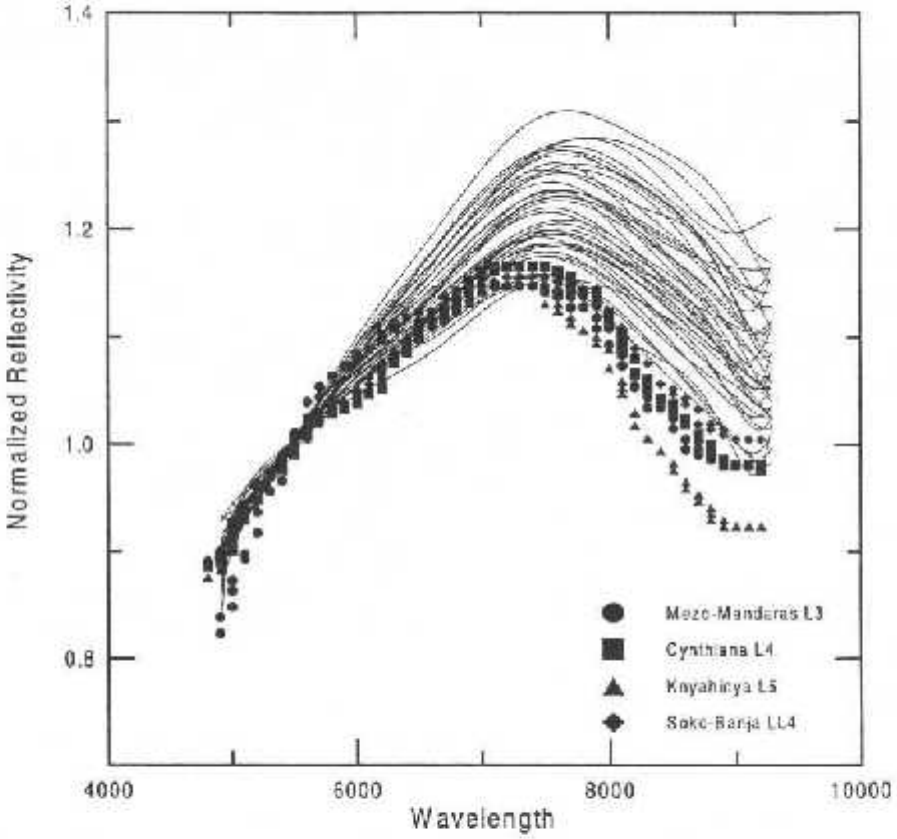

FIG. 4. Spectra of the Flora clan obtained in this survey (except the five possible interlopers) are compared with four ordinary chondrites' spectra. The Mezo-Mandaras, Cynthiana, and Knyahinya are L3, L4, and L5 types respectively and Soko-Banja is LL4 type (Gaffey 1976). All the spectra are normalized around 5500 Å and are fitted by a polynomial for clarity.

to the lower part of the spectral distribution presented here is younger and shows a composition similar to ordinary chondrites.

In this work, we have shown that the spectra of the members of the Flora clan span a continuous range of reflectivities which is consistent with the existence of a space weathering process, although the present data do not exclude completely the other coincidental possibilities. Further studies on the detailed mechanism of the space weathering should be pursued, for example by laboratory experiments.

ACKNOWLEDGMENTS

The authors thank M. Kelley and the late F. Migliorini for the detailed revision and for many suggestions that much improved the paper. They also express their sincere regret for the loss of F. Migliorini. M. Florczak, D. Lazzaro, and C. A. Angeli thank CNPq for its financial support during the present research.

REFERENCES

Arnold, J. R. 1969. Asteroid families and "jet streams," *Astron. J.* **74**, 1235–1242.

Bell, J. F. 1994. Ordinary chondrites in space and time [Abstract]. *Lunar Planet. Sci.* **25**, 89–90.

Bell, J. F., P. D. Owensby, B. R. Hawke, and M. J. Gaffey 1988. The 52-color asteroid survey: Final results and interpretation [Abstract]. *Lunar Planet Sci.* **19**, 57–58.

Bell, J. F., D. R. Davis, W. K. Hartmann, and M. J. Gaffey 1989. Asteroids: The big picture. In *Asteroids II* (T. Gehrels, Ed.), pp. 921–945. Univ. of Arizona Press, Tucson.

Binzel, R. P., S. J. Bus, T. H. Burbine, and J. M. Sunshine 1996. Spectral properties of near-Earth asteroids: Evidence for sources of ordinary chondrite meteorites. *Science* **273**, 946–948.

Brouwer, D. 1951. Secular variations of the orbital elements of minor planets. *Astron. J.* **56**, 9–32.

Carr, M. H., R. L. Kirk, A. McEwen, J. Veverka, P. Thomas, J. W. Head, and S. M. Murchie 1994. The geology of Gaspra. *Icarus* **107**, 61–71.

Carusi, A., and E. Massaro 1978. Statistics and mapping of asteroid concentrations in the proper elements' space. *Astron. Astrophys. Suppl. Ser.* **34**, 81–90.

Chapman, C. R. 1996. S-type asteroids, ordinary chondrites, and space weathering: The evidence from Galileo's fly-bys of Gaspra and Ida (Invited Review). *Meteorit. Planet. Sci.* **31**, 699–725.

Chapman, C. R., and M. J. Gaffey 1979. Reflectance spectra for 277 asteroids. In *Asteroids* (T. Gehrels, Ed.), pp. 655–687. Univ. of Arizona Press, Tucson.

Cloutis, E. A., M. J. Gaffey, T. L. Jackowski, and K. L. Reed 1986. Calibrations of phase abundance, composition, and particle size distribution for olivine-orthopyroxene mixtures from reflectance spectra. *J. Geophys. Res.* **91,** 641–653.

Farinella, P., D. R. Davis, A. Cellino, and V. Zappalà 1992. From asteroid clusters to families: A proposal for a new nomenclature. In *Asteroids Comets Meteors 91* (A. W. Harris and E. Bowell, Eds.), pp. 165–168. Lunar & Planetary Institute, Houston.

Feierberg, M. A., H. P. Larson, and C. R. Chapman 1982. Spectroscopic evidence for undifferentiated S-type asteroids. *Astrophys. J.* **257,** 361–372.

Froeschlé, Ch., and H. Scholl 1986. The secular resonance ν_6 in the asteroidal belt. *Astron. Astrophys.* **166,** 326–332.

Gaffey, M. J. 1976. Spectral reflectance characteristics of the meteorite classes. *J. Geophys. Res.* **81,** 905–920.

Gaffey, M. J. 1984. Rotational spectral variations of Asteroid (8) Flora: Implications for the nature of the S-type asteroids and for the parent bodies of the ordinary chondrites. *Icarus* **60,** 83–114.

Gaffey, M. J., J. F. Bell, R. H. Brown, T. H. Burbine, J. L. Piatek, K. L. Reed, and D. A. Chaky 1993. Mineralogical variations within S-type asteroid class. *Icarus* **106,** 573–602.

Granahan, J. C., F. P. Fanale, M. Robinson, R. W. Carlson, L. W. Kamp, K. P. Klaasen, W. D. Smythe, P. R. Weissman, M. Belton, D. Cooke, K. Edwards, A. S. McEwen, L. A. Soderblom, B. T. Carcich, P. Helfenstein, D. Simonelli, P. Thomas, and J. Veverka 1994. A Galileo multiinstrument spectral analysis of 951 Gaspra [Abstract]. *Lunar Planet. Sci.* **25,** 453–454.

Hardorp, J. 1978. The Sun among the stars. *Astron. Astrophys.* **63,** 383–390.

Hirayama, K. 1918. Groups of asteroids probably of common origin. *Astron. J.* **31,** 185–188.

Hirayama, K. 1919. Further notes on the families of asteroids. *Proc. Phys. Math. Soc. Japan Ser. III* **1,** 52–59.

Hood, L. L., and C. P. Sonett 1994. Galileo magnetic field signature: No evidence that Gaspra is differentiated [Abstract]. *Lunar Planet. Sci.* **25,** 561–562.

Johnson, T. V., and D. L. Matson 1973. Spectrophotometry of (43) Ariadne: A possible chondritic composition (Abstract). *Bull. Am. Astron. Soc.* **5,** No. 2, 308.

Kivelson, M. G., L. F. Bargatze, K. K. Khurana, D. J. Southwood, R. J. Walker, and P. J. Coleman, Jr. 1993. Magnetic field signatures near Galileo's closest approach to Gaspra. *Science* **261,** 331–334.

Lindblad, B. A., and R. B. Southworth 1971. A study of asteroid families and streams by computer techniques. In *Physical Studies of Minor Planets* (T. Gehrels, Ed.), NASA SP-267 pp. 337–352. U.S. Govt. Printing Office, Washington, D.C.

Luu, J. X., and D. C. Jewitt 1990. Charge couple devide of asteroids. 1. Near-Earth and 3:1 resonance asteroids. *Astron. J.* **99,** 1985–2011.

McCord, T. B., and M. J. Gaffey 1974. Asteroid: Surface composition from reflection spectroscopy. *Science* **186,** 352–355.

Migliorini, F., V. Zappalà, R. Vio, and A. Cellino 1995. Interlopers within asteroid families. *Icarus* **118,** 271–291.

Migliorini, F., A. Morbidelli, V. Zappalà, B. J. Gladman, M. E. Bailey and A. Cellino 1997. Vesta fragments from ν_6 and 3:1 resonances: Implications for V-type NEAs and HED meteorites. *Meteorit. Planet. Sci.*, in press.

Pieters, C. M., and L. A. McFadden 1994. Meteorite and asteroid reflectance spectroscopy: clues to early Solar System process. *Annu. Rev. Earth Planet. Sci.* **22,** 457–497.

Scholl, H., and Ch. Froeschlé 1991. The ν_6 secular resonance region near 2AU: A possible source of meteorites. *Astron. Astrophys.* **245,** 316–321.

Sears, D. W. G., and R. T. Dodd 1988. Overview and classification of meteorites. In *Meteorites and the Early Solar System* (J. F. Kerridge and M. S. Matthews, Eds.), pp. 3–31. Univ. of Arizona Press, Tucson.

Tedesco, E. F. 1979. The origin of Flora family. *Icarus* **40,** 375–382.

Tedesco, E. F. 1997. "IMPS Diameters and Albedos V1.0." Planetary Data System-Small Bodies Node (PDSSBN) (M. A'Hearn, University of Maryland, College Park, Maryland). Available http://pdssbn.astro.umd.edu.

Tholen, D. J. 1989. Asteroid taxonomic classification. In *Asteroids II* (R. P. Binzel, T. Gehrels, and M. S. Matthews, Eds.), pp. 1139–1161. Univ. of Arizona Press, Tucson.

Tholen, D. J. 1997. Ephemeris program EPHEM, Version 1.1. Celestech, Honolulu, Hawaii.

Tüg, H. 1977. Vertical extinction on La Silla. *Messenger* **11,** 7–8.

Veeder, G. J., D. L. Matson, and J. C. Smith 1978. Visual and infrared photometry of asteroids. *Astron. J.* **83,** 651–663.

Wetherill, G. W., and C. R. Chapman 1988. Asteroid and meteorites. In *Meteorites and the Early Solar System* (J. Kerridge and M. S. Matthews, Eds.), pp. 35–67. Univ. of Arizona Press, Tucson.

Wiesel, W. 1978. Fragmentation of asteroids and artificial satellites in orbit. *Icarus* **34,** 99–116.

Williams, J. G. 1992. Asteroid families—An initial search. *Icarus* **96,** 251–280.

Xu, S., R. P. Binzel, T. H. Burbine, and S. J. Bus 1995a. Small main-belt asteroid spectroscopic survey: Initial results. *Icarus* **115,** 1–35.

Xu, S., R. P. Binzel, T. H. Burbine, and S. J. Bus 1995b. "Small Main-Belt Asteroid Spectroscopic survey." Planetary Data System—Small Bodies Node (PDSSBN) (M. A'Hearn, University of Maryland, College Park, Maryland). Available http://pdssbn.astro.umd.edu

Zappalà, V., A. Cellino, P. Farinella, and A. Milani 1994. Asteroid families: Extension to unnumbered multi-opposition asteroids. *Astron. J.* **107,** 772–801.

Zappalà, V., P. Bendjoya, A. Cellino, P. Farinella, and Cl. Froeschlé 1995. Asteroid families: Search of a 12,487 asteroid sample using two different clustering techniques. *Icarus* **116,** 291–314.

Zellner, B., D. J. Tholen, and E. F. Tedesco 1985. The eight-color asteroid survey: Results for 589 minor planets. *Icarus* **61,** 355–416.

APPENDIX: RELATIVE REFLECTIVITY OF 47 FLORA CLAN ASTEROIDS

The spectra are presented by increasing asteroid number. They are normalized around 5500 Å by convention.

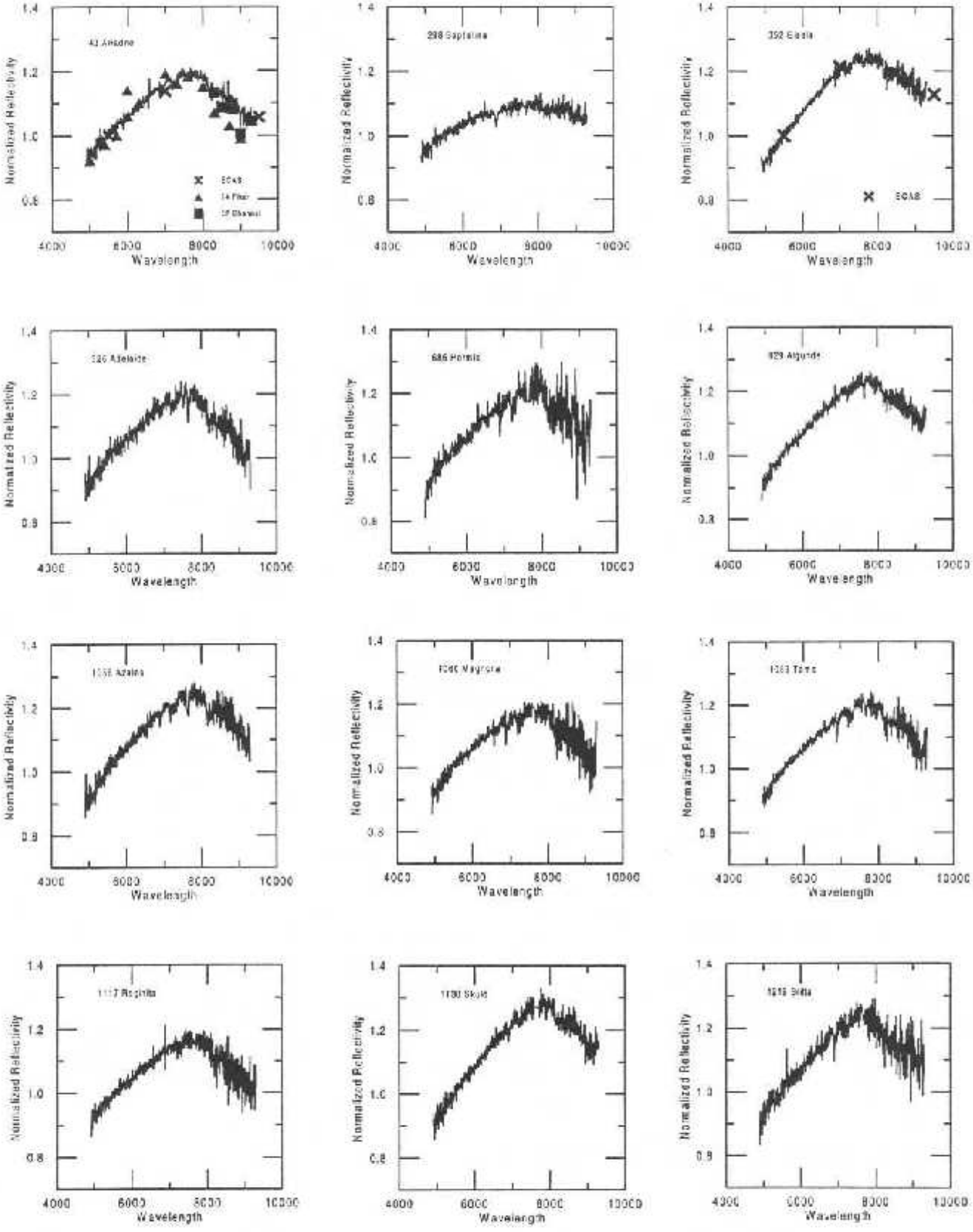

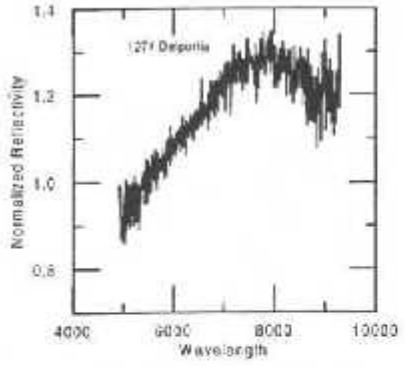
1271 Desportia
Normalized Reflectivity
Wavelength

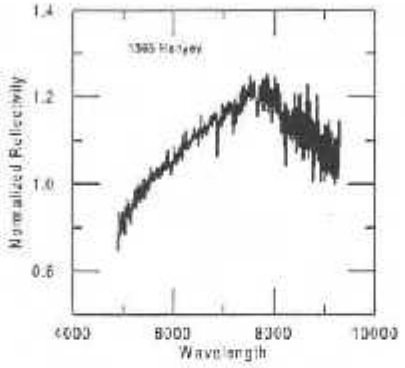
1365 Hetgyey
Normalized Reflectivity
Wavelength

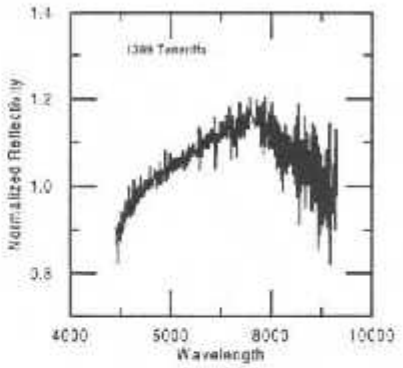
1388 Tenerife
Normalized Reflectivity
Wavelength

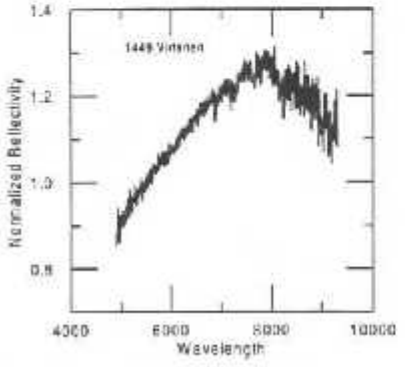
1449 Virtanen
Normalized Reflectivity
Wavelength

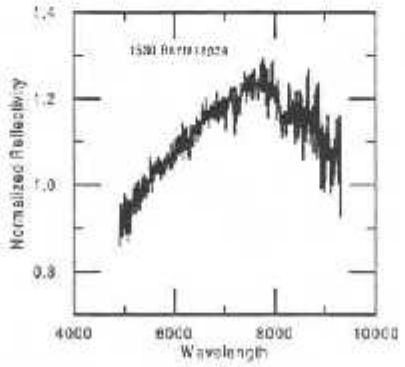
1580 Betrattista
Normalized Reflectivity
Wavelength

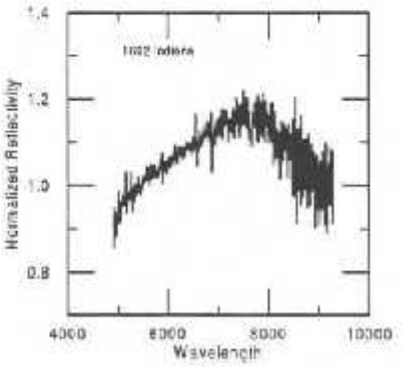
1602 Indiana
Normalized Reflectivity
Wavelength

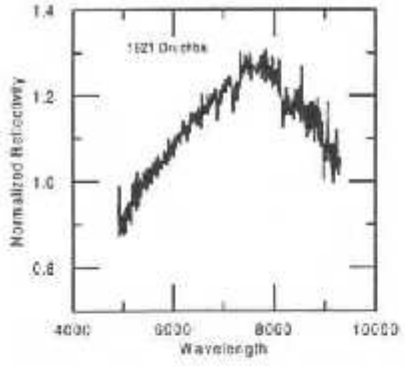
1621 Drachma
Normalized Reflectivity
Wavelength

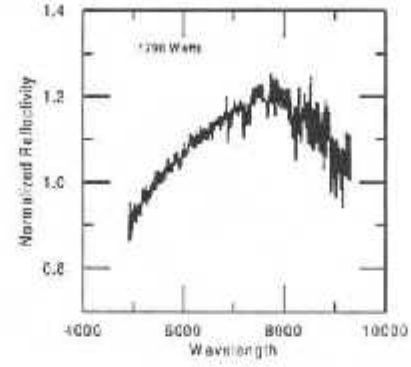
1790 Wam
Normalized Reflectivity
Wavelength

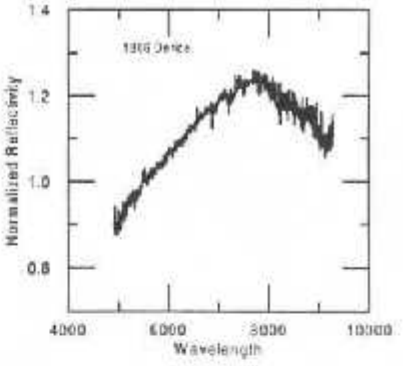
1866 Sisyphus
Normalized Reflectivity
Wavelength

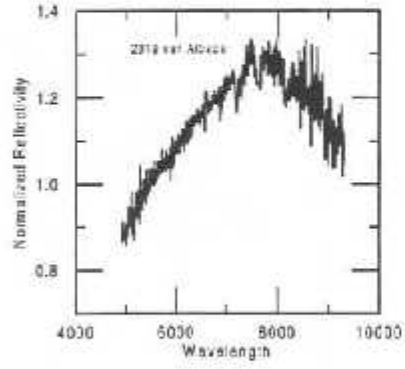
2312 van Albada
Normalized Reflectivity
Wavelength

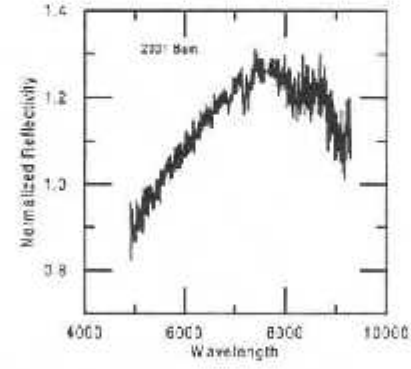
2331 Bam
Normalized Reflectivity
Wavelength

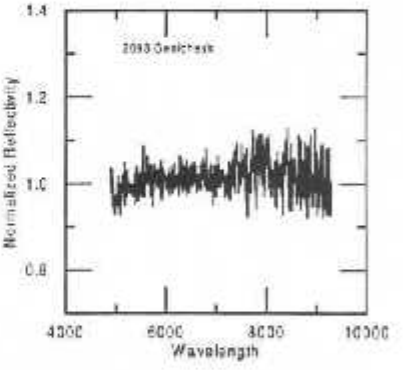
2393 Geelchaik
Normalized Reflectivity
Wavelength

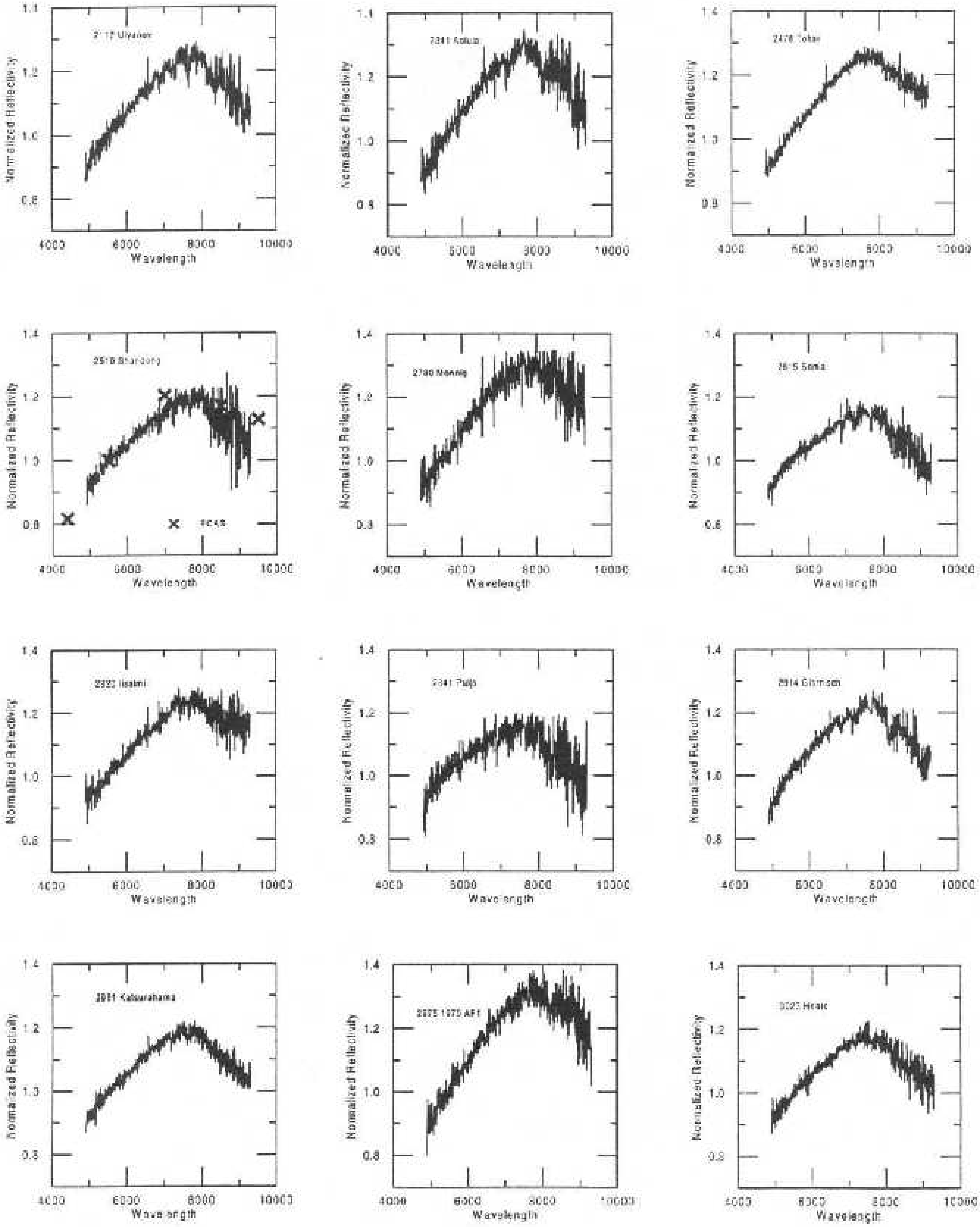
Normalized Reflectivity
Wavelength
4000
6000
8000
10000
0.8
1.0
1.2
1.4

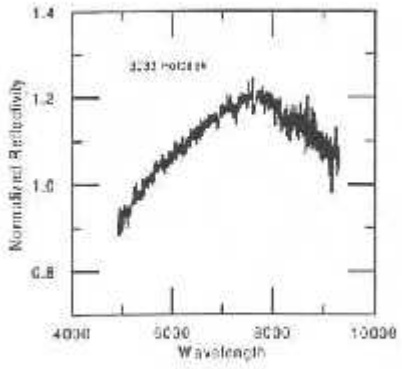
Normalized Reflectivity
Wavelength

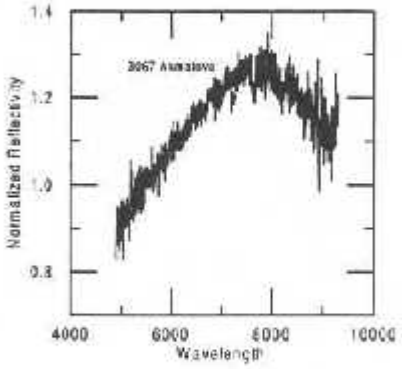
3067 Akhiezer
Normalized Reflectivity
Wavelength

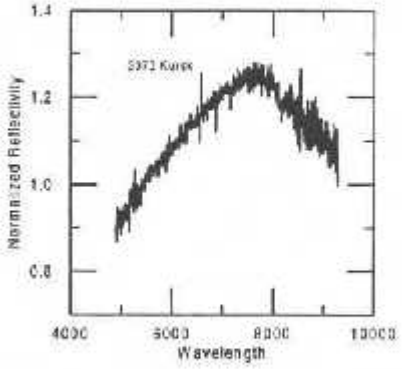
Normalized Reflectivity
Wavelength

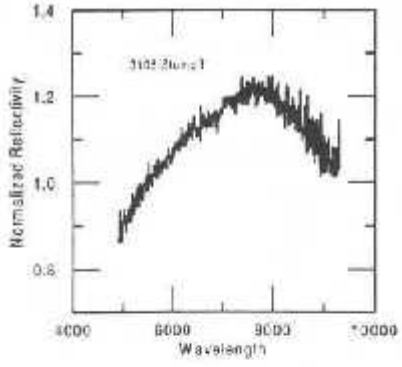
Normalized Reflectivity
Wavelength

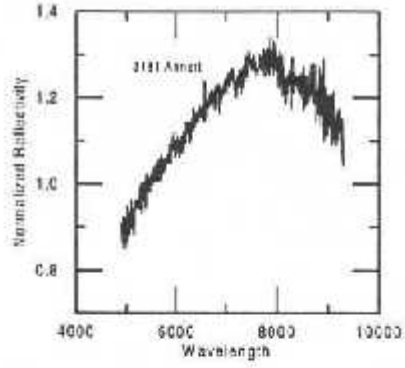
Normalized Reflectivity
Wavelength

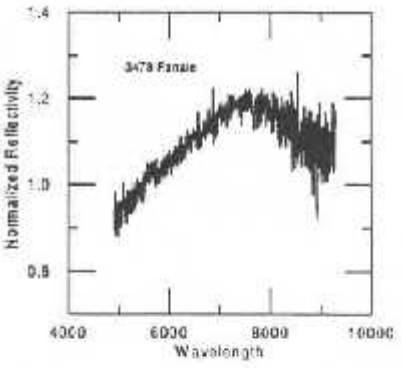
3478 Fanale
Normalized Reflectivity
Wavelength

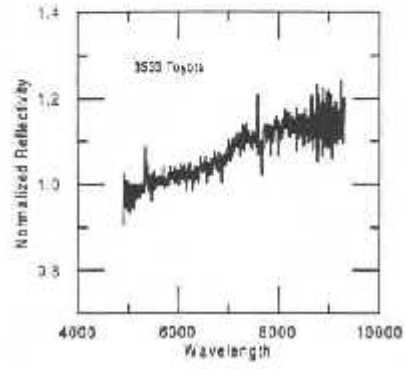
Normalized Reflectivity
Wavelength

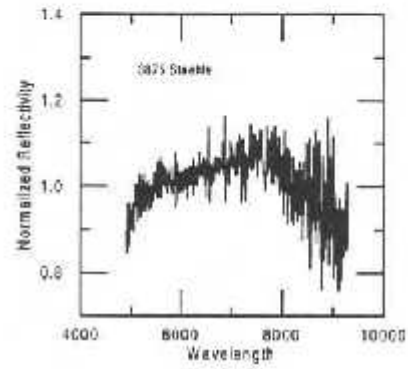
Normalized Reflectivity
Wavelength

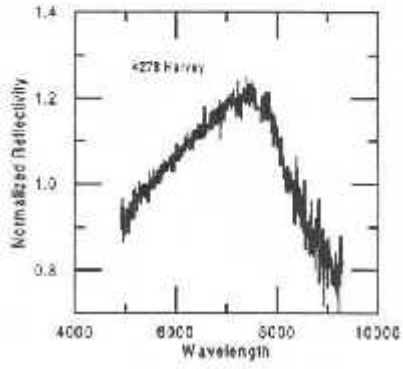
Normalized Reflectivity
Wavelength

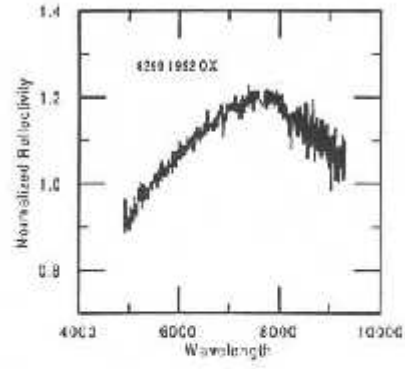
Normalized Reflectivity
Wavelength

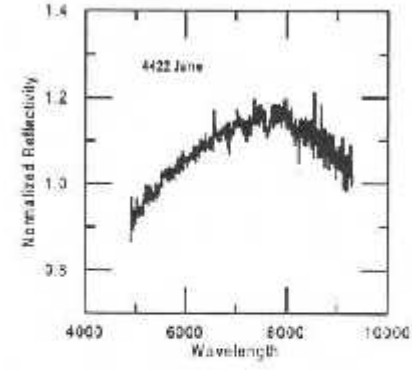
Normalized Reflectivity
Wavelength

c) Família de Themis

Descoberta por Hirayama em 1918, esta é uma das famílias mais bem identificadas dinamicamente, possuindo semi-eixo maior próprio entre 3,06 a 3,23 U.A.. Seus maiores membros são: 24 Themis com 182 km de diâmetro, 171 Ophelia com 117 km, 90 Antiope com 120 km e 268 Adorea com 140 km. Os restantes tem diâmetros inferiores a 100 Km. A figura 1 (ver seção c.1, a seguir) mostra a distribuição dos elementos próprios desta família em relação ao seu tamanho.

Adicionando as massas de todos os membros desta família podemos concluir que o corpo original deve ter tido no mínimo 300 km de diâmetro. Segundo o modelo colisional proposto por Marzari e co-autores (1995), a família de Themis foi formada de uma colisão entre um corpo alvo de 380 km e um projétil de 190 km, a cerca de 2,3 bilhões de anos atrás. Do ponto de vista dinâmico, esta família é peculiar pois está próxima da ressonância 2/1 com Júpiter, e sua distribuição é fortemente interrompida na borda desta ressonância (Morbidelli *et al.*, 1995), sendo esta possivelmente responsável pela eliminação de parte dos fragmentos originais.

Segundo o trabalho de Zappalà e co-autores (1995), esta família possui 550 membros, com um pequeno número de objetos de fundo (Migliorini *et al.*, 1995). Com o objetivo de caracterizar espectroscopicamente os objetos desta família e obter alguns dados sobre sua origem e evolução, observamos 36 asteróides desta população. Nossos resultados são descritos brevemente a seguir, enquanto que o artigo completo referente a esta família é apresentado em seguida. As figuras e tabelas citadas aqui são referentes ao artigo.

Os espectros obtidos possuem características similares aos asteróides do tipo C e seus subtipos B, G e F. Apenas 2, 461 Saskia e 1171 Rusthawelia, diferem dos demais, possuindo um espectro próximo dos asteróides do tipo P. A figura 2 mostra uma comparação de nossos espectros com os dados de ECAS (Zellner *et al.*, 1985) para os asteróides classificados como C e seus subtipos.

Como muitos asteróides destes tipos taxonômicos possuem bandas que indicam um processo de alteração aquosa, analisamos os espectros desta família. Encontramos

15 objetos que possuem estas bandas com o mínimo centrado em 0,60-0,65, ou 0,7, ou 0,8-0,9 μm, ou ainda em uma combinação destas bandas. Outros 11 asteróides possuem uma indicação da existência desta banda, mas suas profundidades se confundem com o ruído. A figura 3 mostra um ajuste polinomial dos espectros ilustrando estas bandas de absorção. Dos 4 objetos anteriormente classificados como do tipo F, apenas 954 Li mostra uma possível banda de alteração aquosa, confirmando de certa forma a hipótese levantada por Sawyer (1991) e Vilas e co-autores (1993, 1994) de que estes asteróides teriam uma composição pouco ou nada alterada.

Nossos resultados indicam que o corpo original da família de Themis era alterado termicamente o suficiente para ocorrer uma hidratação. O fato de termos objetos que apresentam bandas de alteração aquosa e outros não, pode significar que esta hidratação não tenha ocorrido de forma homogênea no corpo original. Assim a distribuição de composição pode ser devida ao fato de que os fragmentos teriam tido origem em partes distintas do corpo.

Encontramos também uma dependência das bandas de alteração aquosa com o diâmetro: 60 % dos objetos maiores do que 50 km possuem esta banda e 35 % não a apresentam. Esta tendência já tinha sido observada por Vilas e Sykes (1996) na análise de uma amostra de objetos do tipo C e subtipos. Eles propuseram que os corpos maiores poderiam ser fragmentos do interior de corpos originais onde o aquecimento teria sido mais eficiente. A figura 5 mostra todos os espectros dos objetos desta família (mostramos o ajuste polinomial deste espectros para melhor compreenção) normalizados em 0,7 μm, onde vemos que a distribuição espectral para os objetos maiores que 50 km é ligeiramente menor do que para os objetos menores que 50 km. Isto pode significar que os eventos colisionais que geram preferencialmente objetos menores, devem fazer com que estes apresentem uma diversidade maior em sua composição, pois seriam originários de partes distintas de um corpo maior. Por outro lado, os objetos maiores sofreriam um processo colisional menos intenso, mantendo sua superfície mais intacta, e inclusive recapturando gravitacionalmente partes de sua superfície retirada através de uma colisão.

Analisando a distribuição do albedo com o diâmetro (fig 6) encontramos também uma maior diversidade de albedos para os objetos menores, embora este resultado não seja

muito confiável devido aos grandes erros dos albedos. Entretranto esta tendência parece confirmar a hipótese de que o corpo original de Themis apresentava uma leve diferenciação sendo que os corpos menores viriam das camadas mais externas. Não descartamos a hipótese de que um processo de alteração espacial ocorreu preferencialmente em corpos menores, ou de que o alvo e o projétil da colisão original tivessem uma composição levemente diferente. Estas duas últimas hipóteses são menos prováveis pois, na primeira, não é conhecido um processo físico-químico capaz de provocar este efeito, enquanto que a segunda acarretaria em duas populações bem distintas, o que não é verificado.

Comparamos também nossos resultados com os de Di Martino e co-autores (1997) sobre a família de Veritas, que se encontra aproximadamente à mesma distância heliocêntrica e que difere apenas em excentricidade e inclinação. Eles encontraram uma maior heterogeneidade na composição e uma menor quantidade de objetos com alteração aquosa. Esta heterogeneidade na composição leva-nos a supor que os eventos térmicos sofridos pelos corpos originais ocorreram em épocas e/ou forma diferentes. Como o corpo original de Themis era maior, é de se supor que este corpo tenha sofrido um processo térmico mais eficiente devido à maior presença de radionuclídeos (Grimm e McSween, 1993), o que explicaria a maior quantidade de objetos com indicação de alteração aquosa. Uma outra possibilidade seria a de que o evento colisional que originou a família de Veritas fosse anterior ao de Themis, fazendo com que o corpo original de Themis sofresse por mais tempo este tipo de aquecimento. Entretanto, isto não está de acordo com os modelos de formação destas duas famílias, os quais indicam que a família de Themis é mais velha do que a de Veritas (Milani e Farinella, 1994). Outra hipótese seria a de que Veritas não seja uma família, o que contradiz as análises estatísticas de Zappalà e co-autores (1995) que confirmam a existência de uma família com alto grau de confiabilidade.

ASTRONOMY & ASTROPHYSICS
SUPPLEMENT SERIES

Astron. Astrophys. Suppl. Ser. 134, 1–10 (1998)

A spectroscopic study of the Themis family*,**,***

M. Florczak[1,2], D. Lazzaro[1], T. Mothé-Diniz[1], C.A. Angeli[1], and A.S. Betzler[1]

[1] CNPq/Observatório Nacional Depto. Astrofísica, 20921-400 Rio de Janeiro, Brazil
e-mail: florczak@on.br, lazzaro@on.br
[2] CEFET, Depto. Física, 80000 Curitiba, Brazil

Received July 3; accepted September 4, 1998

Abstract. We present spectroscopic observations of 36 asteroids, members of the Themis family. These observations were carried on at the European Southern Observatory in the wavelength range 4900 – 9200 Å. Most of the objects present a spectra similar to C-type asteroids and some of them present indicative of aqueous alteration. We discuss the implications of these results on the formation and evolution of this family.

Key words: minor planets, asteroids

1. Introduction

Themis is one of the most statistically reliable family in the asteroid belt. First discovered by Hirayama (1918), along with Eos and Koronis, it has been identified as a family in all subsequent works (see Zappalà et al. 1995, and references therein). According to a modern view (Farinella et al. 1992) the term "family" should be attributed only to clusters of asteroids whose physical properties support a common origin. Thus, the study of surface composition of Themis members is fundamental to define or, at least, constrain its collisional origin. Furthermore, if there is no doubt, from a statistical and physical point of view, that these are indeed fragments resulting from the breakup of a parent-body, thus important constraints on the latter can be obtained. The information about whether parent-body was differentiated or primitive will lead, consequently, to constraints on the primordial temperature of the solar nebula which is fundamental for a correct modelling of the Solar System formation.

A very striking feature of Themis family is its closeness to the border of the 2/1 mean motion resonance, as shown by Morbidelli et al. (1995). This resonance corresponds to the Hecuba gap, the widest of all the gaps in the asteroid belt, on which much work has been done in the last years trying to understand its depletion mechanism (see Henrard et al. 1995; Morbidelli 1996; Moons 1997; Ferraz-Mello et al. 1998). According to Morbidelli et al. (1995), when the Themis family is plotted in an appropriate resonant phase space, its rightmost limit is coincident with the border of the 2/1 resonance. As a consequence they suggest that the catastrophic event which gave rise to Themis family might once have populated the resonance zone. Due to some depletion mechanism all the objects were then swept off this region, creating the gap. If this assumption is true, then it implies that fragments, similar to those present today in the Themis family, might have been "transported" to other regions of the asteroid belt. It has also been suggested (Dermott et al. 1992, and references therein) that collisions in the Themis family could contribute to the formation of the Zodiacal Cloud. A precise surface characterization of asteroids members of Themis family can, therefore, help to investigate the fate of fragments injected in the Hecuba gap.

In the present paper we report spectroscopic observations of 36 asteroids, members of the Themis family, and discuss the implications of these results on the formation and evolution of this family. In the next section we present a short characterization of the Themis family and discuss some hypothesis on the fragmentation which gave origin to it. The observations and data reduction are presented in Sect. 3 along with a discussion of their implications on the origin and evolution of the family. A summary of the main results of the present work is given in the last section.

* Based on observations made with the 1.52 m telescope at the European Southern Observatory (La Silla, Chile) under the agreement with the CNPq/ Observatório Nacional.
** Table A1 is available at the CDS via anonymous ftp 130.79.128.5 or http://cdsweb.u-strasbg.fr/Abstract.html
*** Appendix A is only available at the journal, http://www.edpsciences.com

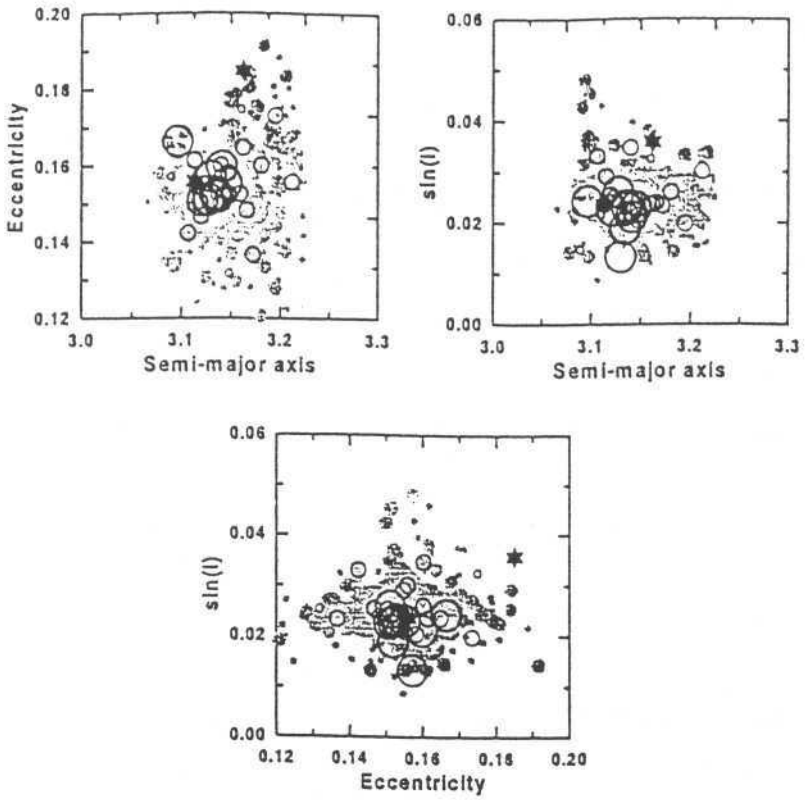

Fig. 1. Distribution of the Themis family in proper elements phase space: a) semi-major axis × eccentricity, b) semi-major axis × sine of inclination, and c) eccentricity × sine of inclination. The size of the circles is proportional to the diameter of the objects and the open circles indicate those observed in the present work (available on-line)

2. The Themis family

Themis family is located in the outer part of the main belt with proper semi-major axis in the region from 3.06 to 3.23 AU. The orbits have relatively high eccentricities and small inclinations. The Themis family, as determined by Zappalà et al. (1995) has 550 members: four – 24 Themis, 90 Antiope, 171 Ophelia, and 268 Adorea – with a diameter greater than 100 km, ten with diameter in the range 50 – 100 km while the remaining are smaller than 50 km. The expected size limit of completeness for this family corresponds to 20 km (Zappalà & Cellino 1995). According to Migliorini et al. (1995), the expected number of interlopers is relatively low, even if one or two can be expected at sizes as large as 40 km.

The distributions of the proper elements in the $a - e$, $a - \sin(i)$ and $e - \sin(i)$ planes are shown in Fig. 1, using Milani & Knezevic (1994) proper elements. In this figure the sizes of the circles are proportional to the diameter of the objects and the open circles indicate objects observed in the present work. The two stars indicate objects which might be interlopers as will be discussed in the next section. A core-halo structure, in which a dense "core" is surrounded by a "halo" of decreasing density, was initially described by Williams (1979, 1992). However, more recent studies do not present such a distribution but mostly a vertical dispersion at the border coincident with the 2/1 resonance. Zappalà et al. (1995) even introduce the denomination of "tribe" for this family due to its particular space distribution.

Since the pioneer work of Hirayama (1918) it has been assumed that families of asteroids are the outcome of one, or more, large impact of a body with a smaller "projectile" leading to the complete fragmentation or to the erosion of the parent body. From a statistical point of view this hypothesis is confirmed by the clustering observed when the planetary perturbations are removed, i.e., in the proper elements phase space. In this sense Themis family is undonbtedly one of the most reliable. However, the breakup mechanism which originated any family, as well as the subsequent evolution of its fragments, still rely on a wide set of working hypotheses and initial parameters which may not be the real ones (see, for example, Farinella et al. 1982; Fujiwara 1982; Zappalà et al. 1984; Davis et al. 1985; Farinella & Davis 1992; Bottke et al. 1994; Marzari et al. 1995). Notwithstanding the limitation of these models, some hypotheses on the Themis family formation are mostly accepted: i) The parent body was completely disrupted; ii) The family is the outcome of a very energetic collision, probably unique in all the asteroid belt, with original parent body and projectile of 380 km and 190 km, respectively (Marzari et al. 1995); iii) Such a collision has

a very low probability to occur over the age of the Solar System; iv) The large remnants are probably "rubble-pile" shaped by their self-gravitation (Fujiwara 1982; Farinella et al. 1982). The mineralogical characterization of Themis family members' surfaces can, therefore, help to constrain the collisional model of its formation.

3. Observations and data reduction

The observations were carried on at the European Southern Observatory at La Silla (Chile) using a 1.5-m telescope equipped with a Boller and Chivens spectrograph and a CCD 2048 × 2048 pixels with a readout noise of ±7 electrons. A grating of 225 gr/mm with a dispersion of 330 Å/mm in the first order was used. The CCD has a square 15 μm pixel, giving a dispersion of about 5 Å/pixel in the wavelength direction. The useful spectral range is about $4900 < \lambda < 9200$ Å with a FWHM of 10 Å. The spectra were taken through a 5 arcsec slit oriented in the East-West direction. The slit width has been chosen in order to minimize the consequences of atmospheric differential refraction and reduce the loss of light at both ends of the spectrum. This is important since a substantial loss of light may lead to an erroneous spectral characterization of the object. Care was taken also in guarantee that the observations were made as near as possible to the meridian of the asteroid.

The spectra of Themis family asteroids were obtained in five observing runs in January/97, March/97, July/97, December/97, January/98 and March/98. The atmospheric conditions were good to excellent during all the observations. The observational circumstances, from EPHEM program (Tholen 1997), are listed in Table 1, which shows the distance from the Sun, from the Earth, the solar phase angle, the estimated visual magnitude and the diameter. The given diameters are from IRAS (Tedesco 1997) whenever available, otherwise are estimated through the absolute magnitude and a visual albedo of 0.081 which is the mean albedo of Themis' family objects.

The spectral data reduction was performed using the Image Reduction and Analysis Facility (IRAF) package and taking much care to ensure a proper calibration of the spectra. The bias level of each night was determined through an average of the many bias images taken in the night. This "averaged bias" was then subtracted from each frame and pixel-to-pixel variations were removed dividing the resulting image by a normalized medium "flat field". The IRAF apsum package was used to sum the pixel values within a specified aperture and to subtract the background level. Wavelength calibration was performed using a He-Ar lamp, obtained several times during each night, and spectra were corrected from airmass by using the mean extinction curve of La Silla (Tüg 1977). Different solar analogs (Hardorp 1978) were observed in each observational run in order to compute reflectivities. It must be pointed out that in each night of observation were observed at least two solar analogs in order to estimate the quality of the night. The ratios between the spectra of the solar analogs for each night show no substantial variation. The influence of different solar analog on the resulting spectra has also been checked showing differences less than $1\%/10^3$ Å. In Table 1 are given only the solar analogs used to obtain the spectra presented. All asteroid spectra are normalized around 5500 Å by convention, unless otherwise specified.

4. Spectroscopic results and discussion

The obtained spectra, normalized at 5500 Å, are given in the Appendix. In these figures only one spectrum per object is given and the crosses indicate observations from the ECAS survey (Zellner et al. 1985). Most of the asteroids show similar featureless spectra, characteristic of C-, B-, F- and G-type asteroids. Two of them, 461 Saskia and 1171 Rusthawelia, display P-type spectra. In effect, Tholen (1989) also classifies the latter as P-type.

In order to compare the overall characteristic of the Themis family, a polynomial has been fitted to each spectrum and the result is presented in Fig. 2a along with ECAS spectra represented by dash lines. In this figure, spectra of a same asteroid obtained in different nights are also individually included. The figure shows a limited spread of the superficial composition between the members of the Themis family. The compositional distribution is completely contained in the distribution of the C-type class and its sub-classes B, F and G as can be seen in Figs. 2b to 2e. In these figures, the distribution of broadband spectra obtained from ECAS's survey for each of the above classes is plotted. This result, therefore, is consistent with a probable common origin of the observed asteroids except 461 Saskia and 1171 Rusthawelia which might be background objects. It must be recalled that in the region around 3.2 AU the P class objects should be abundant (Bell et al. 1989). The compositional analysis of a significative sample of Themis members, therefore, supports the dynamical/statistical indication of a common origin of the family, probably resulting from the breakup of a C-type parent body. In this scenario, the asteroids 461 and 1171 would be background objects. It is noteworthy that only 1171 Rusthawelia lies at the border of the family while 461 Saskia is contained well inside the nuclear region.

Considering that a collisional origin of the Themis family can be inferred, a question remains on whether the original parent body, or its fragments, experienced some degree of aqueous alteration. This information can set some constraints on the primordial nebula and the temperature gradient, or events, during the first stages of the Solar System formation. We recall that aqueous alteration is the low temperature (< 320 K) chemical alteration of materials by liquid water (Vilas & Sykes 1996, and references

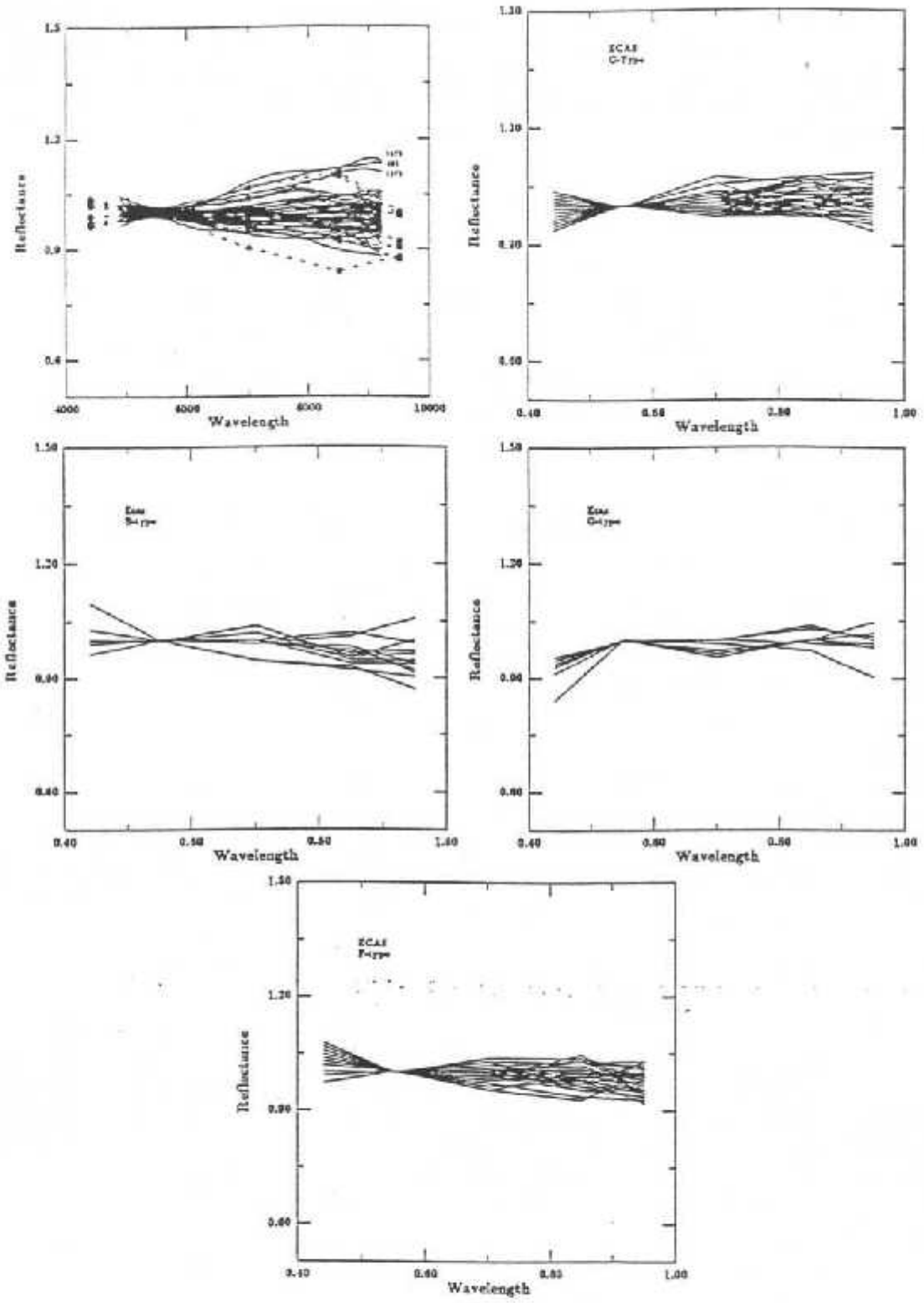

Fig. 2. a) Spectra of the Themis family presented in this work normalized around 5500 Å and fitted by a polynomial for clarity along with ECAS data (Zellner et al. 1985) represented by the dashed lines. b) Distribution of broadband spectra of C-type objects obtained from ECAS's survey. c) Same as b) for B-type objects. d) Same as b) for G-type objects. e) Same as b) for F-type objects

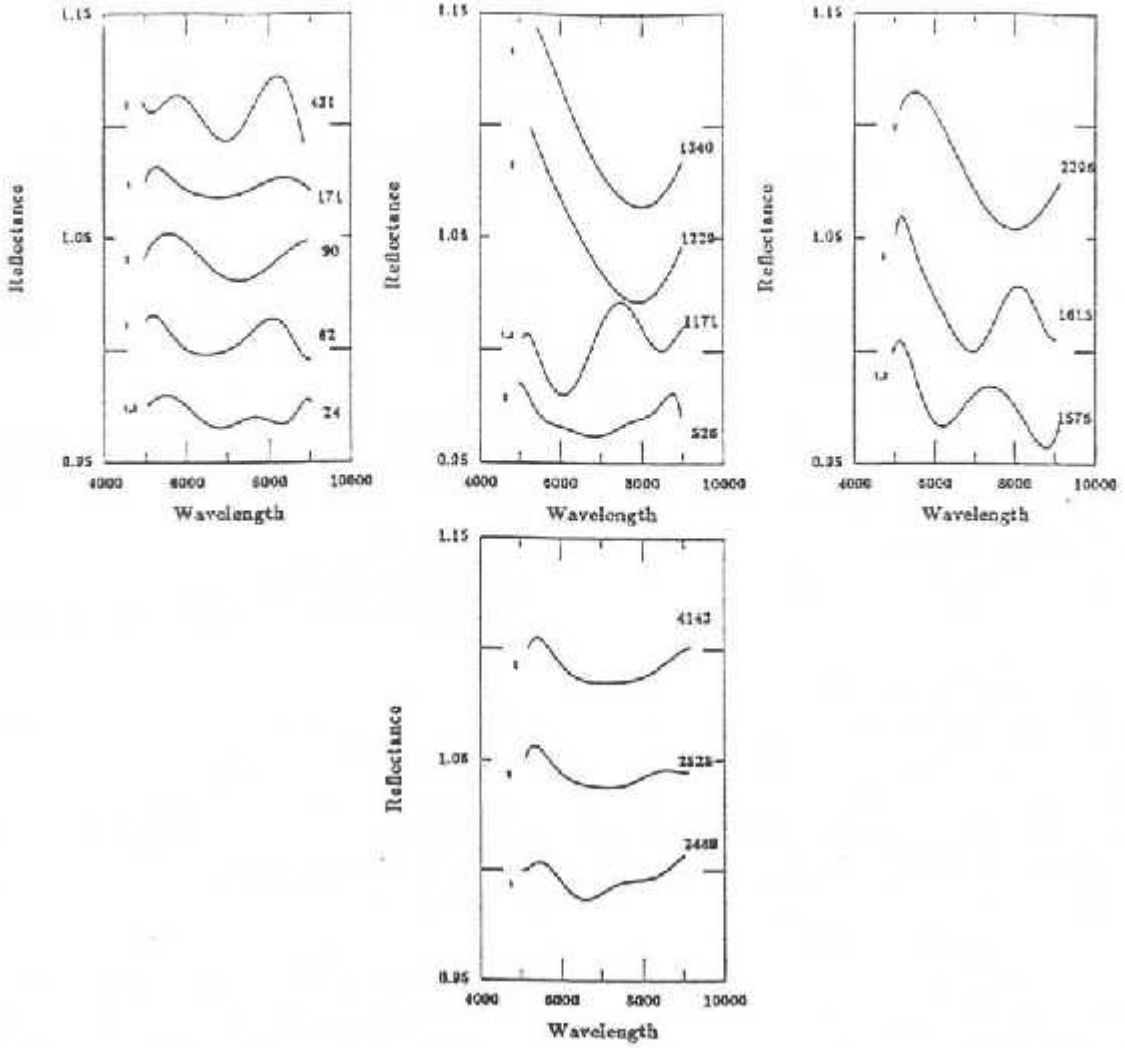

Fig. 3. Asteroids presenting absorption bands with minimum at 0.6 – 0.65 (1), 0.7 (2), and 0.80 – 0.90 μm (3), indicative of aqueous alteration in their surfaces. Each spectrum is fitted by a polynomial to increase the identification of the bands. For each spectrum is given the identified band (1, 2 or 3) at its left and the asteroid number at its right

therein). In order to investigate this aspect of the Themis family, aqueous alteration was searched in the spectra following the procedure described by Vilas et al. (1993, 1994). Indication of aqueous alteration, identifiable by the presence of absorption bands with minimum at 0.60–0.65, 0.7 or 0.8 – 09 μm, is clearly present in the spectra of 15 asteroids[1] among the observed ones. Since these bands are sometimes very swallow, their identification is highly dependent on the noise of the spectra so that we adopted the criterion defined by Vilas et al. (1993) in which a band is identified if its depth is greater than the peak-to-peak scatter. If a more relaxed criterion is adopted, 11 more objects could also present aqueous alteration in their surface. As already pointed out by Vilas et al. (1993), in some cases the 0.65 and 0.90 μm absorption bands seem to overlap with the 0.70 μm band making their identification difficult. In Figs. 3a to 3d we show the polynomial fit to the spectra of asteroids that show clear indication of aqueous alteration through the 0.7, 0.65 or 0.90 μm absorption band. The asteroids 316, 637, 846, 848, 954, 1487, 1539, 1691, 2519, 2524, and 3128 may also present indication of aqueous alteration but with a lesser degree of confidence and, therefore, are not included in these plots.

In Figs. 4a and 4b we present the distributions of the observed asteroids as a function of the presence or not of aqueous alteration. In these figures the triangles and squares represent objects with and without indication of aqueous alteration, respectively. The stars represent objects that may present aqueous alteration and the size of all the symbols is proportional to the diameter of the asteroids. Considering the taxonomy of the observed objects,

[1] Asteroids 1229, 1340 and 2296 present a strong unusual absorption band between 0.8 and 0.9 μm, confirmed in spectra obtained in different nights, with the exception of 1229 observed once.

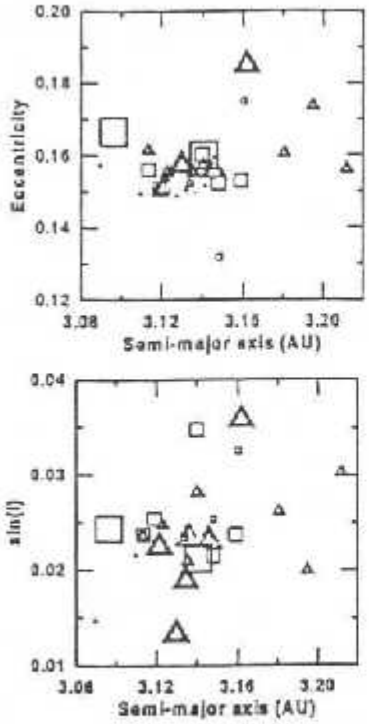

Fig. 4. Distribution, in the proper elements space, of the observed asteroids as a function of the presence (triangles) or not (squares) of aqueous alteration. The stars represent objects which may present aqueous alteration but with a lesser degree of confidence. The size of all the symbols is proportional to the diameter of the asteroids

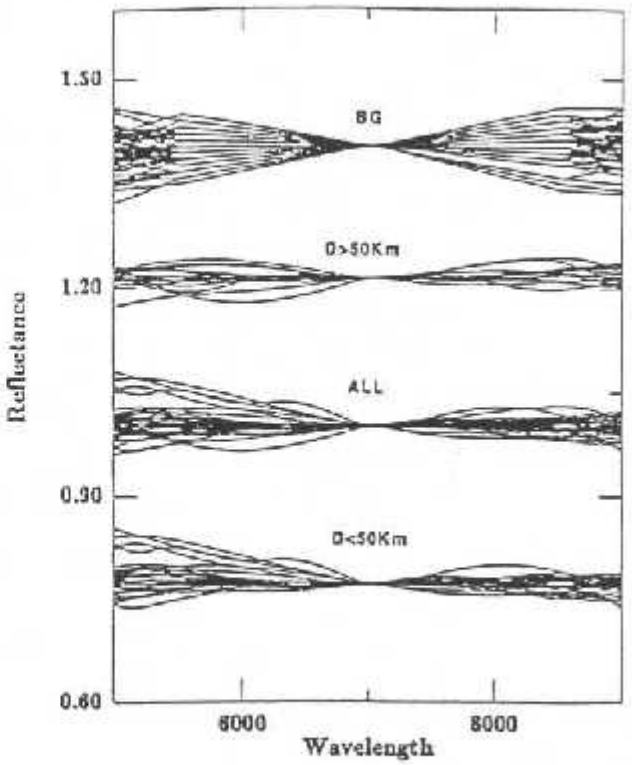

Fig. 5. Spectra normalized at 0.7 μm of bakground objects from ECAS (Zellner et al. 1985), of all the asteroids observed in the present work and of the observed asteroids with diameter greater and smaller than 50 km

all those classified by Tholen (1989) as F do not present indication of thermal metamorphism. This is clear in three of them: 268 Adorea, 468 Lina, and 621 Werdandi, classified as FC, CPF and FCX, respectively. Another asteroid classified as FCX, 954 Li, might or not present aqueous alteration by our analysis. These results confirm earlier suggestions (Sawyer 1991; Vilas et al. 1993; Vilas et al. 1994) that F-class asteroids may be unaltered material or that they are less or differently altered. In a recent paper, Hiroi et al. (1996) plot the UV absorption strength (the most prominent absorption band indicative of aqueous alteration) vs. IRAS diameter for the C, G, B and F asteroids. In their plot the F-type asteroids all present the smallest absorption band or the total absence of it. This fact is interesting since it can indicate a different evolution of this type of objects. In particular for the Themis family, it would imply a different degree of thermal alteration in different parts of the original parent body or a distinct origin of these objects. This last assumption seems not to be supported by the limited spread out in composition shown by our spectra.

Analyzing the percentage of asteroids presenting indication of aqueous alteration as function of the diameter, a trend is apparent: it decreases with the diameter of the objects. The percentage changes from nearly 60% to 35% for asteroids with diameter greater and smaller than 50 km, respectively. This trend is expected by Vilas & Sykes (1996) if we suppose the break-up of a thermally altered parent body. In their model, the bigger fragments should retain more information on the interior of the parent body where the heating event should have been more effective. If in the 11 objects which may have aqueous alteration this fact is confirmed, then the above percentages would increase to nearly 80% and 70%, respectively, and the trend is less evident.

The above results tend to indicate that the parent body of the Themis family was thermally altered and the distribution of compositions can be attributed to fragments coming from different parts of the original body. Following Vilas & Sykes (1996), if the original parent body was altered due to a thermal event in the later phases of the Solar System formation, then all the resulting fragments from a breakup should also present signs of aqueous alteration, in particular the greatest ones. This is true for the Themis family and the percentage of asteroids presenting absorption bands due to aqueous alteration decreases with the object size, as expected by Vilas & Sykes (1996).

The dependence of the distribution of surface compositions with the diameter was further investigated. In Fig. 5 it can be seen the spectra, normalized at 0.7 μm, of the observed asteroids of the Themis family along with

background objects from ECAS (Zellner et al. 1985). The figure also presents our spectra divided in asteroids with diameter greater and lesser than 50 km, respectively. As can be seen, the distribution is slightly larger for the small asteroids. It is noteworthy to point out that this result is also expected by Vilas & Sykes (1996). In their model the small asteroids would be fragments resulting from the breakup of a thermally altered large asteroid. Since these fragments would come from diverse compositional units of the original body, they will present a great degree of differences between them. On the other hand, the larger asteroids should be reaccreted bodies representing the original core displaying, therefore, a smaller degree of diversity.

In Fig. 5 we notice that the distribution of spectra of the Themis family is similar or sligtly smaller than that of background objects. It must be pointed out, however, that a direct comparison is quite imprecise since the two types of spectra, ECAS and ours, were obtained with different techniques. A better comparison would be with a background defined from SMASS (Xu et al. 1995) or from an analogous survey. Since there are too few spectra of this region in the SMASS, the real representation of the background is not guaranteed.

We also analyzed the distribution of IRAS albedo in the Themis family, where a slight correlation with the diameter seems apparent. In Fig. 6 it can be seen a larger dispersion of albedos as the objects' sizes decrease. In particular, higher albedos are displayed by smaller asteroids. However, it must be pointed out that the error bars associated to the individual IRAS albedo are greater as the diameter decreases. Taking into account this fact the trend is less apparent even if it still remains an indication, which is compatible with our spectra (Fig. 5). If this specific albedo distribution between family members is real it can imply in, at least, three distinct scenarios:

- A space weathering process acting distinctly depending on the size of the objects.
- The original parent body presented a slightly differentiated crust. In this case most of the smaller asteroids would be part of the crust presenting an albedo distinct from the bigger ones, which would be mostly reaccreted bodies from the nucleus. If this is the case, the nucleus would have an albedo around 0.02 to 0.07, and crust values greater than 0.08. This hypothesis would imply that lighter materials present in the crust would be more reflective than the denser materials of the nucleus.
- The collision that gave rise to the Themis family occurred between a parent-body and a projectile of slightly different composition. We recall that Marzari et al. (1995) in their model of Themis' family collisional evolution, obtained the best result with a parent-body and projectile sizes of 380 km and 190 km, respectively. Since the two bodies probably were not formed in the same region (otherwise the collision velocity would not lead to the catastrophic breakup of a so big object) different compositions can be expected. Moreover, since the projectile body was relatively large, its fragments would be a considerable part of the remnants. This hypothesis is, obviously, the most difficult to be accepted in view of the quite homogeneous results from the spectroscopic observations.

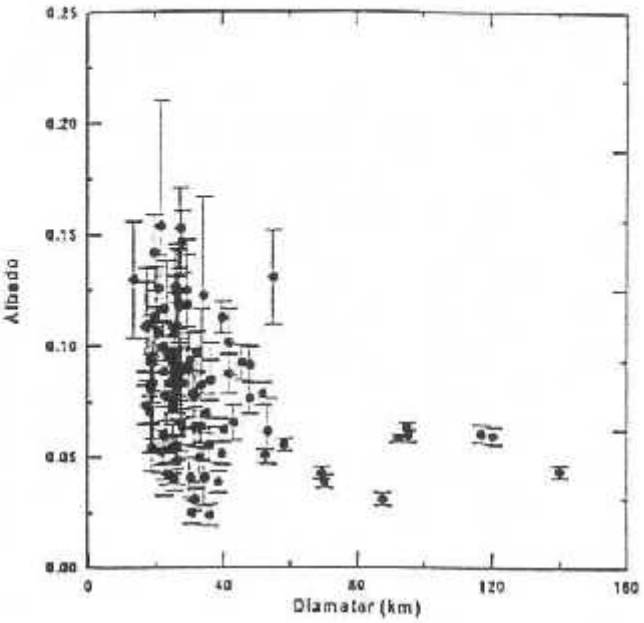

Fig. 6. Distribution of the albedos of Themis family members as a function of their diameters. A larger dispersion is apparent as the object size decreases

Among the observed objects with a known albedo, the presence of aqueous alteration was found in both low and (relatively) high albedo objects of the Themis family. Unfortunately the number of objects with available albedos and spectra is not statistically significative to permit us to find a relation between aqueous alteration and the above scenarios.

Finally the results for the Themis family were also compared to those obtained by Di Martino et al. (1997) for the Veritas family. It must be recalled that these two families occupy nearly the same heliocentric region in the outer belt. From a dynamical point of view, the greatest difference between these families is that while Themis family presents relatively high eccentricities (from .12 to .19, proper elements) and small inclinations, Veritas family members have small eccentricities (around 0.06) but relatively high inclinations (around 10 degrees). Since the two families lie at the same heliocentric distance, it seems obvious to expect that a temperature gradient, or event, should act similarly on the two original bodies. However, a remarkable greater inhomogeneity is apparent in the Veritas family, as can be seen comparing our Fig. 5 with Fig. 3 of Di Martino et al. (1997) paper (note that the scales in two plots are identical) (OR: ...comparing Fig. 5a

with b taken from Di Martino et al. 1997). Moreover, only three asteroids of this family seem to present indications of aqueous alteration. These results set the basis for several scenarios for the origin of the two families:

1) The heating event that thermally altered Themis original body occurred after the breakup of the Veritas family. This assumption, however, is not supported by the dynamical analysis of this family. In effect, Milani & Farinella (1994) proved that Veritas should be one of the youngest families in the asteroid belt due to the chaoticity of 490 Veritas, as well as other members;
2) Since the original parent body of the Themis family was larger than that of Veritas (around 100 km) the thermal event was more efficient in the former. This result would favor the hypothesis that the thermal event was due to the ^{26}Al decay (Grimm & McSween 1993), since larger bodies would retain more radionuclides which would generate a greater and throughout heating of the asteroid;
3) The Veritas family was not originated from the breakup of a large body, but it would just represent a clustering of background objects. Again this assumption is not supported by the statistical clustering analysis of this family, which confirms a highly reliable Veritas family (Zappalà et al. 1995).

5. Summary

In this section we summarize the important points presented in this paper:

- Most of the observed 36 members of Themis family show featureless spectra similar to C-, B-, G- and F-type. The distribution of these spectra is completely contained in the range of the above classes;
- A limited spread of the distribution of superficial composition is apparent, confirming the dynamical indication of a probable common origin from the fragmentation of a parent-body;
- Two objects, 461 Saskia and 1171 Rusthawelia, display a spectra similar to P-type suggesting that they might not be members of the Themis family but just background objects;
- Indication of aqueous alteration is clear in 15 objects and is possibly present in 11 more. This result tends to indicate that the parent-body of Themis family was probably thermally altered. This hypothesis is also supported by the larger percentage of objects presenting aqueous alteration among the big asteroids than among the small ones;
- A slight correlation between albedos and diameters is found: as the asteroid diameter decreases a larger dispersion of albedos is present and higher albedos are displayed by smaller asteroids. The same slight correlation is apparent in our spectra as discussed above.
- Comparison between Themis and Veritas families, which lie nearly at the same heliocentric distance, shows a greater inhomogeneity among the latter one. On the other hand, the presence of aqueous alteration is more prominent in the Themis family. One of the possible explanations is that since the original parent body of Themis was larger than that of Veritas a thermal event leading to metamorphism (probably due to the ^{26}Al decay) was more efficient in the former.

From the analysis of 36 members of Themis family we can conclude that a compositional homogeneity is present as would be expected from the collisional breakup of an original parent body. On the other hand, a slight heterogeneity is also apparent from the presence or not of aqueous alteration and from slightly distinct albedo populations between the family.

Acknowledgements. We acknowledge the technical staff of the ESO for their prompt help whenever needed. We are also grateful to V. Zappalà for valuable comments and remarks which much improved this paper. M.F. was supported by CAPES while D.L., T.M-D., C.A.A., and A.S.B. by CNPq, through diverse fellowships and grants. Support by FAPERJ is also acknowledged.

References

Bell J.F., Davis D.R., Hartmann W.K., Gaffey M.J., 1989, Asteroids: The big picture, in: Asteroids II, Binzel R., Gehrels T., Matthews M.S. (eds.). Univ. of Arizona Press, Tucson, p. 921
Bottke W.F., Nolan M.C., Greenberg R., Kolvoord R.A., 1994, Icarus 107, 255
Davis D.R., Chapman C.R., Weidenschilling S.T., Greenberg R., 1985, Icarus 62, 30
Dermott S.F., Gomes R.S., Durda D.D., Gustafson B.A.S., Jayaraman S., Xu Y.L., Nicholson P.D., 1992, Dynamics of the Zodiacal Cloud. In Chaos, Resonance and Collective Dynamical Phenomena in the Solar System, Ferraz-Mello S. (ed.), IAU Symposium 152. Dordrecht, p. 333-347
Di Martino M., Migliorini F., Zappalà V., Manara A., Barbieri C., 1997, Icarus 127, 112
Farinella P., Davis D.R., 1992, Icarus 97, 111
Farinella P., Paolicchi P., Zappalà V., 1982, Icarus 52, 409
Farinella P., Davis D.R., Cellino A., Zappalà V., 1992. A proposal for a new nomenclature, in: Asteroids Comets Meteors 1991, Harris A.W., Bowell E. (eds.), Lunar Planet Inst. Huston, p. 165
Ferraz-Mello S., Nesvorný D., Michtchenko T.A., 1998, Chaos, diffusion, escape and permanence of resonant asteroids in gaps and groups. In Solar System Formation and Evolution, Lazzaro D., Vieira Martins R., Ferraz-Mello S., Fernandez J., Beugé C. (eds.), ASP Conf. Ser. (in press)
Fujiwara A., 1982, Icarus 52, 433
Grimm R.E., McSween H.Y., 1993, Sci 259, 653
Hardorp J., 1978, A&A 63, 383
Henrard J., Watanabe N., Moons M., 1995, Icarus 115, 336
Hirayama K., 1918, AJ 31, 185

Hiroi T., Zolensky M.E., Pieters C.M., Lipschutz M.E., 1996, Meteor. Planet. Sci 31, 321
Marzari F., Davis D., Vanzani V., 1995, Icarus 113, 168
Migliorini F., Zappalà V., Vio R., Cellino A., 1995, Icarus 118, 271
Milani A., Farinella P., 1994, Nat 370, 40
Milani A., Knezevic Z., 1994, Icarus 107, 219
Moons M., 1997, Cel. Mech. Dyn. Astr. 65, 175
Morbidelli A., 1996, AJ 111, 2453
Morbidelli A., Zappalà V., Moons M., Cellino A., Gonczi R., 1995, Icarus 118, 132
Sawyer S.R., 1991, A High Resolution CCD Spectroscopic Survey of Low Albedo Main Belt Asteroids, Ph.D. dissertation, University of Texas
Tedesco E.F., 1997, "IMPS diameters and albedos V1.0" Planetary Data System - Small Bodies Node (PDSSBN); A'Hearn M., University of Maryland, College Park, Maryland (available http://pdssbn.astro.umd.edu)
Tholen D., 1989, Asteroid taxonomic classification, in: Asteroids II, Binzel R., Gehrels T., Matthews M.S. (eds.). Univ. of Arizona Press, Tucson, p. 1139
Tholen D., 1997, Ephemeris program EPHEM, Version 1.1, Celestech, Honolulu, Hawaii
Tüg H., 1977, Messenger 11, 7
Vilas F., Sykes M.V., 1996, Icarus 124, 483
Vilas F., Larson S.M., Hatch E.C., Jarvis K.S., 1993, Icarus 105, 67
Vilas F., Jarvis K.S., Gaffey M.J., 1994, Icarus 109, 274
Williams J.G., 1979, Proper elements, families and belt boundaries, in: Physical Studies of Minor Planets, Gehrels T. (ed.), NASA SP-267, U.S. Government Printing Office. Washington, p. 177
Williams J.G., 1992, Icarus 96, 251
Xu S., Binzel R.P., Burbine T.H., Bus S.J., 1995, Icarus 115, 1
Zappalà V., Cellino A., 1995, Main belt asteroids, In Present and future inventory, ASP Conf. Ser.
Zappalà V., Farinella P., Knezevic Z., Paolicchi P., 1984, Icarus 59, 261
Zappalà V., Cellino A., Farinella P., Knezevic Z., 1990, AJ 100, 2030
Zappalà V., Cellino A., Farinella P., Milani A., 1994, AJ 107, 772
Zappalà V., Bendjoya P., Cellino A., Farinella P., Froeschlé Cl., 1995, Icarus 116, 291
Zellner B., Tholen D.J., Tedesco E.F., 1985, Icarus 61, 355

Table A1. Observational circumstances: Exp is the number of exposures, R and Δ are the heliocentric and geocentric distances, respectively, α is the solar phase, m_v is the visual magnitude, and D is the diameter ((*) IRAS diameter)

Asteroid	UT Date dd/mm/yy	Exp.	R(AU)	Δ (AU)	α	m_v	D (km)	Analog
24 Themis	16,20/03/97	03	2.708	1.975	16.7	11.6	181.66	HD44594
62 Erato	07,13/07/97	03	3.291	2.277	1.5	13.3	95.39*	HD44585
90 Antiope	05,06/03/98	03	3.484	2.500	2.5	13.2	120.07*	HD44595
171 Ophelia	07,09/07/97	02	3.479	3.427	16.9	14.6	116.69*	HD44585
	24,30/12/97	03	3.352	3.053	16.8	14.2		HD44594
268 Adorea	09,15/07/97	04	3.341	2.601	13.6	13.8	139.89*	HD44585
316 Goberta	08/07/97	02	3.641	2.757	9.1	15.4	47.92*	HD44585
431 Nephele	09/01/97	02	2.814	2.716	20.4	14.1	95.03*	HD44594
461 Saskia	13/07/97	01	3.577	2.627	6.8	13.8	37.95	HD44585
468 Lina	17/03/97	02	3.694	2.759	6.2	15.4	69.34*	HD44594
526 Jena	07,08,09/03/98	03	2.869	2.119	15.1	14.9	41.49*	HD44595
621 Werlandi	04/07/97	02	3.477	2.736	12.9	16.1	27.15*	HD44585
637 Chrysothemis	16/03/97	02	2.713	1.720	1.4	14.5	29.87	HD44594
846 Lipperta	08/07/97	02	3.596	2.943	13.8	16.2	52.42*	HD44585
848 Inna	06,13/07/97	03	2.572	1.823	18.3	15.2	31.28	HD44585
954 Li	09/01/97	01	3.597	3.008	13.7	15.9	58.03*	HD44594
1003 Lilofee	09/01/97	01	2.845	2.652	20.2	15.6	43.18	HD44594
1171 Rusthawelia	07,13/07/97	03	2.896	2.327	18.7	15.0	70.13*	HD44585
1229 Tilia	08/03/98	01	3.712	2.720	0.5	16.2	27.65*	HD44595
1340 Yvette	06,07/03/98	03	2.843	1.851	0.9	14.8	25.87*	HD44595
1487 Boda	15/07/97	02	3.096	2.080	0.9	14.8	29.16*	HD44585
1539 Borrelly	04/01/98	01	3.214	2.462	12.9	15.8	35.91	HD44594
1576 Fabiola	07,14/07/97	03	3.225	2.251	6.2	15.8	27.25*	HD44585
1615 Bardwell	04,14/07/97	02	2.934	2.204	15.0	16.3	27.78*	HD44585
1691 Oort	26/12/97	01	3.045	2.310	14.2	16.0	30.57	HD44594
	03/01/98	01						HD44594
2296 Kugultinov	06,07/03/98	03	2.697	1.722	4.8	15.0	26.02	HD44595
2489 Suvorov	06,14/07/97	03	2.617	1.669	10.1	15.8	18.85	HD44585
2519 Annagerman	09/07/97	01	2.613	2.026	20.8	15.9	26.02	HD44585
2524 Budovicium	06,13/07/97	04	2.635	1.618	0.4	14.1	31.39*	HD44585
2525 O'Steen	06,13/07/97	03	2.759	1.901	13.7	14.9	37.61	HD44585
3128 Obruchev	06,14/07/97	02	2.675	2.098	20.4	16.3	23.73	HD44585
3274 Maillen	04/07/97	01	2.811	1.938	12.8	15.5	18.00	HD44585
3507 Vilas	06,14/07/97	03	2.756	2.160	19.4	16.2	26.02	HD44585
3615 Safronov	04,14/07/97	03	2.824	2.527	21.0	16.5	28.53	HD44585
3663 Tisserand	04,13/07/97	02	2.718	1.767	9.5	16.5	15.68	HD44585
3832 Shapiro	04,13/07/97	02	3.033	2.057	6.5	17.0	15.68	HD44585
4143 1981 QN_1	09,15/07/97	03	2.626	1.656	8.3	16.3	18.00	HD44585

Appendix A: Spectra of observed asteroids

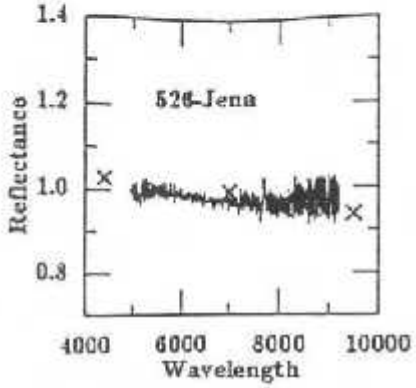
526-Jena
Reflectance
Wavelength
1.4
1.2
1.0
0.8
4000
6000
8000
10000

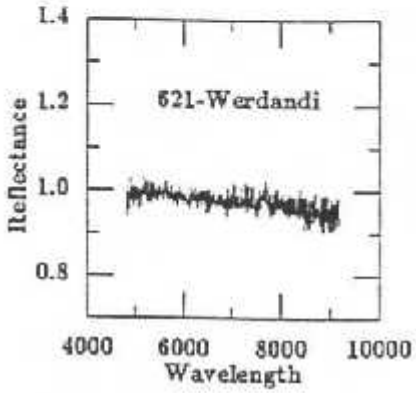
621-Werdandi
Reflectance
Wavelength
1.4
1.2
1.0
0.8
4000
6000
8000
10000

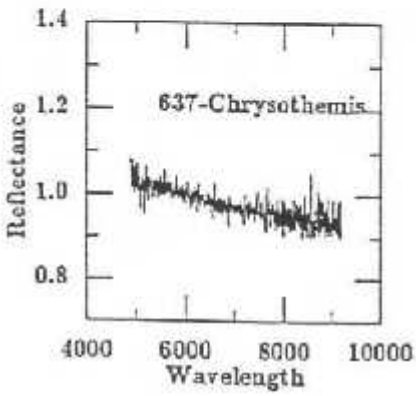
637-Chrysothemis
Reflectance
Wavelength
1.4
1.2
1.0
0.8
4000
6000
8000
10000

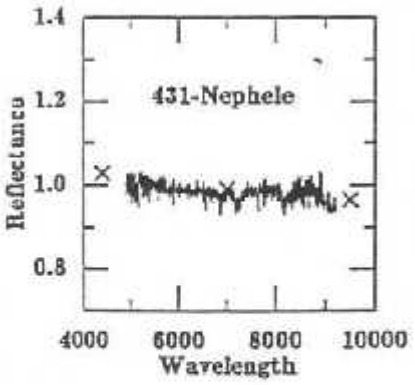
431-Nephele
Reflectance
Wavelength
1.4
1.2
1.0
0.8
4000
6000
8000
10000

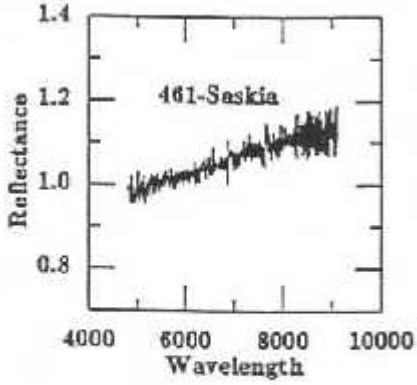
461-Saskia
Reflectance
Wavelength
1.4
1.2
1.0
0.8
4000
6000
8000
10000

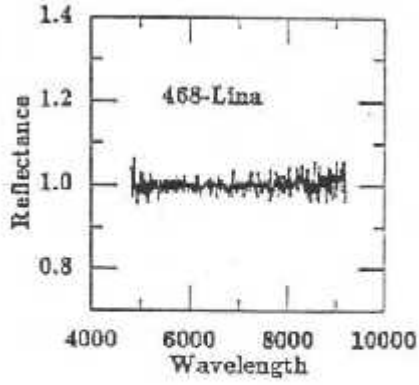
468-Lina
Reflectance
Wavelength
1.4
1.2
1.0
0.8
4000
6000
8000
10000

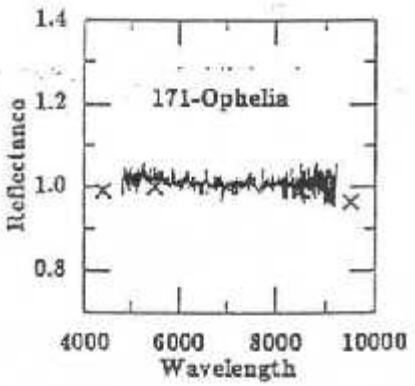
171-Ophelia
Reflectance
Wavelength
1.4
1.2
1.0
0.8
4000
6000
8000
10000

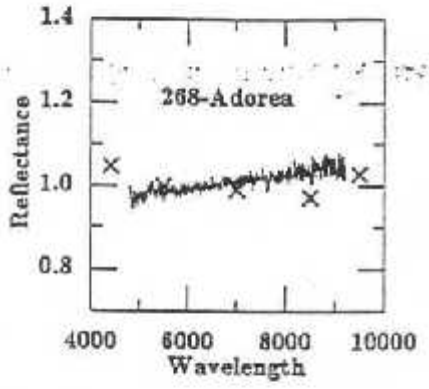
268-Adorea
Reflectance
Wavelength
1.4
1.2
1.0
0.8
4000
6000
8000
10000

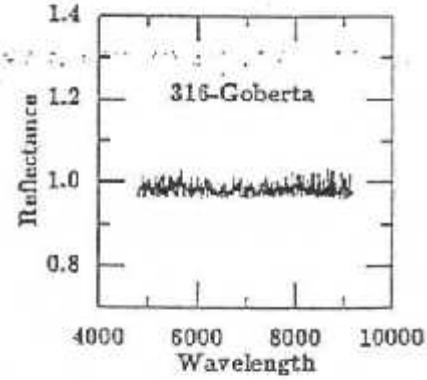
316-Goberta
Reflectance
Wavelength
1.4
1.2
1.0
0.8
4000
6000
8000
10000

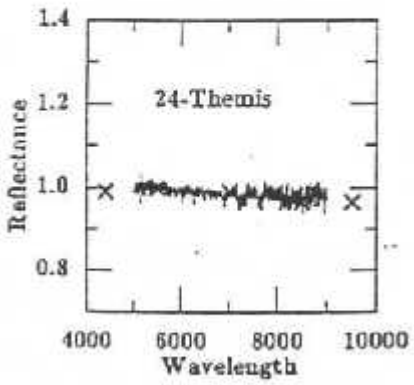
24-Themis
Reflectance
Wavelength
1.4
1.2
1.0
0.8
4000
6000
8000
10000

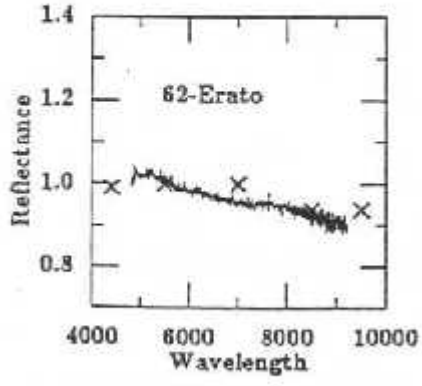
62-Erato
Reflectance
Wavelength
1.4
1.2
1.0
0.8
4000
6000
8000
10000

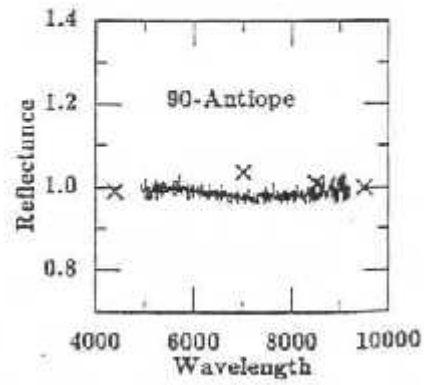
90-Antiope
Reflectance
Wavelength
1.4
1.2
1.0
0.8
4000
6000
8000
10000

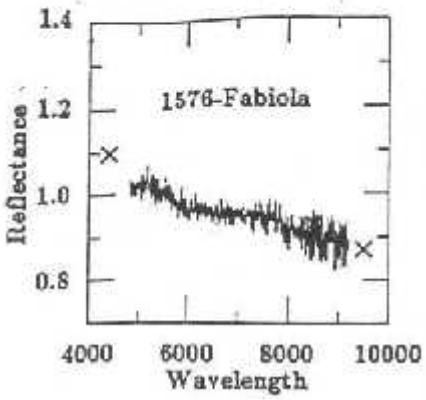
1576-Fabiola
Reflectance
Wavelength
1.4
1.2
1.0
0.8
4000
6000
8000
10000

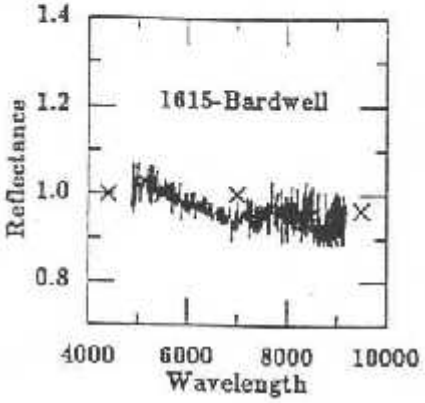
1615-Bardwell
Reflectance
Wavelength
1.4
1.2
1.0
0.8
4000
6000
8000
10000

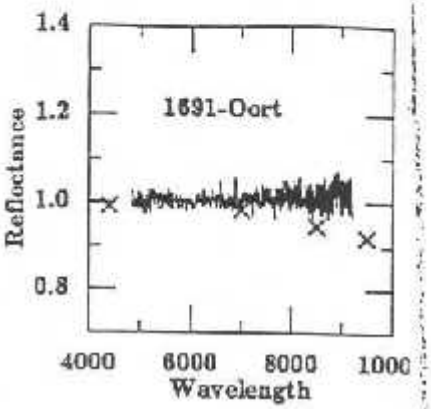
1691-Oort
Reflectance
Wavelength
1.4
1.2
1.0
0.8
4000
6000
8000
1000

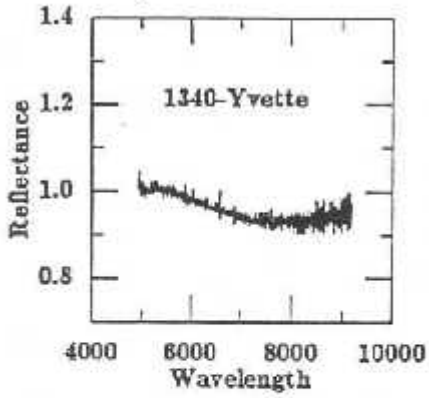
1340-Yvette
Reflectance
Wavelength
1.4
1.2
1.0
0.8
4000
6000
8000
10000

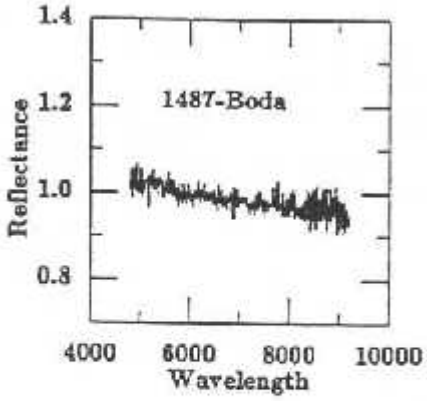
1487-Boda
Reflectance
Wavelength
1.4
1.2
1.0
0.8
4000
6000
8000
10000

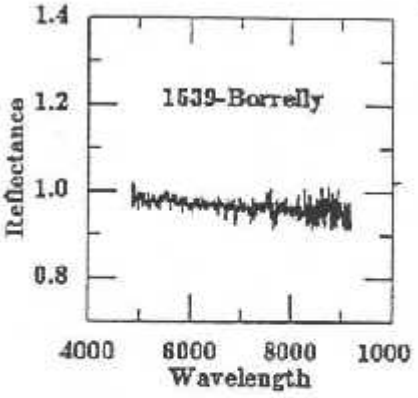
1539-Borrelly
Reflectance
Wavelength
1.4
1.2
1.0
0.8
4000
6000
8000
1000

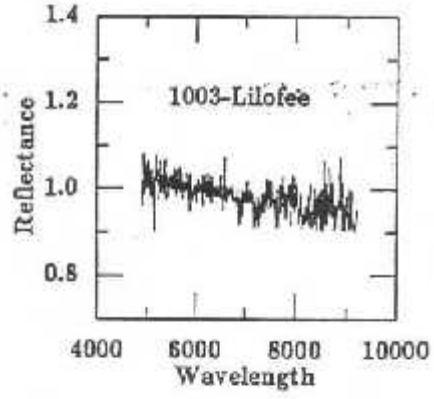
1003-Lilofee
Reflectance
Wavelength
1.4
1.2
1.0
0.8
4000
6000
8000
10000

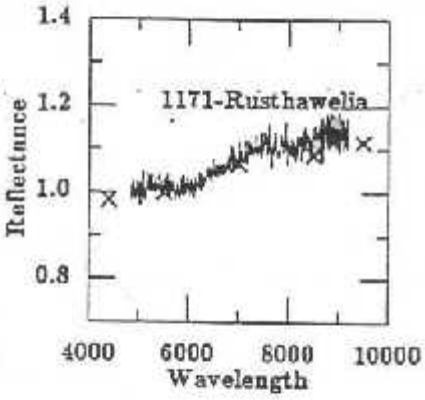
1171-Rusthawelia
Reflectance
Wavelength
1.4
1.2
1.0
0.8
4000
6000
8000
10000

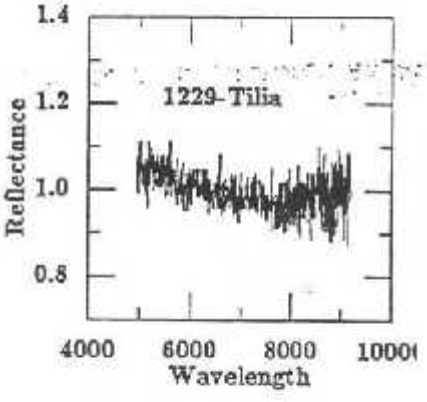
1229-Tilia
Reflectance
Wavelength
1.4
1.2
1.0
0.8
4000
6000
8000
10000

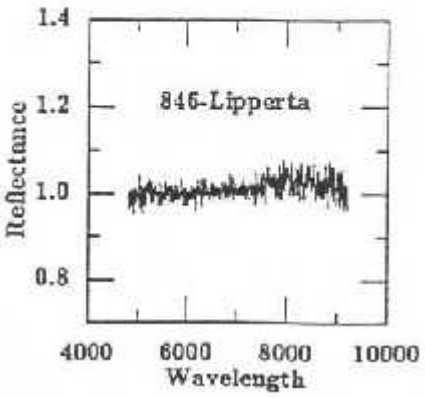
846-Lipperta
Reflectance
Wavelength
1.4
1.2
1.0
0.8
4000
6000
8000
10000

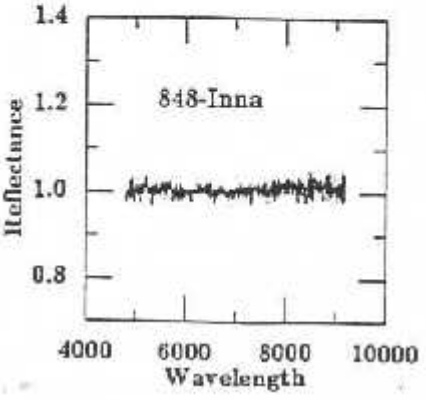
848-Inna
Reflectance
Wavelength
1.4
1.2
1.0
0.8
4000
6000
8000
10000

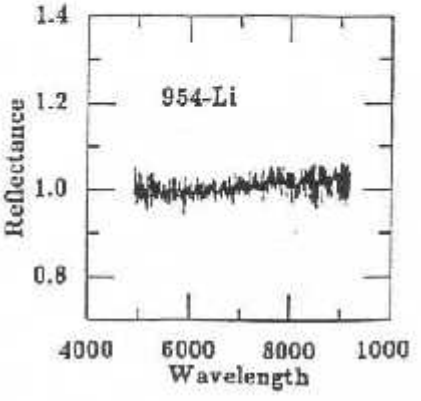
954-Li
Reflectance
Wavelength
1.4
1.2
1.0
0.8
4000
6000
8000
1000

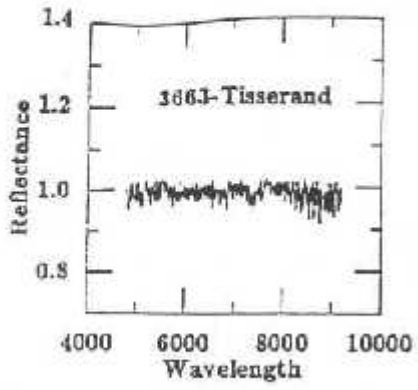
3663-Tisserand
Reflectance
Wavelength
1.4
1.2
1.0
0.8
4000
6000
8000
10000

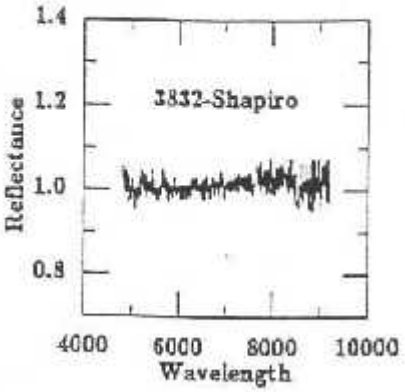
3832-Shapiro
Reflectance
Wavelength
1.4
1.2
1.0
0.8
4000
6000
8000
10000

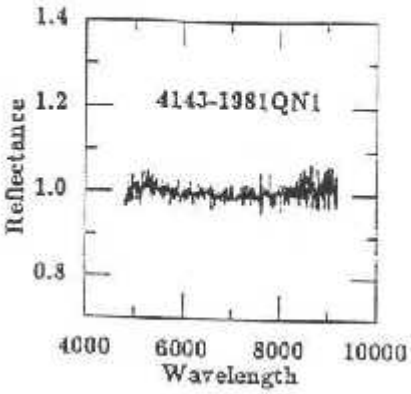
4143-1981QN1
Reflectance
Wavelength
1.4
1.2
1.0
0.8
4000
6000
8000
10000

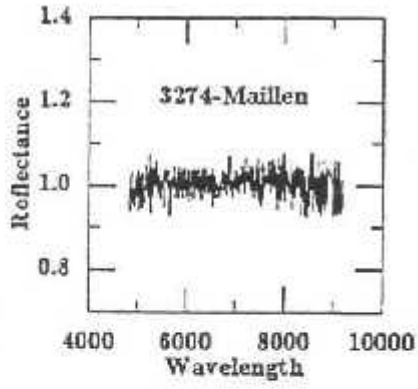
3274-Maillen
Reflectance
Wavelength
1.4
1.2
1.0
0.8
4000
6000
8000
10000

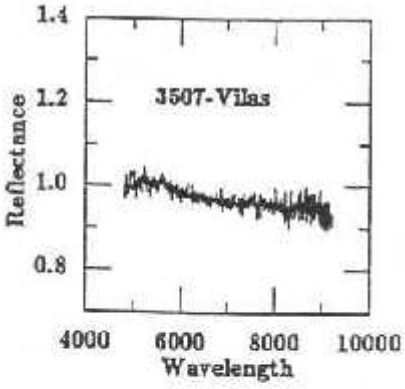
3507-Vilas
Reflectance
Wavelength
1.4
1.2
1.0
0.8
4000
6000
8000
10000

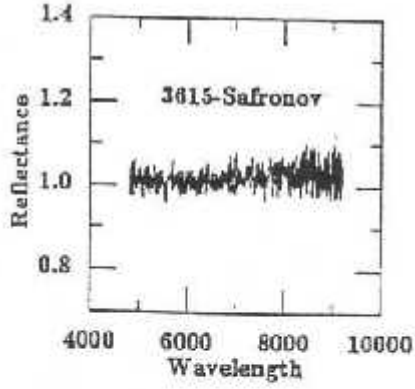
3615-Safronov
Reflectance
Wavelength
1.4
1.2
1.0
0.8
4000
6000
8000
10000

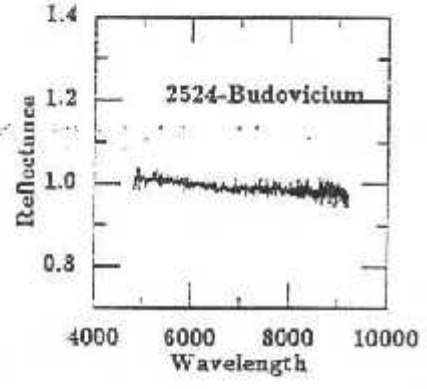
2524-Budovicium
Reflectance
Wavelength
1.4
1.2
1.0
0.8
4000
6000
8000
10000

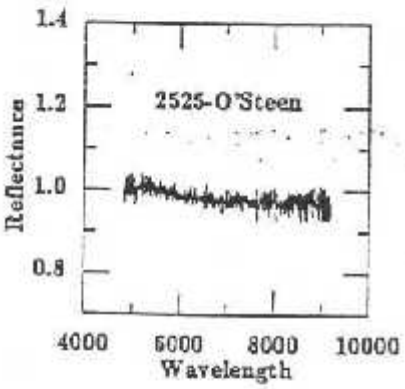
2525-O'Steen
Reflectance
Wavelength
1.4
1.2
1.0
0.8
4000
6000
8000
10000

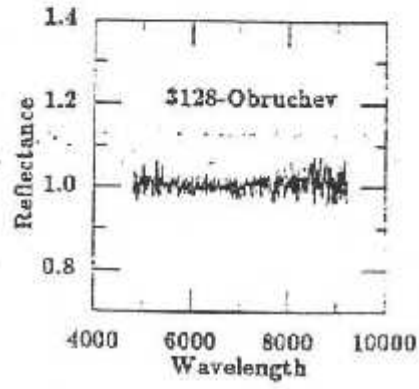
3128-Obruchev
Reflectance
Wavelength
1.4
1.2
1.0
0.8
4000
6000
8000
10000

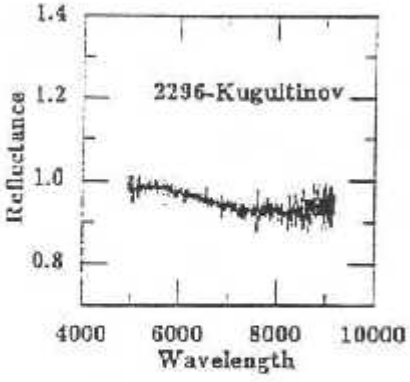
2296-Kugultinov
Reflectance
Wavelength
1.4
1.2
1.0
0.8
4000
6000
8000
10000

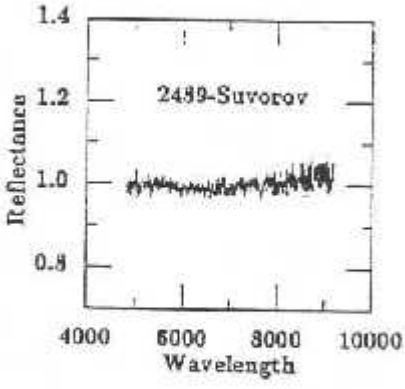
2489-Suvorov
Reflectance
Wavelength
1.4
1.2
1.0
0.8
4000
6000
8000
10000

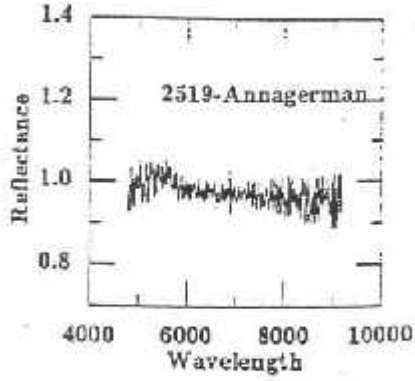
2519-Annagerman
Reflectance
Wavelength
1.4
1.2
1.0
0.8
4000
6000
8000
10000

3.3.4 - Objetos Candidatos à Missão Espacial ROSETTA

Rosetta é uma missão espacial da Agência Espacial Européia (ESA), com o objetivo de investigar objetos primitivos do Sistema Solar, com um estudo *in situ* de um núcleo cometário e o sobrevôo de dois asteróides do cinturão principal. Seu lançamento está previsto para 22 de janeiro de 2003 pela Ariane V.

O objetivo principal desta missão é estudar a origem dos cometas, a relação entre os cometas e o material interestelar e suas implicações sobre a origem do Sistema Solar. As medidas a serem feitas têm como finalidade:

- uma caracterização global do núcleo, determinação das propriedades dinâmicas, composição e morfologia superficial;
- a determinação das composições químicas, mineralógicas e isotópicas dos materiais voláteis e superficiais do núcleo cometário;
- a determinação das propriedades físicas e a interrelação entre os voláteis e o material superficial do núcleo cometário;
- uma caracterização de asteróides, incluíndo a determinação de propriedades dinâmicas, composição e morfologia superficial.

O cometa escolhido como alvo desta missão é o 46 P/Wirtanem, e os dois asteróides escolhidos para o sobrevôo são Otawara e Siwa (decisão tomada em 1998).

Estes sobrevôos terão características similares aos da missão Galileo de Gaspra e Ida. Como estes dois asteróides são do tipo S, foi dada prioridade na escolha de objetos mais primitivos como os do tipo D ou C, ou ainda objetos mais evoluídos termicamente, como os dos tipo V ou M. Por esta razão realizamos, nos anos de 1995, 1996 e 1997, observações espectroscópicas em 14 asteróides candidatos a esta missão. O artigo a seguir descreve detalhadamentes os nossos resultados, que podem ser resumidos em:

- até a época de publicação de nossos dados os asteróides 3840 Mimistrobell e 2703 Rodari eram os dois prováveis candidatos, sendo que Mimistrobell tinha sido observado por Barucci e Lazzarin (1995), sendo classificado pelas autoras como do

tipo S. Nossos dados mostram que Rodari também possui um espectro do tipo S, fazendo com que não seja um candidato ideal baseado no objetivo científico da missão, citado acima.

- nossos dados mostram que 5 objetos possuem espectros do tipo C, 7 do tipo S, um do tipo E e um apresenta características de E e M indistinguíveis (tab. 3).
- baseado no tipo espectral (C) e no tamanho (140 km de diâmetro), indicamos 140 Siwa como um forte candidato a esta missão, já que seu tipo espectral é mais primitivo do que o tipo S, e seu tamanho, o maior entre todos os candidatos, pode indicar uma menor evolução colisional.

Pergamon

Planet. Space Sci., Vol. 46, No. 1, pp. 75–82, 1998

0032–0633/98 $19.00 + 0.00

PII: S0032-0633(97)00128-1

Compositional type characterization of Rosetta asteroid candidates*

M. Antonietta Barucci,[1] Alain Doressoundiram,[1] Marcello Fulchignoni,[1,2] Marcos Florczak,[1,3] Monica Lazzarin[4] and Claudia Angeli[4]

[1]Observatoire de Paris, 92195 Meudon Principal Cedex, France
[2]Université "Denis Diderot" de Paris VII, Paris, France
[3]ON/CNPq, Dep. Astrofisica, 20921 Rio de Janeiro, Brazil
[4]Dip. di Astronomia, Vicolo dell'Osservatorio, 35122 Padova, Italy

Received 26 March 1997; accepted 8 June 1997

Abstract. The final selection of the two Rosetta target asteroids will be made in a successive phase of the Rosetta project development, when the engineering parameters will be frozen. In this paper we present spectroscopic observations of the possible Rosetta candidates and we discuss the results obtained, particularly the definition of their compositional type. We examine the possibility to select some more "primitive" candidates. On the basis of its size and spectral type, we suggest including the asteroid 140 Siwa as one of the asteroid targets of the Rosetta mission. © 1998 Elsevier Science Ltd

1. Introduction

The ESA Rosetta mission (launch in January 22, 2003) was scheduled to have a rendezvous with comet P/Wirtanen and two fly-bys to the asteroids 3840 Mimistrobell and 2530 Shipka (Announcement of Opportunity, ESA, March 1995). In 1996, ESA defined a new mission baseline, changing the second asteroid fly-by to 2703 Rodari, selected by the Rosetta Project on the basis of the minimum Δv cost criterion. The present Rosetta trajectory (Fig. 1) is a Mars–Earth–Earth gravity assisted (MEEGA) trajectory. The Mimistrobell fly-by is scheduled for September 16, 2006 in between the two Earth swing-bys, while the Rodari one will take place on April 5, 2008 in the last leg of the cruise toward comet P/Wirtanen. Visible spectra of these two candidates have been obtained with observations at the Canadian–French–Hawaiian telescope (CFHT) by Barucci and Lazzarin (1995) for Mimistrobell and in 1996 for Rodari (which results are presented in this paper). On the basis of the spectra of these two objects, they have been classified as S-type objects, which means they contain a mixture of pyroxene, olivine and Fe–Ni metal. Even though a more detailed knowledge of S-type asteroids is of high scientific interest (Gaffey *et al.*, 1993), it would be appropriate to select a "more primitive" candidate as an asteroid target in order:

1. to meet closely the primary objectives of the Rosetta mission, which is devoted to the investigation of the pristine Solar System materials;
2. to increase our knowledge on the "diversity" of the asteroid population, which is one of the most interesting characteristics of these objects.

For these reasons we present in the first part of Section 3 the results obtained for the possible alternative candidates, indicated by ESOC for the baseline launch window on January 22, 2003 to comet P/Wirtanen, on the basis of the closeness of the encounter with the Rosetta spacecraft with minimum Δv cost during the fly-by (see Table 1). In the second part of the section the observations of the asteroid candidates (ESA SCI(93)7) for other possible cometary scenarios are presented.

2. Observations and data reduction

All the observations have been performed at the European Southern Observatory (ESO) of La Silla (Chile) during several campaigns (1995, 1996 and 1997) except 2703 Rodari which has also been observed at Mauna Kea Observatory, Hawaii, on June 20, 1996. At ESO we used the 1.5 m telescope with a Boller and Chivens spectrograph and a CCD (2048 × 2048 pixels). The CCD has square 15 μm pixel, giving a dispersion of about 5 Å pixel^{-1} in the wavelength direction. The spectral range is about $0.48 < \lambda < 0.92$ μm with a FWHM of about 10 Å. The spec-

*Based on observations carried out at the Canadian–French–Hawaiian Telescope (CFHT), Hawaii, and at the European Southern Observatory (ESO) of La Silla, Chile
Correspondence to: M. A. Barucci

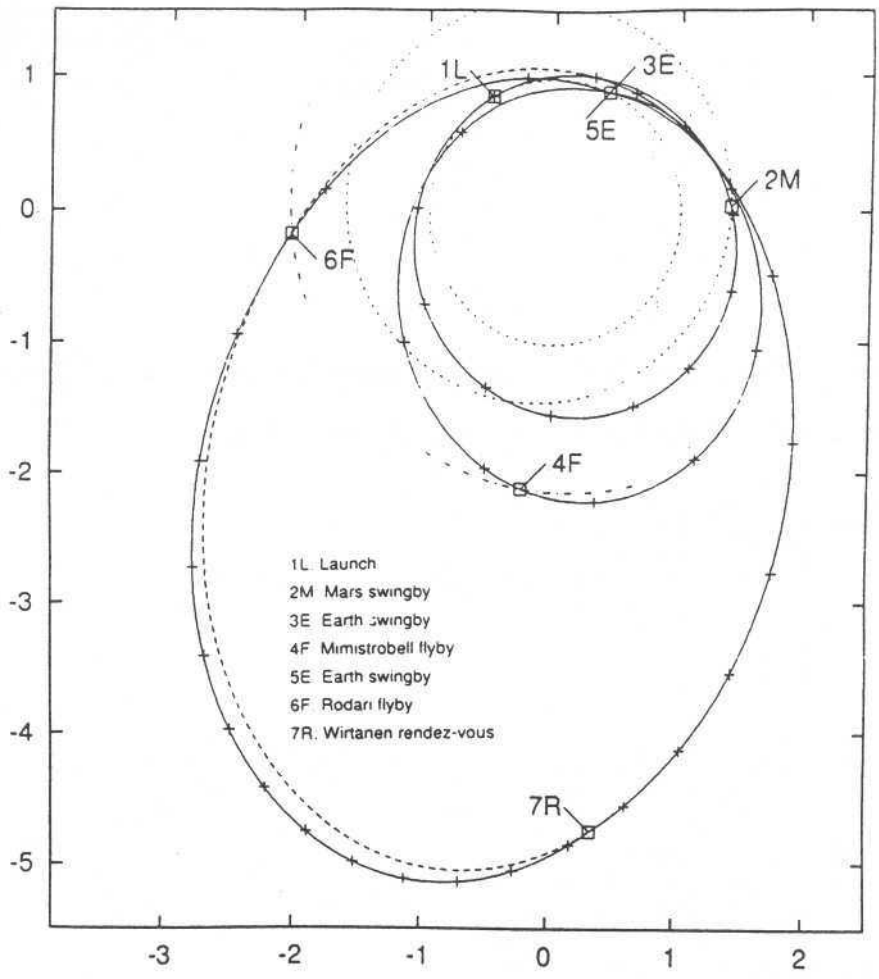

Fig. 1. The projection on the ecliptic plane of the Rosetta baseline trajectory. The Rosetta trajectory is represented with a solid line. The orbits of Earth and Mars are represented with dotted lines, and the orbit of the asteroids Mimistrobell and Rodari are represented with dot-dashed lines (courtesy of G. Schwehm)

tra were taken through a slit oriented in the East–West direction ranging between 2 and 4″.

At the Mauna Kea Observatory we used the 3.6 m Canadian–French–Hawaiian telescope equipped with the MOS (MultiObject Spectrograph) and the CCD STIS2 (2048 × 2048 pixels). The grism used is the V150 with a dispersion of 433 Å mm^{-1}. The spectral range covered is $0.4 < \lambda < 0.98$ μm with a spectral dispersion of 7 Å pixel^{-1}. A spectral resolution of about 30 Å has been obtained with a slit aperture of 1.7″.

Particular care was taken to ensure proper calibration of the asteroid spectra and several solar analog spectra have been secured during each night. The reflectance spectra are the result of the division by the solar analog spectra (Hardorp, 1980). Table 2 lists the observational parameters for the asteroids observed. In order to calibrate the observational data, bias, flatfield, calibration lamp and spectrophotometric standard star spectra were secured at different intervals throughout the observational period each night.

The spectra were reduced using the software packages Midas and IRAF according to standard procedures described by Lazzarin *et al.* (1995).

3. Results

We present the spectra obtained for (i) asteroids that may be selected within the present launch baseline and (ii) possible candidates of alternative missions to be launched between 2003 and 2004. For each object, the diameter has been given: for the asteroids 140 Siwa, 732 Tjilaki and 1071 Brita the diameter has been determined by IRAS (Tedesco *et al.*, 1992) while for all the other asteroids an estimation has been computed using (e.g., Fowler and Chillemi, 1992):

$$\log D = 3.1236 - 0.5 \log p_v - 0.2H$$

where D is the diameter in kilometers, H is the absolute magnitude and p_v is the geometric albedo. The albedo p_v used is the typical mean albedo of the taxonomic class

Table 1. MEEGA mission to Wirtanen with 0 to 3 asteroid fly-bys (Rosetta Project Courtesy)

		Date	Day	Cost Δv ($m\,s^{-1}$)	Total Δv ($m\,s^{-1}$)
without asteroid fly-by (reference)					
Launch		20/01/03	0		
Mars		26/08/05	949	51	51
Earth		28/11/05	1042	14	65
Earth		28/11/07	1773	3	68
Wirtanen		13/06/11	3136	1328	1396
with one asteroid fly-by during					
1 leg	2 leg				
3840 Mimistrobell		19/09/06	1334	67	1463
1981 ES33		09/12/06	1417	93	1489
	2703 Rodari	04/05/08	1930	56	1452
	732 Tjilaki	07/06/08	1964	165	1561
	140 Siwa	22/07/08	2010	29	1425
	1992 Galvarino	21/08/08	2040	188	1584
	1515 Perrotin	21/09/08	2069	221	1617
	4258 Ryazanov	03/12/08	2143	26	1422
with two asteroid fly-bys during					
1 leg	2 leg	(same dates and days as 1 fly-by)			
3840 Mimistrobell	2703 Rodari			92	1488
3840 Mimistrobell	140 Siwa			298	1694
3840 Mimistrobell	1992 Galvarino			215	1611
3840 Mimistrobell	1515 Perrotin			260	1656
3840 Mimistrobell	4258 Ryazanov			334	1730
1981 ES33	2703 Rodari			246	1642
1981 ES33	140 Siwa			155	1551
1981 ES33	1992 Galvarino			299	1695
1981 ES33	4258 Ryazanov			122	1518
	140 Siwa + 4258 Ryazanov			187	1583
with three asteroid fly-bys during					
1 leg	2 leg	(same dates and days as 1 fly-by)			
3840 Mimistrobell	140 Siwa + 4258 Ryazanov			268	1664

(Birlan *et al.*, 1996b) attributed to the asteroid in the framework of the Barucci classification (Barucci *et al.*, 1987). The physical parameters of the observed asteroids are listed in Table 3.

3.1. *Alternative asteroids with fly-by to comet P/Wirtanen*

The asteroids reported in Table 1 are potential candidates for a mission to the comet P/Wirtanen with the same launch window. This selection has been done on the basis of Δv cost criterion. All the asteroids listed have been observed spectroscopically except 1981 ES33, which was too faint to be observed during the allocated time.

140 Siwa is the largest object included in the list of the possible alternative asteroid candidate (diameter of 110 km). An estimation of the rotational period (Schober and Stanzel, 1979; Harris and Young, 1980) gives a value >22 h, while Lagerkvist *et al.* (1992) give an estimation of 18.5 h. We observed this object several times during three runs to check possible morphological variations on its surface with the rotation. The eight spectra obtained are shown in Fig. 2. The object belongs to C class. No evidence for aqueous alteration has been found. All the spectra are similar. We computed the reflectivity gradient S' in the wavelength range 5000–8000 Å and we obtained values ranging between $4.4 \pm 0.1\%/10^3$ Å for the spectrum of 1997/01/02, and $9.5 \pm 0.1\%/10^3$ Å for the spectrum of 1995/06/20.

732 Tjilaki is a main-belt asteroid with a diameter of 38 km. This object has been observed at ESO on March 26, 1996. The obtained spectrum (Fig. 3) is less red than the one obtained by Xu *et al.* (1995). They classified this object as D type, while the slope of our spectrum is typical of C asteroids, with a reflectivity gradient S' (computed in the wavelength range 5000–8000 Å) equal to $4.7 \pm 0.1\%/10^3$ Å. A similar slope has been observed by D. Lazzaro (personal communication). A rotational period of 12.342 h has been determined by Florczak *et al.*, 1997.

1515 Perrotin is a main-belt asteroid with a diameter of about 9 km. It has been observed at ESO during two nights (March 26 and 28, 1996). The obtained spectra are shown in Fig. 4. The asteroid has a typical S class spectrum. No differences are evident in the two spectra.

1992 Galvarino has an estimation of the diameter between 5 and 9 km, depending on the albedo value

Table 2. Observational characteristics of the Rosetta candidates

Asteroid	Date (UT)	Exp. (n.)	r (AU)	Δ (AU)	Phase angle (°)	m_v	Solar analog
140 Siwa	1995/06/20	1	2.353	1.509	17.3	12.0	HD1835/HR6060
	1996/10/15	2	2.596	1.627	6.5	12.0	HD280/HD44594
	1996/10/16	1	2.598	1.626	6.1	11.9	HD280/HD44594
	1996/10/17	2	2.601	1.625	5.7	11.9	HD280/HD44594
	1997/01/03	2	2.778	2.322	19.7	13.4	HD44594/HD1835
732 Tjilaki	1996/03/26	1	2.481	2.040	22.9	15.3	HD76151
1071 Brita	1995/06/20	1	3.084	2.249	12.6	15.1	HD1835/HR6060
1515 Perrotin	1996/03/26	1	3.139	2.228	8.8	17.4	HD76151
	1996/03/28	1	3.141	2.215	8.1	17.4	HD144585
1992 Galvarino	1997/01/03	1	3.107	2.212	8.9	17.6	HD44594/HD1835
2446 Lunacharsky	1996/03/28	2	1.977	2.078	28.4	17.2	HD144585
	1996/10/15	1	2.167	1.550	24.7	16.7	HD280/HD44594
	1996/10/16	1	2.169	1.562	24.8	16.9	HD280/HD44594
2703 Rodari	1996/06/21	1	2.206	1.738	26.6	17.6	16 Cyg B
	1996/10/15	1	2.275	1.485	19.1	17.1	HD280/HD44594
	1996/10/16	1	2.276	1.496	19.4	17.1	HD280/HD44594
3057 Mälaren	1995/06/21	1	2.132	1.329	21.3	16.7	HD1835/HR6060
3103 Eger	1996/10/15	1	0.923	0.505	83.1	16.6	HD280/HD44594
	1996/10/16	1	0.925	0.509	82.6	16.6	HD280/HD44594
	1996/10/17	1	0.927	0.513	82.2	16.6	HD280/HD44594
3328 1985 QD1	1995/06/21	1	2.747	1.939	15.3	16.2	HD1835/HR6060
3837 Carr	1996/03/27	1	2.356	1.448	12.8	16.3	HD144585
4258 Ryazanov	1996/05/22	1	2.992	1.993	3.9	15.9	HD144585
5224 Abbe	1996/05/21	1	2.264	1.266	5.7	17.0	HD144585
6173 1983 AD	1996/03/27	1	2.413	1.516	13.2	16.4	HD144585

Table 3. Physical parameters of Rosetta candidates

Asteroid	Diameter (km)	Taxonomic class	Rotation period (h)
140 Siwa	110*	C	~18.5
732 Tjilaki	38*	C	12.342
1071 Brita	50*	C	–
1515 Perrotin	9	S	–
1992 Galvarino	5–9	EM	7.004
2446 Lunacharsky	16	C	3.613
2703 Rodari	6	S	–
3057 Mälaren	6	S	–
3103 Eger	2	E	5.709
3328 1985 QD1	14	S	–
3837 Carr	8	S	–
4258 Ryazanov	14	S	–
5224 Abbe	8	C	–
6173 1983 AD	8	S	–

*Diameter determined by IRAS, the other values are only an estimation

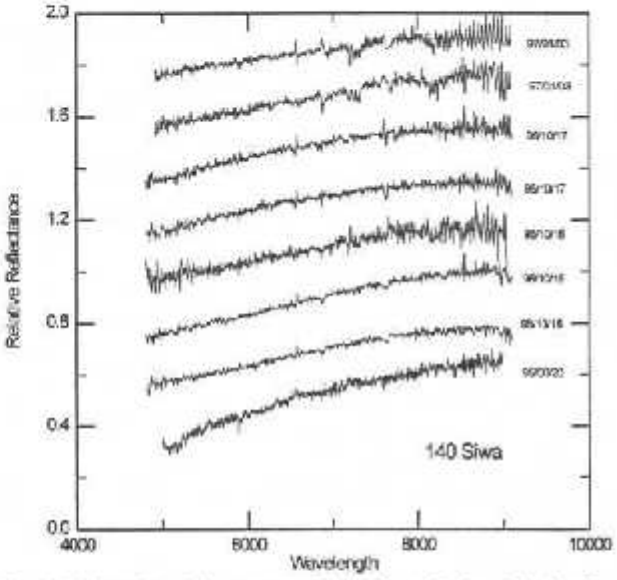

Fig. 2. Eight reflectivity spectra of 140 Siwa obtained during five different days. All spectra have been normalized to unity at 5500 Å and have been offset vertically for clarity

assumed. Birlan *et al.* (1996a) observed it by CCD photometry and determined a rotational period of 7.004 h. The spectrum obtained is presented in Fig. 5. The red part of the spectrum is very noisy. Tentatively, it can be classified as E or M type.

2703 Rodari (diameter of about 6 km) has been observed at CFHT on 1996/06/21 and at ESO (October 15 and 16, 1996). The spectra are shown in Fig. 6, and they exhibit a typical behavior of S type objects. No variations between these spectra are evident.

4258 Ryazanov is a main-belt asteroid with a diameter of about 14 km. It has been observed at ESO on 1996/05/22 and its spectrum, characteristic of S type objects, is shown in Fig. 7.

3.2. *Alternative launch windows*

The following observed asteroids include some of the possible asteroid fly-bys for other Rosetta comet rend-

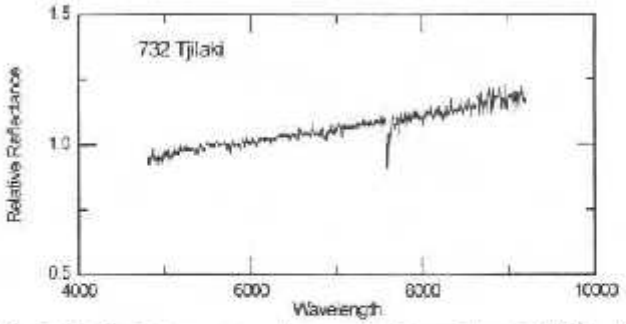

Fig. 3. Reflectivity spectrum (normalized to unity at 5500 Å) of 732 Tjilaki

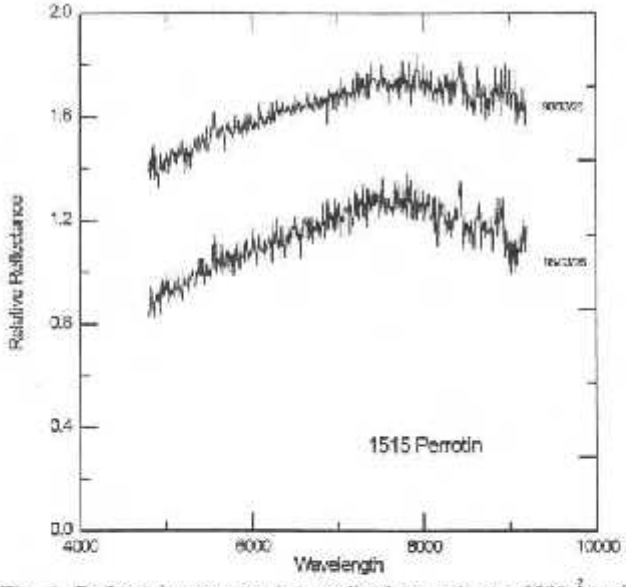

Fig. 4. Reflectivity spectra (normalized to unity at 5500 Å) of 1515 Perrotin. The two spectra have been offset vertically for clarity

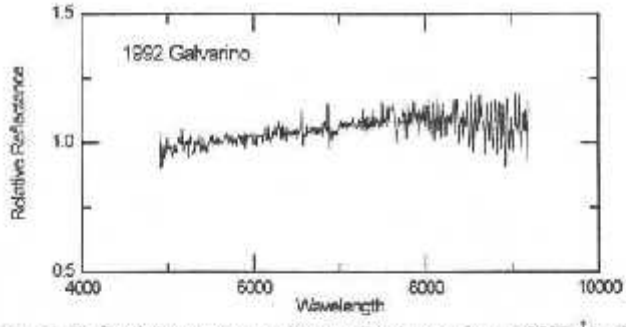

Fig. 5. Reflectivity spectrum (normalized to unity at 5500 Å) of 1992 Galvarino

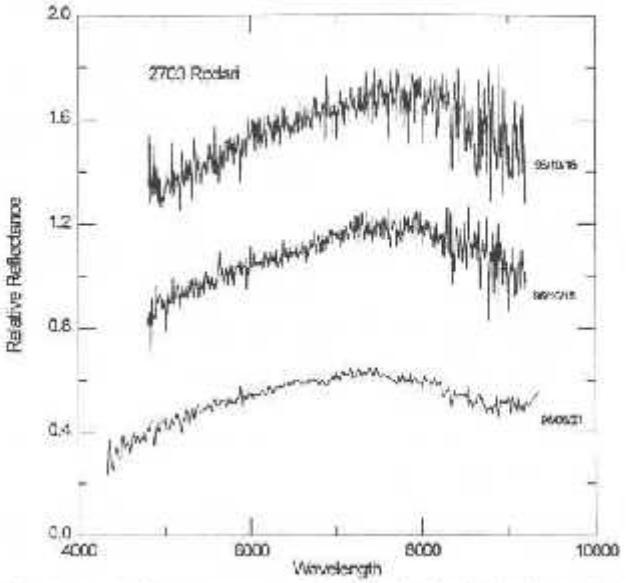

Fig. 6. Reflectivity spectra of 2703 Rodari obtained at ESO (the first two) and the third at Hawaii. The spectra have been normalized to unity at 5500 Å and have been offset vertically for clarity

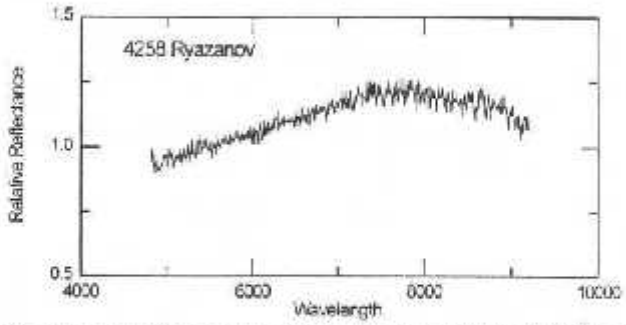

Fig. 7. Reflectivity spectrum (normalized to unity at 5500 Å) of 4258 Ryazanov

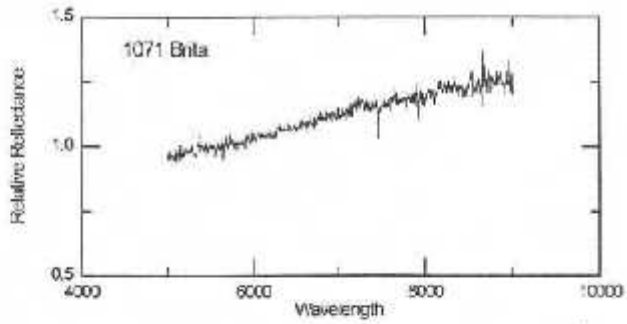

Fig. 8. Reflectivity spectrum (normalized to unity at 5500 Å) of 1071 Brita

ezvous opportunities with launch between 2002 and 2004 (SCI(93)7).

1071 Brita is a main-belt asteroid with a diameter of 50 km. It was the programmed fly-by asteroid with the rendezvous to the comet P/Schwassmann–Wachmann 3 and spacecraft launch on 2003/07/18 (SCI(93)7). The asteroid has been observed at ESO on 1995/06/20. The spectrum is shown in Fig. 8 and the computed reflectivity gradient S' (5000–8000 Å) is equal to $8.2 \pm 0.1\%/10^3$ Å. The object was observed in 1992 by Xu *et al.* (1995). The spectrum is typical of a C class asteroid.

3057 Mälaren is a main-belt asteroid with a diameter of about 6 km. It is the candidate for a fly-by, together with the asteroid 494 Virtus, for the mission to comet P/Neujmin 2 (launch on 2003/09/29). The asteroid has

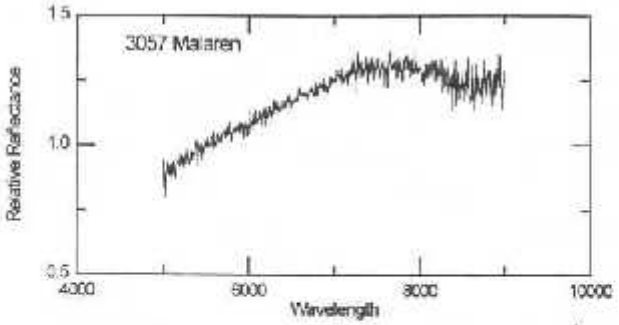

Fig. 9. Reflectivity spectrum (normalized to unity at 5500 Å) of 3057 Mälaren

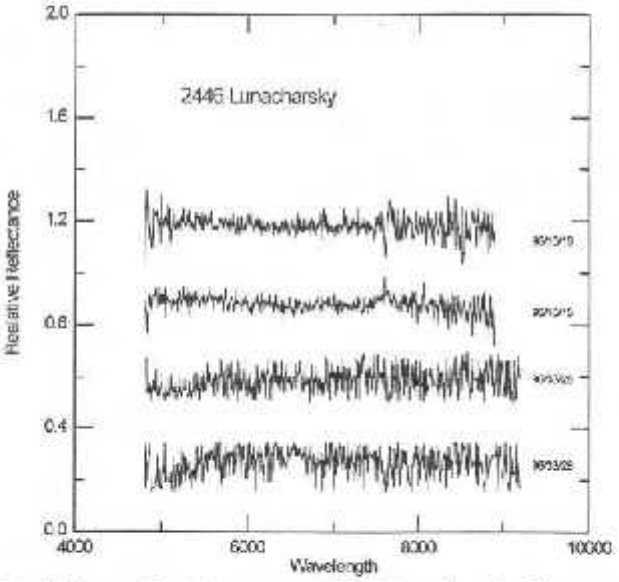

Fig. 10. Four reflectivity spectra of 2446 Lunacharsky. The spectra have been normalized to unity at 5500 Å and have been offset vertically for clarity

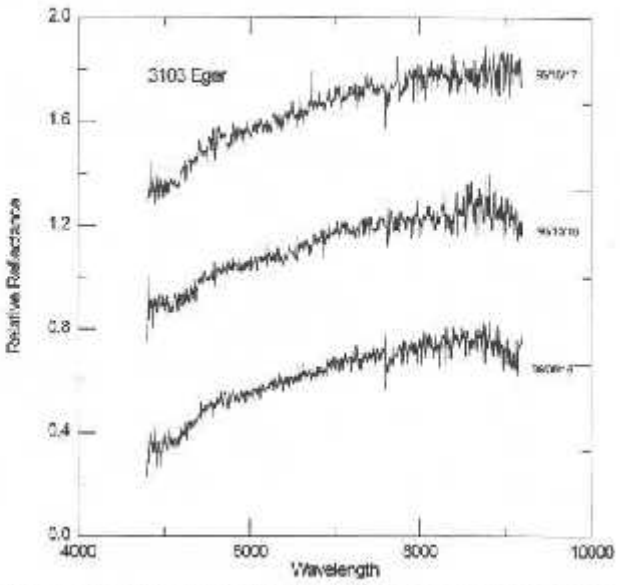

Fig. 11. Reflectivity spectra of 3103 Eger. The spectra have been normalized to unity at 5500 Å and have been offset vertically for clarity

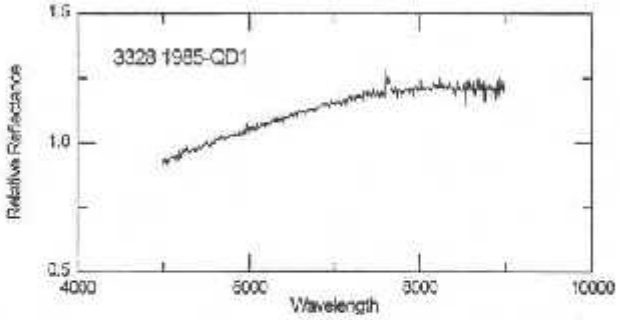

Fig. 12. Reflectivity spectrum (normalized to unity at 5500 Å) of 3328 1985-QD1

been observed at ESO on 1995/06/21 and the spectrum (Fig. 9) is typical of S class objects.

2446 Lunacharsky and **3103 Eger** are both candidates for the fly-by asteroids with the rendezvous to the comet P/Finlay (launch on 2004/05/11). 2446 Lunacharsky is a main-belt object with a diameter of about 6 km, while 3103 Eger is an Apollo with a diameter of about 2 km. 2446 Lunacharsky has been observed during three nights at ESO. In Fig. 10 the flat spectra characteristic for C type asteroids are shown. No detectable variations are present in the different spectra. CCD photometry have been carried out at ESO and a rotational period of 3.613 h has been determined (Florczak *et al.*, 1997). 3103 Eger has been observed during three nights and the spectra obtained are shown in Fig. 11. These spectra are typical of E class. Previous visible and near-infrared spectroscopy observations have been carried out by Gaffey *et al.* (1992) who classified this NEA objects as E type. They also affirmed the analogy of this object with the enstatite achondrite meteorites. A rotational period of 5.709 h has been obtained (Wisniewski, 1991; De Sanctis *et al.*, 1994).

3328 1985 QD1 is an asteroid of the Eos family (Zappala *et al.*, 1995; Doressoundiram *et al.*, 1997) with a diameter of about 14 km. It is the fly-by candidate, with the asteroid 1453 Fennia, for the mission to comet P/Schwassmann–Wachmann 3 (launch on 2002/04/19). The spectrum (Fig. 12) has been obtained at ESO on 1995/06/21 and, as for other Eos family members, belongs to S type.

3837 Carr is a main-belt object (diameter of about 8 km). It is one of the two asteroid candidates, with 1983 WM, for a mission to the comet P/Brooks 2 (launch on 2004/05/25). The observation has been performed at ESO on 1996/03/27 and the spectrum (Fig. 13) indicates an S-type object.

5224 Abbe and **6173 1983 AD** (both with a diameter of about 8 km) are the back-up targets for a debated mission to the comet P/Wirtanen (launch on 2003/11/03). These objects have been observed at ESO on 1996 and the spectra are shown in Figs 14 and 15. The spectrum of the asteroid 5224 Abbe is characteristic of C type with reflectivity gradient of $7.4 \pm 0.1\%/10^3$ Å (computed in the wavelength range 5000–8000 Å), while the spectrum of 6173 1983 AD is typical of S class.

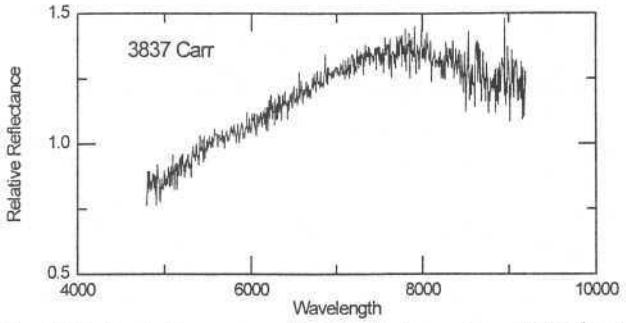

Fig. 13. Reflectivity spectrum (normalized to unity at 5500 Å) of 3837 Carr

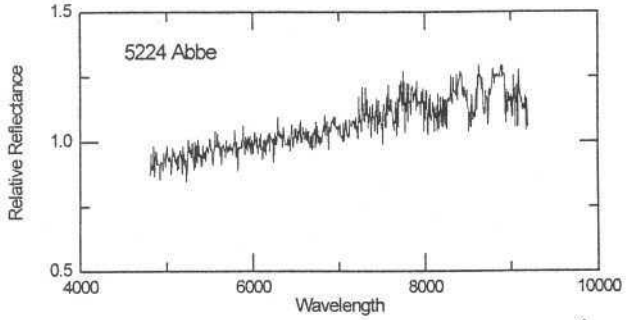

Fig. 14. Reflectivity spectrum (normalized to unity at 5500 Å) of 5224 Abbe

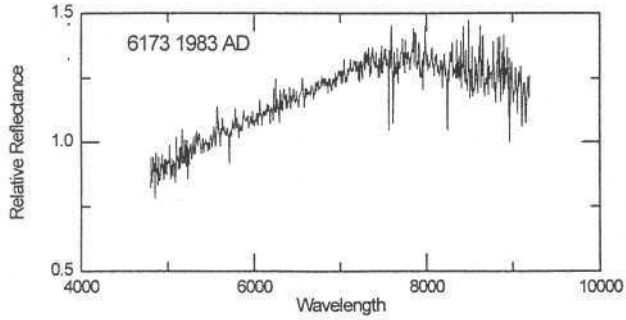

Fig. 15. Reflectivity spectrum (normalized to unity at 5500 Å) of 6173 1983 AD

4. Conclusions

Up to now, we have *in situ* observations of only two S-type asteroids (951 Gaspra and 243 Ida, obtained from Galileo spacecraft). Details on the nature of these two objects are given by Granahan *et al.* (1994), Belton *et al.* (1995) and Chapman (1996).

The asteroid targets of the Rosetta mission baseline 3840 Mimistrobell and 2703 Rodari, belong again to S class as well as 433 Eros, the main target of the NEAR (NASA) mission.

In our opinion the ideal selection in the present framework baseline of the mission has to include the asteroid 140 Siwa because of its size and its spectral type. The data obtained indicate that Siwa is a more pristine object (C type) which has probably been less altered by collisions than smaller ones. The presence of several primitive-type asteroids between the possible alternative targets (both to P/Wirtanen or other comets) suggests that a careful selection procedure is needed in order to explore "primitive bodies" and to meet the primary goal of the Rosetta mission.

The final selection of the two Rosetta target asteroids will be made in a successive phase of the Rosetta project development, when the engineering parameters will be frozen. We hope that this work will help in choosing the best candidates.

References

Barucci, M. A., Capria, M. T., Coradini, A. and Fulchignoni, M. (1987) Classification of asteroids using G-mode analysis. *Icarus* **72,** 304–324.

Barucci, M. A. and Lazzarin, M. (1995) Visible spectroscopy of the Rosetta Asteroid Targets: 3840 Mimistrobell and 2530 Shipka. *Icarus* **118,** 216–218.

Belton, M. J. S., Chapman, C. R., Thomas, P. C., Davies, M. E., Greenberg, R., Klaasen, K., Byrnes, D., D'Amario, L., Synnott, S., Johnson, T. V., McEwen, A., Merline, W. J., Davies, D. R., Petit, J.-M., Storrs, A., Veverka, J. and Zellner, B. (1995) Bulk density of asteroid 243 Ida from the orbit of its satellite Dactyl. *Nature* **374,** 785–788.

Birlan, M., Barucci, M. A., Angeli, C., Doressoundiram, A. and De Sanctis, C. (1996a) Rotational properties of nine small asteroids. *Planet. Space Sci.* **44,** 555–558.

Birlan, M., Fulchignoni, M. and Barucci, M. A. (1996b) Effects of IRAS albedo correction on the G-mode asteroid taxonomy. *Icarus* **124,** 352–354.

Chapman, C. R. (1996) S-type asteroids, ordinary chondrites, and space weathering: the evidence from Galileo's fly-bys of Gaspra and Ida. *Meteorites Planet. Sci.* **31,** 699–725.

De Sanctis, M. C., Barucci, M. A., Angeli, C. A., Fulchignoni, M., Burchi, R. and Angelini, P. (1994) Photometric and CCD observations of 10 asteroids. *Planet. Space Sci.* **42,** 859–864.

Doressoundiram, A., Barucci, M.A., Fulchignoni, M. and Florczak, M. (1997) EOS family: a spectroscopic study. *Icarus*, in press.

Gaffey, M. J., Reed, K. L. and Kelley, M. S. (1992) Relationship of E-type Apollo Asteroid 3103 (1982 BB) to the Enstatite Achondrite Meteorites and the Hungaria Asteroids. *Icarus* **100,** 95–109.

Gaffey, M. J., Bell, J. F., Brown, R. H., Burbine, T. H., Piatek, J. L., Reed, K. L. and Chaky, D. A. (1993) Mineralogical variations within the S-type asteroid class. *Icarus* **106,** 573–602.

Granahan, J. C., Fanale, F. P., Robinson, M. S., Carlson, R. W., Kamp, L. W., Klaasen, K. P., Weissman, P. R., Belton, M., Cook, D., Edwards, K., McEwen, A. S., Soderblom, L. A., Carcich, B. T., Helfienstein, D., Simonelli, D., Thomas, P. C. and Veverka, J. (1994) A Galileo multi-instrument spectral analysis of 951 Gaspra. *Lunar Planet Sci. Conf.*, Vol. XXV, pp. 453–454.

Florczak, M., Dotto, E., Barucci, M. A., Birlan, M., Erikson, A., Fulchignoni, M., Perret, L. and Thebault, P. (1997) Rotational properties of main belt asteroids. *Planet. Space Sci.* **45,** 1423–1435.

Fowler, J. W. and Chillemi, J. R. (1992) IRAS asteroid data processing. In *Tech. Rep. PL-TR-92-2049. The IRAS Minor Planet Survey*, pp. 17–43. Phillips Laboratory, Hanscom AF Base, MA, 1992.

Hardorp, J. (1980) The Sun among the stars. *Astron. Astrophys.* **91,** 221–232.

Harris, A. W. and Young, J. W. (1980) Asteroid rotation III—1978 observations. *Icarus* **43,** 20–32.

Lagerkvist, C.-I., Magnusson, P., Debehogne, H., Hoffman, M., Erikson, A., De Campos, A. and Cutispoto, G. (1992) Photoelectric photometry of asteroids obtained at ESO and Hoher List Observatory. *Astron. Astrophys. Sup. Ser.* **95**, 461–470.

Lazzarin, M., Barbieri, C. and Barucci, M. A. (1995) Visible spectroscopy of dark, primitive asteroids. *Astron. J.* **110**, 3058–3072.

Schober, H. J. and Stanzel, R. (1979) On the light variations of the C-type asteroids 140 Siwa and 790 Tretonia. *Astron. Astroph. Suppl.* **38**, 265–268.

Tedesco, E. F., Veeder, G. J., Fowler, J. W. and Chillemi, J. R. (1992) *Tech. Rep. PL-TR-92-2049. The Iras Minor Planet Survey*. Phillips Laboratory, Hanscom AF Base, MA.

Xu, S., Binzel, R. P., Burbine, T. H. and Bus, S. J. (1995) Small main-belt asteroid spectroscopic survey: initial results. *Icarus* **115**, 1–35.

Wisniewski, W. Z. (1991) Physical studies of small asteroids. I—Lightcurves and taxonomy of 10 asteroids. *Icarus* **90**, 117–122.

Zappala, V., Bendjoya, P., Cellino, A., Farinella, P. and Froeschle, C. (1995) Asteroids families: Search of a 12487 Asteroids sample using two different clustering techniques. *Icarus* **116**, 291–314.

3.4 - Conclusões

Realizamos várias missões de observação espectroscópica de famílias de asteróides, de asteróides do tipo C, de alguns objetos com órbitas próximas à da Terra e de candidatos à missão espacial Rosetta. Quanto às famílias, encontramos que os membros estudados de Eos, Themis e Flora apresentam um comportamento espectral similar, confirmando os resultados dinâmicos de uma origem comum.

Na família de Eos encontramos que seus membros possuem espectros identificados como do tipo K com uma forte identidade espectroscópica, ou seja, um máximo localizado entre 8000 e 8500 $\AA$. Por outro lado, a diversidade espectral encontrada entre os membros, nos leva a concluir que o corpo original desta família deva ter sido parcialmente diferenciado. Com relação à família de Flora encontramos que seus membros apresentam características de tipo S, onde a diversidade espectral encontrada parece indicar que um processo de alteração mineralógica superficial está agindo nestes objetos. Devido ao fato de encontrarmos semelhanças entre os membros menos alterados e os meteoritos condritos ordinários, sugerimos que a composição mineralógica destes asteróides seja parecida com a destes meteoritos.

Encontramos nos membros da família de Themis uma característica espectral de C e seus subtipos B, G e F, sendo que parte destes objetos apresenta indícios de que um processo de alteração aquosa está agindo em sua superfície. O fato de que parte destes objetos não apresenta indícios de alteração aquosa nos leva a concluir que provavelmente o corpo original desta família deve ter sido parcialmente diferenciado. Para os asteróides de tipo taxonômico C encontramos vários deles que apresentam bandas que sugerem um processo de alteração aquosa em seus materiais.

Com relação aos asteróides próximos da órbita da Terra, encontramos alguns semelhantes aos meteoritos condritos ordinários e um objeto com tipo espectral C . Nos outros asteróides, embora não houvesse nenhum meteorito análogo, sugerimos que um processo de alteração de composição superficial pode estar agindo, escondendo sua real composição, provavelmente do tipo similar aos condritos ordinários. No que diz respeito à missão espacial Rosetta, observamos 14 asteróides candidatos e sugerimos 140 Siwa como um alvo ideal entre aqueles por nós analisados.

Capítulo 4

Propriedades Rotacionais de Asteróides

4.1 - Introdução

A rotação dos asteróides é resultado de uma combinação de seus momentos angulares individuais iniciais, com o momento que estes objetos ganharam ou perderam nas colisões subseqüentes à sua formação. Desta forma, o conhecimento da distribuição atual das taxas de rotação poderá nos ajudar a compreender o cenário evolutivo destes objetos.

Quando se analisa as taxas de rotação, encontra-se diferenças na distribuição entre os tipos taxonômicos mais comuns e entre as famílias de asteróides. Lagerkvist (1983) e Lagerkvist e Williams (1987) verificaram que a taxa de rotação dos asteróides do tipo M era maior do que a dos S e C, fato que poderia ser explicado considerando-se a maior densidade média dos objetos de tipo M. Além disto, Binzel (1988) encontrou uma distribuição de taxas de rotação com um valor médio maior para os membros da família de Eos em comparação com os de Koronis. Em seu modelo de evolução colisional, Binzel propõe que a família de Eos tenha uma idade próxima à do Sistema Solar enquanto Koronis seria muito mais jovem, com idade entre 2 e 4 bilhões de anos.

Analisando as taxas de rotação em função do diâmetro, Binzel e co-autores (1989) encontraram para os objetos maiores ($D > 200$ km e $125 \leq D \leq 200$ km) que estas poderiam ser ajustadas por uma distribuição maxwelliana, implicando que estes asteróides teriam alcançado um avançado processo colisional. Por outro lado, os asteróides com $D < 125$ km apresentavam um excesso de objetos lentos, sugerindo que suas taxas de rotação teriam sido influenciadas por eventos catastróficos. Fulchignoni e co-autores (1995) e Angeli (1995),

analisando a distribuição de rotação de pequenos asteróides (D < 50 km) encontraram que esta distribuição poderia ser uma combinação linear de três distribuições maxwellianas, com valores médios de rotação de 4,1, 8,7 e 24,7 horas. A existência de objetos (2/3 do total) com um período rotacional de 8,7 horas, próximo ao dos grandes planetas do Sistema Solar (período médio igual a 7,62 horas), os levaram a sugerir que as rotações foram pouco afetadas por colisões após as fases primordiais de formação. Em relação aos tipos taxonômicos eles confirmaram que os asteróides do tipo M possuem uma taxa de rotação média maior do que os de outros tipos, enquanto os C e P seriam os mais lentos.

Por estas razões, determinar as propriedades rotacionais dos asteróides é fundamental para entender sua evolução colisional. Estas propriedades, tais como o período de rotação, a forma do objeto e a direção do eixo de rotação podem ser obtidas através da análise de suas curvas de luz. Estas curvas são a variação de luminosidade do objeto durante um certo período de tempo. Os fatores que levam à variação da intensidade da luz solar refletida pelo asteróide são: a) as mudanças das distâncias asteróide–Terra e asteróide–Sol; b) a rotação do asteróide; c) as mudanças do ângulo de fase solar (ângulo Sol–asteróide–Terra) (fig. 4.1).

Podemos *corrigir* os fatores geométricos utilizando as magnitudes reduzida e absoluta. Magnitude reduzida é a magnitude de um asteróide supondo que este esteja a uma distância padrão de 1 U.A. do Sol e da Terra, enquanto que a magnitude absoluta seria a magnitude reduzida quando o asteróide está com um ângulo de fase igual a zero (ver seção 5.2). A magnitude absoluta seria então uma grandeza invariante do ponto de vista geométrico.

A mudança do brilho devida à rotação do asteróide normalmente ocorre sem que haja uma variação significativa de sua configuração geométrica, com exceção dos asteróides que possuem rotação longa ou complexa, que discutiremos a seguir. Desta forma, podemos obter o período de rotação em poucas noites (boas) de observação. Portanto, em uma dada configuração geométrica a variação no brilho do asteróide será função apenas da mudança da área superficial de reflexão solar, e/ou da mudança de albedo (fig. 4.2). Se o asteróide for uma esfera sem variações de albedo sua curva de luz será uma linha reta; do contrário, será do tipo senoidal. Se admitirmos uma rotação pura, ou seja, em torno do eixo principal de

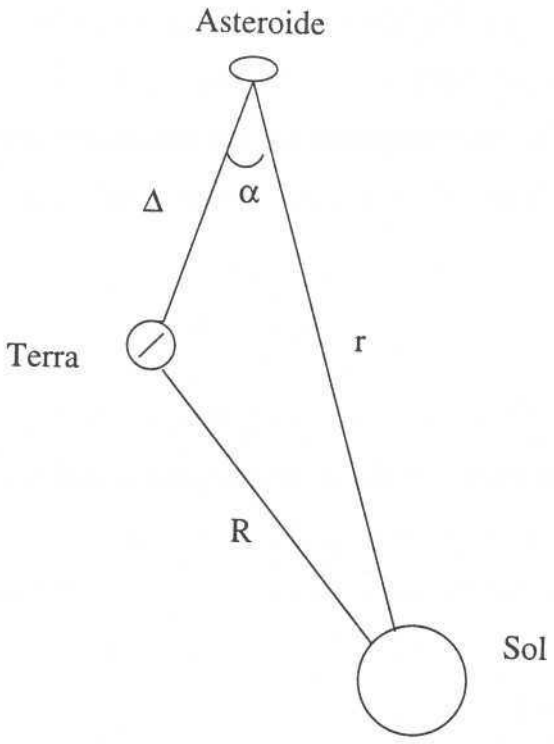

Figura (4.1) *Configuração geométrica do Sol, Terra e asteróide. O ângulo α é chamado de ângulo de fase solar.*

momento de inércia, então o período poderá ser obtido através de uma análise de Fourier. A curva de luz pode ser representada pela seguinte função (Harris *et al.*, 1989):

$$V(\alpha,t) = V(\alpha) + \sum_{l=1}^{n} \left[A_l \sin \frac{2\pi\, l}{P}(t-t_o) \times B_l \cos \frac{2\pi\, l}{P}(t-t_o) \right] \qquad (4.1)$$

onde $V(\alpha,t)$ é a magnitude reduzida em um ângulo de fase α e um tempo t, $V(\alpha)$ é a magnitude média em um ângulo de fase α, A_l e B_l são os coeficientes de Fourier, P é o

período de rotação do objeto e t_a é uma constante escolhida como o instante próximo do meio do intervalo de observação.

A amplitude de uma curva de luz (Δm) nos fornece uma estimativa da forma do asteróide. Considerando um asteróide como um elipsóide com os eixos a, b e c diferentes, obteríamos em uma rotação completa 2 máximos e 2 mínimos (fig. 4.2), e considerando que a variação da luz refletida seja apenas devida à mudança da área de reflexão, teríamos uma relação entre a amplitude dos eixos do elipsóide dada por:

$$\Delta m = 2,5 \log \frac{\mathrm{a}}{\mathrm{b}}. \tag{4.2}$$

A determinação da forma e da orientação do eixo de rotação é mais complexa do que o período, devido à dificuldade de se extrair uma grandeza tridimensional através de dados bidimensionais. Para isto são necessárias muitas observações em vários ângulos de fase solar distintos. Atualmente outras técnicas, além da fotometria, são utilizadas para determinação da forma tais como o radar, as ocultações estelares e observações *in locu*, através de missões espaciais.

A hipótese descrita acima de uma rotação pura é baseada na análise das curvas de luz de asteróides, que aparentemente não exibem múltiplos períodos, os quais seriam resultado de uma precessão e/ou cambalhotamento (Sher, 1971). Por outro lado, podemos supor que colisões que não passam pelo centro de massa do asteróide tendem a desalinhar o eixo de rotação do eixo principal, causando uma precessão livre ou um cambalhotamento. Burns e Safronov (1973) deduziram uma expressão aproximada para o intervalo de tempo necessário para o alinhamento dos eixos de rotação com o momento de inércia principal devido à dissipação interna de energia. Este tempo, que chamaremos de *tempo de relaxação*, foi deduzido como sendo dado por:

$$\tau \approx \frac{\mu Q}{\rho k^2 r^2 \omega^3} \tag{4.3}$$

onde μ é o coeficiente de rigidez do material que compõe o asteróide, Q é um fator que indica a perda de energia por ciclo de oscilação, k é um fator numérico relativo ao formato

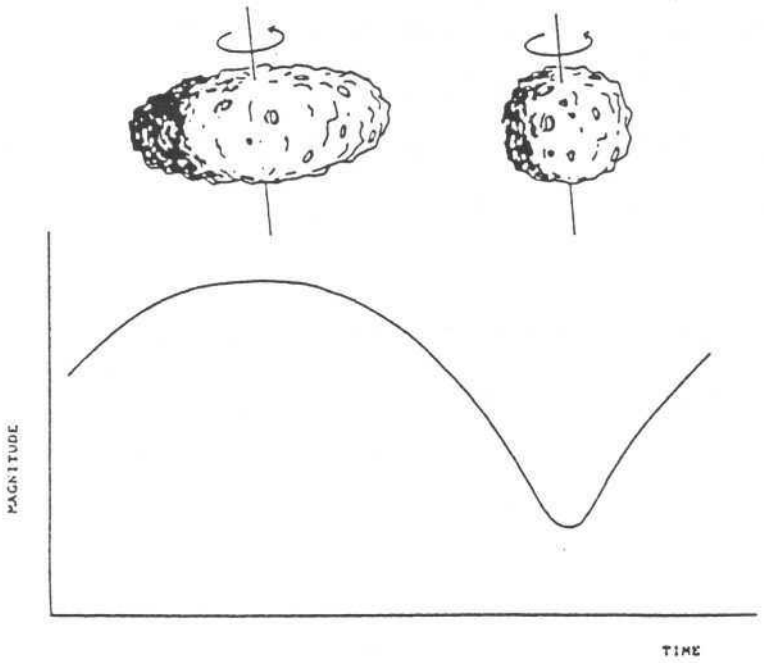

Figura (4.2) *Um asteróide visto em meia fase rotacional, e sua curva de luz correspondente (Angeli, 1995).*

do corpo (aproximadamente 0,01 para uma esfera e 0,1 para um corpo altamente alongado), r é o raio médio do corpo e ω é a frequência angular de rotação. Calculando τ para alguns asteróides, os autores encontraram valores entre 10^5 e 10^8 anos concluíndo que grande parte dos asteróides se encontra num estado puro de rotação, já que as estimativas de probabilidade de que ocorra pelo menos uma colisão entre 2 asteróides fornecem tempos superiores a 10^8 anos.

Mais recentemente, as análises das curvas de luz de 4179 Toutatis (Spencer et al, 1995), 253 Mathilde (Mottola et al, 1995) e 3288 Seleucus (Harris, 1994b) indicaram que estes asteróides provavelmente se encontram num estado de rotação complexo. Por outro lado, nestes últimos anos tem aumentado o número de objetos para os quais o período tem sido estimado como sendo longo (superior a um dado valor) e mal determinado, sugerindo

novas observações e uma análise mais detalhada de seu comportamento rotacional. Devemos ressaltar o efeito de um *bias* observacional que ocorre na determinação dos períodos rotacionais de asteróides, onde muitos não são publicados justamente pelo fato de não se obter um bom valor. Isto poderia não ser originário de uma observação onde os dados obtidos são de baixa qualidade, mas sim de uma rotação complexa do objeto. Desta forma, teríamos uma quantidade muito maior de asteróides com rotação complexa e/ou rotação longa do que a prevista até o momento.

A fim de estudar o comportamento rotacional de asteróides, realizamos várias missões de observação com o objetivo de aumentar as estatísticas do número de objetos com período conhecido, dando ênfase aos asteróides pequenos e aos candidatos à missão *Rosetta*, e de analisar o comportamento rotacional de objetos cujos períodos eram mal determinados e considerados longos.

4.2 - Observações e Reduções

As observações fotoelétricas e CCD foram realizadas nos anos de 1995 e 1996, nos telescópios de 0,60 m do Observatório do Pico dos Dias (Brasil), de 1,2 m do Observatório de Haute–Provence (França) e de 1,5 m Danish, 0,9 m Dutch, 0,6 m Bochum e 0,5 m do European Southern Observatory (ESO, Chile).

As observações fotoelétricas foram reduzidas com o sistema de redução fotométrica do ESO, RANBO2, e as observações CCD com o IRAF. As imagens foram corrigidas de *bias* e *flat-field* como descrito no capítulo 3. A correção da extinção atmosférica e a transformação ao sistema padrão de magnitudes foram feitas usando-se estrelas padrão (Landolt, 1983; Graham, 1982; Lasker *et al.*, 1988), como descrito por Hardie (1962).

Quando as condições do céu são consideradas boas, ou seja, com baixa dispersão na determinação da extinção atmosférica, é obtida a magnitude reduzida (V) através da seguinte relação:

$$V = V_o - 5\log(r\Delta) \tag{4.4}$$

onde r é a distância do asteróide ao Sol, V_o é a magnitude instrumental e Δ a distância do asteróide à Terra (fig. 4.1). Para a obtenção do período rotacional ajustamos a função descrita através da equação 4.1, usando o método dos mínimos quadrados. Na prática procuramos determinar uma solução onde, fixando um valor inicial para o período (estimado visualmente) e usando um valor fixo para o grau da equação (n), fazemos variar o período em torno deste valor inicial de forma a obter a menor dispersão. Em seguida testamos esta solução para maiores graus da equação 4.1.

Se a noite não for fotométrica, ou ocorrer algum problema na transformação ao sistema padrão, podemos ainda obter as magnitudes diferenciais usando estrelas de comparação do mesmo campo do asteróide. Desta forma o ajuste descrito acima é feito sobre a diferença entre a magnitude do asteróide e aquela de uma estrela de comparação. Normalmente usamos três estrelas de comparação, de forma a eliminar algum problema intrínseco à estrela como, por exemplo, uma variabilidade.

4.3 - Resultados

Nas seções seguintes apresentaremos os resultados obtidos do estudo das propriedades rotacionais de asteróides do cinturão principal e de asteróides com período longo. Para cada um dos assuntos apresentamos um resumo dos principais resultados e, em seguida, o artigo correspondente.

4.3.1 - Asteróides do Cinturão Principal

Com o objetivo de aumentar os dados sobre a rotação de asteróides realizamos uma campanha de observação durante o ano de 1996, obtendo 64 curvas de luz para 15 asteróides. Destes, 13 objetos possuem um diâmetro inferior a 50 km e dois em torno de 100 km. Dois objetos, 732 Tjilaki e 2446 Lunacharsky eram candidatos à missão Rosetta, aumentando o interesse na determinação de seu estado rotacional em vista da missão espacial. Obtivemos o período rotacional para 12 asteróides e estimamos um valor mínimo para 2. Os asteróides 424 Gratia e 491 Carina, com diâmetros de 87 e 97 km respectivamente, tiveram períodos determinados com boa precisão, sendo iguais a 19,47 e 14,87

horas. Estes valores estão bem acima do valor médio, 8,8 h, encontrado por Angeli (1995) para asteróides com diâmetro superior a 50 km.

Para os objetos menores do que 50 km tivemos uma maior distribuição dos períodos calculados. Os períodos rotacionais de 440 Theodora, 727 Nipponia, 888 Parysatis, 1626 Sadeya e 2446 Lunacharsky foram estimados em 4,828, 4,6, 5,49, 3,438 e 3,614 horas respectivamente. Somente para 727 Nipponia o período foi mal determinado, havendo a possibilidade de estar errado. Estes valores estão próximos daqueles de uma população considerada de rotação rápida, cujo valor médio foi estimado em 4,1 horas por Angeli e que representavam 25 % de toda a população dos pequenos objetos dentro de sua amostra. Apenas 783 Nora apresentou um período muito lento, 34,4 horas, bem maior do que o valor médio encontrado para uma população com rotação lenta, que é em torno de 24 horas e que representa aproximadamente 10 % da população de pequenos objetos. Para este objeto já havia na literatura uma estimativa de que o período seria longo (Lagerkvist *et al.*, 1992).

Para os outros pequenos asteróides, ou seja, 446 Aeternitas, 732 Tjilaki, 2209 Tianjin e 3776 Vartiovuori, encontramos os seguintes períodos: 15,85, 12,34, 9,47 e 7,7 horas respectivamente. Estes valores estão entre os valores médios encontrados por Angeli para a maior parte dos asteróides pequenos, 8,7 horas, e da população de rotação lenta, 24 horas. Para 1246 Chaka e 1507 Vaasa foram encontrados apenas valores inferiores para o período, ou seja, 20 e 14 horas, respectivamente. Para 1995 Shane não obtivemos nenhuma estimativa razoável. Todos estes resultados são descritos em detalhe no artigo a seguir.

Pergamon

Planet. Space Sci., Vol. 45, No. 11, pp. 1423–1435, 1997

0032-0633/97 $17.00+0.00

PII: S0032-0633(97)00121-9

Rotational properties of main belt asteroids: photoelectric and CCD observations of 15 objects*

M. Florczak,[1,2,3] E. Dotto,[3,4] M. A. Barucci,[3] M. Birlan,[5] A. Erikson,[6] M. Fulchignoni,[3,7] A. Nathues,[6] L. Perret[3] and P. Thebault[3]

[1]ON/CNPq, Dep. Astrofisica, 20921 Rio de Janeiro, Brazil
[2]CEFET, Dep. Fisica, 80000 Curitiba, Brazil
[3]Observatoire de Paris, 92195 Meudon Principal Cedex, France
[4]Universita di Padova, Dip. di Fisica, V. Marzolo 8, 35131 Padova, Italy
[5]Astronomical Institute of the Romanian Academy, str. Cutitul de Argint 5, Bucharest 28, Romania
[6]DLR, Institute of Planetary Exploration, Rudower Chausse 5, D-12489 Berlin, Germany
[7]Université Paris 7, Paris, France

Received 19 March 1997; accepted 20 May 1997

Abstract. In this paper we present the results of several observational campaigns carried out during 1996 at the 1.2 m telescope of the Haute Provence Observatory (France) and at the 1.5 m Danish, 0.9 m Dutch, 0.6 m Bochum and 0.5 m telescopes of the European Southern Observatory (ESO, La Silla, Chile), in order to enlarge the available sample of know asteroid rotational periods.

A total of 64 single night lightcurves for 15 asteroids were obtained. The rotational periods have been determined for 12 objects, with different quality code: 424 Gratia (P_{syn} = 19.47 h), 440 Theodora (P_{syn} = 4.828 h), 446 Aeternitas (P_{syn} = 15.85 h), 491 Carina (P_{syn} = 14.87 h), 727 Nipponia (P_{syn} = 4.6 h), 732 Tjilaki (P_{syn} = 12.34 h), 783 Nora (P_{syn} = 34.4 h), 888 Parysatis (P_{syn} = 5.49 h), 1626 Sadeya (P_{syn} = 3.438 h), 2209 Tianjin (P_{syn} = 9.47 h), 2446 Lunacharsky (P_{syn} = 3.613 h) and 3776 Vartiovuori (P_{syn} = 7.7 h). For 1246 Chaka, 1507 Vaasa and 1994 Shane the complete rotational phase was not covered and for two of them it was possible to find only an indication of the rotational period.

Introduction

The knowledge of the asteroid spin rate is an important tool to gain information on the collisional evolution state of the asteroid population. Binzel *et al.* (1989) showed that the intermediate size range is important in terms of collisional evolution: the limit between 100 km and 125 km is considered as very representative because it seems to be the transition region between the larger primordial asteroids and the population of the smaller objects which are supposed to be the fragments, results of collisional events. Fulchignoni *et al.* (1995), analysing the rotational rate distribution for a sample of 516 main belt asteroids, found, for small objects ($D \leq 50$ km), the superimposition of three sub-populations: the more populated (similar to the distribution of larger objects) and the slow and the rapid rotator ones. Harris (1996), analyzing the rotational spin of asteroids with mean diameter $D \leq 10$ km, pointed out an absence of very rapid rotators, and an excess of slow rotators: the first characteristic (cut-off for period of less than 2.25 h) seems to imply a "rubble pile" structure, while the excess of slow rotators can be due to a state of non-principal axis rotation, or "tumbling" (Harris, 1994).

In order to enlarge the available data set of asteroid spins, we are carrying out a long-term observing program.

In this paper we present 64 lightcurves of 15 asteroids, obtained during 1996 by CCD observations at the 1.2 m telescope of the Haute Provence Observatory (France) and at 0.9 m Dutch, 1.5 m Danish and 0.6 m Bochum telescopes of the European Southern Observatory (ESO, La Silla, Chile) and by photoelectric observations carried out with the 0.5 m telescope at ESO. For all the objects, with the exception of 783 Nora, lightcurves were measured for the first time. The survey has been carried out on small asteroids: 13 out of the 15 observed objects have a diameter $D < 50$ km, while the remaining objects have a diameter of about 90 km.

Two of the observed asteroids (732 Tjilaki and 2446

*Based on observations carried out at the European Southern Observatory (ESO), La Silla, Chile.

Correspondence to: M. A. Barucci. E-mail: BARUCCI@obspm.fr.

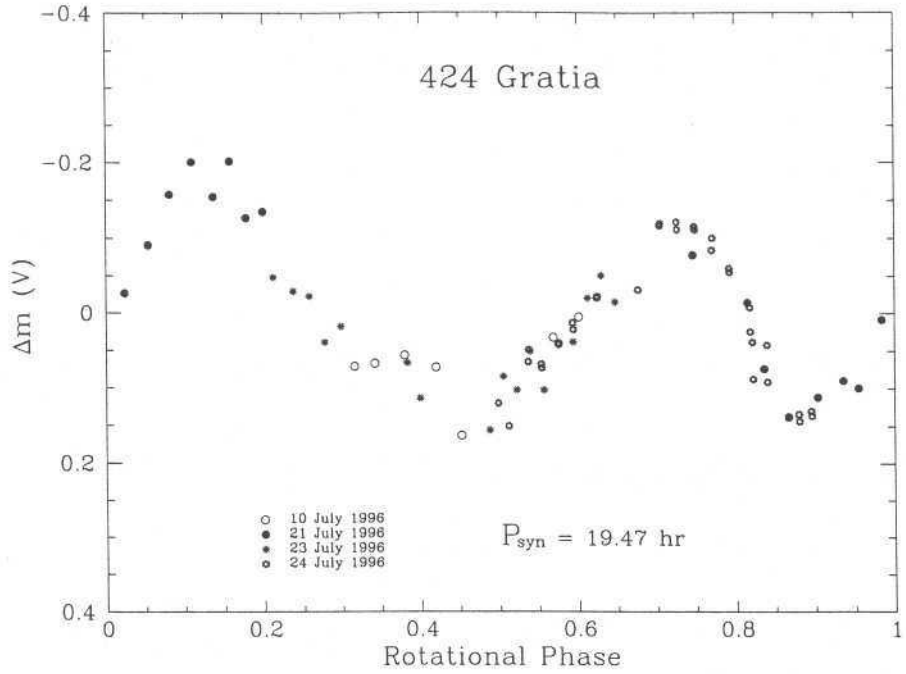

Fig. 1. Composite lightcurve of the asteroid 424 Gratia in rotational phase. Zero phase corresponds to U.T. 1996 July 22.0

Lunacharsky) are possible candidates for the Rosetta mission : 732 Tjilaki is an alternative candidate for the mission to comet P/Wirtanen, while 2446 Lunacharsky is a candidate for other Rosetta comet rendezvous opportunities (ESA, SCI(93)7).

Observations and data reduction

All the observations reported here have been obtained in the V-band. The transformation to the standard system has been carried out observing groups of standard stars, taken from the Harvard E-regions (Graham, 1982), Landolt (1983) and Guide Star Photometric Catalog (Lasker *et al.*, 1988). The data reduction procedure has been carried out using the standard method described by Hardie (1962). The photoelectric observations have been reduced using the ESO photometric reduction package RANBO2. The CCD observations have been reduced with either the software package IRAF or ASTPHOT, a synthetic aperture photometric package developed at DLR. When the conditions of the sky were not photometric, the data have been reduced only taking into account the differential extinction between the asteroid and the comparison star. The aspect data, calculated using the Ephemerides Program Ephem (version 1.1, Tholen, 1996) and the telescope used are listed in Table 1 : the mean magnitude level $V(1,\alpha)$, reported in the ninth column, corresponds to the zero level of the respective composite lightcurve. We determined the synodic rotational period, and the corresponding uncertainty for 12 asteroids, by applying Fourier analysis as described in Harris *et al.* (1989). The composite or single lightcurves of the observed asteroids, corrected for the lightime, are presented in Figs 1–15.

Results

The main results are listed in Table 2: the synodic rotational period (when determined), the corresponding reliability code (according to Harris and Young, 1983), the amplitude of the lightcurve and the diameter of each object. The observations of individual objects are discussed below.

424 *Gratia*

This asteroid was observed at the ESO during four nights (10, 21, 23, 24 July 1996) for a total of more then 30 h. The composite lightcurve, shown in Fig. 1, has been obtained with a period of 19.47 ± 0.01 h. The lightcurve is quite regular with an amplitude of 0.32 ± 0.02 mag.

440 *Theodora*

We observed this asteroid at the 0.9 m Dutch telescope of the ESO during two nights (24 and 25 July 1996) for a total of about 18 h. The composite lightcurve, shown in Fig. 2, is quite symmetric with well defined maxima and minima. The computed rotational period is 4.828 ± 0.004 h and the maximum amplitude of the light variation is 0.43 ± 0.03 mag.

446 *Aeternitas*

This asteroid was observed at the 0.5 m ESO telescope during three nights (8–10 July 1996) for a total of about

Table 1. Aspect data of the observed asteroids

Date (0 UT)	R.A. (2000)	Decl (2000)	Longitude (2000)	Latitude (2000)	r (AU)	Δ (AU)	Phase	V (mag)	Observed
424 Gratia									
96/07/10	19 34 13	−24 02 37	290.7	−2.3	2.996	1.981	1.39	—	0.5m ESO
96/07/21	19 24 11	−24 48 49	288.3	−2.7	2.988	1.982	3.35	—	0.5m ESO
96/07/23	19 22 24	−24 56 32	287.9	−2.8	2.986	1.985	4.11	—	0.5m ESO
96/07/24	19 21 31	−25 00 17	287.7	−2.8	2.985	1.988	4.49	—	0.9m Dutch ESO
440 Theodora									
96/07/24	20 08 49	−19 44 45	299.4	−0.3	2.444	1.428	0.57	—	0.9m Dutch ESO
96/07/25	20 07 43	−19 47 24	299.1	−0.4	2.444	1.428	1.07	—	0.9m Dutch ESO
446 Aeternitas									
96/07/08	19 13 18	−38 25 31	284.1	−15.9	2.484	1.491	6.47	—	0.5m ESO
96/07/09	19 12 16	−38 29 16	283.9	−15.9	2.483	1.491	6.54	—	0.5m ESO
96/07/10	19 11 13	−38 32 48	283.7	−15.9	2.483	1.491	6.64	—	0.5m ESO
91 Carina									
96/02/09	09 18 51	−00 57 21	141.7	−15.8	3.133	2.174	5.00	—	1.5m Danish ESO
96/02/10	09 18 08	−00 49 38	141.5	−15.7	3.134	2.173	4.93	—	1.5m Danish ESO
96/02/11	09 17 24	−00 41 47	141.3	−15.6	3.135	2.174	4.88	—	1.5m Danish ESO
96/02/22	09 09 50	+00 50 59	138.9	−14.7	3.145	2.195	6.07	9.6	0.6m Bochum ESO
96/02/23	09 09 12	+00 59 50	138.7	−14.7	3.145	2.199	6.29	9.6	0.6m Bochum ESO
96/02/24	09 08 35	+01 08 44	138.5	−14.6	3.146	2.203	6.52	9.6	0.9m Dutch ESO
96/02/25	09 07 58	+01 17 40	138.3	−14.5	3.147	2.208	6.76	9.6	0.9m Dutch ESO
96/02/26	09 07 22	+01 26 37	138.1	−14.4	3.148	2.212	7.00	9.6	0.9m Dutch ESO
96/02/27	09 06 47	+01 35 36	137.9	−14.3	3.149	2.217	7.26	9.6	0.9m Dutch ESO
727 Nipponia									
96/07/23	19 32 20	−14 08 50	291.8	+7.5	2.646	1.641	4.16	—	0.5m ESO
96/07/24	19 31 26	−14 16 47	291.6	+7.4	2.645	1.642	4.48	—	0.9m Dutch ESO
732 Tjilaki									
96/02/09	07 21 16	+08 27 30	109.9	−13.5	2.501	1.607	11.94	—	0.9m Dutch ESO
96/02/11	07 20 02	+08 41 53	109.6	−13.3	2.500	1.619	12.65	—	0.9m Dutch ESO
96/02/13	07 18 54	+08 56 21	109.3	−13.1	2.499	1.631	13.35	—	0.9m Dutch ESO
96/02/17	07 16 57	+09 25 20	108.7	−12.7	2.498	1.658	14.71	11.4	0.6m Bochum ESO
96/02/18	07 16 32	+09 32 34	108.6	−12.6	2.497	1.666	15.04	11.4	0.6m Bochum ESO
96/02/19	07 16 09	+09 39 47	108.5	−12.5	2.497	1.673	15.36	11.4	0.6m Bochum ESO
96/02/20	07 15 48	+09 46 58	108.4	−12.4	2.497	1.681	15.68	11.5	0.6m Bochum ESO
96/02/21	07 15 29	+09 54 07	108.3	−12.3	2.496	1.689	15.99	11.5	0.6m Bochum ESO
96/02/22	07 15 11	+10 01 15	108.2	−12.1	2.496	1.697	16.30	11.5	0.6m Bochum ESO
96/02/23	07 14 55	+10 08 21	108.1	−12.0	2.495	1.706	16.60	11.5	0.6m Bochum ESO
783 Nora									
96/02/09	09 35 16	−13 57 39	140.8	−0.3	2.805	1.819	0.71	—	0.9m Dutch ESO
96/02/10	09 34 17	−14 05 23	140.5	−0.3	2.803	1.817	0.28	—	0.9m Dutch ESO
96/02/11	09 33 19	−14 13 07	140.3	−0.2	2.802	1.816	0.22	—	0.9m Dutch ESO
96/02/17	09 27 27	−14 59 13	138.7	−0.0	2.796	1.814	2.89	11.4	0.6m Bochum ESO
96/02/18	09 26 29	−15 06 47	138.4	+0.0	2.794	1.815	3.34	11.4	0.6m Bochum ESO
96/02/19	09 25 32	−15 14 18	138.2	+0.0	2.793	1.816	3.79	11.5	0.6m Bochum ESO
96/02/20	09 24 34	−15 21 45	137.9	+0.1	2.792	1.817	4.23	11.5	0.6m Bochum ESO
96/02/21	09 23 38	−15 29 08	137.7	+0.1	2.791	1.819	4.67	11.6	0.6m Bochum ESO
96/02/22	09 22 41	−15 36 27	137.4	+0.2	2.790	1.821	5.11	11.6	0.6m Bochum ESO
96/02/23	09 21 46	−15 43 42	137.2	+0.2	2.788	1.823	5.54	11.6	0.6m Bochum ESO
96/02/24	09 20 51	−15 50 51	136.9	+0.3	2.787	1.826	5.98	11.6	0.9m Dutch ESO
96/02/25	09 19 57	−15 57 55	136.7	+0.3	2.786	1.829	6.41	11.6	0.9m Dutch ESO
96/02/26	09 19 03	−16 04 54	136.4	+0.4	2.785	1.832	6.83	11.6	0.9m Dutch ESO
96/02/28	09 17 19	−16 18 34	136.0	+0.5	2.782	1.839	7.67	11.6	0.9m Dutch ESO
888 Parysatis									
96/07/21	19 20 49	−17 42 45	288.5	+4.3	2.977	1.971	3.49	—	0.5m ESO
96/07/24	19 18 10	−18 00 21	287.9	+4.1	2.927	1.975	4.57	—	0.9m Dutch ESO
1246 Chaka									
96/10/03	00 20 14	+37 50 37	20.6	+32.3	1.882	0.968	17.32	—	1.2m OHP
96/10/04	00 19 20	+37 47 30	20.4	+32.3	1.884	0.969	17.16	—	1.2m OHP

Table 1—*Continued.*

Date (0 UT)	R.A. (2000)	Decl (2000)	Longitude (2000)	Latitude (2000)	r (AU)	Δ (AU)	Phase	V (mag)	Observed
1507 Vaasa									
96/10/05	00 35 19	+25 35 30	17.8	+19.9	1.814	0.845	11.35	—	1.2m OHP
96/10/06	00 34 24	+25 30 58	17.6	+19.9	1.816	0.846	11.18	—	1.2m OHP
1626 Sadeya									
96/02/09	07 07 14	+01 27 53	107.3	−20.9	1.903	1.021	18.29	—	1.5m Danish ESO
96/02/10	07 06 35	+01 20 09	107.1	−21.0	1.905	1.030	18.71	—	1.5m Danish ESO
96/02/11	07 05 59	+01 12 46	107.0	−21.2	1.908	1.039	19.11	—	1.5m Danish ESO
96/02/12	07 05 25	+01 05 42	106.8	−21.3	1.911	1.048	19.51	—	1.5m Danish ESO
96/02/22	07 02 13	+00 10 58	106.1	−22.3	1.939	1.148	22.96	12.5	0.6m Bochum ESO
96/02/23	07 02 08	−00 06 52	106.1	−22.4	1.942	1.159	23.26	12.5	0.6m Bochum ESO
1994 Shane									
96/10/03	00 07 31	−17 42 59	8.2	+15.4	2.198	1.217	6.99	—	1.2m OHP
96/10/04	00 06 48	−17 33 29	8.0	+15.3	2.199	1.219	7.02	—	1.2m OHP
2209 Tianjin									
96/07/25	18 12 45	−20 34 02	272.2	+2.8	2.959	2.033	9.74	—	0.9m Dutch ESO
96/07/26	18 12 08	−20 35 16	271.1	+2.8	2.959	2.039	10.07	—	0.9m Dutch ESO
2446 Lunacharsky									
96/07/12	22 03 02	−18 05 56	325.7	−5.7	2.031	1.124	17.48	—	0.9m Dutch ESO
96/07/13	22 02 42	−18 09 52	325.6	−5.7	2.032	1.117	17.04	—	0.9m Dutch ESO
3776 Vartiovuori									
96/07/12	18 07 18	−57 10 18	270.4	−33.7	3.128	2.265	11.56	—	0.9m Dutch ESO
96/07/13	18 06 05	−57 10 04	270.2	−33.7	3.129	2.269	11.69	—	0.9m Dutch ESO

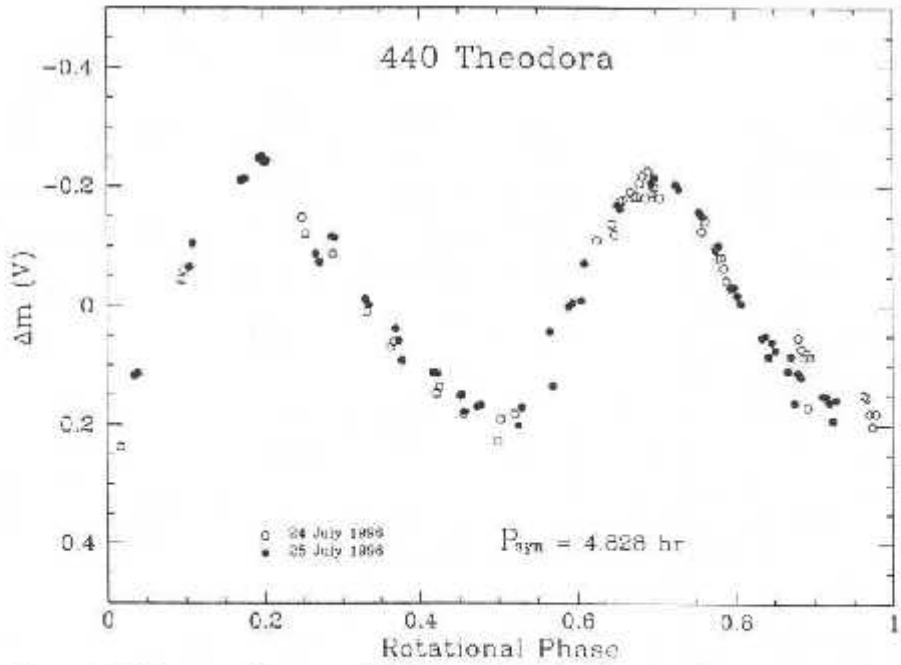

Fig. 2. Composite lightcurve of the asteroid 440 Theodora in rotational phase. Zero phase corresponds to U.T. 1996 July 25.0

Table 2. Physical parameters of the observed asteroids

Asteroid	Rotational Period (hr)	Reliability Code[a]	Amplitude (mag)	D (km)
424 Gratia	19.47±0.01	3	0.32±0.02	87[b]
440 Theodora	4.828±0.004	3	0.43±0.03	19[c]
446 Aeternitas	15.85±0.01	2	>0.33	45[b]
491 Carina	14.87±0.01	3	0.12±0.02	97[b]
727 Nipponia	4.6±0.1	1	0.14±0.02	32[b]
732 Tjilaki	12.34±0.01	3	0.19±0.03	38[b]
783 Nora	34.4±0.5	2	0.08±0.02	40[b]
888 Parysatis	5.49±0.01	3	0.23±0.02	44[b]
1246 Chaka	>20	1	—	18[b]
1507 Vaasa	>14	1	—	10[c]
1626 Sadeya	3.438±0.009	3	0.22±0.02	30[c]
1994 Shane	—	—	—	26[c]
2209 Tianjin	9.47±0.01	3	0.42±0.02	16[b]
2446 Lunacharsky	3.613±0.004	3	0.41±0.02	10[c]
3776 Vartiovuori	7.7±0.1	2	0.12±0.02	24[b]

[a]Meaning of the reliability codes:
1: the result is based on fragmentary lightcurves, may be completely wrong;
2: the result is based on less than full coverage, so that the period may be wrong by 30% or so;
3: sure result with no ambiguity and full lightcurve coverage.
[b]by IRAS (Tedesco *et al.*, 1992)
[c]estimation by Tholen (1996), based on the values of the magnitude and the location on the Solar System.

17 h. Figure 3 shows the composite lightcurve obtained with a rotational period of 15.85±0.01 h with an amplitude larger than 0.33 mag. The rotational phase is not well covered, only two minima and one maximum are defined, and therefore the period is given with a quality code 2.

491 *Carina*

We observed this object at ESO for 9 nights during 1996 for about 35 h. The composite lightcurve shown in Fig. 4 has been obtained fitting the data with a synodical period of 14.87±0.01 h. The lightcurve amplitude is 0.12±0.02 mag.

727 *Nipponia*

This asteroid was observed at the 0.5 m and 0.9 m Dutch telescopes of the ESO during two nights (23–24 July 1996). More than 11 h of observations are available, but because the poor quality of the data, only a tentative solution for the rotational period can be given. Figure 5 shows the composite lightcurve obtained with $P_{syn} = 4.6 \pm 0.1$ h and a quality code 1.

732 *Tjilaki*

This asteroid has been considered as an asteroid target in the Phase A study of the Rosetta mission for an alternative (non baseline) mission to comet P/Wirtanen. We observed this asteroid at ESO for 10 nights during February 1996 for about 35 h and the best fitting rotational period is 12.34±0.01 h. The composite light-curve obtained, shown in Fig. 6, is very asymmetric with a difference between

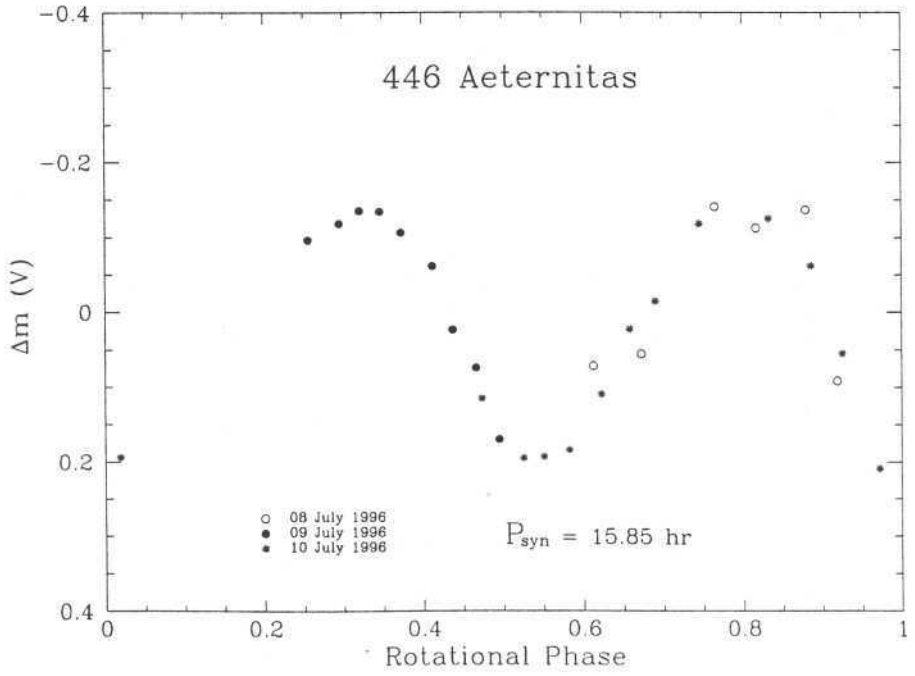

Fig. 3. Composite lightcurve of the asteroid 446 Aeternitas in rotational phase. Zero phase corresponds to U.T. 1996 July 9.0

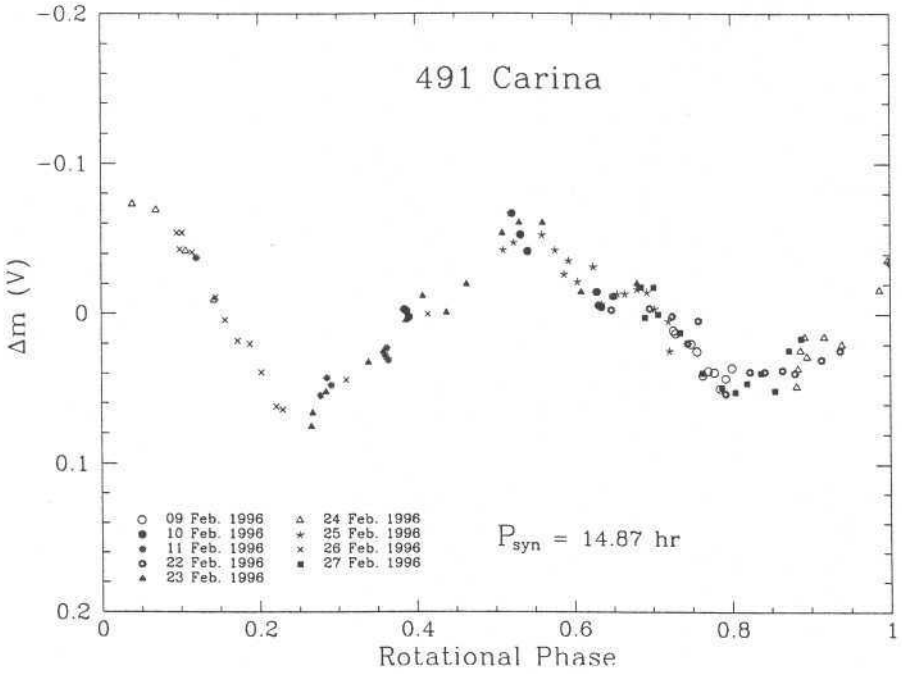

Fig. 4. Composite lightcurve of the asteroid 491 Carina in rotational phase. Zero phase corresponds to U.T. 1996 February 21.0

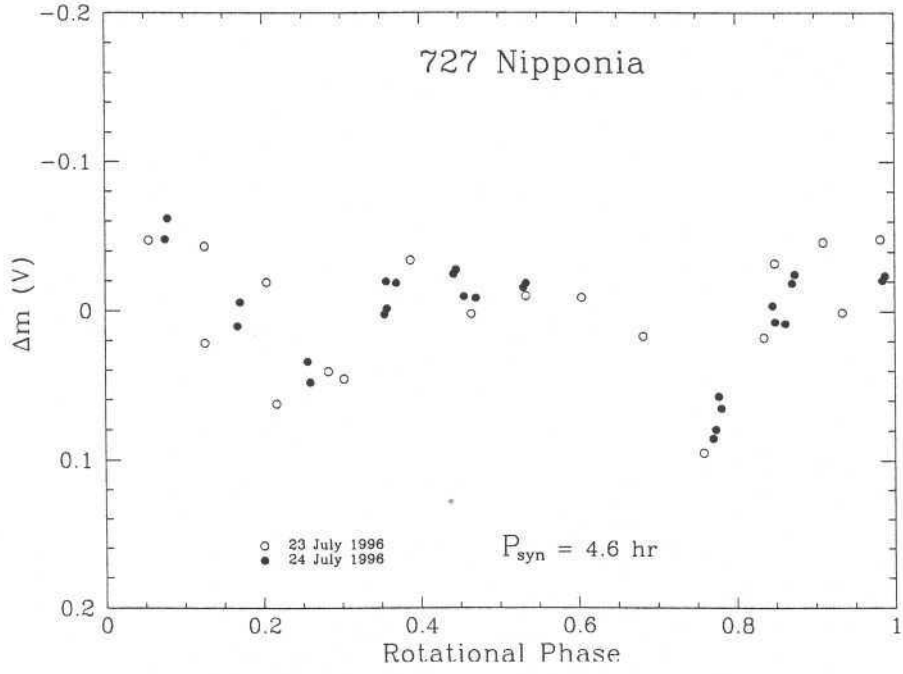

Fig. 5. Composite lightcurve of the asteroid 727 Nipponia in rotational phase. Zero phase corresponds to U.T. 1996 July 24.0

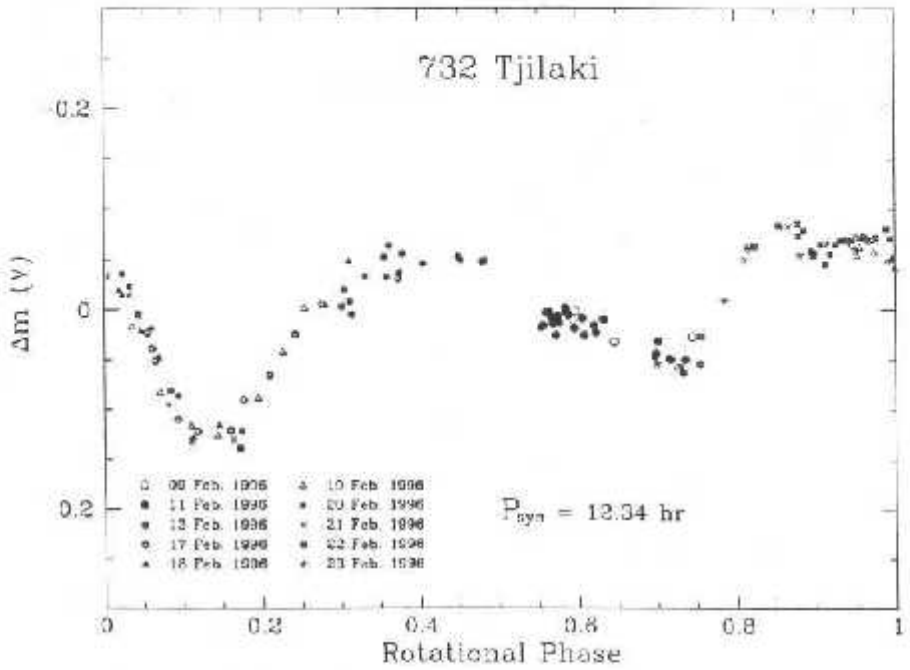

Fig. 6. Composite lightcurve of the asteroid 732 Tjilaki in rotational phase. Zero phase corresponds to U.T. 1996 February 17.0

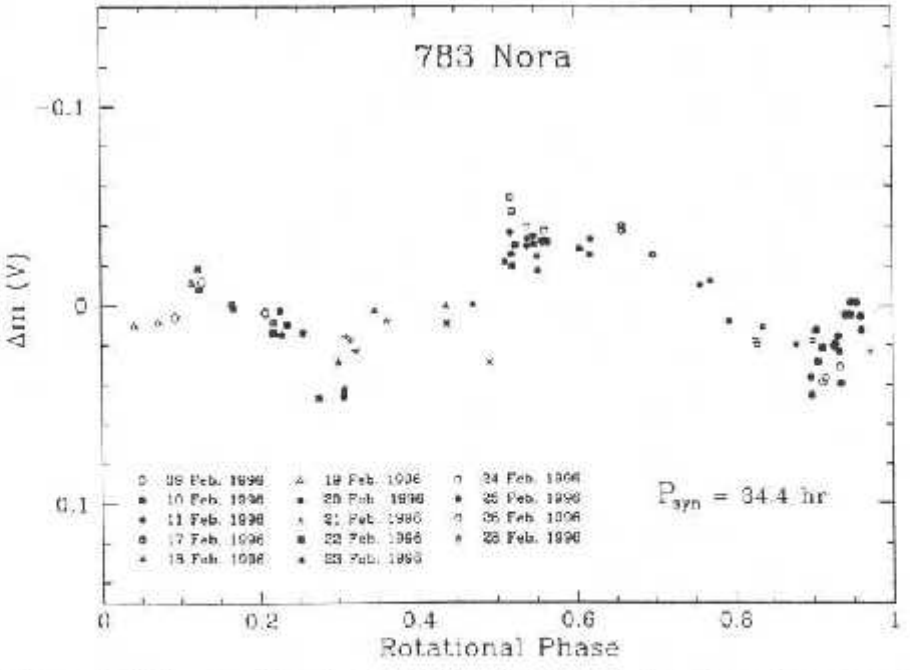

Fig. 7. Composite lightcurve of the asteroid 783 Nora in rotational phase. Zero phase corresponds to U.T. 1996 February 19.0

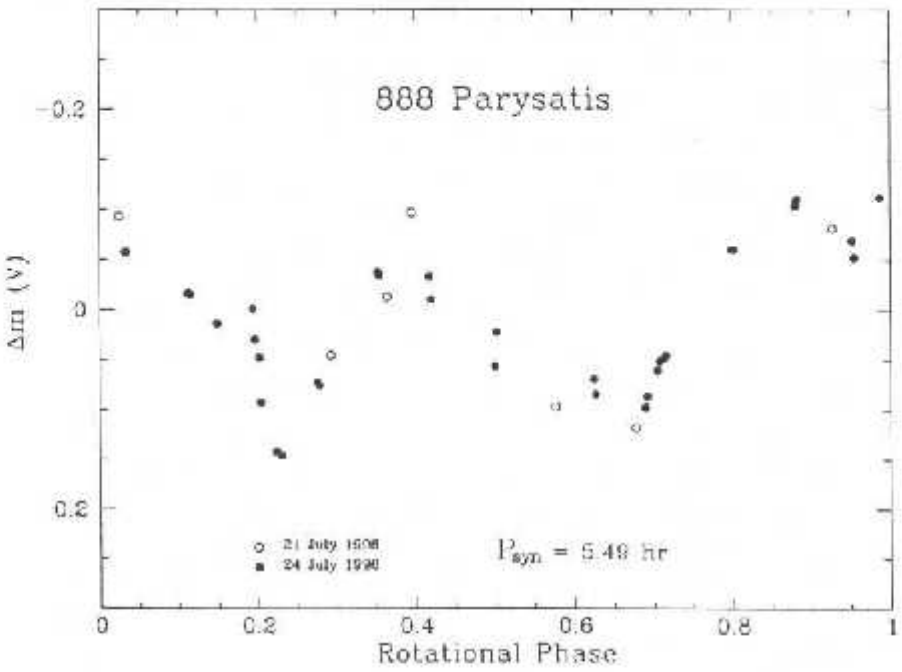

Fig. 8. Composite lightcurve of the asteroid 888 Parysatis in rotational phase. Zero phase corresponds to U.T. 1996 July 24.0

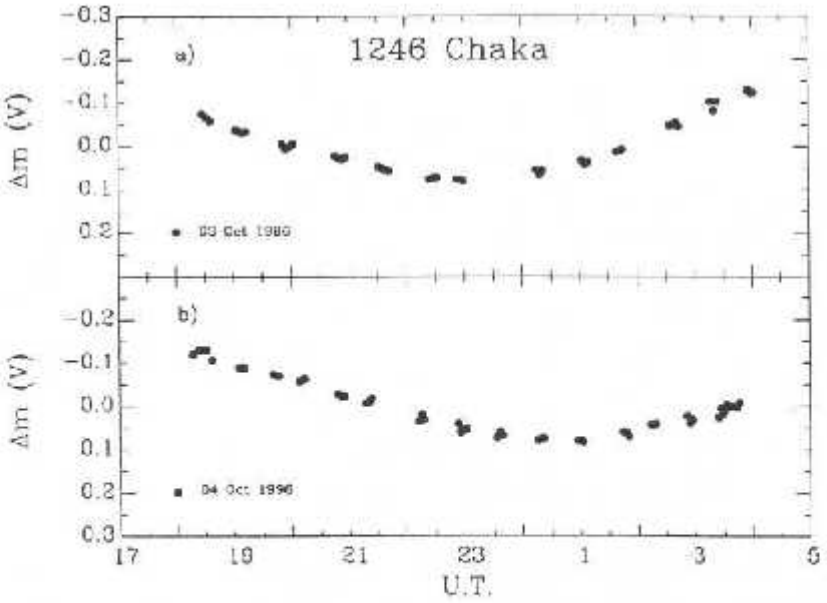

Fig. 9. Single night lightcurves of the asteroid 1246 Chaka for the nights (a) 1996, October 3 and (b) 1996, October 4

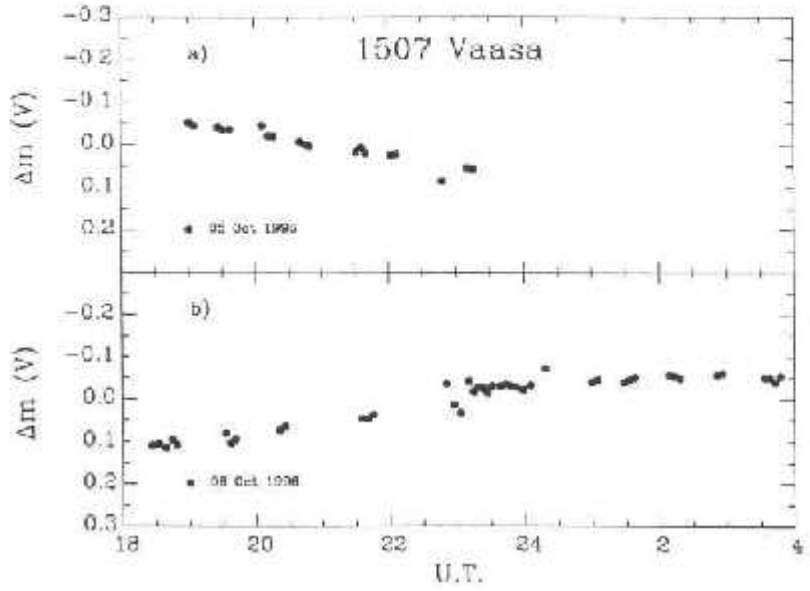

Fig. 10. Single night lightcurves of the asteroid 1507 Vaasa for the nights (a) 1996, October 5 and (b) 1996, October 6

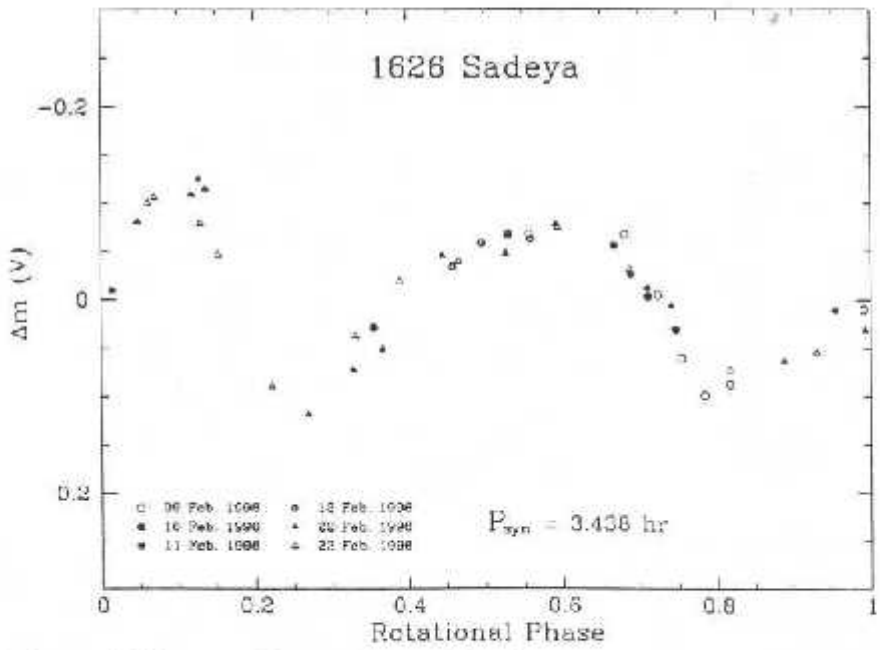

Fig. 11. Composite lightcurve of the asteroid 1626 Sadeya in rotational phase. Zero phase corresponds to U.T. 1996 February 17.0

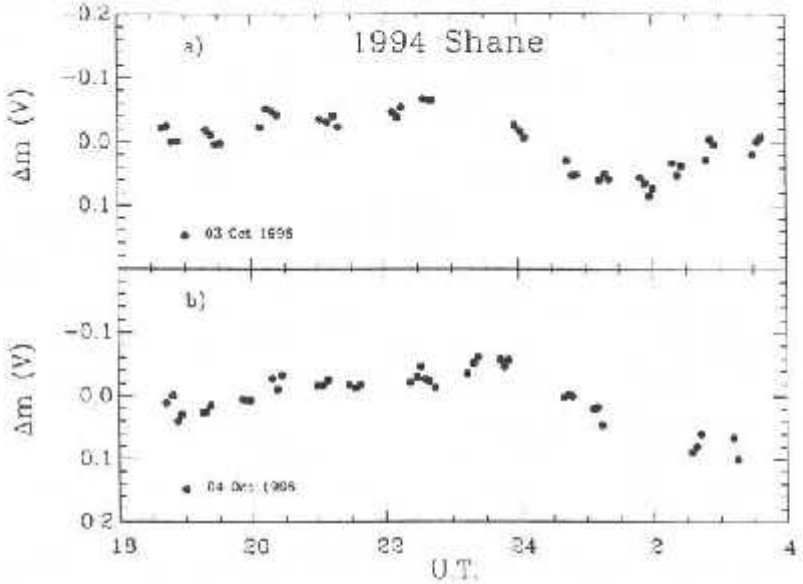

Fig. 12. Single night lightcurves of the asteroid 1994 Shane for the nights (a) 1996, October 3 and (b) 1996, October 4

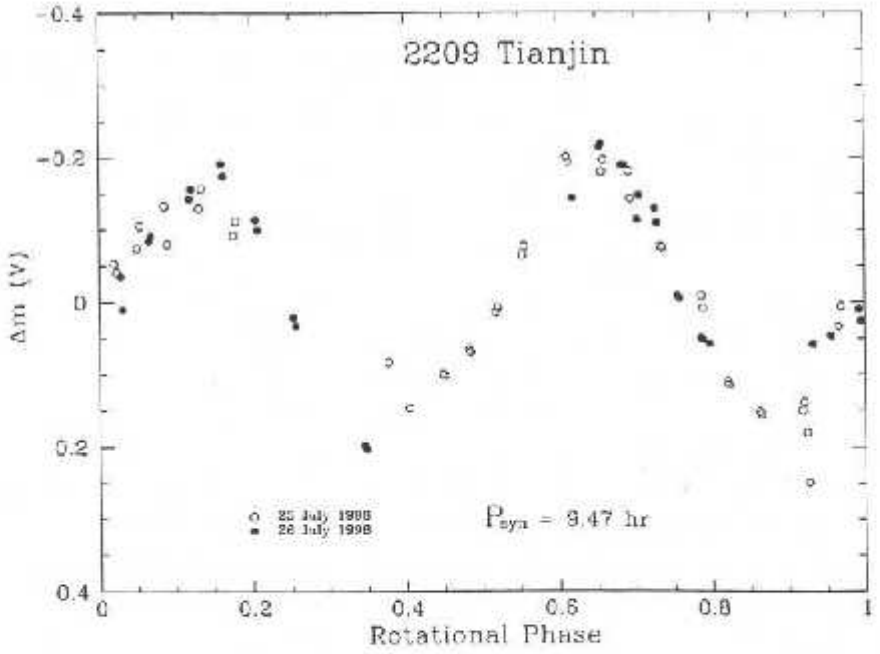

Fig. 13. Composite lightcurve of the asteroid 2209 Tianjin in rotational phase. Zero phase corresponds to U.T. 1996 July 26.0

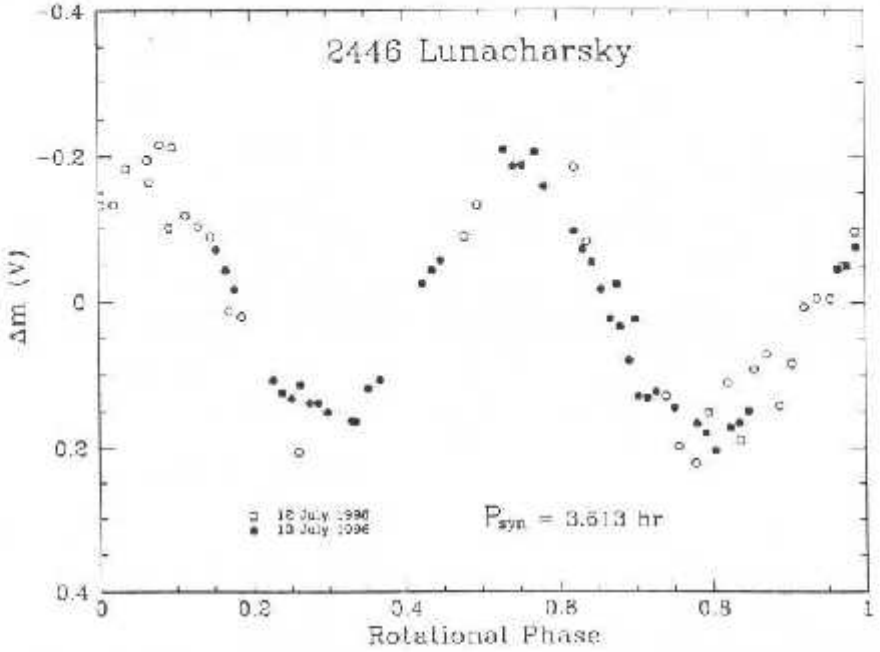

Fig. 14. Composite lightcurve of the asteroid 2446 Lunacharsky in rotational phase. Zero phase corresponds to U.T. 1996 July 13.0

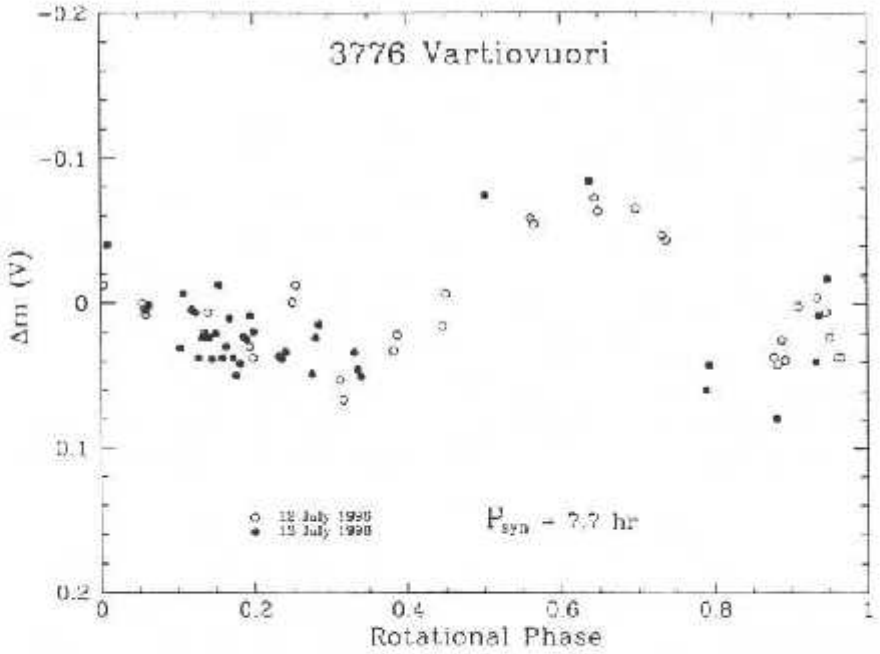

Fig. 15. Composite lightcurve of the asteroid 3776 Vartiovuori in rotational phase. Zero phase corresponds to U.T. 1996 July 13.0

the principal and secondary minima of 0.07 mag. The lightcurve amplitude is 0.19 ± 0.03 mag.

783 *Nora*

This object was observed for one night during the 1990 apparition (Lagerkvist *et al.*, 1992) and the lightcurve obtained suggested a long rotational period. During the 1996 apparition we reobserved 783 Nora during 14 nights. The obtained data are very close to the opposition, phase angles ranging between 0.2 and 8°. Figure 7 shows the composite lightcurve with a rotational period of 34.4 ± 0.5 h. However, owing to the long rotational period, the large dispersion and the small amplitude (0.08 ± 0.02 mag), alternative rotational periods cannot be completely excluded.

888 *Parysatis*

We observed 888 Parysatis at ESO during two nights (21–24 July 1996) for a total of about 15 h. The composite lightcurve, shown in Fig. 8, has been obtained by fitting the single night lightcurves with a rotational period of 5.49 ± 0.01 h. The obtained amplitude is 0.23 ± 0.02 mag.

1246 *Chaka*

1246 Chaka was observed at the 1.2 m telescope of the OHP during 2 nights (3–4 October) for a total of about 20 h. The two single night lightcurves (Fig. 9) display two different wide minima suggesting a period longer than 20 h.

1507 *Vaasa*

We observed 1507 Vaasa during two nights (5 and 6 October) in 1996 at the 1.2 m telescope of the OHP for about 14 h. The available single night lightcurves, shown in Fig. 10, did not allow us to determine an unique rotational period. From the available data it seems longer then 14 h.

1626 *Sadeya*

1626 Sadeya was observed during 1996 for 6 nights 9, 10, 11, 12, 22, 23 February) at ESO for more than 13 h. The composite lightcurve, shown in Fig. 11, is very asymmetric with a principal maximum wider and brighter than the secondary one. The computed rotational period is 3.438 ± 0.009 h and the amplitude obtained is 0.22 ± 0.02 mag.

1994 *Shane*

This object has been observed at the 1.2 m telescope of the OHP during two nights (3 and 4 October 1996). The individual lightcurves are shown in Fig. 12 and seem to cover the same maximum. This constrains the rotational period to be either 12 h or a longer multiple of 6 h (such as 18 or 24 h) but no definitive conclusion can be drawn from the available data.

2209 *Tianjin*

2209 Tianjin was observed with the 0.9 m Dutch telescope at ESO during two nights in 1996 (25–26 July) for a total of about 16 h. The composite lightcurve, obtained with a rotational period of 9.47 ± 0.01 h, is shown in Fig. 13 with a maximum amplitude of 0.42 ± 0.02 mag.

2446 *Lunacharsky*

We observed this object in 1996 at the 0.9 m Dutch telescope at ESO (12–13 July) for more than 9 h. Figure 14 shows the composite lightcurve, obtained fitting the observed data with a rotational period of 3.613 ± 0.004 h. The lightcurve is quite asymmetric with an amplitude of 0.41 ± 0.02 mag.

3776 *Vartiovuori*

3776 Vartiovuori was observed at the 0.9 m Dutch telescope of the ESO for more than 15 h (12–13 July 1996). The composite lightcurve, shown in Fig. 15, has been obtained fitting the single night lightcurves with a rotational period of 7.7 ± 0.1 h. However, a somewhat longer rotational period (11.5 h) cannot be completely excluded with the available data.

Acknowledgements. E. Dotto and M. Florczak thank ESA and CNPq, respectively, for the financial support during the present research.

References

Binzel, R., Farinella, P., Zappalà, V., Cellino V. (1989) Asteroid rotation rates: distributions and statistics. In *Asteroids II*, eds. R. Binzel, T. Gehrels, and M. S. Matthews, pp. 416–441. University of Arizona Press, Tucson, AZ.

Fulchignoni, M., Barucci, M. A., Di Martino, M. and Dotto, E. (1995) On the evolution of the asteroid spin. *Astron. Astrophys.* **299**, 929–932.

Graham, J. A. (1982) UBVRI standard stars in the E-regions. *P.A.S.P.* **94**, 244–265.

Hardie, R. H. (1962) Photoelectric reductions. In *Astronomical techniques*, Vol. II. *Stars and Stellar Systems*, ed. A. W. Hintler, pp. 178–208. The University of Chicago Press, Chicago and London.

Harris, A. W. (1994) Tumbling asteroids. *Icarus* **107**, 209–211.

Harris, A. W. (1996) The rotation rates of very small asteroids: evidence for "rubble-pile" structure. *Lunar Planet. Sci.* **XXVII**, 493–494.

Harris, A. W. and Young, J. W. (1983) Asteroid rotation—IV. 1979 observations. *Icarus* **54**, 59–109.

Harris, A. W., Young, J. W., Bowell, E., Martin, L. J., Millis, R. L., Poutanen, M., Scaltriti, F., Zappalà, V., Schober, H. J. and Zeigler, H. W. (1989) Photometric observations of asteroids 3, 24, 60, 261 and 863. *Icarus* **77**, 171–186.

Lagerkvist, C.-I., Magnusson, R., Debehogne, H., Hoffmann, M., Erikson, A., De Campos, A. and Cutispoto, G. (1992) Physical studies of asteroids—XXV Photoelectric photometry of asteroids obtained at FSO and Hoher List Observatory. *Astron. Astrophys. Supl. Ser.* **95**, 461–470.

Landolt, A. U. (1983) UBVRI photometric standard stars around the celestial equator. *Astron. J.* **88**, 439–460.

Lasker, B. M., Sturch, C. R., Lopez, C., Mallamas, A. D., McLaughlin, S. F., Russell, J. L., Wisniewski, W. Z., Gillespie, B. A., Jenkner, H., Siciliano, E. D., Kenny, D., Baumert, J. H., Goldberg, A. M., Henry, G. W., Kemper, E. and Siegel, M. J. (1988) The guide star photometric catalog. *Astroph. J. Suppl. Ser.* **68**, 1–90.

Tedesco, E. F., Veeder, G. J., Fowler, J.W. and Chillemi, J. R. (1992) The Irus Minor Planet Survey PL-TR-92-2049.

Tholen, D. J. (1996) Ephemerides Program Ephem version 1.1, Celestech.

4.3.2 - Asteróides com Período de Rotação Longo

A distribuição dos asteróides com período de rotação conhecido (734 até o ano de 1997) mostra que a grande maioria tem um período de rotação entre 5 e 10 horas (fig 4.3). Apenas 66 possuem um período superior a 24 horas, sendo que a qualidade da determinação destes períodos é, em sua grande maioria, ruim. Em muitos casos não temos um período definido mas apenas uma estimativa de um valor mínimo; por exemplo, encontramos tabelado "período superior a 24, 40, 50, etc, horas". Harris (1994a) analisou a curva de luz de alguns destes asteróides com período de rotação longo e propôs como explicação uma forma muito irregular juntamente com um estado rotacional excitado. Harris se referiu a estes asteróides como *tumbling asteroids*. Este estado de rotação excitado poderia, segundo ele, ser devido a uma colisão recente ou ser remanescente dos processos caóticos originais. Neste segundo caso, seria necessário que o tempo de dissipação da energia rotacional fosse superior à idade do Sistema Solar. Harris substituiu na equação 4.3 obtida por Burns e Safronov (1973) valores considerados típicos para objetos do Sistema Solar, encontrando a seguinte relação:

$$P \approx 17 D^{2/3} \tau^{1/3} \qquad 4.5$$

onde P é o período de rotação em horas, D é o diâmetro do corpo em quilômetros e τ é o tempo de relaxação.

Na figura 4.3 vemos um gráfico que mostra a equação 4.5 obtida para três diferentes tempos de relaxação. Podemos notar que 6 objetos se encontram abaixo da linha de 4,5 bilhões de anos. Isto implica que se estes asteróides se encontram em um estado excitado de rotação, deveriam levar um tempo maior do que a idade do Sistema Solar para chegar a um estado de rotação onde o eixo de rotação teria o máximo momento de inércia. Por outro lado, estes objetos possuem um diâmetro inferior a 50 km, cujo tempo estimado para que sofram pelo menos uma colisão no cinturão é de $\sim 10^8$ anos (Housen et al, 1991). Conseqüentemente, Harris concluiu que estes asteróides são fortes candidatos a

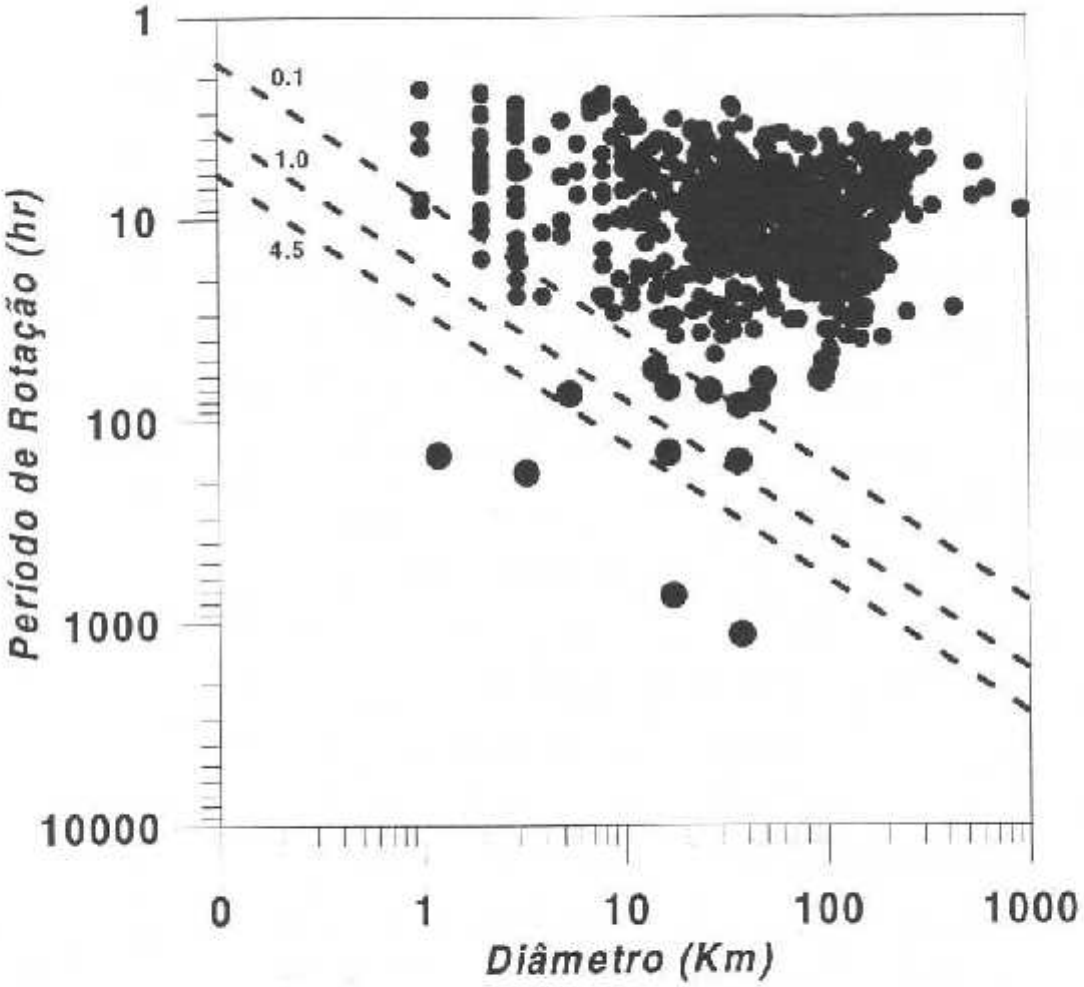

Figura (4.3) *Distribuição dos períodos de rotação em função do diâmetro para 734 asteróides. As três linhas se referem à equação 4.5 com tempos de relaxação de 100 milhões, 1 e 4,5 bilhões de anos respectivamente. Os objetos que estão abaixo da linha de 4,5 bilhões de anos são fortes candidatos a se encontrarem num estado de rotação excitado.*

"tumbling", já que muito provavelmente sofreram uma colisão e ainda não tiveram tempo de atingir um estado de rotação puro.

É importante ressaltar que alguns outros efeitos também podem causar irregularidades nas curvas de luz, fazendo com que não possamos estimar com segurança os períodos de rotação dos objetos, podendo levar à conjectura de que sejam asteróides "tumbling", tais como: a forma irregular dos asteróides, binárias de contato (como Castalia e Toutatis), e satélites de asteróide (como Dactyl, satélite de 243 Ida).

Com o objetivo de aumentar nosso conhecimento sobre os asteróides que exibem uma rotação aparentemente longa e/ou complexa, selecionamos 22 objetos no *Ephemerides of Minor Planets* cujos períodos de rotação eram considerados longos e com qualidade ruim. Todas as estimativas para os períodos de rotação destes objetos eram superiores a 12 horas. Realizamos então várias campanhas de observação fotométrica a fim de obter suas curvas de luz, e também observações espectroscópicas a fim de verificar a existência de algumas características composicionais peculiares. Nossos resultados podem ser resumidos em:

a) Obtivemos curvas de luz para 10 destes objetos (a tabela 2a mostra as estimativas dos períodos de rotação e amplitude média das curvas de luz para 5 asteróides). Dois objetos apresentam períodos inferiores a 10 horas e três superiores a 20 horas. A qualidade na determinação destes períodos permanece ruim. Uma rotação complexa não pode ser determinada com os nossos dados, já que seria necessária uma campanha observacional de monitoramento durante um período muito longo de observação sem grandes interrupções, de forma a se obter uma curva de luz completa . Isto não foi possível devido a problemas meteorológicos e à distribuição de tempo de telescópio para este projeto. Para 4 objetos, as curvas de luz obtidas não permitiram sequer uma estimativa de período.

b) Na análise dos espectros de 18 destes asteróides não encontramos qualquer característica de composição peculiar. Em termos de distância heliocêntrica os espectros obtidos são os esperados, entre tipos S e C, correspondentes aos tipos taxonômicos mais comuns encontrados nestas regiões. A maior parte dos objetos do tipo C apresentam também indicação de um processo de alteração aquosa (ver capítulo 3).

9013 Elsevier PSS Ms 991 December 1998 MFC

PERGAMON

JOURNAL LOGO

Planetary and Space Science 00 (1998) 000–000

A contribution to the study of asteroids with long rotational period[1]

Cláudia A. Angeli[a,*], Daniela Lazzaro[a], Marcos A. Florczak[a,b], Alberto S. Betzler[a,c], Jorge M. Carvano[a]

[a] *Observatório Nacional, Dep. de Astrofísica, Rua Gal. José Cristino 77, 20921-400 Rio de Janeiro, Brazil*
[b] *CEFET, Dep. Faisica, 80000 Curitiba, Brazil*
[c] *Universidade Federal do Rio de Janeiro, Obs. Valongo, Rio de Janeiro, Brazil*

Received 27 March 1998; received in revised form 13 October 1998; accepted 18 October 1998

Abstract

We report the results of new photometric and/or spectroscopic observations of 22 asteroids, selected among a sample of presumed *slow rotators*. All the available previous estimations of their rotation periods give values larger than 12 h. It has been recently suggested by Harris (1994) that some of these asteroids could be in a motion of non-principal axis rotation, due to a primordial excited state. The observations reported here were carried on at the Observatório do Pico-dos-Dias (Brazil), at the Observatoire de Haute-Provence (France), and at the European Southern Observatory (Chile). More than 60 single night lightcurves were obtained. Rotation periods and the corresponding composite lightcurves were obtained for 5 objects. Spectroscopic observations were also carried on to increase the knowledge on these objects and verify the hypothesis of a common origin. We have obtained reflectivity spectra covering 0.5–0.6 μm for 18 objects with orbital semi-major axes between 2.23 and 3.15 AU. For most of them (11) the spectra suggest a C-type composition, and for the others an S or E-type. Between the C-type asteroids, all but two show features associated with an aqueous alteration process.

1. Introduction

The analysis of the asteroid rotation periods can give us information about the collisional evolution of the asteroid population. Several works aiming to understand the global collisional evolution of the asteroids have been undertaken since the seventies. McAdoo and Burns (1973), analysing 64 rotation periods known at that time, concluded that the smaller asteroids rotate faster than the larger ones. Later, studying a sample of 182 asteroids, Harris and Burns (1979) also concluded that there was a tendency for smaller asteroids to rotate faster than larger ones. The rotation rate dispersions seemed to be consistent with a tridimensional Maxwellian distribution, as we suppose would be the case for a collisionally evolved system. On the other hand, Tedesco and Zappalà (1980), analysing data for 134 main belt asteroids, did not find a defined relationship between asteroid sizes and rotation rates, even if they identified a large asteroid group ($D \geqslant 175$ km) which seemed to rotate faster than the other asteroids in the sample. Burns and Tedesco (1979) also concluded that the asteroids with $D > 175$ km rotate faster than the others. Like other authors, they concluded that a much larger database would be necessary to confirm this tendency.

Dermott and Murray (1982) have analysed the same sample of 134 asteroids studied by Tedesco and Zappalà (1980) and have shown that the rotation frequencies were dependent on the asteroid taxonomic type and diameter. Farinella et al. (1981) have reanalysed Harris and Burns (1979) and Tedesco and Zappala's (1980) results, concluding that the larger asteroids rotate faster than those of intermediate size. They also suggested that it seemed to have an excess of slow rotators among the asteroids of small to intermediate size. Dermott et al. (1984) and Binzel (1984), analyzing samples of 217 and 66 objects, respectively, suggested the existence of two populations: the slow and the fast asteroids.

Binzel et al. (1989) have summarized the knowledge on asteroid rotation rates with the study of 375 rotation periods known with a quality code $\geqslant 1$. The results of their analyses have confirmed that the distribution of the larger asteroids ($125 \leqslant D < 200$ km and $D \geqslant 200$ km) can be fitted by Maxwellian distributions. The whole

* Corresponding author. Tel./fax: 55-21 580 7181; e-mail angeli@on.br

[1] Observations carried on at the Observatório do Pico dos Dias, operated by the Laboratório Nacional de Astrofísica (Brazil), at the Observatoire de Haute-Provence (France), and at the European Southern Observatory (Chile), under the agreement with the CNPq/ Observatório Nacional (Brazil).

S0032-0633/98/$—see front matter
PII: S0032-0633(98)00122-6

sample and the different sub-samples of smaller sizes deviate from a Maxwellian and even from a linear combination of two Maxwellians. However, for the sample in the range of $50 \leqslant D < 125$ km, a very good fit is obtained with the combination of two Maxwellian functions. The asteroids with $D < 125$ km show an excess of slow rotators and their non-Maxwellian distributions suggest that their rotation rates might be more strongly affected by processes like catastrophic perturbation events.

More recently, Fulchignoni et al. (1995) analysed the rotation periods of 516 asteroids with a quality code $\geqslant 2$. They obtained very good fits to the distributions of the larger asteroids with one Maxwellian function, and of the smaller asteroids with a linear combination of three Maxwellian functions. Angeli (1995), studying a sample of 585 asteroids, obtained results very close to those of Fulchignoni et al. (1995). The sample was composed of all the rotation periods published (with quality code $\geqslant 2$) in the literature until July 1995, plus the rotation periods (20) computed by the author between 1992 and 1995, that is, 13% (69 objects) more than the amount contained in the previous analysis. As in the work by Fulchignoni et al., the whole sample has been divided in two sets: the larger asteroids ($D > 50$ km) and the smaller ones ($D \leqslant 50$ km). A very good fit has been obtained to the distribution of the larger asteroids, with only one Maxwellian function. The best fit obtained for the smaller asteroids considers the linear combination of three Maxwellian functions and suggests that three distinct populations can explain the observed distribution. The first population superimposes exactly the larger objects population, is represented by a Maxwellian distribution with a mean period of 8.7 h, and contains 2/3 of the whole sample. The second population contains the fast rotators (Maxwellian function with a mean period of 4.1 h) and is formed by 25% of the whole population; and the third population account mainly for the slow rotators (Maxwellian function with a mean period of 24.7 h), composed by 0.11 of the whole sample. It is important to stress out that this population of slow rotators is probably underrepresented in the sample, because their rotation periods are in general computed with a very low precision (quality code 1).

At the moment, a very modest amount of rotation periods of slow rotation objects is available from lightcurve analysis. Although these periods are not known with a high precision, Harris (1994) suggests that it can be question of objects presenting a complex rotation motion around more than one rotation axis. Following Harris (1994), the damping time scale of rotational wobble, for small asteroids with a long rotation period, to a state of principal-axis rotation about the axis of maximum moment of inertia is expected to be considerably longer than the age of the Solar System. These objects may, therefore, exhibit non-principal-axis rotation, which in an extreme case may lead to the appearance of an irregular 'tumbling' in space. For two of these objects, 4179 Toutatis (Spencer et al., 1995), and 253 Mathilde (Mottola et al., 1995), worldwide campaigns allowed the determining of a principal rotation and a wobbling around it, somehow confirming this hypothesis.

A complete and secure statistical picture of asteroid rotation properties must take into account the rotation of these slow objects, but further observations and reliable period determinations are still needed. In order to enlarge the knowledge about the rotational behavior of these slow asteroids and increase the reliability in the determination of their periods, we started a systematic observational program. We have observed 22 asteroids photometrically and/or spectroscopically, whose results are presented below.

2. Observations and reductions

2.1. Photometry

The photometric observations reported here were performed at the Observatório do Pico-dos-Dias (OPD, Brazil), on a 0.6 m telescope, and at the Observatoire de Haute-Provence (OHP, France), on a 1.2 m telescope. All the observations were carried out using CCD cameras in the V band. In the OPD observations a CCD EEV-385 × 576 was used, with a focal-plane reducing optics giving a 7.2′ × 5.5′ field and yielding a scale image of 1.12″ pix. In the OHP observations a CCD camera Tek 512 × 512 with a scale image of 0.82″ pix and a 7′ × 7′ field was used.

The observational circumstances and the aspect data are listed in Table 1(a). The UT date and hour, right ascension, declination, ecliptic longitude and latitude, heliocentric (r) and topocentric (Δ) distances, and solar phase angle are given. These values were obtained using EPHEM program by Tholen (1997). The mean magnitude level $V(1,\alpha)$, reported in the ninth column, corresponds to the zero level of the respective composite lightcurve for the asteroids 588 and 2260; for 141, 249 and 1646 they correspond to an average magnitude value of the night. This is done because for these three asteroids some nights were not of good quality, so the composite lightcurves have been made just with relative magnitudes (the differential extinction between the asteroid and a comparison star). So, for 141, 249 and 1646 the values given in Table 1 do not correspond to the zero level of the lightcurves, but to an average value of the magnitude of the respective night. In the last column the telescope size is given, and the times reported have not been corrected for light-travel time. The images were reduced using DAOPHOT, a routine of the Image Reduction and Analysis Facility (IRAF) package, and calibrated using standard methods with bias and dome flat-field images.

Table 1(a)
Aspect data of the observed asteroids

Date (00:00UT)		R.A. (2000) h min s	Decl (2000)	Long. (2000)	Lat. (2000)	r (AU)	Δ (AU)	Phase (deg)	V(1,α) (mag)	Tel.
58 Concordia										
1995	08 14	01 44 31.03	+07°47'41.5	27.0	−2.8	2.882	2.258	19.17	—	0.6 m*
	08 18	01 45 28.43	+07°43'57.2	27.2	−2.9	2.823	2.210	18.57	—	0.6 m*
	10 01	01 32 17.06	+04°44'10.6	23.1	−4.5	2.822	1.847	5.72	—	0.6 m*
	10 03	01 30 48.30	+04°31'34.5	22.6	−4.6	2.822	1.841	4.94	—	0.6 m*
1997	02 11	07 41 18.32	+16°40'17.5	114.2	−4.6	2.648	1.738	10.21	—	0.6 m*
	02 13	07 39 26.23	+16°52'28.2	113.8	−4.5	2.647	1.757	11.35	—	0.6 m*
	03 11	07 33 25.96	+18°15'33.9	112.1	−3.4	2.636	1.987	18.93	—	0.6 m*
	03 12	07 33 35.12	+18°17'48.0	112.1	−3.3	2.635	1.998	19.13	—	0.6 m*
120 Lachesis										
1995	08 18	23 37 28.39	−01°45'21.4	354.1	+0.6	3.230	2.310	8.87	—	0.6 m*
	10 01	23 05 42.23	−03°47'07.1	346.0	+1.8	3.250	2.298	6.46	—	0.6 m*
	10 03	23 04 26.05	−03°52'07.7	345.7	+1.9	3.251	2.310	7.11	—	0.6 m*
141 Lumen										
1995	08 13	02 26 39.51	+27°10'11.7	43.1	+11.9	2.094	1.716	28.70	—	0.6 m*
	08 14	02 27 27.79	+27°19'24.5	43.3	+12.0	2.094	1.709	28.67	9.705±0.033	0.6 m*
	08 15	02 28 34.74	+27°32'26.5	43.7	+12.1	2.094	1.698	28.62	9.668±0.033	0.6 m*
	09 28	02 52 03.53	+35°40'03.2	51.2	+18.3	2.105	1.311	21.21	9.124±0.033	0.6 m*
	10 01	02 50 52.74	+36°11'56.8	51.1	+18.9	2.107	1.284	19.92	—	0.6 m*
	10 02	02 50 57.65	+36°10'25.1	51.2	+18.8	2.107	1.285	19.99	9.415±0.033	0.6 m*
	10 03	02 50 35.53	+36°17'25.1	51.1	+19.0	2.108	1.279	19.67	9.266±0.033	0.6 m*
1997	02 12	10 49 24.29	+01°33'37.8	163.1	−5.4	3.050	2.102	6.20	—	0.6 m*
	02 14	10 48 31.30	+01°35'14.7	162.9	−5.5	3.052	2.098	5.84	8.885±0.033	0.6 m*
	03 12	10 24 30.95	+02°40'48.1	156.9	−6.7	3.088	2.121	5.10	8.820±0.027	0.6 m*
	03 13	10 23 39.86	+02°43'42.0	156.6	−6.8	3.089	2.125	5.45	8.880±0.027	0.6 m*
249 Ilse										
1995	08 13	22 15 31.62	−14°20'36.0	330.6	−3.3	1.998	0.995	5.67	—	0.6 m*
	08 14	22 14 30.34	−14°18'54.2	330.3	−3.1	1.996	0.991	5.09	11.795±0.011	0.6 m*
	08 15	22 13 27.99	−14°17'11.3	330.1	−3.0	1.994	0.987	4.52	11.543±0.011	0.6 m*
	08 17	22 11 20.44	−14°13'40.5	329.7	−2.8	1.991	0.981	3.37	—	0.6 m*
	08 18	22 10 15.42	−14°11'52.2	329.4	−2.7	1.989	0.979	2.80	11.580±0.011	0.6 m*
1997	02 12	10 26 34.66	+11°05'20.4	154.3	+1.2	2.663	1.688	4.06	11.690±0.011	0.6 m*
	02 14	10 24 26.05	+11°10'45.4	153.7	+1.1	2.667	1.686	3.12	—	0.6 m*
	03 12	09 57 38.14	+12°09'33.2	147.3	−0.2	2.711	1.774	8.64	11.974±0.010	0.6 m*
437 Rhodia										
1996	01 26	08 33 02.85	+10°53'09.8	127.8	−7.6	2.935	1.957	2.60	—	0.6 m*
	01 28	08 30 58.87	+10°58'02.6	127.3	−7.7	2.937	1.958	2.61	—	0.6 m*
1997	05 11	13 17 34.51	−17°53'09.0	204.6	−8.9	2.438	1.500	11.23	—	0.6 m*
	05 12	13 16 52.36	−17°45'01.3	204.4	−8.9	2.435	1.502	11.66	—	0.6 m*
	05 13	13 16 11.71	−17°36'56.8	204.2	−8.8	2.432	1.505	12.07	—	0.6 m*
588 Achilles										
1995	08 14	20 58 33.72	−17°50'59.0	311.9	−0.6	5.660	4.656	1.58	8.655±0.014	0.6 m*
	08 15	20 58 02.82	−17°52'09.4	311.8	−0.6	5.659	4.658	1.77	8.710±0.014	0.6 m*
	08 17	20 57 01.52	−17°54'26.8	311.6	−0.6	5.657	4.663	2.15	8.643±0.014	0.6 m*
	08 18	20 56 31.16	−17°55'33.7	311.4	−0.6	5.656	4.666	2.33	8.677±0.014	0.6 m*
617 Patroclus										
1995	04 25	12 37 02.30	+13°02'24.4	183.2	+15.6	5.922	5.073	5.64	—	1.2 m
	04 26	12 36 36.47	+13°02'03.7	183.1	+15.5	5.922	5.081	5.77	—	1.2 m
	04 27	12 36 11.05	+13°01'37.8	183.0	+15.5	5.922	5.089	5.90	—	1.2 m
	06 05	12 26 39.28	+11°41'32.9	181.3	+13.3	5.910	5.549	9.49	—	0.6 m
1996	04 24	14 02 55.76	−05°41'43.8	210.6	+6.3	5.749	4.750	1.27	—	0.6 m
1997	05 12	15 36 06.26	−25°29'38.7	237.7	−5.9	5.432	4.432	1.62	—	0.6 m
	05 13	15 35 29.81	−25°29'55.2	237.6	−6.0	5.432	4.429	1.49	—	0.6 m
	05 14	15 34 53.25	−25°30'09.6	237.5	−6.0	5.431	4.427	1.37	—	0.6 m
1236 Thals										
1995	08 12	20 27 46.45	−45°20'09.8	297.8	−25.4	1.948	1.019	16.49	—	0.6 m
	08 13	20 26 47.74	−45°20'09.1	297.7	−25.3	1.947	1.021	16.82	—	0.6 m
	08 14	20 25 50.52	−45°19'42.6	297.5	−25.3	1.945	1.023	17.15	—	0.6 m
	08 17	20 23 09.00	−45°15'50.5	297.0	−25.1	1.939	1.030	18.16	—	0.6 m
	09 27	20 23 54.48	−39°40'23.8	298.7	−19.7	1.875	1.244	29.52	—	0.6 m

Table 1(a)
Continued

Date (00:00UT)		R.A. (2000) h min s	Decl (2000)	Long. (2000)	Lat. (2000)	r (AU)	Δ (AU)	Phase (deg)	$V(1,\alpha)$ (mag)	Tel
1646 Rosseland										
1995	08 12	21 15 19.62	−20°32′30.9	314.9	−4.4	2.292	1.283	2.89	—	0.6 m
	08 13	21 14 23.66	−20°40′57.3	314.7	−4.4	2.291	1.283	3.32	12.112±0.010	0.6 m
	08 14	21 13 27.82	−20°49′18.0	314.4	−4.5	2.290	1.283	3.78	12.231±0.010	0.6 m
	08 15	21 12 32.20	−20°57′32.7	314.2	−4.6	2.288	1.283	4.25	12.261±0.010	0.6 m
	08 17	21 10 41.93	−21°13′41.5	313.7	−4.7	2.286	1.285	5.23	—	0.6 m
	08 18	21 09 47.44	−21°21′34.9	313.5	−4.7	2.284	1.287	5.72	12.156±0.010	0.6 m
2260 Neoptolemus										
1995	08 14	21 20 44.49	−32°47′39.3	312.3	−16.4	5.183	4.212	3.54	10.041±0.011	0.6 m
	08 15	21 20 11.03	−32°50′44.1	312.1	−16.4	5.183	4.215	3.64	10.025±0.011	0.6 m
	08 18	21 18 31.17	−32°59′27.2	311.7	−16.4	5.182	4.223	3.97	10.073±0.011	0.6 m

* Observatório do Pico dos Dias, Brazil.
" Observatoire de Haute-Provence, France.

Table 1(b)
Observational circumstances. Exp is the number of exposures, r and Δ are the heliocentric and geocentric distances, respectively, α is the solar phase angle, m_v is the visual magnitude and in the last column the solar analog is given

Asteroids	UT Date	Exp.	r (AU)	Δ (AU)	α (deg)	m_v	Solar Analog
50 Virginia	16/03/97	2	3.100	2.218	10.04	14.07	HD44594
58 Concordia	19/11/96	1	2.687	2.157	19.94	13.67	HR2290
105 Artemis	17/11/96	1	2.624	1.926	17.92	13.08	HR1405
	03/01/97	1	2.685	2.611	21.33	13.91	HD44594
141 Lumen	16/03/97	2	3.093	2.143	6.53	12.80	HD44594
	19/03/97	1	3.097	2.162	7.55	12.87	HD44594
169 Zelia	18/11/96	1	2.407	1.520	12.67	13.14	HR2290
249 Ilse	17/03/97	2	2.719	1.813	10.63	15.46	HD44594
324 Bamberga	17/03/97	2	2.824	2.253	18.59	11.86	HD44594
357 Ninina	18/11/96	2	2.961	2.834	19.47	14.32	HR2290
437 Rhodia	17/03/97	2	2.581	1.746	14.64	14.50	HD44594
488 Kreusa	17/03/97	2	2.756	1.985	15.45	12.35	HD44594
	20/03/97	1	2.760	1.961	14.67	12.29	HD44594
521 Brixia	17/03/97	2	3.430	3.204	16.81	14.68	HD44594
	20/03/97	1	3.427	3.157	16.75	14.64	HD44594
628 Christine	18/11/96	1	2.528	1.850	19.13	13.57	HR2290
716 Berkeley	19/11/96	1	3.013	2.791	19.11	16.43	HR2290
870 Manto	20/11/96	1	2.656	1.923	16.85	16.53	HR2290
1031 Arctica	12/01/97	1	2.883	2.001	10.38	14.02	HD44594
1621 Druzhba	02/01/97	2	1.965	1.419	28.35	15.11	HD44594
1646 Rosseland	21/11/96	1	2.235	1.778	25.37	15.98	HR2290
2014 Vasilevskis	12/01/97	1	2.692	2.329	21.02	16.71	HD44594

Flux calibration was performed using standard stars from Landolt (1983). The images were corrected for extinction by using photometry of field stars in the asteroid images and of Landolt stars, taken at different air masses. The errors given in Tables 1 and 2 take into account the aperture error given by DAOPHOT and the quality of the night. Fourier analyses of the data in order to obtain the composite lightcurves were performed using the method described by Harris et al. (1989).

2.2. *Spectrosopy*

The spectroscopic observations were performed at the European Southern Observatory at La Silla (Chile) using

a 1.5 m telescope equipped with a Boller and Chivens spectrograph and a Ford CCD 2048 × 2048 pixels with a readout noise of ±7 electrons. We used the 225 gr/mm grating with a dispersion of 0.033 μm/mm in the first order. The CCD has a square 15 μm pixel, giving a dispersion of about 5 Å/pixel in the wavelength direction. The spectral range is about $0.5 < \lambda < 0.9$ μm with a FWHM of 10 Å. The spectra were taken through a 5 arcs slit oriented in the East–West direction in order to eliminate possible loss of light due to atmospheric differential refraction. The observational circumstances and the aspect data are listed in Table 1(b). All the values were obtained from EPHEM program by Tholen (1997).

The spectral data reduction was performed using the Image Reduction and Analysis Facility (IRAF) package. Pixel-to-pixel variations were removed by subtracting the bias level from each frame and dividing it by a flat field. The IRAF apsum package was used to sum the pixel values within a specified aperture and to subtract the background level. Wavelength calibration was performed using a He–Ar lamp and spectra were corrected from airmass by using the mean extinction curve of La Silla. We used the solar analog HD 44,594 to compute reflectivities, but we observed two other solar analogs (HR 2290 and HR 1405) (Hardorp, 1979) to compare the quality of the night. All asteroid spectra are normalized around 0.55 μm by convention.

3. Results

3.1. Photometric lightcurves

In Table 2(a) the estimated diameter of each asteroid and the values obtained for the synodic rotation period and the amplitude of the composite lightcurves are reported. The lightcurves are plotted in Figs. 1–10, and in the composite ones each symbol corresponds to a different night. A reliability code 1, meaning a result based on fragmentary or inconclusive coverage, which may be completely wrong (Harris and Young, 1983), has been attributed to all the obtained periods. Below, we make some specific remarks about each asteroid.

Table 2(a)
Physical parameters of the observed asteroids

Asteroid		Diameter (km)	Rot. Period (h)	Amplitude (mag.)
58 Concordia		97.7★		
120 Lachesis		178★		
141 Lumen	(95)	135★	20.0 ± 0.3	>0.29
	(97)	20.0 ± 0.3	>0.18	
249 Ilse	(95)	37.2★	42.6 ± 0.3	>0.16
	(97)	42.6 ± 0.3	>0.84	
437 Rhodia		14.3★		
588 Achilles		147★	7.0 ± 0.1	≥0.22
617 Patroclus		149★		
1236 Thais		26.3★		
1646 Rosseland		16.5*	68.9 ± 0.3	>0.45
2260 Neoptolemus		85.0★	8.5 ± 0.1	>0.43

★ Diameters by the IRAS Minor Planet Survey.
* Diameters by D.J. Tholen, ephemeris program EPHEM, 1997.

Table 2(b)
Presence of hydration bands on the observed asteroids

Asteroid	Semi-major axis (AU)	Diameter (km)	Estimated P (h)	Hydration
50 Virginia	2.651	54.2*	17.88	Yes
58 Concordia	2.700	97.7★	>16	Yes
105 Artemis	2.372	123★	16.84	Yes
141 Lumen	2.666	135★	20.0†	Yes
169 Zelia	2.358	36.5★	>16	—
249 Ilse	2.378	37.2★	42.6†	Yes
324 Bamberga	2.685	242★	29.43	No
357 Ninina	3.149	110★	>20	Yes
437 Rhodia	2.385	14.3★	56	—
488 Kreusa	3.149	158★	>28	Yes
521 Brixia	2.740	121★	>24	Yes
628 Christine	2.581	51.2★	>14	—
716 Berkeley	2.811	25.5★	>17	—
870 Manto	2.322	14.5*	>24	—
1031 Arctica	3.046	78.0★	51.0	Yes
1621 Druzhba	2.230	11.0★	>12	—
1646 Rosseland	2.360	16.5*	68.9†	No
2014 Vasilevskis	2.403	17.5*	36.25	—

★ Diameters by the IRAS Minor Planet Survey.
* Diameters by D.J. Tholen, ephemeris program EPHEM, 1997.
† This work.

58 Concordia was observed in 1995 (4 nights) and 1997 (4 nights). The rotational period previously estimated for this asteroid was $P > 16$ h, with an amplitude larger than 0.07 mag. (Gil-Hutton, 1993). It must be noted that just a single lightcurve was published in that work. The single night lightcurves for each apparition are shown in Fig. 1 (a) and (b). Magnitude variations of small amplitude are visible in some of these lightcurves, but no estimation can be made about the rotational period.

120 Lachesis was observed during 3 nights in 1995. The rotation period previously estimated for this object was $P > 20$ h (Debehogne et al., 1983), with an estimated lightcurve amplitude larger than 0.1 mag., when only three single lightcurves were published. More recently, Hainaut-Rouelle et al. (1995) provided a new estimation of the amplitude (larger than 0.14 mag.), but their two single lightcurves did not allow a better estimation of the rotation period. The single night lightcurves are shown in Fig. 2, but the small number of points for each night does not allow an estimation for the rotation period.

141 Lumen was observed during 7 nights in 1995 and 4 nights in 1997. The first rotational period estimated for this asteroid was $P > 18$ h (Wetterer and Flower, 1992),

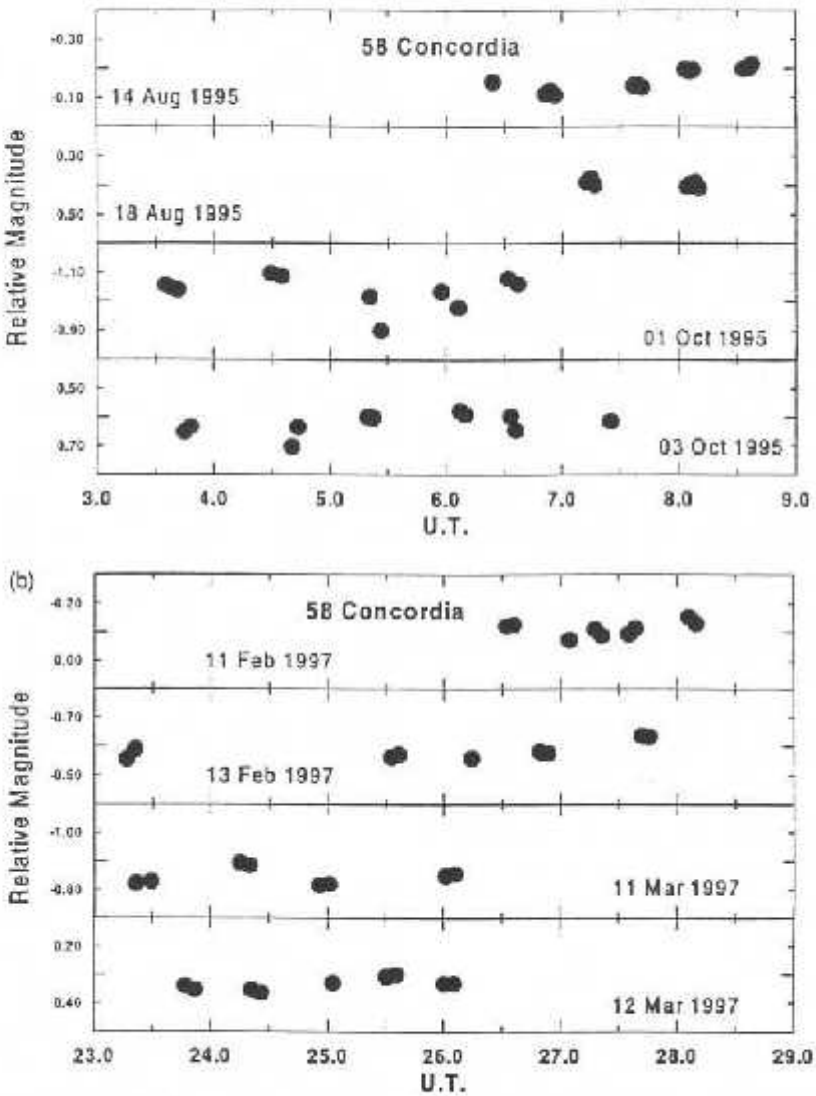

Fig. 1. (a) Single night lightcurves of the asteroid *58 Concordia* for the 1995 apparition. All the plots have the same scale, but the different values in the *y*-axis are due to a different comparison star for each night; (b) single night lightcurves of the asteroid *58 Concordia* for the 1997 apparition. As in (a), the different values in the *y*-axis are due to a different comparison star for each night.

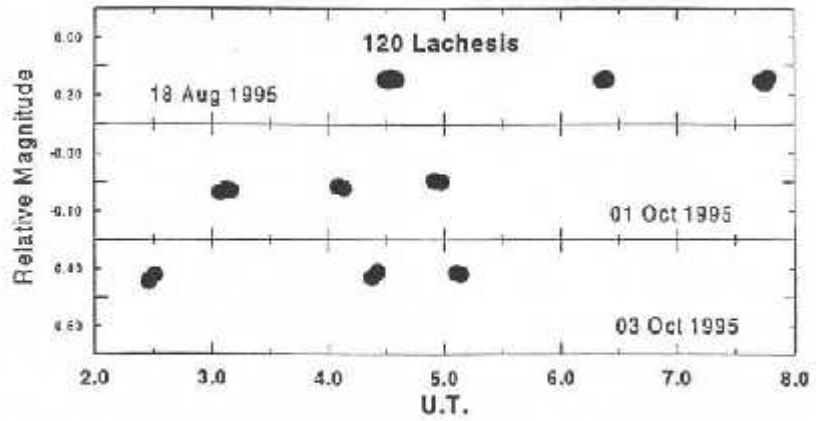

Fig. 2. Single night lightcurves of the asteroid *120 Lachesis*. All the plots have the same scale, but the different values in the *y*-axis are due to a different comparison star for each night.

with an amplitude larger than 0.2 mag., when only an individual lightcurve was published. More recently, Holliday (1996) based on 7 nights of observations in November 1995, reported a rotation period of 19.67 ± 0.01 h with quality code 1 and lightcurve amplitude of 0.13 mag. We divided the whole data in two sets according to the year of the observation. After some tests the period of 20.0 ± 0.3 h revealed to be the best fit to the data, with the composite lightcurves showing clearly two maxima and two minima. In the 1995 lightcurve (Fig. 3a) the principal maximum seems to be much brighter than the secondary one (>0.11 mag.), and in the 1997 lightcurve (Fig. 3b) one maximum is not well defined. The lightcurves are relatively good, but in some parts they remain without coverage.

249 Ilse was observed in 1995 (5 nights) and 1997 (3 nights). This asteroid has been observed by Lagerkvist (1978), who did not detect any variation in its lightcurve over a period of 4.5 h. The periods previously estimated for this asteroid were $P = 42.62$ h (Binzel and Mulholand, 1983) and $P = 85.24$ h (Binzel, 1987). Due to the precarious coverage, neither published composite lightcurves is of very good quality. Our data fit the period of 42.6 h, but not that of 85.24 h. In Fig. 4(a) is shown the composite lightcurve obtained with the 1995 data set, and in Fig. 4(b) the one obtained with the 1997 data set. Both are poorly covered and the second one has a very large amplitude (>0.84 mag.).

437 Rhodia was observed in 1996 (2 nights) and 1997 (3 nights). The rotation period previously estimated for this asteroid was $P = 56 \pm 1$ h (Binzel, 1987). We present the five obtained single night lightcurves (Fig. 5), because it is not possible to confirm or to refute this estimation with our data set.

588 Achilles was observed during 4 nights in August 1995. The rotation period previously estimated for this asteroid was $P > 12$ h with an amplitude larger than 0.12 mag. (Zappalà et al., 1989). The published single lightcurves do not show a definite behavior. Achilles has been observed before by Lagerkvist and Sjölander (1979), but only one single lightcurve was published at that time. The authors estimated $P > 0.4$ days for this asteroid. The best fit obtained with our data provides $P = 7.0 \pm 0.1$ h, with a lightcurve amplitude larger than 0.22 mag. The composite lightcurve shows the principal maximum narrower and much brighter than the secondary one and presents a relatively poor coverage (Fig. 6).

617 Patroclus was observed in 1995 (4 nights), 1996 (1 night) and 1997 (3 nights). The rotation period previously estimated for this asteroid was $P > 40$ h (Gonano et al., 1991), with an estimated lightcurve amplitude larger than 0.1 mag., but no lightcurve (single or composite) was published. In Fig. 7 (a, b and c) we show all the eight single night lightcurves obtained. Among the three data sets, the 1997 one seems to present larger variations of magnitude, but due to the poor coverage of most of the lightcurves, no conclusion can be drawn from the available data.

1236 Thaïs was observed during 5 nights in August 1995. The rotation period previously estimated for this object was $P > 72$ h, with a lightcurve amplitude larger than 0.08 mag. (Schober and Schroll, 1983). Here was show our five single night lightcurves (Fig. 8), and, despite some small amplitude magnitude variations, no estimation can be made about the rotation period.

1646 Rosseland was observed for 6 nights in August 1995. The rotation period previously estimated for this object was $P = 69.2$ h, with a poorly sampled and very irregular lightcurve with amplitude of 0.13 mag. (Binzel and Mulholand, 1983). After several trials, the composite lightcurve that best fits our data provides $P = 68.9 \pm 0.3$ h, but the most of this lightcurve remains without coverage. The two minima seem to have nearly the same magnitude, but the two maxima are very poorly covered and the lightcurve amplitude seems to be greater than 0.45 mag. (Fig. 9).

2260 Neoptolemus was observed during 3 nights in August 1995. The rotation period previously estimated was $P > 12$ h (Binzel and Sauter, 1992) with a lightcurve amplitude larger than 0.26 mag. (based on 3 h of coverage, with seven measurements). No lightcurve was published at that time. The best fit obtained with our data provides $P = 8.5 \pm 0.1$ h, with a poorly covered lightcurve of amplitude larger than 0.43 mag. (Fig. 10). The maxima and the minima are not well defined, but no other period could fit the data.

3.2. Spectra

We obtained reflectivity spectra over the wavelength from 0.5 to 0.9 μm for 18 asteroids candidates for a long rotation period. For most of them (11) the spectra suggest a C-type composition (Fig. 11a and b) and for the others an S or E-type (Fig. 11c).

The five asteroids for which we also present lightcurves, i.e., *58 Concordia, 141 Lumen, 249 Ilse, 1646 Rosseland* and *437 Rhodia*, exhibit a C-type composition, except the last one. Between the C-type asteroids, all but one, *1646 Rosseland*, show features associated with an aqueous alteration process. Previous classification by Tholen (1984) indicated for 58 and 141 a C- and CPF-type, respectively. In the case of *50 Virginia*, also classified as C-type, Rivkin et al. (1995) obtained a spectrum which clearly shows absorption features in the 3 μm region, diagnostic of hydrated minerals. Xu et al. (1995) obtained a spectrum of *1646 Rosseland* attributing to it a CX-type classification. For *437 Rhodia* that are no previous classification and our spectra suggest an E-type composition.

Another six objects, *105 Artemis, 324 Bamberga, 357 Ninina, 488 Kreusa, 521 Brixia*, and *1031 Arctica*, also present a C-type composition, most of them (5) showing

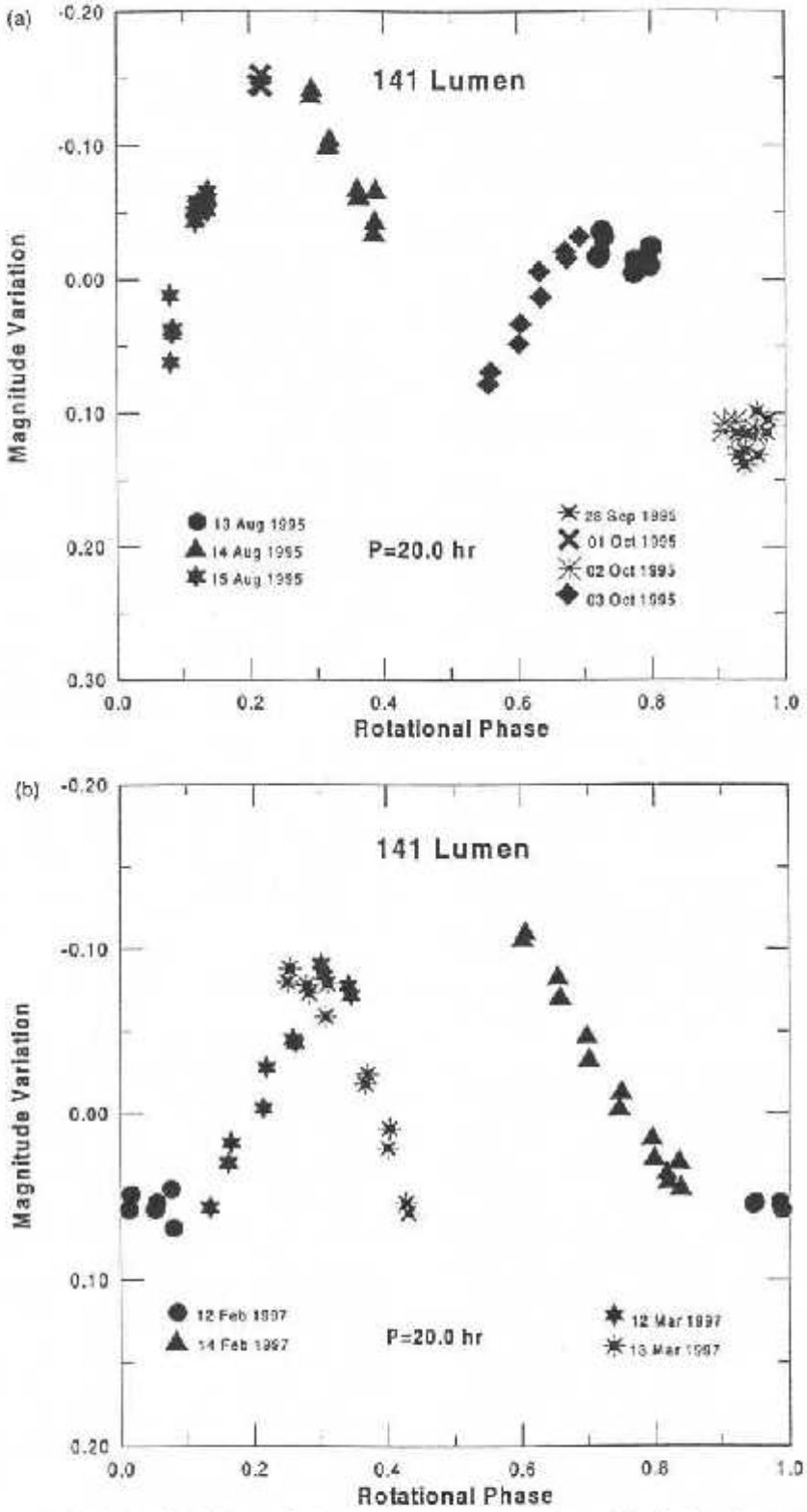

Fig. 3. (a) Composite lightcurve of the asteroid *141 Lumen* for the 1995 data in rotational phase. The 0 phase time corresponds to UT 07 h 58 min 39 s of 28 September, 1995; (b) composite lightcurve of the asteroid *141 Lumen* for the 1997 data in rotational phase. The 0 phase time corresponds to UT 17 h 56 min 6 s of 12 March, 1997.

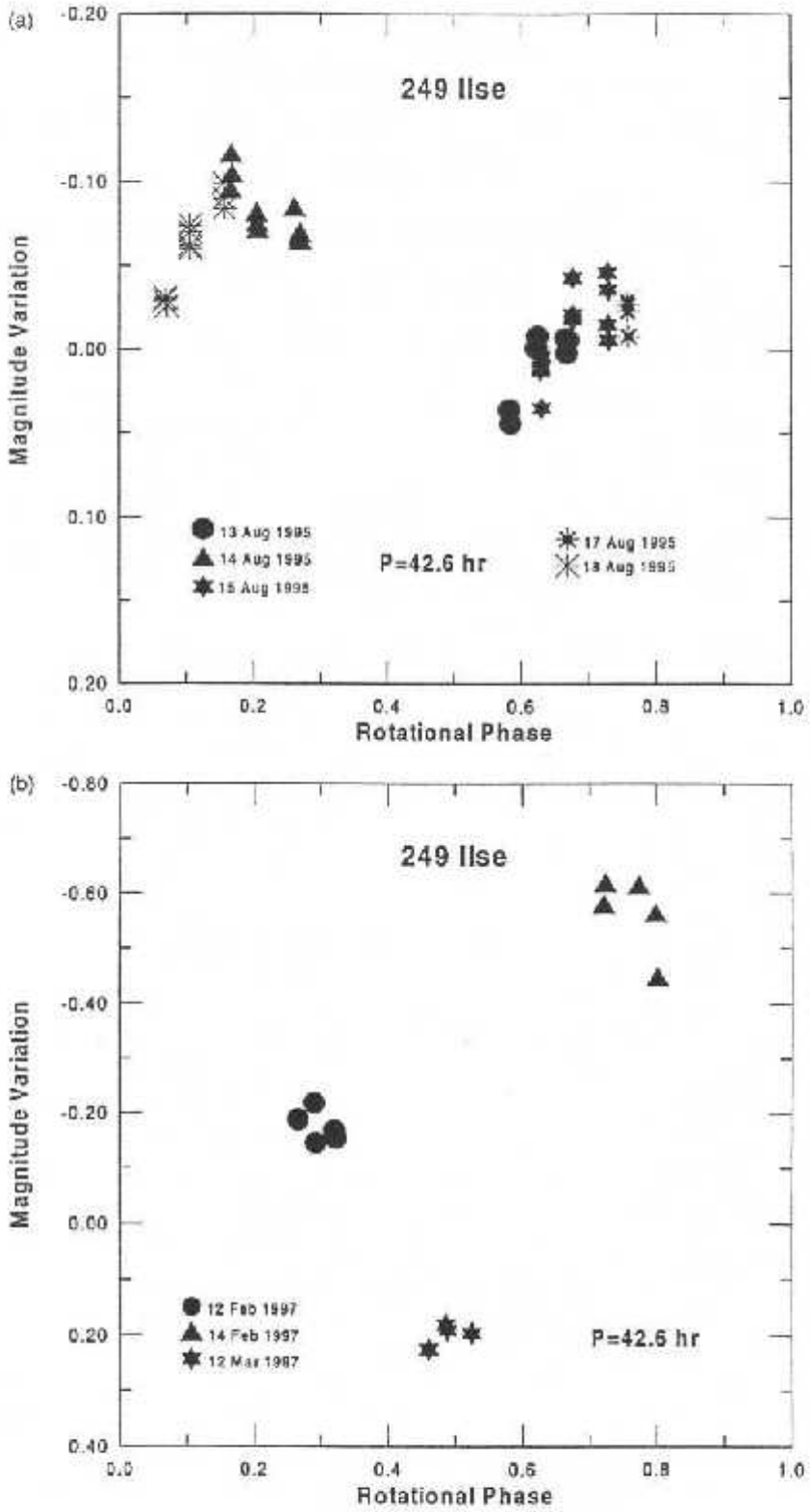

Fig. 4. (a) Composite lightcurve of the asteroid *249 Ilse* for the 1995 data in rotational phase. The 0 phase time corresponds to UT 18 h 00 min 11 s of 15 August, 1995; (b) composite lightcurve of the asteroid *249 Ilse* for the 1997 data in rotational phase. The 0 phase time corresponds to UT 13 h 48 min 1 s of 14 February, 1997.

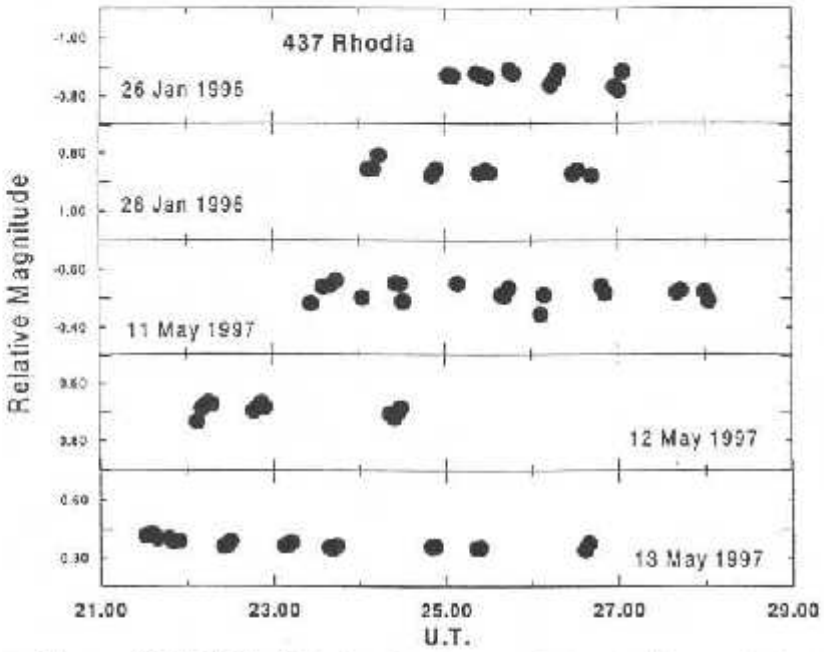

Fig. 5. Single night lightcurves of the asteroid *437 Rhodia*. All the plots have the same scale, but the different values in the *y*-axis are due to a different comparison star for each night.

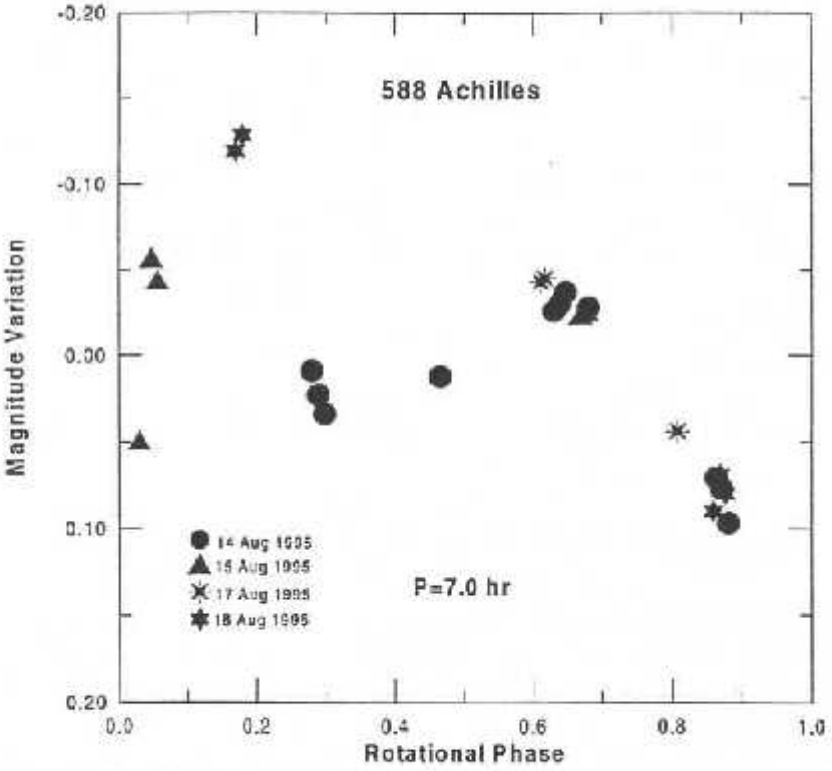

Fig. 6. Composite lightcurve of the asteroid *588 Achilles* in rotational phase. The 0 phase time corresponds to UT 21 h 59 min 59 s of 13 August, 1995.

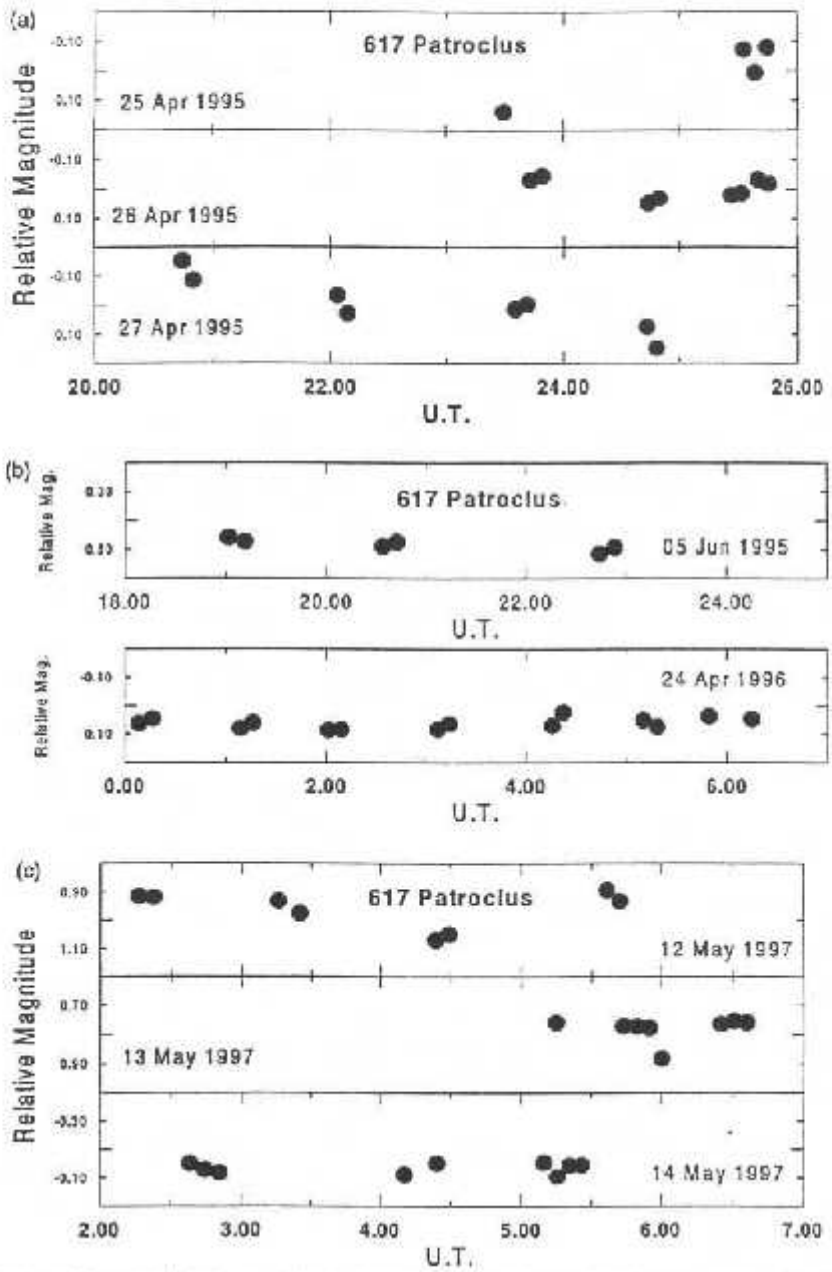

Fig. 7. (a) Single night lightcurves of the asteroid *617 Patroclus* for April 1995; (b) single night lightcurves of the asteroid *617 Patroclus* for June 1995 and April 1996. Both plots have the same scale, but the different values in the *y*-axis are due to a different comparison star for each night; (c) single night lightcurves of the asteroid *617 Patroclus* for the 1997 apparition. As in (b), the different values in the *y*-axis are due to a different comparison star for each night.

features associated with an aqueous alteration process (Fig. 11b). These asteroids were classified by Tholen (1984) as: C-type for *105*, *488* and *521*, CX-type for *357* and *1031*, and CP-type for *324*.

The spectra of C-type asteroids varies from neutral to slightly red, probably darkened by organic materials associated with carbonaceous chondrites. The presence of aqueous alteration in some C-type asteroids was discovered by Vilas et al. (1994), resulting from a low temperature chemical alteration of materials by liquid water, which acts as a solvent producing material like phyllosilicates, sulfates, oxides, carbonates and hydroxides (Barucci et al., 1998). The spectrum shows a broad absorption feature around 0.7 μm with a depth relative to the continuum around 3–7%. This absorption feature is believed to arise from $Fe^{2+} \rightarrow Fe^{3+}$ charge transfer absorptions in phyllosilicate minerals (Vilas and Gaffey, 1989; Vilas et al., 1993).

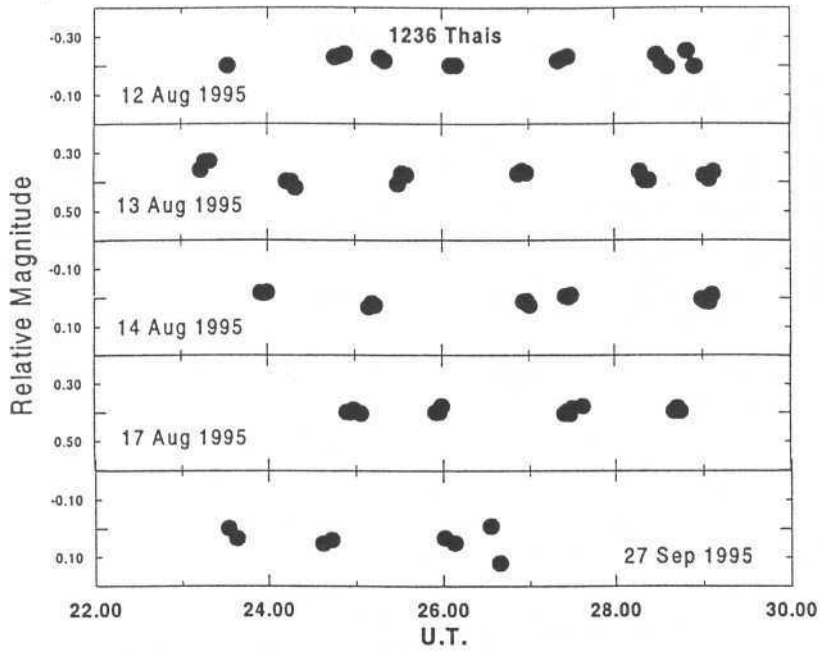

Fig. 8. Single night lightcurves of the asteroid *1236 Thais*. All the plots have the same scale, but the different values in the *y*-axis are due to a different comparison star for each night.

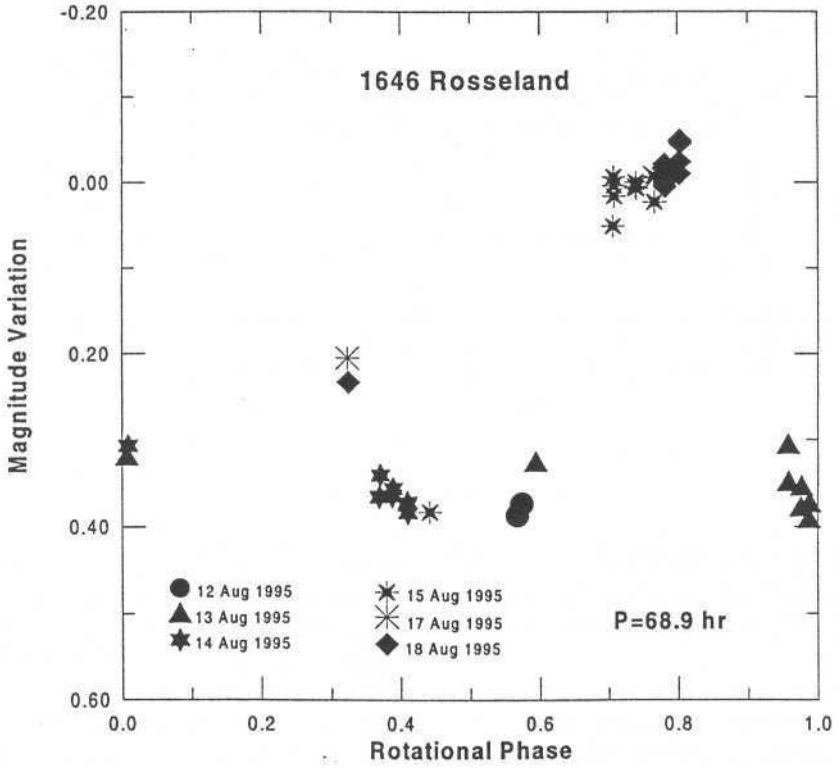

Fig. 9. Composite lightcurve of the asteroid *1646 Rosseland* in rotational phase. The 0 phase time corresponds to UT 21 h 35 min 57 s of 15 August, 1995.

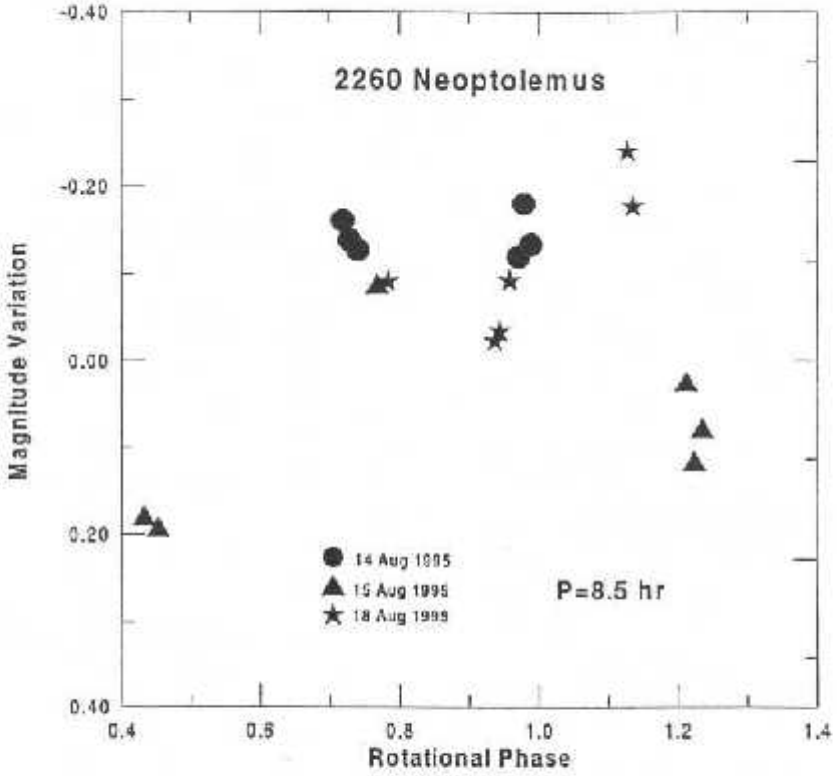

Fig. 10. Composite lightcurve of the asteroid *2260 Neoptolemus* in rotational phase. The 0 phase time corresponds to UT 21 h 29 min 58 s of 14 August, 1995.

The other objects analyzed, *169 Zelia*, *716 Berkeley*, *870 Manto*, *1621 Druzhba* and *2014 Vasilevskis*, present an S-type composition (Fig. 11c). Tholen (1984) also classified *169*, *716* and *1621* as S-type and Xu et al. (1995) confirmed an S-type spectrum for *169* and *2014*.

The last object, *628 Christine*, shows a spectrum similar to *437 Rhodia* which resembles an E-type although it was classified as SD-type by Tholen (1984). More data, on a wider spectral range, is needed to confirm its classification.

4. Discussion

Since our composite lightcurves are not of very good quality, the period determinations are not definitive. Therefore, a reliability code 1, meaning a result based on fragmentary or inconclusive coverage (Harris and Young, 1983), has been attributed to all the obtained periods. Anyway, we cannot exclude the possibility that some of these asteroids do have rotation periods shorter than previously estimated. It must be noted that even the previous estimations were, for the most part, not supported by good quality lightcurves.

A complex rotation cannot be deduced from our data. It is important to stress that, in cases of very long rotation periods, only an international campaign, like that undertaken for *Toutatis* and *Mathilde*, can succeed in making a secure determination of the period and revealing a possible complex rotation.

From our spectroscopical analysis, the long-period asteroids do not present any specific compositional characteristic. In terms of their heliocentric distances these asteroids present an expected composition between S and C-types. The C-type asteroids with indication of aqueous alteration are also in the 'alteration zone' defined by Vilas et al. (1994) and by Barucci et al. (1998).

Due to the supposed long rotation period of most of these asteroids, it would be useful to have available all data acquired up to present. To favour future period determinations by other observers, we make our complete data set available through anonymous ftp to the following address: *lagrange.on.br*

Acknowledgements

The authors acknowledge the technical staff of the OPD, OHP and ESO for their prompt help whenever needed. They also acknowledge M.A. Barucci and A.W. Harris for the detailed revision that much improved the paper, and D. Foryta and O. Winter for their assistance in some of the observations. C.A.A., D.I., A.S.B. and J.M.C. were supported by CNPq, and M.A.F. by CAPES through diverse fellowships and grants.

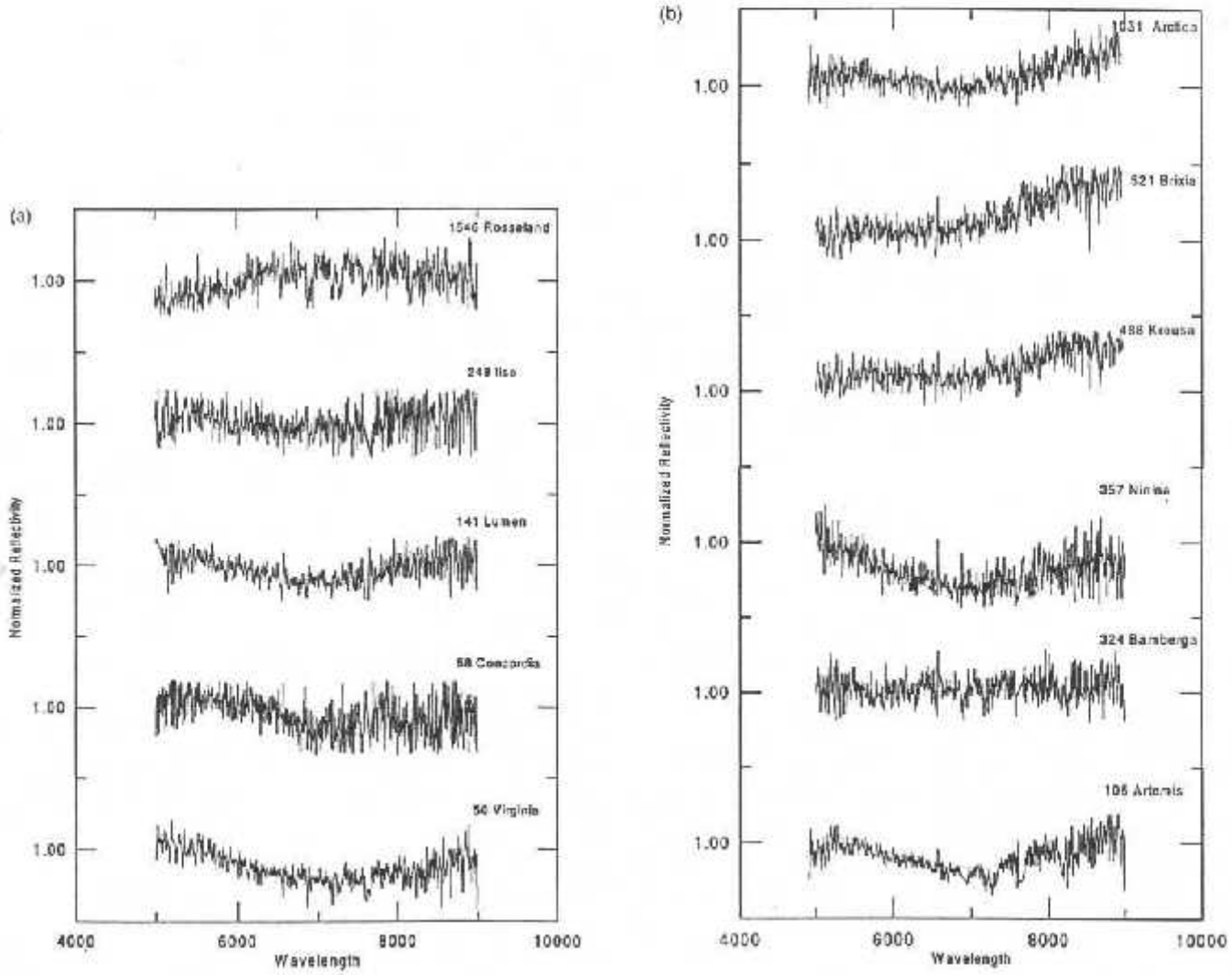

Fig. 11. (a) Spectra of C-type asteroids. Four of them show a broad absorption band around 0.7 μm, indicating an aqueous alteration process. For purpose of clarity, the curves are offset vertically from each other by 0.1; (b) spectra of C-type asteroids. Five of them show a broad absorption band around 0.7 μm. As in (a), the curves are offset vertically by 0.1; (c) spectra of asteroids showing S-type and E-type (*437* and *626*) classifications. The curves are offset vertically from each other by 0.15.

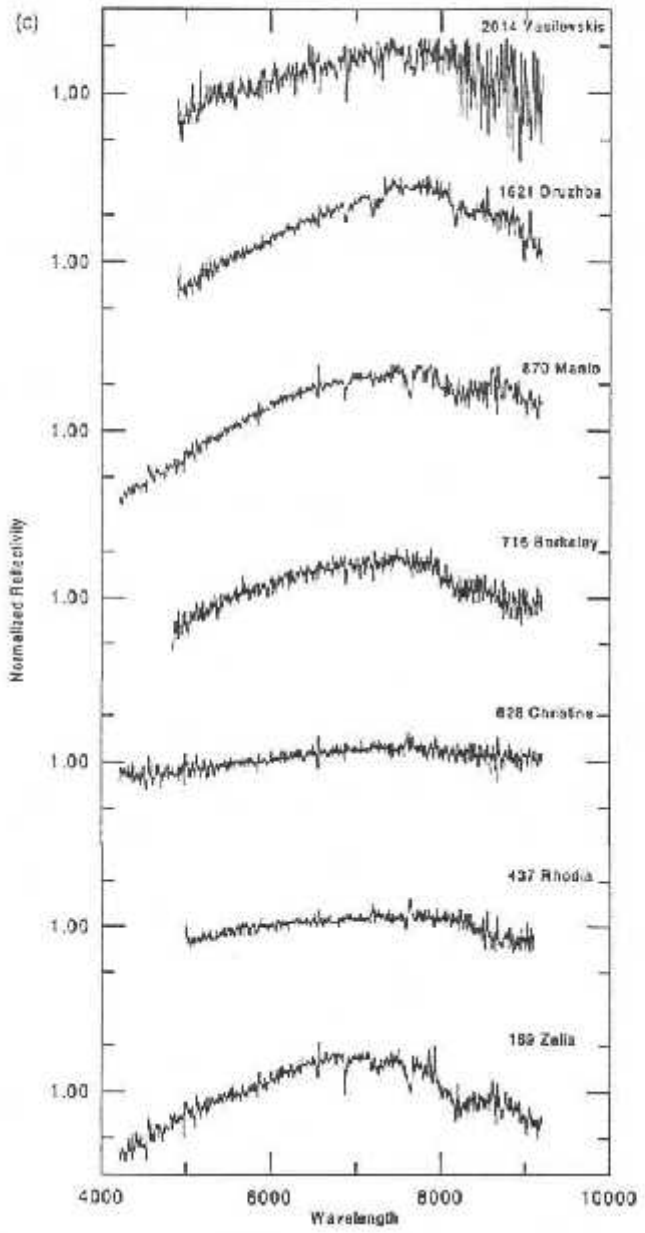

Fig. 11. *Continued.*

References

Angeli, C.A., 1995. Détermination des propriétés rotationnelles d'astéroïdes: Des indices pour interpréter leur histoire évolutive. Thèse de Doctorat, Observatoire de Paris.

Barucci, M.A., Doressoundiram, A., Fulchignoni, M., Florczak, M., Lazzarin, M., Angeli, C.A., Lazzaro, D., 1998. Search for aqueously altered materials on asteroids. Icarus, in press.

Binzel, R.P., 1984. The rotation of small asteroids. Icarus 57, 294–306.

Binzel, R.P., 1987. A photoelectric survey of 130 asteroids. Icarus 72, 135–208.

Binzel, R.P., Mulholand, J.D., 1983. A photoelectric lightcurve survey of small main belt asteroids. Icarus 56, 519–533.

Binzel, R.P., Farinella, P., Zappalà, V., Cellino, A., 1989. Asteroid rotation rates: distributions and statistics. In: Binzel, R.P., Gehrels, T., Matthews, M.S. (Eds.), Asteroids II. University of Arizona Press, Tucson, pp. 416–441.

Binzel, R.P., Sauter, L.M., 1992. Trojan, Hilda, and Cybele asteroids: New lightcurve observations and analysis. Icarus 95, 222–238.

Burns, J.A., Tedesco, E.F., 1979. Asteroid lightcurves: Results for rotations and shapes. In: Gehrels, T. (Ed.), Asteroids. University of Arizona Press, Tucson, pp. 494–527.

Debehogne, H., De Sanctis, G., Zappalà, V., 1983. Photoelectric photometry of asteroids 45, 120, 776, 804, 814 and 1982DV. Icarus 55, 236–244.

Dermott, S.F., Murray, C.D., 1982. Asteroid rotation rates depend on diameter and type. Nature 296, 418–421.

Dermott, S.F., Harris, A.W., Murray, C.D., 1984. Asteroid rotation rates. Icarus 57, 14–34.

Farinella, P., Paolicchi, P., Zappalà, V., 1981. Analysis of the spin rate distribution of asteroids. Astron. Astrophys. 104, 159–165.

Fulchignoni, M., Barucci, M.A., Di Martino, M., Dotto, E., 1995. On the evolution of the asteroid spin. Astron. Astrophys. 299, 929–932.

Gil-Hutton, R.G., 1993. Photoelectric photometry of asteroids 58 Concordia, 122 Gerda, 326 Tamara and 441 Bathilde. Rev. Mexicana Astron. Astrof. 25, 75–77.

Gonano, M., Di Martino, M., Mottola, S., Neukum, G., 1991. Physical study of outer belt asteroids. Adv. Space Res. 11 (12), 197–200.

Hainaut-Rouelle, M.-C., Hainaut, O.R., Detal, A., 1995. Lightcurves of selected minor planets. Astron. Astrophys. Suppl. Series 112, 125–142.

Hardorp, J., 1979. The sun among the stars. Astron. Astrophys. 63, 383–390.

Harris, A.W., 1994. Tumbling asteroids. Icarus 107, 209–211.

Harris, A.W., Burns, J.A., 1979. Asteroid rotation. I. Tabulation and analysis rates, pole positions and shapes. Icarus 40, 115–144.

Harris, A.W., Young, J.W., 1983. Asteroid rotation. IV. 1979 observations. Icarus 54, 59–109.

Harris, A.W., Young, J.W., Bowell, E., Martin, L.J., Millis, R.L., Poutanen, M., Scaltriti, F., Zappalà, V., Schober, H.-J., Debehogne, H., Zeigler, K.W., 1989. Photoelectric observations of asteroids 3, 24, 60, 261 and 863. Icarus 77, 171–186.

Holliday, B., 1996. Lightcurve observations of minor planet 141 Lumen. Minor Planet Bul. 23, 17.

Lagerkvist, C.-I., 1978. Photographic photometry of 110 main-belt asteroids. Astron. Astrophys. Suppl. 31, 361–381.

Lagerkvist, C.-I., Sjölander, N.-G., 1979. Photographic photometry of asteroids with Schmidt telescopes. II. Observations of 11 asteroids during 1977 and 1978. Acta Astronomica 29 (3), 455–461.

Landolt, A.U., 1983. UBVRI photometric standard stars around the celestial equator. Astron. J. 88, 439–460.

McAdoo, D.C., Burns, J.A., 1973. Further evidence for collisions among asteroids. Icarus 18, 285–293.

Mottola, S., Sears, W.D., Erikson, A., Harris, A.W., Young, J.W., Hahn, G., Dahlgren, M., Mueller, B.E.A., Owen, B., Gil-Hutton, R., Licandro, J., Barucci, M.A., Angeli, C., Neukum, G., Lagerkvist, C.-I., Lahulla, F., 1995. The slow rotation of 253 Mathilde. Planet. Space Sci. 43 (12), 1609–1613.

Rivkin, A.S., Howell, E.S., Britt, D.T., Lebofsky, L.A., Nolan, M.C., Branston, D.D., 1995. 3-μm spectrophotometric survey of M- and E-class asteroids. Icarus 117, 90–100.

Schober, H.J., Schroll, A., 1983. Rotation properties of the high-numbered asteroids 1236 Thais and 1317 Silvretta. Astron. Astrophys. 120, 106–108.

Spencer, J.R., Akimov, L.A., Angeli, C., Angelini, P., Barucci, M.A., Birch, P., Blanco, C., Buie, M., Caruso, A., Chiomij, V.G., Colas, F., Dentchev, P., De Sanctis, M.C., Dotto, E., Fulchignoni, M., Green, S., Harris, A.W., Hudevek, T., Kalashnikov, A.V., Kobelev, V.V., Kozhevnikov, V.P., Krugly, Y., Lazzaro, D., Lecacheux, J., MacConnell, J., Michalowski, T., Mohamed, R.A., Mueller, B., Nakamura, T., Neese, C., Noll, K., Osborn, W., Pravec, P., Riccioli, D., Shevchenko, V., Tholen, D.J., Velichko, F., Venditti, C., Venditti, R., Wisniewski, W., Young, J., Zellner, B., 1995. The lightcurve of 4179 Toutatis: evidence for complex rotation. Icarus 117, 71–89.

Tedesco, E.F., Zappalà, V., 1980. Rotational properties of asteroids: correlation and selection effect. Icarus 43, 33–50.

Tholen, D.J., 1984. Asteroid taxonomy from cluster analysis of photometry. PhD. Thesis, University of Arizona.

Tholen, D.J., 1997. Ephemeris program EPHEM.

Vilas, F., Gaffey, M.J., 1989. Phyllosilicate absorption features in main-belt and outer-belt asteroid reflectance spectra. Science 246, 790–792.

Vilas, F., Larson, S.M., Hatch, E.C., Jarvis, K.S., 1993. CCD reflectance spectra of selected asteroids. II. Low albedo asteroid spectra and data extraction techniques. Icarus 105, 67–78.

Vilas, F., Jarvis, K.S., Gaffey, M.J., 1994. Iron alteration minerals in the visible and near infrared spectra of low albedo asteroids. Icarus 109, 274–283.

Wetterer, C.J., Flower, T.F., 1992. CCD photometry of 141 Lumen. Minor Planet Bul. 19, 33.

Xu, S., Binzel, R.P., Burbine, T.H., Bus, S.J., 1995. Small main-belt asteroid spectroscopic survey: initial results. Icarus 115, 1–35.

Zappalà, V., Di Martino, M., Cellino, A., Farinella, P., De Sanctis, G., Ferreri, W., 1989. Rotational properties of outer belt asteroids. Icarus 82, 354–368.

4.4 - Conclusões

Realizamos várias missões de observação fotométrica com a obtenção de curvas de luz para 25 asteróides, sendo que determinamos com boa precisão o período rotacional de 8 deles. Para 3 objetos a precisão foi razoável, podendo estar errada até 30 % e para 8 objetos a estimativa de período é considerada ruim. Para os objetos restantes não foi possível obter uma estimativa razoável.

Em relação aos pequenos objetos, determinamos o período de 12 com diâmetro inferior a 50 km. Destes asteróides, 5 apresentam valores próximos aos de rotação rápida (4,1 horas), 4 têm valores próximos aos de uma população intermediária (8,7 horas) e 3 possuem rotação lenta (> 24 horas). Aproximadamente a metade destes objetos são de rotação rápida, o que não seria esperado pois esta população representa em torno de 25 % do total segundo o trabalho de Angeli (1995). Por outro lado, estes períodos rápidos são os menos influenciados pelo *bias* observacional, já que é muito mais fácil determiná-los. O fato de obtermos também mais objetos com rotação lenta do que o previsto se deve ao fato de que em nosso trabalho escolhemos uma amostra que privilegiava este tipo de rotação. Em relação aos objetos com rotação longa, encontramos apenas 3 com valores bem acima de 24 horas e 2 com valores em torno de 20 horas.

Em vista da nossa amostra ser pequena fica difícil de se tirar conclusões gerais sobre o estado rotacional dos asteróides. Acreditamos serem necessárias mais observações antes de se ter conclusões seguras sobre este assunto.

Capítulo 5

Objetos distantes: Chiron

5.1 - Introdução

Chiron foi descoberto por Charles T. Kowal em 1977, sendo inicialmente classificado como o asteróide 1977UB. Posteriormente, com a realização de novas observações, sua órbita foi determinada com precisão e o objeto passou a ter a identificação de 2060 Chiron *. Desde sua descoberta, este objeto despertou particular interesse devido ao fato de ser o asteróide mais distante do Sol de que se tinha conhecimento. Enquanto a maioria dos asteróides se encontram entre as órbitas de Marte e Júpiter, Chiron orbita entre Saturno e Urano com distância periélica de 8,5 U.A. e afélica de 18,9 U.A.. Sua órbita é caótica, pois cruza a órbita de Saturno estando portanto sujeita a fortes perturbações e a encontros próximos com este (French *et al.*, 1989).

Com a descoberta de 5 asteróides com órbitas similares à de Chiron, foi definida uma nova classe de objetos, os *Centauros*. Os Centauros são um grupo de objetos cujas órbitas cruzam as dos planetas gigantes e parecem ser uma população intermediária entre os cometas de curto período e os objetos do Cinturão de Kuiper (Fernández, 1980).

Em 1987, Chiron começou a apresentar um comportamento distinto do que se espera de um asteróide, tendo sido detectadas variações significativas em seu brilho, sugerindo

* *Chiron na mitologia grega representa um centauro, filho de Kronos (Saturno) e neto de Urano, uma figura metade homem e metade cavalo.*

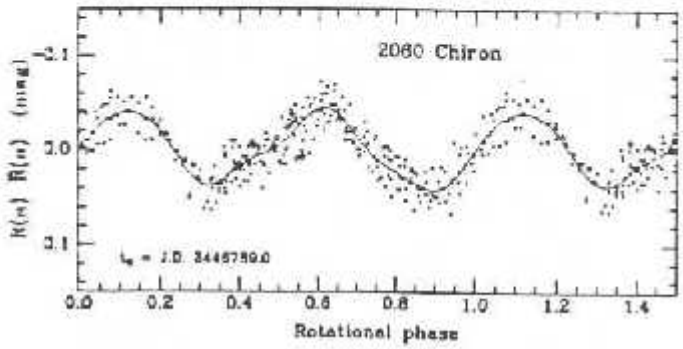

Figura (5.1) *Curva de luz de Chiron obtida por Bus e co-autores (1989). O período rotacional é de aproximadamente 5,9 horas, com uma amplitude de 0,088 magnitude.*

uma possível atividade cometária. Sua curva de luz apresenta três tipos de variações. A primeira é devida à sua rotação, sendo o período estimado em aproximadamente 5,92 horas por Bus e co-autores (1989) e também confirmado por nós (ver seção 5.3.2). A figura 5.1 mostra a curva de luz obtida por Bus e co-autores com uma amplitude de 0,088 magnitude. Este tipo de variação é similar à encontrada em asteróides. Uma segunda variação é do tipo secular, ou seja, um aumento/diminuição contínuo do brilho num período de alguns anos. Desde a sua descoberta até aproximadamente o ano de 1983, Chiron apresentou um aumento suave em sua magnitude, ou seja, seu brilho começou a diminuir. Entretanto, entre os anos de 1985 e 1989 foi detectado um aumento significativo em seu brilho, chegando a uma variação de mais de uma magnitude. Este aumento no brilho foi atribuído a uma atividade cometária, sendo esperado que esta continuasse durante a aproximação ao periélio de Chiron (French *et al.*, 1989) (fig. 5.2).

A terceira variação é do tipo impulsiva, que ocorre em curtos intervalos de tempo e sugere a existência de jatos cometários. Luu e Jewitt (1990b) observaram um aumento

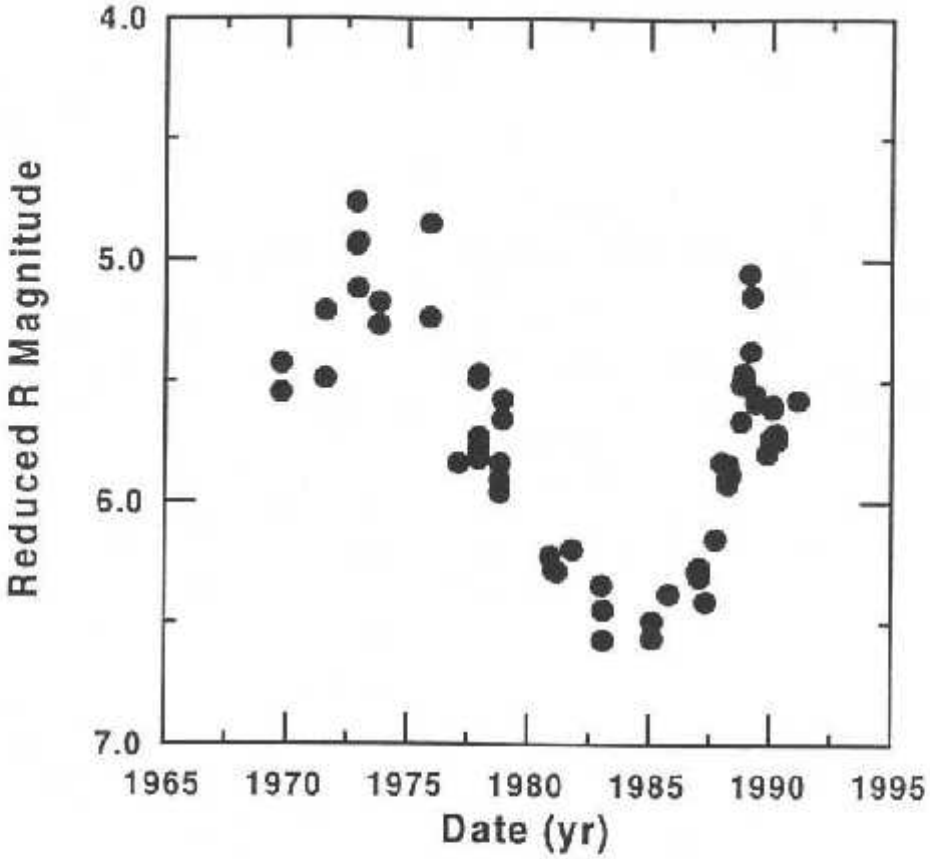

Figura (5.2) *Variação secular do brilho de Chiron desde sua descoberta até o ano de 1990.*

do brilho da ordem de 10 % em 29 de janeiro de 1990, enquanto que Buratti e Dunbar (1991), 9 dias depois, observaram o contrário, ou seja, um decréscimo desta mesma ordem no brilho (ver fig. 5.3).

Em 1989, quando Chiron estava em torno de seu brilho máximo, foi detectada sua coma (Meech e Belton, 1990), e este objeto passou a ser considerado um cometa. Mas mesmo sendo um cometa, Chiron é ainda um objeto incomum devido ao seu grande tamanho, da ordem de 180 km, e à sua atividade cometária em regiões muito distantes do Sol. Devemos salientar que em cometas *típicos* a atividade é devida essencialmente à volatilização da água, o que ocorre em torno de 3 U.A.. Em distâncias da ordem de 10 U.A. a água não pode ser volatilizada, sugerindo que em Chiron outras moléculas, tais como CO, CN, N_2 ou CH_4, sejam responsáveis por sua atividade. De fato, em 1991 Bus e

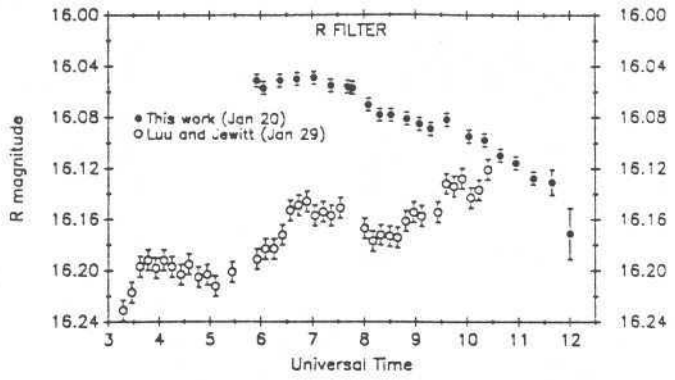

Figura (5.3) *Curvas de luz de Chiron obtidas por Luu e Jewitt (1991) e Buratti e Dunbar (1991), mostrando suas variações impulsivas.*

colaboradores detectam a molécula de CN.

O fato da atividade cometária de Chiron ser intensa a grandes distâncias do Sol nos fornece uma forte evidência de que o nível de atividade não é uma função apenas da distância heliocêntrica. Provavelmente, a atividade cometária de Chiron deve ser uma combinação entre o nível de aquecimento solar, a direção de seu eixo de rotação, a localização dos materiais voláteis próximos à superfície e o tipo de composição superficial. A figura 5.4 mostra a órbita de Chiron e as posições aproximadas onde foram detectados seus efeitos cometários. A grande variabilidade de Chiron e a taxa provável de produção de gás CN e CO em sua coma sugere que a fonte de atividade em Chiron deve ser inferior a 1 % de sua superfície (Stern e Campins, 1996). A existência de jatos de matéria, inicialmente sugerida pelas flutuações de curto período no brilho, foi também confirmada através de ocultações estelares (Elliot *et al.*, 1994).

Com o objetivo de melhor compreender a atividade deste objeto foi realizado um monitoramento do comportamento de Chiron em sua aproximação e passagem pelo periélio.

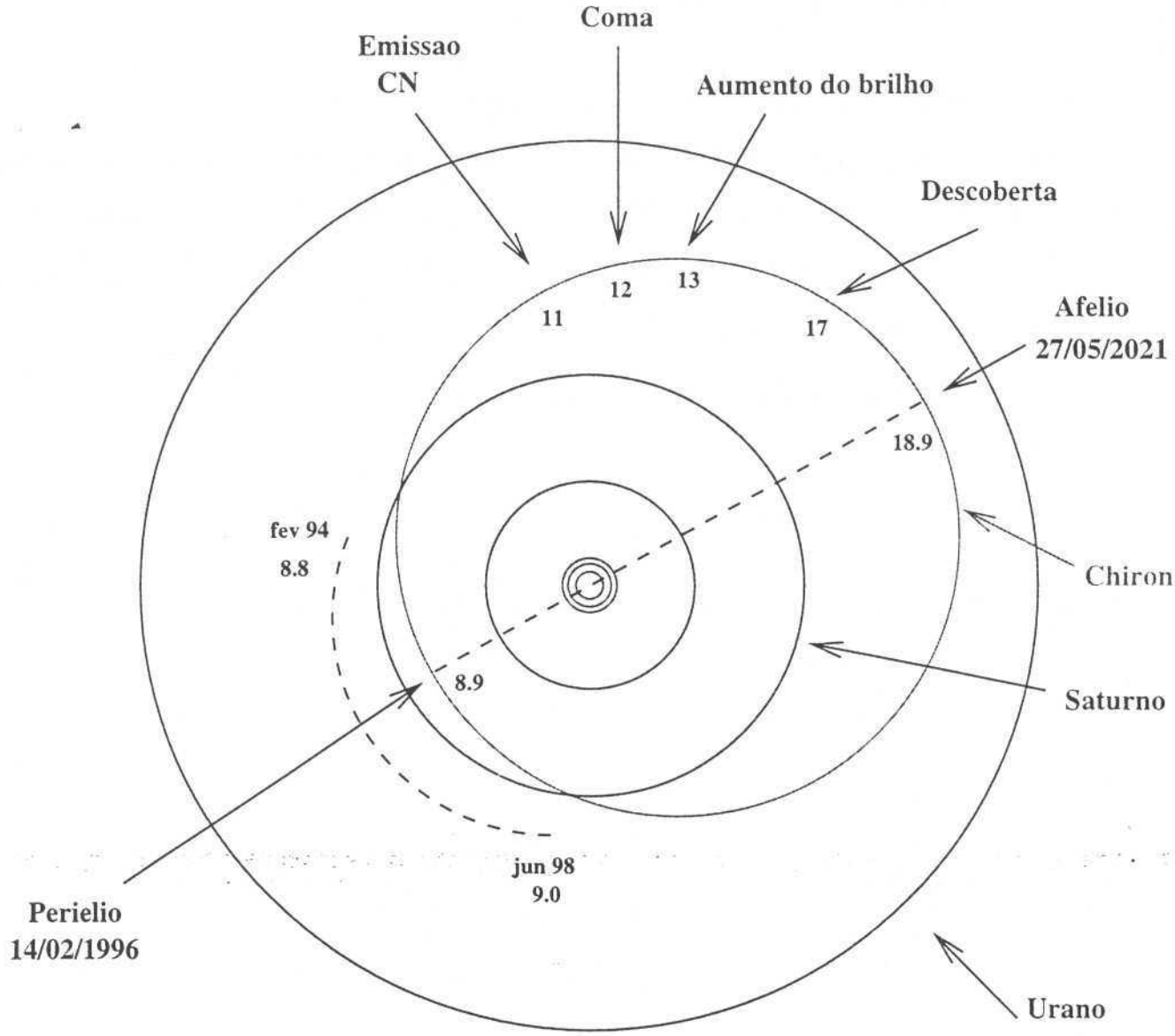

Figura (5.4) *A órbita de Chiron e as posições aproximadas onde ocorreram as detecções de atividade cometária.*

Para isto foram realizadas diversas missões de observação durante os anos de 1994 a 1996, que são descritas a seguir.

5.2 - Observações e Reduções

As observações fotométricas foram realizadas nos anos de 1994 a 1996 principalmente no Observatório do Pico dos Dias (OPD, Brasil), e em menor quantidade no Observatório de Haute-Provence (OHP, França). No OPD utilizamos os telescópios de 1,6 e 0,6 m e no OHP o de 1,2 m, acoplados a câmeras CCD. As reduções seguiram os mesmos procedimentos descritos no capítulo 4.

A magnitude absoluta foi obtida através da equação (Bowell *et al.*, 1989):

$$H(\alpha) = H - 2,5 \log [(1 - G)\, \Phi_1(\alpha) + G\Phi_2(\alpha)] \tag{5.1}$$

onde H é a *magnitude absoluta*, que é a magnitude com um ângulo de fase igual a zero. G é um parâmetro que indica o gradiente da curva de fase, que vale aproximadamente zero para corpos de baixo albedo e 1 para altos albedos. Estes dois parâmetros fundamentais podem ser obtidos através das seguintes relações:

$$\begin{aligned} 10^{-0,4V(\alpha)} &= a_1\Phi_1(\alpha) + a_2\Phi_2(\alpha) \\ H &= -2,5 \log(a_1 + a_2) \\ G &= \frac{a_1}{a_1 + a_2} \end{aligned} \tag{5.2}$$

onde $V(\alpha)$ (ver eq. 4.4) é a magnitude reduzida para diferentes valores de α, e a_1 e a_2 são constantes auxiliares para um dado asteróide. As funções Φ são calculadas através das seguintes relações:

$$\begin{aligned} \Phi_i &= W\Phi_{is} + (1 - W)\Phi_{il} \\ W &= \exp\left(-90,56 \tan^2 \frac{1}{2}\alpha\right) \end{aligned}$$

$$\Phi_{is} = 1 - \frac{C_i \sin\alpha}{0,119 + 1,341 \sin\alpha - 0,754 \sin^2\alpha}$$

$$\Phi_{il} = \exp\left[-A_i \left(\tan\frac{1}{2}\alpha\right) B_i\right] \qquad (5.3)$$

$$A_1 = 3,332 \qquad A_2 = 1,862$$

$$B_1 = 0,631 \qquad B_2 = 1,218$$

$$C_1 = 0,986 \qquad C_2 = 0,238$$

As observações espectroscópicas foram realizadas no European Southern Observatory (ESO, Chile) e no Observatório de Mauna Kea (Havaí) no ano de 1996. O telescópio utilizado no ESO foi o de 1,5 m, com espectrógrafo Boller e Chivens e detetor CCD num intervalo espectral entre 0,48 e 0,92 μm. Em Mauna Kea foi utilizado o telescópio de 3,6 m com o espectrógrafo MOS (Multi Object Spectrograph) e detetor CCD num intervalo espectral entre 0,4 e 0,98 μm. A redução dos dados seguiu os mesmos procedimentos descritos no capitulo 3.

5.3 - Resultados

O objetivo principal de nossas observações fotométricas entre os anos de 1994 e 1995 foi o de monitorar seu comportamento secular. Chiron mostrava uma atividade mínima entre os anos de 1983 e 1985 e máxima entre 1988 e 1991. Nossos resultados, surpreendentemente, mostraram uma volta aos valores similares àqueles da posição de mínima atividade, embora Chiron estivesse se aproximando do perélio. A figura 1 (seção 5.3.1) mostra a variação da magnitude reduzida de Chiron com o tempo, onde podemos notar sua variação de longo período com uma possível periodicidade em torno de 12 a 14 anos. Este período necessita de muitas observações adicionais ao longo dos anos para ser confirmado. Nenhum mecanismo foi por nós encontrado que possa justificar esta suposta variação periódica do brilho.

Calculamos também o valor da magnitude absoluta e do parâmetro G de acordo com o sistema descrito acima e encontramos, com os dados de 1986, um valor de 0,71 ± 0,15 para G, similar ao valor de 0,70 encontrado por Bus e co-autores (1989). Entretanto, quando calculamos o parâmetro G utilizando também os valores de magnitudes reduzidas obtidos por outros autores (fig. 1, seção 5.3.1), obtemos valores bastante diferentes, como seria de se esperar, pois o sistema de magnitude absoluta H-G é definido para um corpo que não possui qualquer tipo de *atmosfera* (como uma atividade cometária). Por isso, vale salientar que este sistema de magnitudes H-G é apropriado para asteróides mas não para cometas.

A passagem de Chiron pelo periélio aconteceu em fevereiro de 1996, sendo a primeira vez que se pôde observar sua máxima aproximação ao Sol. Desde que foi detectada sua atividade cometária a grandes distâncias, era de se esperar também uma atividade no periélio. Por este motivo monitoramos Chiron no primeiro semestre de 1996, realizando observações fotométricas em várias missões e duas observações espectroscópicas no decorrer do semestre.

Nossos resultados fotométricos mostram, em diferentes filtros, que Chiron atingiu um valor mínimo de brilho nos meses de janeiro e fevereiro, e um aumento de aproximadamente 20 % no mês de março, retornando novamente a um mínimo em junho (fig. 4, seção 5.3.2). Entretanto, como o aumento foi detectado quando Chiron estava em uma posição de ângulo de fase mínimo, não nos é permitido afirmar que este aumento seja devido a uma atividade cometária e não a um efeito de ângulo de fase. Por outro lado, detectamos atividade de curto período da ordem de algumas horas durante uma noite. A figura 3 (seção 5.3.2) mostra a variação da magnitude de Chiron na noite de 23 de abril nos filtros V e R. A razão entre as magnitudes de duas estrelas do mesmo campo de Chiron garante que esta variação seja devida à atividade cometária e não a um outro efeito, como problemas atmosféricos. Outra atividade de curto período, da ordem de alguns meses, também foi encontrada em Chiron no início do ano de 1996 (fig. 2, seção 5.3.2).

Com os dados de 1996 obtivemos uma curva de luz composta com 200 pontos (fig. 5, seção 5.3.2), confirmando o período rotacional obtido por Bus e co-autores (1989) e Marcialis e Buratti (1993). Entretanto as amplitudes obtidas por nós e por estes autores são diferentes, o que provavelmente é resultado de uma forma levemente alongada de Chiron, combinada com uma coma esférica, mais ou menos intensa em diferentes épocas, ocultando sua real forma. Por outro lado, estas diferentes amplitudes podem também ser devidas à variação do ângulo entre o eixo de rotação do objeto e o plano orbital (*ângulo de aspecto*).

Em relação à variação secular na magnitude encontramos que o brilho de Chiron se encontra em um mínimo, embora isto não represente uma falta de atividade cometária, pois variações de curto período foram detectadas, como descrito acima. Este comportamento é bastante incomum para um cometa, possuíndo uma maior atividade cometária próximo do afélio e uma menor no periélio.

No ano de 1996 obtivemos dois espectros de Chiron, um no mês de março e outro em junho. Os dois espectros são similares aos asteróides do tipo C, mas com diferentes gradientes de refletividade: o espectro de março se mostra mais inclinado do que o de junho, provavelmente devido a uma atividade cometária nesta época, sugerida pelos resultados de fotometria descritos anteriormente.

Pergamon

Planet. Space Sci., Vol. 44, No. 12, pp. 1547–1550, 1996

0032–0633/96 $15.00 + 0.00

PII: S0032-0633(96)00111-0

2060 Chiron back to a minimum of brightness*

Daniela Lazzaro,[1] Marcos A. Florczak,[1,2] Alberto Betzler,[1,3] Othon C. Winter,[4] Silvia M. Giuliatti-Winter,[4] Claudia A. Angeli[1,5] and Dietmar W. Foryta[6]

[1]Observatório Nacional, Dep. Astrofísica, 20921 Rio de Janeiro, Brazil
[2]CEFET, Dep. Física, 80000 Curitiba, Brazil
[3]Universidade Federal do Rio de Janeiro, Obs. Valongo, Rio de Janeiro, Brazil
[4]UNESP, Grupo de Dinâmica Orbital e Planetologia, Guaratinguetá, Brazil
[5]Observatoire de Paris, EUROPA, 92195 Meudon Principal Cedex, France
[6]Universidade Federal do Paraná, Dep. Física, 80000 Curitiba, Brazil

Received 16 February 1996; revised 17 July 1996; accepted 17 July 1996

Abstract. The results of photometric observations of comet/asteroid 2060 Chiron at the Observatório do Pico dos Dias (Brazil—OPD) and the Observatoire de Haute-Provence (France—OHP) during 1994 and 1995 are presented. The analysis of the data shows a decrease of 2060 Chiron brightness from its peak values of 1988–1991. The absolute magnitude, H_V, varies from a maximum of 6.6 in February 1994 up to a minimum of 6.8 in June 1995. Therefore 2060 Chiron is back to a minimum of activity close to that of 1983–1985. The slope parameter G is found to be $G = 0.71 \pm 0.15$. It is suggested that the H–G magnitude system, generally adopted to present 2060 Chiron brightness, is not the most appropriate due to the cometary activity of this object.

Introduction

2060 Chiron, with an orbit between Uranus and Saturn, was considered as the most distant asteroid known at the time of its discovery (Kowal, 1979). Calculation by Scholl (1979) and Oikawa and Everhart (1979) readily demonstrated that 2060 Chiron is not in a stable path due to its proximity to Saturn and Uranus. Nowadays it is widely accepted that 2060 Chiron originated somewhere in the outer Solar System, probably in the Kuiper belt, and evolved to its present orbit (Hahn and Bailey, 1990).

From the analysis of JHK photometric data Hartmann *et al.* (1982) concluded that 2060 Chiron is a low albedo object composed of dark carbonaceous chondritic material and/or dirty ices matching the C class asteroids. On the other hand, between 1988 and 1989 many observers (Tholen *et al.*, 1988; Bus *et al.*, 1988, 1989; Hartmann *et al.*, 1990) reported the sudden brightening of 2060 Chiron indicative of a cometary behavior.

The presence of a coma around 2060 Chiron was first observed by Meech and Belton (1990) at a heliocentric distance of 11.8 AU. Almost simultaneously Luu and Jewitt (1990) revealed that 2060 Chiron exhibits two kinds of brightness variations: long-term (months to years) and short-term (hours). Short-period variations were also detected by Buratti and Dunbar (1991). Marcialis and Buratti (1993) suggested that the long-term variation can be caused by dissipation and resupply of material in the coma while the short-term variation should be due to the release of volatiles such as CO_2 and CN. It was also argued (Stern, 1989; Meech and Belton, 1990) that outbursts at large heliocentric distances should be due to the sublimation of more volatile ices, such as CO or CO_2. The presence of CN and CO was detected by Bus *et al.* (1991) and Womack and Stern (1995), respectively.

Moreover, the occultation of a star by 2060 Chiron in 1994 revealed the presence of discrete jet features near the nucleus (Elliot *et al.*, 1995). It became clear that the particles in the coma have radii larger than 0.25 μm and originated from a few active areas.

Another quite interesting aspect of 2060 Chiron is its size. Using different techniques the diameter of 2060 Chiron has been estimated as 372 km (Sykes and Walker,

Correspondence to: D. Lazzaro
*Observations carried out at the Observatório do Pico dos Dias, operated by the Laboratório Nacional de Astrofísica (Brazil), and at the Observatoire de Haute-Provence, operated by the Centre National de la Recherche Scientifique (France).

1991), 173 km (Lebofsky *et al.*, 1984) and 182–189 km (Campins *et al.*, 1994; Marcialis *et al.*, 1994). Whatever the precise value is, it is clear that 2060 Chiron is one of the largest comets presently being observed.

The approach of 2060 Chiron to perihelion in February 1996 was the incentive for systematic monitoring of its brightness since 1994. In this paper we present the analysis of photometric observations of 2060 Chiron obtained during 1994 and 1995 which show that the decline in brightness is continuing despite its proximity to perihelion.

Observations and reduction

CCD observations of 2060 Chiron were performed in 1994 and 1995 at the Observatório do Pico dos Dias (Brazil—OPD) and at the Observatoire de Haute-Provence (France—OHP). The first observing run, at the OPD, was done using a 1.6 m telescope on February 8. The 1995 campaign is composed of several short observational runs between February and July on a 0.6 and a 1.2 m telescope of the OPD and OHP, respectively. In Table 1 are shown the mean geometric circumstances for each night of observation as well as the technical specification of the telescope and the CCD used.

The photometric data from these observations are given in Table 2. In this table $V_{obs}(\alpha)$ is the observed magnitude and $V(\alpha)$ the reduced (to unit distance) magnitude at phase angle α. All images were reduced using IRAF (DAOPHOT) and calibrated using standard methods with bias and dome flat-field images. Flux calibration was obtained using standard stars from Landolt (1983). The images from each night were corrected for extinction by using photometry of field stars from 2060 Chiron images and photometry of the Landolt stars taken at different airmasses. Since not all the observations were made under photometric conditions a night quality factor is given in Table 1. The errors given in Table 2 take into account the aperture error given by DAOPHOT and the quality of the night (through the extinction coefficient). It must be pointed out that the non-photometric nights have not been appropriately linked to the photometric ones, so that the values given must be taken with care.

Results and discussion

The basic aim of our observational program was to monitor the photometric secular behavior of 2060 Chiron. Therefore only a few points per night were acquired and no complete lightcurve was obtained. Since all the published data are given in the *H–G* magnitude system, as defined by Bowell *et al.* (1989), we reduced our apparent magnitudes to this system in order to study their photometric variation. The values of H_V, as well as the error envelope, for a slope parameter of 0.70, are given in Table 3. Note that the value of 0.70, used in most of the published data, was determined by Bus *et al.* (1989) from data obtained in 1986, when 2060 Chiron was at a minimum of brightness. As can be seen in Table 3 the mean absolute magnitude H_V, between 1994 and 1995, varied from 6.559 to 6.798 which indicates a minimum of activity.

As 2060 Chiron was initially thought to be an asteroid and only later was cometary behavior noticed, this duality asteroid/comet raises a problem when we analyze the value to be used for the G parameter since it is not an "atmosphereless body". Nevertheless a crude estimate of the G parameter for the nucleus of 2060 Chiron can be obtained by using its photometric data when it has no coma or, at least, when it is at a minimum of activity. A new determination of this parameter from our data gives $G = 0.71 \pm 0.15$ which confirms that the characteristics of 2060 Chiron's surface are probably best represented by a slope parameter around 0.70–0.71. We should, however, remember that this value could also be wrong since the presence of a thin coma cannot be ruled out even during "quiescent" periods (Marcialis and Buratti, 1993).

Since the *H–G* magnitude system does not seem to be appropriate to monitor the behavior of 2060 Chiron we suggest that reduced magnitudes should be used, instead. Reduced magnitudes, $V(\alpha)$, are obtained from observed magnitudes, $V_{obs}(\alpha)$, through the relation $V(\alpha) = V_{obs}(\alpha)$

Table 1. Mean observing geometry for 2060 Chiron for each night it was observed. R and Δ are the heliocentric and geocentric distances, respectively, and α is the solar phase angle. The quality factor, Q, indicates if night was 3—photometric, 2—with thin cirrus and 1—with moonlight. In the telescope column OPD stands for Observatório do Pico dos Dias and OHP for Observatoire de Haute-Provence

UT Date	R (AU)	Δ (AU)	α	Q	Telescope	CCD detector	Scale ($''$ pix^{-1})	Field ($' \times '$)
1994/02/08	8.865	7.927	2.09	2	OPD 1.6 m	EEV-384 × 576	0.57	3.6 × 5.5
1995/03/25	8.538	7.557	1.22	3	OPD 0.6 m	TK-1024 × 1024	0.42	7 × 7
1995/04/26	8.521	7.791	4.86	3	OHP 1.2 m	TK-512 × 512	0.82	7 × 7
1995/04/27	8.521	7.802	4.95	2	OHP 1.2 m	TK-512 × 512	0.82	7 × 7
1995/06/03	8.505	8.316	6.79	2	OPD 0.6 m	EEV-384 × 576	1.12	7.2 × 10.8
1995/06/04	8.505	8.332	6.80	2	OPD 0.6 m	EEV-384 × 576	1.12	7.2 × 10.8
1995/06/05	8.504	8.347	6.82	2	OPD 0.6 m	EEV-384 × 576	1.12	7.2 × 10.8
1995/06/16	8.500	8.520	6.84	1	OPD 0.6 m	EEV-384 × 576	1.12	7.2 × 10.8
1995/07/01	8.495	8.749	6.54	1	OPD 0.6 m	EEV-384 × 576	1.12	7.2 × 10.8
1995/07/02	8.494	8.764	6.51	1	OPD 0.6 m	EEV-384 × 576	1.12	7.2 × 10.8

Table 2. Photometric observations of 2060 Chiron in 1994 and 1995

UT Date	$V_{obs}(\alpha)$	Error	$V(\alpha)$
1994 February 08.2439	15.985	0.008	6.642
1994 February 08.2543	16.004	0.009	6.661
1994 February 08.2658	16.074	0.009	6.731
1994 February 08.2744	16.024	0.010	6.682
1994 February 08.3106	16.051	0.011	6.709
1995 March 25.1590	15.752	0.006	6.702
1995 March 25.1759	15.950	0.006	6.900
1995 April 26.9112	15.900	0.006	6.789
1995 April 26.9143	15.916	0.006	6.805
1995 April 26.9298	15.999	0.007	6.888
1995 April 26.9334	16.151	0.007	7.040
1995 April 27.8552	15.846	0.020	6.733
1995 April 27.9109	15.880	0.021	6.767
1995 April 27.9141	15.865	0.021	6.752
1995 April 27.9502	15.801	0.024	6.688
1995 April 27.9538	16.022	0.024	6.909
1995 April 27.9562	15.914	0.025	6.801
1995 April 27.9747	15.930	0.027	6.817
1995 June 03.9475	16.230	0.010	6.986
1995 June 04.0158	16.361	0.012	7.097
1995 June 04.0212	16.285	0.012	7.018
1995 June 04.9136	16.185	0.010	6.933
1995 June 04.9196	16.192	0.010	6.940
1995 June 04.9915	16.189	0.011	6.937
1995 June 04.9967	16.151	0.011	6.899
1995 June 05.9010	16.206	0.011	6.950
1995 June 16.9542	16.303	0.021	7.003
1995 June 16.9575	16.281	0.021	6.981
1995 July 01.8964	16.184	0.021	6.830
1995 July 01.9041	16.176	0.021	6.820
1995 July 01.9079	16.177	0.021	6.821
1995 July 01.9363	16.143	0.022	6.787
1995 July 01.9400	16.157	0.023	6.802
1995 July 01.9835	16.237	0.031	6.881
1995 July 01.9872	16.253	0.032	6.898
1995 July 02.8956	16.222	0.018	6.863
1995 July 02.9360	16.217	0.016	6.857
1995 July 02.9349	16.221	0.016	6.861
1995 July 02.9485	16.256	0.018	6.896
1995 July 02.9508	16.237	0.017	6.878

$-5\log(r\Delta)$, where r and Δ are the heliocentric and geocentric distance, respectively.

The general behavior of 2060 Chiron's activity reaching a maximum in 1988–1991 and minima in 1983–1985 and

Table 3. Mean absolute magnitudes and the associated error envelope obtained with a slope parameter $G = 0.70$

UT Date	$H_V(\alpha)$	$\pm\Delta H_V$
1994 February 08	6.685	0.017
1995 March 25	6.715	0.032
1995 April 26	6.682	0.032
1995 April 27	6.579	0.032
1995 June 03	6.798	0.019
1995 June 04	6.692	0.019
1995 June 05	6.714	0.019
1995 June 16	6.756	0.019
1995 July 01	6.602	0.012
1995 July 02	6.641	0.008

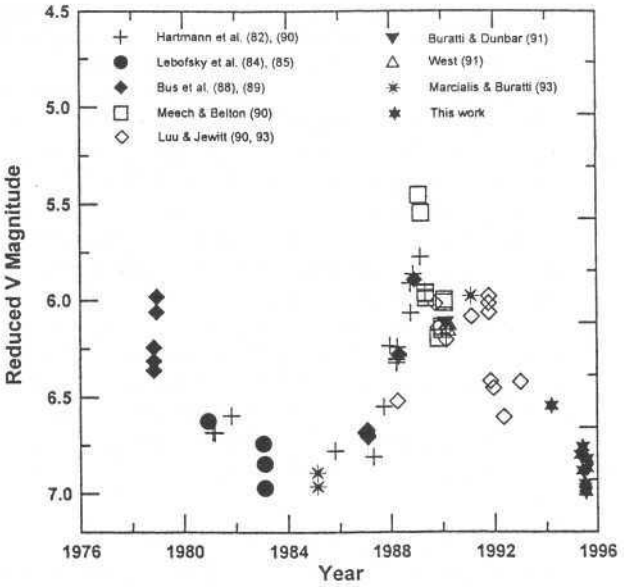

Fig. 1. Reduced magnitudes of 2060 Chiron versus year. The values are taken from the literature and converted to V magnitudes as described in the text

1994–1995 is easily seen in Fig. 1. In this figure are shown all the published data after transformation to reduced V magnitudes. The transformation to the V filter for each data set was performed using the color index determined by the authors in that period. When these values were not specified we adopted color indexes of $+0.37$ for V–R and $+0.54$ or $+0.70$ for B–V, depending on the epoch of observation.

From Fig. 1 it is clear that the magnitudes obtained in this work are much smaller than those determined in the period 1988–1991 and very similar to those of 1983–1985. We therefore conclude that, despite its proximity to perihelion, 2060 Chiron is now in a "quiet" state while a clear outburst was responsible for the peak in 1988–1991.

The decrease in brightness has also been detected by Bergeron and Vanouplines (1995) though their value of this minimum (7.0) differs from ours (6.8). This data has not been included in Fig. 1 due to the lack of precise information on the procedure of acquisition and reduction, but the important fact is that all the observations in 1995 indicate a minimum of activity of 2060 Chiron.

It is interesting to observe that Fig. 1 indicates a possible periodicity, of nearly 12–14 years, for active/non-active behavior of 2060 Chiron. Unfortunately the span of data is still not enough to confirm this periodicity and, at present, there is no obvious mechanisms that could explain such a behavior. A preliminary reduction of some of the pre-discovery plates indicated (Bus *et al.*, 1993) another possible peak of brightness around 1971–1972, but a more detailed analysis of these plates is in preparation (S. Bus, private communication) in order to confirm the exact value of this brightening. Only the years to come and the reduction of all the pre-discovery plates will confirm or not the periodicity *suggested* by Fig. 1.

The important points we would like to stress in this paper can be summarized as follows:

1. Photometric observations of 2060 Chiron, in 1994 and 1995, show that its brightness is decreasing despite its approach to perihelion, reached in early 1996.
2. Figure 1 suggests a possible periodicity, of nearly 12–14 years, for the activity of 2060 Chiron.
3. A new determination of the G parameter was performed resulting in a value of $G = 0.71 \pm 0.15$, very similar to the 0.70 determined by Bus *et al.* (1989). Considering that 2060 Chiron is now at its minimum of activity we conclude that the above values probably best represent its nuclear surface.
4. Since the cometary activity of 2060 Chiron is presently well established, including the observation of short- and long-period duration outbursts as well as discrete jet features, we do not see a good reason for using the H–G magnitude system. We suggest that reduced magnitudes should be preferred instead of absolute ones.

2060 Chiron's activity continues to present its unpredictable character. The monitoring of this very interesting object should be emphasized in the years to come. A continuation of this program is already in progress at the OPD for 1996 and, hopefully, for the following years.

Acknowledgements. The authors acknowledge the technical staff of the OPD and OHP for their prompt help whenever needed. Thanks are also due to A. Casati and A. Kushima for their help with some of the observations. C. Angeli thanks CAPES and S. Giuliatti-Winter thanks CNPq for their financial support during the present research. D. Lazzaro was partially supported by CNPq. We are also grateful to Drs B. Mueller and S. J. Bus for the detailed revision and many suggestions which much improved the paper.

References

Bergeron, D. and Vanouplines, P., 2060 Chiron. *M.P.C.* 25405–25406, 1995.

Bowell, E., Hapke, B., Domingue, D., Lumme, K., Peltoniemi, J. and Harris, A. W., Applications of photometric models to asteroids, in *Asteroids II* (edited by R. P. Binzel, T. Gehrels and M. S. Matthews), pp. 524–556. University of Arizona Press, Tucson, 1989.

Buratti, B. J. and Dunbar, R. S., Observation of a rapid decrease in the brightness of the coma of 2060 Chiron in 1990 January. *Astrophys. J.* **366,** L47–L49, 1991.

Bus, S. J., Bowell, E. and French, L. M., (2060) Chiron. IAU Circular 4684, 1988.

Bus, S. J., Bowell, E., Harris, A. W. and Hewitt, A. V., 2060 Chiron: CCD and electronographic photometry. *Icarus* **77,** 223–238, 1989.

Bus, S. J., A'Hearn, M. F., Schleicher, D. G. and Bowell, E., Detection of CN emission from (2060) Chiron. *Science* **251,** 774–777, 1991.

Bus, S. J., Bowell, E., Stern, S. A. and A'Hearn, M. F., Activity of Chiron near aphelion, in *Proceedings of the Workshop on the Activity of Distant Comets* (edited by W. F. Huebner, H. U. Keller, D. Jewitt, J. Klinger and R. West), pp. 41–43. Southwest Research Institute, San Antonio, 1993.

Campins, H., Tedesco, C., Osip, D., Rieke, G., Rieke, M. and Schulz, B., The color temperature of 2060 Chiron: a warm and small nucleus. *BAAS* **26,** 1152, 1994.

Elliot, J. L., Olkin, C. B., Dunham, E. W., Ford, C. H., Gilmore, D. K., Kurtz, D., Lazzaro, D., Rank, D. M., Temi, P., Bandyopadhyay, R. M., Barroso, J., Barucci, A., Bosh, A. S., Buie, M. W., Bus, S. J., Dahn, C. C., Foryta, D. W., Hubbard, W. B., Lopes, D. F., Marcialis, R. L., McDonald, S. W., Millis, R. L., Reitsema, H., Shleicher, D. G., Sicardy, B., Stone, R. P. and Wasserman, L. H., Jet-like features near the nucleus of Chiron. *Nature* **373,** 46–49, 1995.

Hahn, G. and Bailey, M. E., Rapid dynamical evolution of giant comet Chiron. *Nature* **348,** 132–136, 1990.

Hartmann, W. K., Cruikshank, D. P. and Degewij, J., Remote comets and related bodies: VJHK colorimetry and surface materials. *Icarus* **52,** 377–408, 1982.

Hartmann, W. K., Tholen, D. J., Meech, K. J. and Cruikshank, D. P., 2060 Chiron, colorimetry and cometary behavior. *Icarus* **83,** 1–15, 1990.

Kowal, C. T., Chiron, in *Asteroids* (edited by T. Gehrels), pp. 436–439. University of Arizona Press, Tucson, 1979.

Landolt, A. U., UBVRI photometric standard stars around the celestial equator. *Astron. J.* **88,** 439–460, 1983.

Lebofsky, L. A., Tholen, D. J., Rieke, G. H. and Lebofsky, M., 2060 Chiron: visual and thermal infrared observations. *Icarus* **60,** 532–537, 1984.

Luu, J. X. and Jewitt, D. C., Cometary activity in 2060 Chiron. *Astron. J.* **100,** 913–931, 1990.

Luu, J. X. and Jewitt, D. C., Continued activity in Chiron, in *Proceedings of the Workshop on the Activity of Distant Comets* (edited by W. F. Huebner, H. U. Keller, D. Jewitt, J. Klinger and R. West), pp. 44–53. Southwest Research Institute, San Antonio, 1993.

Marcialis, R. L. and Buratti, B. J., CCD photometry of 2060 Chiron in 1985 and 1991. *Icarus* **104,** 234–243, 1993.

Marcialis, R. L., Hubbard, W. B., Hill, R., Bus, S. J., Elliot, J. L., Olkin, C., McDonald, S., Foust, J., Sopata, L., Bandyopadhyay, R., Meserole, R., Buie, M. W., Spencer, J. R., Wasserman, L. H., Millis, R., Dunham, E., Beichman, C. A., Jarrett, T. H., Young, J., Ford, C. and Herter, T., The 1993 Nov 07 occultation of Ch02 by 2060 Chiron. *BAAS* **26,** 1153, 1994.

Meech, K. J. and Belton, M. J. S., The atmosphere of 2060 Chiron. *Astron. J.* **100,** 1323–1338, 1990.

Oikawa, S. and Everhart, E., Past and future orbit of 1977 UB, object Chiron. *Astron. J.* **84,** 134–139, 1979.

Scholl, H., History and evolution of Chiron's orbit. *Icarus* **40,** 345–349, 1979.

Stern, A., Implications of volatile release from object 2060 Chiron. *Pub. Astron. Soc. Pacific* **101,** 126–132, 1989.

Sykes, M. and Walker, R., Constraints on the diameter and albedo of 2060 Chiron. *Science* **251,** 777–780, 1991.

Tholen, D., Hartmann, W. K. and Cruikshank, D. P., (2060) Chiron, IAU Circular 4554, 1988.

West, R. M., A photometric study of (2060) Chiron and its coma. *Astron. Astrophys.* **241,** 635–645, 1991.

Womack, M. and Stern, S. A., Detection of carbon monoxide in (2060) Chiron. *BAAS* **27,** 1143, 1995.

Pergamon

Planet. Space Sci., Vol. 45, No. 12, pp. 1607–1614, 1997

0032-0633/97 $17.00+0.00

PII: S0032-0633(97)00124-4

Photometric monitoring of 2060 Chiron's brightness at perihelion*

D. Lazzaro,[1]† M. A. Florczak,[1,2,3] C. A. Angeli,[1] J. M. Carvano,[1] A. S. Betzler,[1,4] A. A. Casati,[1,4] M. A. Barucci,[3] A. Doressoundiram[3] and M. Lazzarin[5]

[1]ON/CNPq, Dep. Astrofisica, 20921 Rio de Janeiro, Brazil
[2]CEFET, Dep. Física, Curitiba, 80000 Brazil
[3]Observatoire de Paris, 92195 Meudon Principal Cedex, France
[4]UFRJ, Dep. Astronomia, Rio de Janeiro, Brazil
[5]Universitá di Padova, Dip. di Astronomia, 35122 Padova, Italy

Received 6 December 1996; accepted 20 May 1997

Abstract. The results of photometric and spectroscopic observations of comet/asteroid 2060 Chiron carried on at the Observatório do Pico-dos-Dias (Brazil), at the European Southern Observatory (Chile), and at the Mauna Kea Observatory (Hawaii) during 1996 are presented. The analysis of the photometric data shows that even at a minimum of brightness 2060 Chiron presents some activity. The absolute magnitude, H_r, varied from 6.79 in February to 6.22 in March. Therefore 2060 Chiron is still in a minimum of activity close to that of 1983–1985 and of 1994–1995. © 1998 Elsevier Science Ltd. All rights reserved

1. Introduction

The approach of 2060 Chiron to perihelion, which occurred in February 1996, increased the interest on this Centaur object. Since its discovery it would be the first time that this object could be observed at its maximum approximation to the Sun. Therefore, it would be the best chance to test if its outgassing mechanism is related to heliocentric distance.

It should be recalled that 2060 Chiron, being a Saturn crosser, was considered the most distant asteroid known until its cometary behavior started to be asserted in 1988 (Tholen *et al.*, 1988; Bus *et al.*, 1988; Bus *et al.*, 1989; Hartmann *et al.*, 1990). This cometary activity was detected when 2060 Chiron was at a heliocentric distance of nearly 13 AU which seemed to imply the presence of very volatile ices, such as CN, CO or CO_2 (Stern, 1989; Meech and Belton, 1990). Even though CN and CO have been detected (Bus *et al.*, 1991; Womack and Stern, 1995) this occurred only once up to the present date, probably implying very particular outgassing configurations.

Another quite surprising property observed for 2060 Chiron is that it seems to present a peculiar long-term brightness evolution. In spite of increasing cometary activity as it approaches perihelion the brightness diminishes (Bergeron and Vanouplines, 1995; Lazzaro *et al.*, 1996). The marked increase in brightness which occurred from 1987 up to 1992 was preceded and followed by periods of minima, tending to indicate a somehow periodic behavior (Lazzaro *et al.*, 1996).

To gain more information on the long-term evolution of 2060 Chiron's brightness, a photometric and spectroscopic survey was performed all along its passage through perihelion. In this paper we present the data of these missions showing that despite its minimum of brightness 2060 Chiron is indeed active. In Section 2 we present the photometric and spectroscopic observations and the reduction techniques used. The results and a brief discussion of them are given in Section 3.

2. Observations and reduction

2.1. *Photometry*

CCD photometric observations of 2060 Chiron were performed all along its opposition in 1996 at the Observatório do Pico-dos-Dias, (Brazil). This campaign was composed of several short observational runs between January and June on a 0.6 m telescope. In all the observations a CCD EEV-385 × 576 was used, with a readout noise of 8 electronsRMS and an approximate gain of 10 ADU. A focal-plane reducing optics giving a 7.2′ × 5.5′ field was used

*Observations carried on at the Observatório do Pico dos Dias, operated by the Laboratório Nacional de Astrofisica (Brazil), at the European Southern Observatory (Chile) and at the Mauna Kea Observatory (Hawaii).
†*Correspondence to*: D. Lazzaro

Table 1. Mean observing geometry for 2060 Chiron for each night it was observed [a]

UT date	R (AU)	Δ (AU)	α (°)	Q	"Linking night"
Photometry					
1996/01/27	8.454	8.033	6.19	3	
1996/01/29	8.454	8.004	6.10	3	
1996/01/31	8.454	7.972	6.00	2	01/29
1996/02/01	8.454	7.957	5.94	2	01/29
1996/02/17	8.454	7.740	4.84	2	02/18
1996/02/18	8.454	7.728	4.75	3	
1996/02/29	8.454	7.611	3.72	1	
1996/03/27	8.455	7.463	0.64	3	
1996/04/23	8.455	7.528	2.75	3	
1996/04/24	8.455	7.535	2.86	3	
1996/06/12	8.465	8.133	6.60	3	
Spectroscopy					
1996/03/27	8.455	7.463	0.64	3	
1996/06/21	8.467	8.265	6.83	3	

[a] R and Δ are the heliocentric and geocentric distances, respectively, and α is the solar phase angle. The quality factor, Q, indicates whether a night was photometric (3), with thin cirrus but "linked" to a photometric night (2) or with thin cirrus (1).

yielding a scale image of $1.2''\,\mathrm{pix}^{-1}$. Most of the observations were obtained through filters approximating the V and R of the Johnson system and some in the B filter. In Table 1 are shown the mean geometric circumstances for each night of observation as well as a quality factor indicating whether the night was photometric or not. In the case of non-photometric nights there is also given the photometric night to which it has been linked through the comparison stars in the field.

The photometric data from these observations are given in Table 2 where $\mathrm{Mag}_{\mathrm{obs}}(\alpha)$ is the observed magnitude and α is the solar phase angle given in Table 1. All images were reduced using DAOPHOT, a package of the Image Reduction and Analysis Facility (IRAF), and calibrated using standard methods with bias and dome flat-field images. Flux calibration was obtained using standard stars from Landolt (1983). The images from each night were corrected for extinction by using photometry of field stars from 2060 Chiron images and photometry of the Landolt stars taken at different air masses. Since 2060 Chiron was almost stationary relatively to the field stars, it was possible to link the non-photometric observations to photometric ones, through the comparison stars present on nearby nights. The errors given in Table 2 take into account the aperture error given by DAOPHOT and the quality of the night. It must be pointed out that for one non-photometric night, February 29th, it was not possible to appropriately link it to a photometric one, so that the values given for this night must be taken with care.

2.2. *Spectroscopy*

2060 Chiron has been observed at the European Southern Observatory of La Silla (ESO, Chile) on March 26, 1996 and at the Mauna Kea Observatory, Hawaii, on June 20, 1996. At ESO we used the 1.5 m telescope with a Boller and Chivens spectrograph and a Ford CCD (2048 × 2048 pixels). We used the $225\,\mathrm{gr\,mm}^{-1}$ grating with a dispersion of $330\,\mathrm{mm}^{-1}$ in the first order. The CCD has a square $15\,\mu$m pixel, giving a dispersion of about $5\,\mathrm{pixel}^{-1}$ in the wavelength direction. The spectral range is about $0.48 < \lambda < 0.92\,\mu$m with a FWHM of 10. The spectrum was taken through a long slit oriented in the East–West direction, 2″ wide, to eliminate possible loss of light due to atmospheric differential refraction.

At the Mauna Kea Observatory we used the 3.6 m Canada–France–Hawaii telescope equipped with the MOS (Multi Object Spectrograph) and the CCD STI2 (2048 × 2048 pixels). The grism used is the V150 with a dispersion of $433\,\mathrm{mm}^{-1}$. The spectral range covered is $0.4 < \lambda < 0.98\,\mu$m with a spectral dispersion of $7\,\mathrm{pixel}^{-1}$. A spectral resolution of about 30 has been obtained with a slit aperture of 1″.

The observational circumstances are listed in Table 1 which shows the distance from the Sun, from the Earth, the solar phase angle and the quality of the night.

Particular care was taken to ensure proper calibration of the comet/asteroid spectra and several solar analog spectra have been secured during the two nights. The reflectance spectra, shown in Fig. 1 are the result of the division by the spectrum of the solar analog HD44594 for the ESO observations, and by 16Cygnus B for the CFHT observations (Hardorp, 1979).

3. Results and discussion

3.1. *Photometric evolution*

To analyze the photometric long-term behavior of 2060 Chiron we computed absolute magnitudes of the H–G system (Bowell *et al.*, 1989), as well as reduced ones (Table 3). For this purpose we adopted the commonly used values

Table 2. Photometric observations of 2060 Chiron in 1996

UT date	Filter	$Mag_{obs}(\alpha)$	Error
1996 January 27.1482	V	16.070	0.027
1996 January 27.1551	V	16.076	0.026
1996 January 27.1576	V	16.074	0.025
1996 January 27.1626	V	16.061	0.024
1996 January 27.1708	V	16.058	0.023
1996 January 27.1825	V	16.022	0.021
1996 January 27.1863	V	16.025	0.021
1996 January 27.1899	V	16.027	0.020
1996 January 27.1932	V	16.096	0.020
1996 January 27.1974	V	16.028	0.019
1996 January 27.2095	V	16.051	0.018
1996 January 27.2133	V	16.092	0.019
1996 January 27.2169	V	16.116	0.019
1996 January 27.2203	V	16.103	0.018
1996 January 27.2274	V	16.056	0.018
1996 January 27.2305	V	16.037	0.018
1996 January 27.2366	V	16.079	0.018
1996 January 27.2400	V	16.068	0.018
1996 January 27.2640	V	16.071	0.017
1996 January 27.2725	V	16.052	0.016
1996 January 27.2761	V	16.052	0.016
1996 January 27.2799	V	16.057	0.016
1996 January 27.2831	V	16.036	0.016
1996 January 27.2863	V	16.024	0.016
1996 January 27.2903	V	16.032	0.016
1996 January 27.2941	V	16.056	0.016
1996 January 27.2980	V	16.102	0.016
1996 January 27.3090	V	16.038	0.016
1996 January 27.3131	V	16.035	0.016
1996 January 27.3168	V	16.040	0.017
1996 January 27.3205	V	16.054	0.018
1996 January 29.1300	V	16.003	0.019
1996 January 29.1354	R	15.566	0.016
1996 January 29.1372	R	15.647	0.013
1996 January 29.1401	R	15.638	0.015
1996 January 29.1421	R	15.639	0.015
1996 January 29.1444	V	16.012	0.018
1996 January 29.1473	V	15.994	0.015
1996 January 29.1508	V	16.005	0.013
1996 January 29.1545	B	16.516	0.029
1996 January 29.1667	B	16.634	0.030
1996 January 29.1834	V	16.057	0.013
1996 January 29.1866	V	16.072	0.013
1996 January 29.1894	V	16.052	0.012
1996 January 29.1930	R	15.710	0.011
1996 January 29.1956	R	15.694	0.011
1996 January 29.1973	R	15.701	0.011
1996 January 29.1990	R	15.705	0.012
1996 January 29.2056	B	16.618	0.023
1996 January 29.2104	B	16.691	0.025
1996 January 29.2281	V	16.072	0.013
1996 January 29.2311	V	16.080	0.013
1996 January 29.2338	V	16.034	0.012
1996 January 29.2366	V	16.050	0.012
1996 January 29.2411	R	15.628	0.011
1996 January 29.2434	R	15.654	0.010
1996 January 29.2452	R	15.657	0.010
1996 January 29.2470	R	15.650	0.010
1996 January 29.2506	B	16.579	0.026
1996 January 29.2605	B	16.541	0.021
1996 January 29.2735	R	15.621	0.011
1996 January 29.2751	R	15.611	0.011
1996 January 29.2767	R	15.645	0.010
1996 January 29.2791	B	16.549	0.021
1996 January 29.2855	B	16.574	0.019
1996 January 29.2928	B	16.639	0.018
1996 January 29.3018	V	16.024	0.010

Table 2. Continued

UT date	Filter	$Mag_{obs}(\alpha)$	Error
1996 January 29.3057	V	16.018	0.010
1996 January 29.3102	R	15.648	0.009
1996 January 29.3135	B	16.669	0.023
1996 January 31.2156	R	15.649	0.015
1996 January 31.2184	R	15.630	0.015
1996 January 31.2214	V	16.005	0.024
1996 January 31.2303	V	15.974	0.024
1996 January 31.2423	R	15.614	0.014
1996 January 31.2473	R	15.621	0.014
1996 January 31.2506	V	15.966	0.022
1996 January 31.2552	V	15.950	0.022
1996 January 31.2594	V	15.981	0.022
1996 January 31.2714	R	15.628	0.014
1996 January 31.2739	R	15.658	0.014
1996 January 31.2764	R	15.663	0.014
1996 January 31.2839	V	16.023	0.024
1996 January 31.3085	V	16.043	0.024
1996 January 31.3259	V	15.979	0.024
1996 February 01.2317	V	16.028	0.028
1996 February 01.2352	V	15.992	0.028
1996 February 01.2386	V	15.967	0.028
1996 February 01.2421	V	16.021	0.028
1996 February 01.2462	V	15.990	0.028
1996 February 01.2503	V	15.970	0.026
1996 February 01.3026	V	16.010	0.026
1996 February 17.1739	V	16.042	0.065
1996 February 17.2253	V	16.110	0.059
1996 February 17.2659	V	15.973	0.059
1996 February 17.2771	V	16.004	0.059
1996 February 17.3076	V	16.039	0.062
1996 February 18.1770	R	15.641	0.008
1996 February 18.1801	R	15.626	0.006
1996 February 18.1830	R	15.631	0.006
1996 February 18.1929	V	16.001	0.007
1996 February 18.2123	R	15.629	0.006
1996 February 18.2195	R	15.591	0.006
1996 February 18.2839	R	15.599	0.006
1996 February 18.2876	R	15.580	0.006
1996 February 18.2938	V	16.056	0.006
1996 February 18.2998	V	15.998	0.006
1996 February 18.3057	V	16.019	0.006
1996 February 18.3294	V	15.983	0.008
1996 February 29.0682	V	16.031	0.121
1996 February 29.1700	V	15.934	0.115
1996 February 29.2341	V	15.878	0.113
1996 February 29.2360	V	15.880	0.112
1996 March 27.0172	V	15.678	0.014
1996 March 27.0204	R	15.219	0.010
1996 March 27.0220	R	15.208	0.010
1996 March 27.0240	V	15.630	0.012
1996 March 27.0265	V	15.654	0.012
1996 March 27.0295	R	15.222	0.010
1996 March 27.0311	R	15.209	0.010
1996 March 27.0417	V	15.629	0.012
1996 March 27.0444	V	15.657	0.012
1996 March 27.0474	R	15.214	0.010
1996 March 27.0490	R	15.224	0.010
1996 March 27.0509	V	15.631	0.012
1996 March 27.0537	V	15.654	0.012
1996 March 27.0564	R	15.186	0.009
1996 March 27.0580	R	15.189	0.009
1996 March 27.0722	V	15.632	0.011
1996 March 27.0752	V	15.637	0.011
1996 March 27.0780	R	15.201	0.009
1996 March 27.0795	R	15.201	0.010
1996 March 27.0815	V	15.631	0.011
1996 March 27.0840	V	15.656	0.011

Table 2. Continued

UT date	Filter	$Mag_{obs}(x)$	Error
1996 March 27.0871	R	15.212	0.009
1996 March 27.0886	R	15.208	0.009
1996 March 27.0973	V	15.670	0.011
1996 March 27.0998	V	15.671	0.011
1996 March 27.1157	R	15.268	0.009
1996 March 27.1172	R	15.279	0.009
1996 March 27.2338	V	15.688	0.012
1996 March 27.2363	V	15.680	0.012
1996 March 27.2390	R	15.211	0.009
1996 March 27.2407	R	15.233	0.009
1996 March 27.2555	V	15.725	0.012
1996 March 27.2648	V	15.712	0.013
1996 March 27.2671	V	15.732	0.013
1996 March 27.2698	R	15.281	0.010
1996 April 22.9386	V	15.733	0.013
1996 April 22.9446	V	15.735	0.010
1996 April 22.9512	V	15.734	0.010
1996 April 22.9555	R	15.338	0.008
1996 April 22.9582	R	15.349	0.009
1996 April 22.9767	V	15.706	0.009
1996 April 22.9812	V	15.735	0.009
1996 April 22.9862	R	15.364	0.008
1996 April 22.9892	R	15.358	0.008
1996 April 23.0106	V	15.753	0.009
1996 April 23.0147	V	15.725	0.009
1996 April 23.0190	R	15.389	0.008
1996 April 23.0218	R	15.399	0.008
1996 April 23.0353	V	15.779	0.009
1996 April 23.0394	V	15.778	0.009
1996 April 23.0436	R	15.404	0.007
1996 April 23.0463	R	15.385	0.007
1996 April 23.0497	B	16.435	0.018
1996 April 23.0577	B	16.531	0.018
1996 April 23.0824	V	15.738	0.009
1996 April 23.0869	B	16.220	0.016
1996 April 23.0944	V	15.749	0.008
1996 April 23.0986	R	15.358	0.007
1996 April 23.1169	V	15.757	0.009
1996 April 23.1209	V	15.763	0.009
1996 April 23.1251	R	15.377	0.007
1996 April 23.1278	R	15.377	0.007
1996 April 23.1484	V	15.778	0.009
1996 April 23.1525	V	15.784	0.009
1996 April 23.1568	R	15.392	0.007
1996 April 23.1596	R	15.392	0.008
1996 April 23.1746	V	15.759	0.010
1996 April 23.1786	V	15.764	0.010
1996 April 23.1828	R	15.218	0.007
1996 April 23.1863	R	15.224	0.007
1996 April 23.2040	R	15.336	0.008
1996 April 23.2070	R	15.307	0.008
1996 April 23.9559	V	15.754	0.009
1996 April 23.9612	V	15.756	0.008
1996 April 23.9653	R	15.360	0.007
1996 April 23.9685	R	15.369	0.007
1996 April 23.9827	V	15.790	0.008
1996 April 23.9879	V	15.799	0.009
1996 April 23.9920	R	15.379	0.007
1996 April 23.9951	R	15.420	0.007
1996 April 24.0194	V	15.830	0.008
1996 April 24.0244	V	15.808	0.008
1996 April 24.0290	R	15.420	0.007
1996 April 24.0321	R	15.403	0.007
1996 April 24.0692	V	15.788	0.008
1996 April 24.0743	V	15.785	0.007
1996 April 24.0787	R	15.368	0.006
1996 April 24.0819	R	15.373	0.006

Table 2. Continued

UT date	Filter	$Mag_{obs}(x)$	Error
1996 April 24.1090	V	15.813	0.008
1996 April 24.1141	V	15.785	0.008
1996 April 24.1183	R	15.294	0.010
1996 April 24.1214	R	15.285	0.010
1996 April 24.1246	R	15.392	0.007
1996 April 24.1277	R	15.375	0.007
1996 April 24.1551	V	15.808	0.008
1996 April 24.1601	V	15.804	0.008
1996 April 24.1646	R	15.406	0.007
1996 April 24.1677	R	15.398	0.007
1996 April 24.1970	V	15.762	0.009
1996 April 24.2014	R	15.365	0.007
1996 June 11.9742	V	16.154	0.009
1996 June 11.9782	V	16.155	0.009
1996 June 11.9820	V	16.140	0.009
1996 June 12.0153	R	15.709	0.008
1996 June 12.0228	V	16.118	0.009
1996 June 12.0266	V	16.110	0.009
1996 June 12.0030	B	16.899	0.014
1996 June 12.0303	V	16.082	0.009
1996 June 12.0349	R	15.689	0.008
1996 June 12.0371	R	15.693	0.008
1996 June 12.0391	R	15.683	0.008
1996 June 12.0416	B	16.896	0.015
1996 June 12.0489	B	16.902	0.015
1996 June 12.0560	B	16.945	0.016

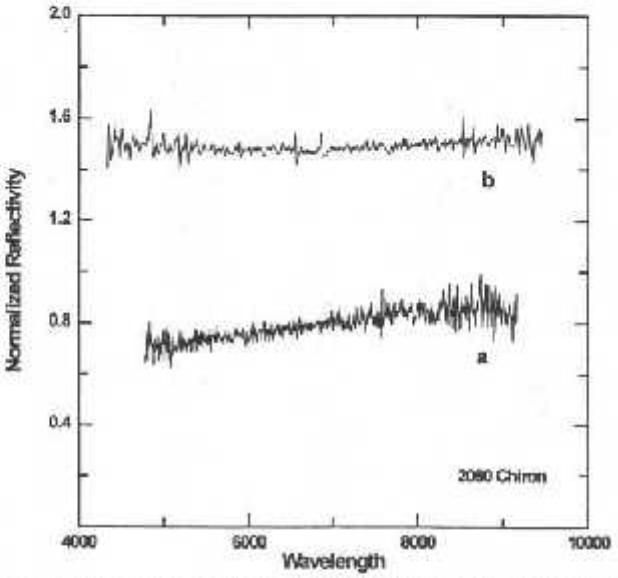

Fig. 1. Reflectivity spectrum of 2060 Chiron, normalized at 1 around 5500 Å, obtained at (a) ESO on 1996/03/27, and (b) CFHT on 1996/06/21. The exposure time was 660 s for spectrum (a) and 360 s for spectrum (b)

of slope parameter, 0.70 ± 0.15 determined by Bus *et al.* (1989). We would like to stress that, as will be discussed in the next section, the use of the H–G system seems inappropriate for 2060 Chiron, and is adopted here just to compare the present values with those published.

The monitoring of 2060 Chiron's brightness in 1996 showed that its mean absolute V magnitude varied from

Table 3. Mean values for each night of observation and each filter, of the observed magnitude, Mag_{obs}, reduced magnitude, Mag_{red}, and absolute magnitudes, $H(\alpha)$, obtained with a slope parameter $G = 0.70$

UT date	Filter	Mag_{obs}	Mag_{red}	$H(\alpha)$
1996 January 27.2312	V	16.058 ± 0.019	6.903	6.714
1996 January 29.2053	V	16.026 ± 0.013	6.885	6.698
1996 January 29.2158	R	15.651 ± 0.012	6.499	6.313
1996 January 29.2420	B	16.601 ± 0.024	7.450	7.263
1996 January 31.2669	V	15.990 ± 0.023	6.847	6.663
1996 January 31.2493	R	15.638 ± 0.014	6.495	6.310
1996 February 01.2497	V	15.997 ± 0.027	6.858	6.674
1996 February 17.2499	V	16.036 ± 0.061	6.955	6.796
1996 February 18.2843	V	16.012 ± 0.007	6.936	6.779
1996 February 18.2205	R	15.614 ± 0.006	6.538	6.381
1996 February 29.1771	V	15.931 ± 0.115	6.889	6.756
1996 March 27.1126	V	15.665 ± 0.012	6.665	6.623
1996 March 27.0958	R	15.222 ± 0.009	6.222	6.180
1996 April 23.0565	V	15.751 ± 0.009	6.732	6.623
1996 April 23.0863	R	15.361 ± 0.008	6.331	6.223
1996 April 23.0648	B	16.395 ± 0.017	7.376	7.267
1996 April 23.0648	B	16.395 ± 0.017	7.376	7.267
1996 April 24.0623	V	15.791 ± 0.008	6.769	6.658
1996 April 24.0779	R	15.374 ± 0.007	6.352	6.240
1996 June 12.0024	V	16.127 ± 0.009	6.941	6.744
1996 June 12.0316	R	15.694 ± 0.008	6.508	6.311
1996 June 12.0374	B	16.910 ± 0.015	7.726	7.528

6.79 in February to 6.22 in March. An almost equal variation was detected in the mean absolute R magnitude, from 6.28 to 6.18, for the same time. In Fig. 2(a) and (b) we present, for each filter, the mean absolute magnitudes and the reduced magnitudes, respectively, obtained in 1996. As can be seen, 2060 Chiron was at a minimum of brightness in January and February, had an increase in March reaching a minimum again in June. A nearly 20% mag increase in activity, in the UV band, was also detected by Parker *et al.* (1996) from data obtained with the Hubble telescope in January and April 1996.

It must be pointed out that the detected increase of nearly 0.1 mag in the span of some months was coincident with the smallest solar phase angle. Although this fact is taken into account when computing absolute magnitudes, we cannot guarantee that the increase was due to 2060 Chiron's cometary activity or to an opposition surge. In the published data the only continuous monitoring reaching small phase angles was made in 1978 by Bus *et al.* (1989) showing an even greater opposition surge, if real. Since a visible coma was not detected in our observations it is impossible, at present, to exclude either possibility.

Short-period activity of the order of hours was also detected during one night. In Fig. 3(a) and (b) are shown the observed magnitude of 2060 Chiron and the ratio of two comparison stars in the field of April 23rd. In contrast to this ratio which stays constant, 2060 Chiron's magnitude presents a complex curve that can be represented by the combination of three components. The first one is periodic, due to the rotation of the object. The second is secular, due to the decrease of brightness after the peak detected in March. And the third component is rather random, corresponding to peaks of brightening. A similar short-period activity was also detected in 1989 by Luu and Jewitt (1990) and in 1990 by Buratti and Dunbar (1991).

All published data of 2060 Chiron are compiled in Fig. 4 where its brightness secular evolution is shown through reduced V magnitudes. From this figure it is clear that 2060 Chiron is now at its minimum of brightness. However, we would like to stress that presently 2060 Chiron has an activity, as mentioned above. In other words, a minimum of brightness does not mean inactivity. This fact suggests that the minimum detected in 1984–1986 cannot be taken as proof of 2060 Chiron's inactivity at that instant. It must be recalled that 2060 Chiron then was at almost 13 AU. A small activity, such as the present one, would possibly be below the observational limit. This understanding is crucial in modelling 2060 Chiron's activity.

A Fourier analysis of the composite lightcurve was performed using the method described by Harris *et al.* (1989) giving a period of 5.9178 ± 0.0015 h in agreement with the value obtained by Marcialis and Buratti (1993). The composite lightcurve is plotted in Fig. 5 together with the fifth-order fit (continuous line). Each symbol corresponds to a different night. The quite high dispersion, around 3, is most probably due to the activity detected in the object and to the fact that the data are spread out over a period of several months. The peak-to-peak variation of the lightcurve is 0.06 ± 0.01 mag. This value, taking into account the high dispersion of the data, is rather close to that obtained by Bus *et al.* (1989), 0.08, when 2060 Chiron was at a minimum of activity as nowadays. It is interesting to note that these values are greater than those obtained by Luu and Jewitt (1990), 0.045, and by Buratti and Dunbar (1991), 0.020, when the comet was at a maximum of brightness. Such a behavior of the lightcurve can be under-

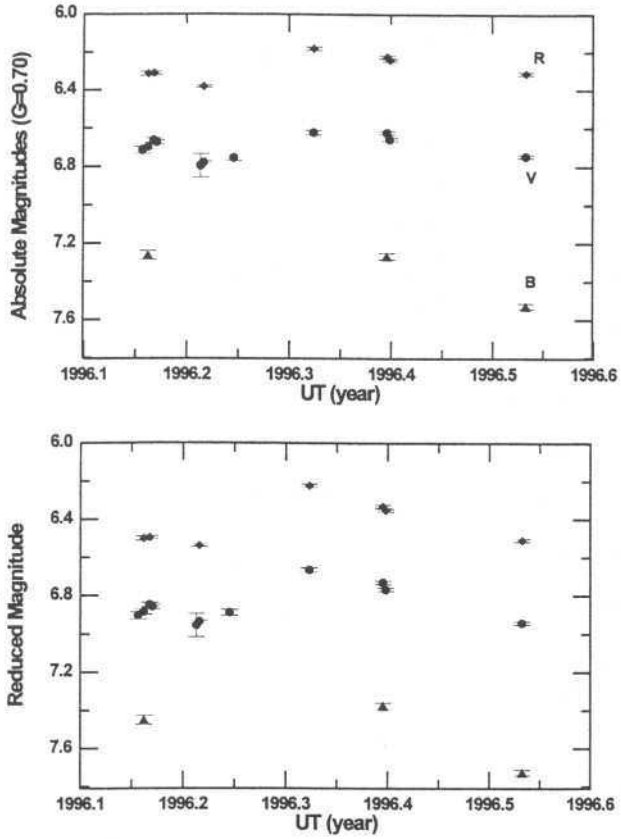

Fig. 2. 2060 Chiron mean brightness during 1996 for each filter used. The brightness is represented by (a) absolute H_V magnitudes, and (b) reduced magnitudes

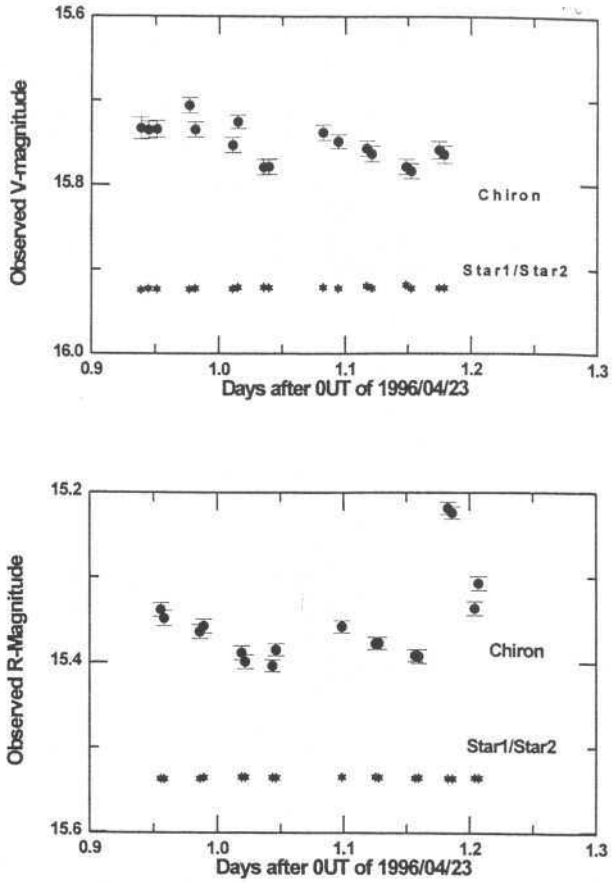

Fig. 3. Observed magnitudes of 2060 Chiron during April 23rd, 1996. The stars represent the ratio between two comparison stars in the field that has been arbitrarily vertically displayed in order to fit into the plot

stood if we assume that 2060 Chiron has a slightly elongated shape but the presence of a spherical coma may suppress the amplitude variation during its high activity. On the other hand, when it has low activity the effect of the coma disappears and the amplitude variation becomes greater. However, we cannot preclude the possibility that these differences could also be due to different inclinations of 2060 Chiron's rotation axis.

The data obtained allow us to determine a broadband colorimetry for 2060 Chiron in 1996. The V–R index varies from 0.382 ± 0.01 in January up to 0.417 ± 0.008 in April. The B–V index varies from 0.565 ± 0.027 in January to 0.644 ± 0.019 in April, although the precision of these values are less than the V–R values, and are based on insufficient data. Considering that the solar values of V–R and B–V are around 0.36 and 0.66 (Hardorp, 1979), respectively, the values obtained indicate that 2060 Chiron had a rather gray color in April. It is worth to point out that the slight bluer color of 2060 Chiron in January has no clear explanation but it could be due, in part, to the greater phase angle.

3.2. *The G parameter*

The slope parameter, G, as introduced by Bowell *et al.* (1989), is used to represent the scattering properties of an asteroid's surface. Since 2060 Chiron was initially thought

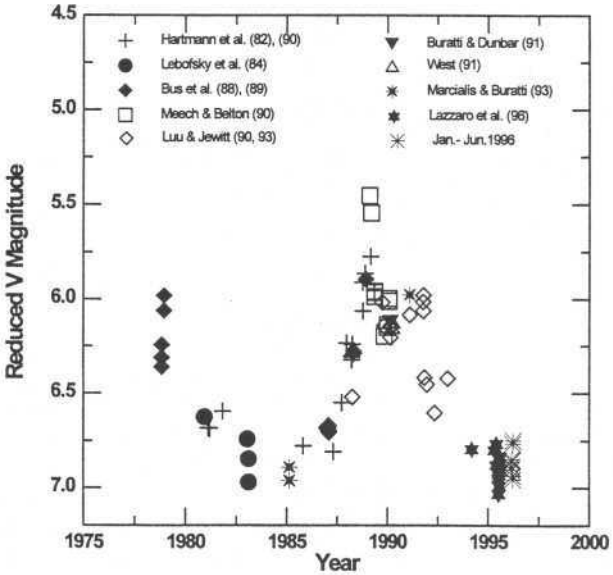

Fig. 4. Reduced V magnitudes of 2060 Chiron vs. year. The values are taken from literature and converted to V magnitudes

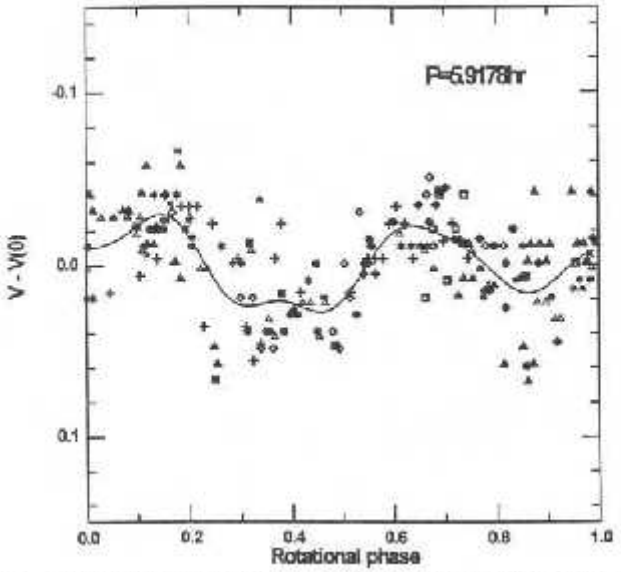

Fig. 5. Composite lightcurve with 200 points of 2060 Chiron during 1996. Absolute magnitudes, with $G = 0.70$ were used in order to include the effects of phase angle. The continuous line indicates the fifth-order fit giving a period of 5.9287 h

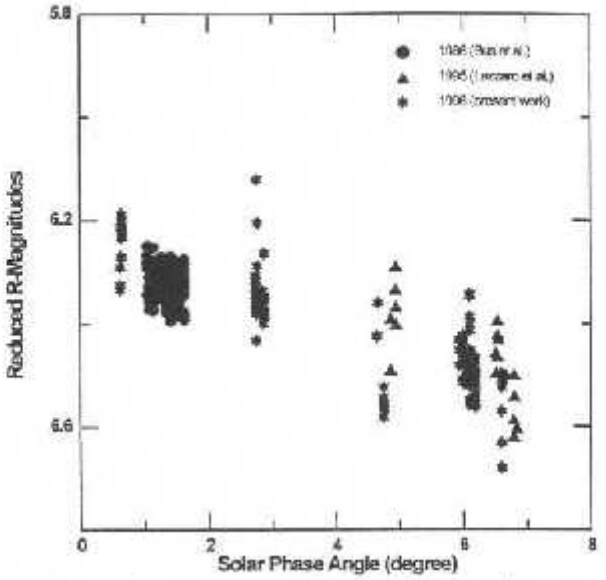

Fig. 6. Reduced R magnitudes of 2060 Chiron vs. phase angle for different sets of data

to be an asteroid, this parameter was determined by Bus *et al.* (1989), giving a value of 0.70 ± 0.15. While these authors state that little significance should be attached formally to this value of G in view of their limited span of phase angles, all data published afterwards adopted their value in order to assert the secular photometric evolution of 2060 Chiron.

In our previous paper (Lazzaro *et al.*, 1996) we pointed out that, in view of the cometary activity of 2060 Chiron, the H–G system seemed to be inappropriate for monitoring its photometric behavior. However, 2060 Chiron appeared again to be in a quiet state similar to that of the Bus *et al.* observational period, so that a new determination of this parameter was performed. The value of 0.71 ± 0.15 was obtained confirming the previous value. Therefore, it seemed to support somehow the idea that the characteristics of 2060 Chiron's surface could be represented by a slope parameter around 0.70–0.71.

Since the mean brightness of 2060 Chiron in 1996 was still at a minimum we decided to perform yet another new analysis of the slope parameter. This new analysis indicated a very different value, 0.42 ± 0.01. However, as discussed in the previous section, 2060 Chiron underwent some cometary activity in 1996, which possibly invalidates this new determination. It is important to note that, since we cannot discard the fact that in 1986 and in 1995 the comet/asteroid presented some degree of activity, even the value of 0.70–0.71 must be used with care. Moreover, if we analyze the different sets of data used in the determinations of the slope parameter (Fig. 6) it is clear that the data for any of the values are too restricted in phase angle to be significant. Not even all the combined data at minima of 2060 Chiron's brightness, assuming no cometary activity, span an interval of phase angles sufficient to constrain well the slope parameter. We do believe that reduced magnitudes should be preferred to absolute ones.

3.3. *Chiron's color*

The two optical spectra show a featureless quite flat continuum: the first with a small positive slope and the second with a flatter continuum.

The reflectivity gradient S' is equal to $2.3 \pm 0.1\%/10^3$ in the wavelength range 500–900 nm for the first spectrum of Fig. 1 while S' is equal to $0.4 \pm 0.1\%/10^3$ for the second one, computed in the same wavelength range. The higher S' value obtained during the March observations corresponds to an increase of 2060 Chiron's brightness probably due to an increase of the dust production. It is worth noting that the values obtained from spectroscopy are in agreement with the broadband photometry.

These values are not consistent with the mean slope of the optical spectra of cometary nuclei, $S' = 14 \pm 5\%/10^3$, computed by Jewitt and Luu (1990) and Fitzsimmons *et al.* (1994). This difference supports the idea that 2060 Chiron is a peculiar object.

The spectra obtained here reveal a small difference from those reported by Luu (1993): they show a slight negative slope (the slope has been computed in the wavelength range 380–630 nm) even if they affirmed that the spectrum of 2060 Chiron becomes nearly neutral at longer wavelengths. The negative reflectivity gradient was confirmed by Fitzsimmons *et al.* (1994) with observations performed during the same period. We cannot exclude that small changes in color may also be due to observations performed during different rotational phases (different area on 2060 Chiron's surface) or to the phase angle effect on the spectrum continua.

4. Summary

In this section we summarize the important points presented in this paper:

1. Photometric observations of 2060 Chiron in 1996 show that its brightness is still at a minimum despite having passed through its maximum approach to the Sun.
2. Even at a minimum of brightness 2060 Chiron presents cometary activity of long- (months) and short-period (hours). This activity could be now detected owing to an almost continuous monitoring and to its greater approach to Earth. We can therefore infer that 2060 Chiron has probably always some degree of activity and the outgassing models developed for this very particular object must be reexamined in the light of the new data.
3. Although the slope parameter, G, is useful in homogenizing the data for different phase angles, its value hardly represents the surface scattering properties of 2060 Chiron due to its activity. A more detailed study should be realized to assert how this fact affects the considerations on 2060 Chiron's brightness evolution.
4. A composite lightcurve was obtained with period of 5.9178 h and a peak-to-peak variation of 0.06 mag. This value is rather close to that determined by Bus *et al.* (1989) when 2060 Chiron was at a minimum of brightness as nowadays. The difference between the amplitudes obtained when 2060 Chiron was at a minimum and at a maximum of brightness can be attributed to a slightly elongated shape of the comet that is diluted when an extended coma is present. We do not preclude that these differences could also be explained by different inclinations of 2060 Chiron's rotation axis.
5. From broadband colorimetry we can assert a rather gray color for 2060 Chiron, with values around solar values.
6. The visible spectra of 2060 Chiron show quite flat featureless continua. The spectral behavior differs from the typical comet nuclei spectra which are generally redder in color. Small variations in the reflectivity gradients S' have been found among the available spectroscopical observations and this could probably be due to variations in the comet dust production.

Acknowledgements. The authors acknowledge the technical staff of the Observatório do Pico-dos-Dias, ESO and Mauna Kea Observatory for their prompt help whenever needed. Thanks are also due to D. Foryta and O. C. Winter for their help in some of the observations. M. A. Florczak, D. Lazzaro, C. A. Angeli, J. M. Carvano, A. S. Betzler and A. A. Casati thanks CNPq for its financial support during the present research.

References

Bergeron, D. and Vanouplines, P. (1995) 2060 Chiron, pp. 25405–25406. M.P.C.

Bowell, E., Hapke, B., Domingue, D., Lumme, K., Peltoniemi, J. and Harris, A. W. (1989) Applications of photometric models to asteroids. In *Asteroids II*, eds. R. P. Binzel, T. Gehrels and M. S. Matthews, pp. 524–556. Univ. of Arizona Press, Tucson, AZ.

Buratti, B. J. and Dunbar, R. S. (1991) Observation of a rapid decrease in the brightness of the coma of 2060 Chiron in 1990 January. *Astrophys. J.* **366,** L47–L49.

Bus, S. J., Bowell, E. and French, L. M. (1988) (2060) Chiron, *IAU Circular* 4684.

Bus, S. J., Bowell, E., Harris, A. W. and Hewitt, A. V. (1989) 2060 Chiron: CCD and electronographic photometry. *Icarus* **77,** 223–238.

Bus, S. J., A'Hearn, M. F., Schleicher, D. G. and Bowell, E. (1991) Detection of CN emission from (2020) Chiron. *Science* **251,** 774–777.

Fitzsimmons, A., Dahlgren, M., Lagerkvist, C.-I., Magnusson, P. and Williams, I. P. (1994) A spectroscopic survey of D-type asteroids. *Astron. Astrophys.* **282,** 634.

Hardorp, J. (1979) The Sun among the stars. *Astron. Astrophys.* **63,** 383–390.

Harris, A. W., Young, J. W., Bowell, E., Martin, L. J., Millis, R. L., Poutanen, M., Scaltriti, F., Zappalà, V., Dchober, H.-J., Debehogne, H. and Zeigler, K. W. (1989) Photoelectric observations of asteroids 3 Juno, 24 Themis, 60 Echo, 261 Prymno, and 863 Benkoela. *Icarus* **77,** 171–186.

Hartmann, W. K., Tholen, D. J., Meech, K. J. and Cruikshank, D. P. (1990) 2060 Chiron, colorimetry and cometary behavior. *Icarus* **83,** 1–15.

Jewitt, D. C. and Luu, J. X. (1990) CCD spectra of asteroids II. The Trojans as spectral analogs of cometary nuclei. *Astron. J.* **100,** 933–944.

Landolt, A. U. (1983) UBVRI photometric standard stars around the celestial equator. *Astron. J.* **88,** 439–460.

Lazzaro, D., Florczak, M. A., Betzler, A., Winter, O. C., Giuliatti-Winter, S. M., Angeli, C. A. and Foryta, D. W. (1996) 2060 Chiron back to a minimum of brightness. *Planet. Space Sci.* **44,** 1547–1550.

Lebofsky, L. A., Tholen, D. J., Rieke, G. H. and Lebofsky, M. A. (1984) 2060 Chiron: visual and thermal infrared observations. *Icarus* **60,** 535.

Luu, J. X. and Jewitt, D. C. (1990) Cometary activity in 2060 Chiron. *Astron. J.* **100,** 913–931.

Luu, J. X. (1993) Spectral diversity among the nuclei of Comets. *Icarus* **104,** 138–148.

Marcialis, R. L. and Buratti, J. (1993) CCD photometry of 2060 Chiron in 1985 and 1991. *Icarus* **104,** 234–243.

Meech, K. J. and Belton, M. J. S. (1990) The atmosphere of 2060 Chiron. *Astron. J.* **100,** 1323–1338.

Parker, J. M., Stern, A. and Festou, M. C. (1996) Ultraviolet spectra of Chiron observed with the HST/FOS. *ACM96–Cospar Colloquium 10*, abstract.

Stern, A. (1989) Implications of volatile release from object 2060 Chiron. *Publ. Astron. Soc. Pacific* **101,** 126–132.

Tholen, D., Hartmann, W. K. and Cruikshank, D. P. (1988) (2060) Chiron, *IAU Circular* 4554.

West, R. (1991) A photometric study of 2060 Chiron and its coma. *Astron. Astrophys.* **241,** 635.

Wormack, M. and Stern, S. A. (1995) Detection of carbon monoxide in (2060) Chiron. *BAAS* **27,** 1143.

5.4 - Conclusões

Nossas observações de Chiron mostraram que seu brilho diminuiu, alcançando um valor considerado mínimo (pouca ou nenhuma atividade cometária), apesar de sua passagem pelo periélio. Obtivemos uma curva de luz composta que confirma o período rotacional de 5,9 horas e detectamos uma possível atividade de curto período no início do ano de 1996. Verificamos também que o sistema H-G de magnitude absoluta não é apropriado para Chiron.

Apesar da obtenção de resultados muito reveladores sobre a atividade deste objeto, ainda não foi possível se elaborar um modelo que explique de forma satisfatória os processos atuantes em Chiron. Em particular, a atividade secular peculiar deste objeto necessita de dados sobre um intervalo de tempo maior antes de se elaborar um modelo.

Capítulo 6

Conclusões e Perspectivas Futuras

O trabalho desta tese foi baseado em observações espectroscópicas e fotométricas de asteróides visando uma melhor compreensão destes objetos. Para isto, foram selecionadas algumas populações que nos permitiram trabalhar dentro de assuntos distintos na área tais como: famílias de asteróides, processos de alteração físico-química superficial, relação asteróides-meteoritos, propriedades rotacionais, entre outros. Entre os princiais resultados obtidos, podemos destacar:

- encontramos características espectrais comuns entre si nos membros das famílias estudadas – Eos, Flora e Themis – confirmando, do ponto de vista mineralógico, uma provável origem comun;
- nos membros da família de Flora encontramos evidências de que um processo de "envelhecimento" espacial está agindo em sua superfície, camuflando sua real composição, a qual seria similar à dos meteoritos condritos ordinários. Esta composição também foi inferida para muitos dos objetos próximos da Terra observados;
- nos membros da família de Eos encontramos uma diversidade espectral que nos levou a concluir que o corpo original deve ter sido parcialmente diferenciado;
- em parte dos objetos da família de Themis foram encontrados indícios de um processo de alteração aquosa, implicando que o corpo orginal deve ter sido parcialmente alterado;
- analisando uma amostra significativa de asteróides do tipo C encontramos também indícios de alteração aquosa, a qual caracteriza a ocorrência de um evento térmico a baixa temperatura;

- das observações fotométricas obtivemos curvas de luz para 25 asteróides, tendo determinado o período rotacional para 19 destes;
- as observações de Chiron revelaram que, apesar de sua aproximação ao periélio, seu brilho se encontra com valores mínimos.

Acreditamos que o conjunto de dados obtido seja importante no estudo dos asteróides, tanto de um ponto de vista individual quanto global. Vale salientar que ao longo do trabalho foram estudados mais de 230 asteróides, o que representa um número bastante significativo. Mas, mais importante do que conhecer algumas propriedades físico-químicas de um asteróide, é entender este objeto como membro de uma população, seja ela de família, de objetos lentos ou de cometas "esquisitos". Foi essencialmente este o espírito que norteou o presente trabalho, e os resultados acima mencionados são uma boa amostra disto.

Entretanto, apesar do número de dados obtidos, estes ainda não são suficientes para se tentar melhorar os modelos de formação e evolução do cinturão, e do Sistema Solar, atualmente existentes. Dados adicionais são necessários para confirmar e precisar certos aspectos observados em nossas análises. Como bom exemplo podemos citar a definição precisa da extensão do(s) evento(s) térmico(s) ocorrido(s) no cinturão intermediário e no externo, assim como o processo que gerou este(s) evento(s). Este ponto é de fundamental importância na elaboração de qualquer modelo coerente de formação do cinturão dos asteróides e, provavelmente, de todo o Sistema Solar. Outro exemplo é o estudo evolutivo do cinturão através das famílias e do estado rotacional de asteróides, em particular dos pequenos. Até que ponto as colisões influenciaram o estado rotacional atual? Será que os pequenos asteróides (diâmetro inferior a 50km) podem guardar o período rotacional original? O que é este período?

Para responder a estas e a muitas outras perguntas precisamos conhecer melhor este universo de pequenos corpos, não apenas do ponto de vista dinâmico mas, principalmente, físico-químico. Pretendemos continuar neste caminho para futuramente tentar abordar o problema da formação do cinturão, tendo à mão condições de contorno mais precisas do que as atualmente disponíveis.

Bibliografia

ADAMS, J.B. (1974). Visible and infrared diffuse reflectance spectra of pyroxenes as applied to remote sensing of solid objects in the solar system. *J. Geophys. Res.*, **79**, 4829-4836.

ANGELI C.A. (1995). Determination des propriétés rotationnelles d'astéroÇdes: des indices pour interpréter leur histoire évolutive. Thèse de Doctorat, Observatoire de Paris.

ARNOLD, J.R. (1969). Asteroid families and "jet streams". *Astron. J.*, **74**, 1235-1242.

BARUCCI, M.A., M. LAZZARIN (1995). Visible spectroscopy of the Rosetta targets: 3840 Mimistrobell and 2530 Shipka. *Icarus*, **118**, 216-218.

BARUCCI, M.A., M.T. CAPRIA, A. CORADINI e M. FULCHIGNONI (1987). Classification of asteroids using G-mode analysis. *Icarus*, **72**, 304-324.

BELL, J.F. (1988). A probable asteroidal parent body for the CO or CV chondrite. *Meteoritics*, **23**, 256-257.

BELL, J.F. (1989). Mineralogical clues to the origin of asteroid dynamical families. *Icarus*, **78**, 426-440.

BELL, J.F., D.R. DAVIS, W.K. HARTMANN e M.J. GAFFEY (1989). Asteroids: the big picture. In *Asteroids II* (R.P. Binzel, T. Gehrels e M.S. Matthews, eds.), Univ. Arizona Press, Tucson, 921-945.

BENDJOYA, Ph. (1993). A classification of 6479 asteroids into families by means of the wavelet clustering method. *Astron. Astrophys. Suppl. Ser.*, **102**, 25-55.

BINZEL, R.P. (1988) . *Evolution in the Eos and Koronis families: observational and numerical results.* **Icarus,**, 73 303-313.

BINZEL, R.P., P. FARINELLA, V. ZAPPALÀ e A. CELLINO (1989). Asteroid rotation rates: distributions and statistics In *Asteroids II* (R.P. Binzel, T. Gehrels e M.S. Matthews, eds.), Univ. of Arizona Press, Tucson, 416-441.

BINZEL, R.P. e S. XU (1990). Chips off of asteroid 4 Vesta: evidence for the parent body of basaltic achondrite meteorites. *Science,* **260**, 186-191.

BINZEL, R.P., M.A. BARUCCI e M. FULCHIGNONI (1991) The origins of the asteroids. *Science,* **265**, 88-94.

BINZEL, R.P., S.J. BUS, T.H. BURBINE e J.M. SUNSHINE (1996). Spectral properties of near-Earth asteroids: evidence for sources of ordinary chondrite meteorites. *Science,* **273**, 946-948.

BOWELL, E., B. HAPKE, D. DOMINGUE, K. LUMME, J. PELTONIEMI e A. HARRIS (1989). Application of photometric models to asteroids. In *Asteroids II* (R.P. Binzel, T. Geherels e M. S. Matthews, eds), Univ. of Arizona Press, Tucson, 524-556.

BROUWER, D. (1951). Secular variations of the orbital elements of minor planets. *Astron. J.,* **56**, 9-32.

BURATTI, B.J. e R.S. DUNBAR (1991). Observation of a rapid decrease in the brightness of the coma of 2060 Chiron in 1990 January. *Astrophys. J.,* **366**, L47-L49.

BURNS, J. (1993). Mineralogical applications of crystal field theory. Cambrigde Univ. Press., New York.

BURNS, J. e V. SAFRONOV (1973). Asteroid nutation angles. *M.N.R.A.S.,* **165**, 403-411.

BUS, S.J., E. BOWELL, A.W. HARRIS e A.V. HEWITT (1989). 2060 Chiron: CCD and electronographic photometry. *Icarus,* **77**, 223-238.

BUS, S., M. A'HEARN, D. SCHLEICHER e E. BOWELL (1991). Detection of *CN* emission from (2060) Chiron. *Science,* **251**, 774-777.

CHAPMAN, C.R. (1996). S-type asteroids, ordinary chondrites, and space weathering: The evidence from Galileo's fly-bys of Gaspra and Ida (Invited Review). *Meteoritics and Planet. Sci.,* **31**, 699-725.

CHAPMAN, C.R., T.B. McCORD E C. PIETERS (1973). Minor planets related objects: spectrophotometric study of the composition of (1985) Toro. *Astron. J.,* **78**, 502-505.

CLOUTIS, E.A., M.J. GAFFEY, T.L. JACKOWSKI e K.L. REED (1986). Calibrations of phase abundance, composition, and particle size distribution for olivine-orthopyroxene mixtures from reflectance spectra. *J. Geophys. Res.*, **91**, 641-653.

CLOUTIS, E.A. e M.J. GAFFEY (1991). Pyroxene spectroscopy revisited: spectral–compositional correlations and relationship to geothermometry. *J. Geophys. Res.*, **96**, 22809-22826.

CUNNINGHAM, C.J. (1988a). The baron and his celestial police. *Sky and Telescope,* **75**, 271-272.

CUNNINGHAM, C.J. (1988b). Introduction to asteroids. Richmond: Willmann-Bell.

DI MARTINO, M., F. MIGLIORINI, V. ZAPPALÀ, A. MANARA e C. BARBIERI (1997). Veritas asteroid family: remarkable spectral differences inside a primitive parent body. *Icarus,* **127**, 112-120.

ELLIOT, J.L. *et al.* (1994). Jet-like features near the nucleus of Chiron. *Nature,* **373**, 46-49.

FARINELLA, P., D.R. DAVIS, A. CELLINO e V. ZAPPALÀ (1992). From asteroid clusters to families: a proposal for a new nomenclature. In *Asteroids Comets Meteors 91* (A. W. Harris and E. Bowell, eds.), Lunar and Planetary Institute, Houston, 165-166.

FEIERBERG, M.A., H.P. LARSON e C.R. CHAPMAN (1982). Spectroscopic evidence for undifferentiated S-type asteroids. *Astrophys. J.,* **257**, 361-372.

FEIERBERG, M.A., L.A. LEBOFSKY e D.J. THOLEN (1985). The nature of C-class asteroids from 3 micron spectrophotometry. *Icarus,* **63**, 183-191.

FERNÁNDEZ, J.A. (1980). On the existence of a comet belt beyond Neptune. *Mon. Not. Roy. Astron. Soc.,* **216**, 565-570.

FERNÁNDEZ, J.A. e A. BRUNINI (1998). Origin and evolution of the Oort cloud. In Solar System Formation and Evolution (D. Lazzaro, R. Vieira Martins, S. Ferraz-Mello, J. Fernández e C. Beaugé, Eds.), ASP Conference Series, Vol 149, 107-116.

FITZSIMMONS, A., M. DAHLGREN, C.-I. LAGERKVIST, P. MAGNUSSON e I.P. WILLIAMS (1994). A spectroscopic suervey of D-type asteroids. *Astron. Astrophys.,* **282**, 634-642.

GRIMM, R.E. e H.Y. McSWEEN (1993). Heliocentric zoning of the Asteroid belt by aluminum-26 heating. *Science,* **259**, 653-655.

FESTOU, M., H. RICKMAN e R. WEST (1993). Comets. *Astron. Astrophys. Rev.,* **5**, 37-163.

FRENCH, L., F. VILAS, W. HARTMANN e D.THOLEN (1989). Distant asteroids and Chiron. In *Asteroids II* (R. Binzel, T. Geherels e M. S. Matthews, eds), Univ. of Arizona Press, Tucson, 468-486.

FULCHIGNONI, M., M.A. BARUCCI, M. DI MARTINO e E. DOTTO (1995). On the evolution of the asteroid spin *Astron. Astrophys.,* **299**, 929-932.

GAFFEY, M.J. (1976). Spectral reflectance characteristics of the meteorite classes. *J. Geophys. Res.,* **81**, 905-920.

GAFFEY, M.J. (1978). Mineralogical characterizations of surface materials: evidence for unsampled types (abstract). *Meteoritcs,* **13**, 471-473.

GAFFEY, M.J. (1984). Rotational spectral variations of asteroid (8) Flora: Implications for the nature of the S-type asteroids and for the parent bodies of the ordinary chondrites. *Icarus,* **60**, 83-114.

GAFFEY, M.J. e McCORD (1979). Mineralogical and petrological characterizations of asteroid surface materials. In *Asteroids* (T. Gehrels, eds), Univ. of Arizona Press, Tucson, 688-723.

GAFFEY, M.J., J.F. BELL e D.P. CRUIKSHANK (1989). Reflectance spectroscopy and asteroid surface mineralogy. In *Asteroids II* (R.P. Binzel, T. Geherels e M. S. Matthews, eds), Univ. of Arizona Press, Tucson, 98-127.

GAFFEY, M.J., K.L. REED e M.S. KELLEY (1992). Relationship of E-type Apollo asteroid 3103 (1982 BB) to the enstatite achondrite meteorites and the Hungaria asteroids. *Icarus,* **100**, 95-109.

GAFFEY, M.J., J. F. BELL, R. H. BROWN, T. H. BURBINE, J. L. PIATEK, K. L. REED e D. A. CHAKY (1993). Mineralogical variations within S-type asteroid class. *Icarus* **106**, 573-602.

GEHRELS, T. (1979). The asteroids: history, surveys, techniques, and future work. In *Asteroids* (T. Gehrels eds), Univ. of Arizona Press, Tucson, 3-24.

GRADIE, J.C. e E.F. TEDESCO (1982). Compositional structure of the asteroid belt. *Science*, **197**, 1405-1407.

GRAHAM, J.A. (1982). UBVRI standard stars in the E-regions. *P.A.S.P.*, **94**, 244-265.

HARDIE, R.H. (1962). Photoelectric reductions. In *Astronomical techniques*, Vol. II. *Stars and Stellar Systems*, (A. W. Hintler, eds), Univ. of Chicago Press.

HARDORP, J. (1978). The Sun among the stars. *Astron. Astrophys.*, **63**, 383-390.

HARRIS, A. (1994a). Tumbling asteroids. *Icarus*, **107**, 209-211.

HARRIS, A. (1994b). Tumbling asteroids 2: 3288 Seleucus. *B.A.A.S.*, **26**, 1165.

HARRIS, A.W. *et. al* (1989). Photoelectric observations of asteroids 3, 24, 60, 261, and 863. *Icarus*, **77**, 171-186.

HAYASHI, C., K. NAKAZAWA e Y. NAKAGAWA (1985). Formation of the Solar System. In *Protostars and Planets II*, (D. Black e M. Matthews, eds) The University of Arizona Press, Tucson, 32-40.

HIRAYAMA, K. (1918). Groups of asteroids probably of common origin. *Astron. J.*, **31**, 185-188.

HIROI, T., M.E. ZOLENSKY, C.M. PIETERS e M.E. LIPSCHUTZ (1993). Thermal metamorphism of the C, G, B, and F asteroids seen from the 0.7 μm and UV absorption strengths in comparison with carbonaceous chondrites. *Meteoritics & Planetary Sciences*, **31**, 321-327.

HOUSEN, K., SCHIMIDT, R. e K. HOlSAPPLE (1991). Laboratory simulations of large scale fragmentation events. *Icarus*, **94**, 180-190.

JEWITT, D. e J. LUU (1995). The Solar System beyond Neptune. *Astron. J.*, **109**, 1867-1876.

JOHNSON, T.V. e F.P. FANALE (1973). Optical properties of carbonaceous chondrites and their relationship to asteroid. *J. Geophys. Res.*, **78**, 8507-8518.

KOZAI, Y. (1994). Kiyotsugu Hirayama and his families of asteroids. In *Seventy-Five Years of Hirayama Asteroid Families* (Y. Kozai, R.P. Binzel e T. Hirayama eds), ASP Conference Series, Vol. 63, 3-6.

LAGERKVIST, C.-I. (1983). Studies of small asteroids. In *Highlights of Astronomy*, (R.W. West, eds), Vol. 6, 371-376.

LAGERKVIST, C.-I, R. MAGNUSSON, H. DEBEHOGNE, M. HOFFMANN, A. ERIKSON, A. DE CAMPOS e G. CUTISPOTO (1992). Physical studies of asteroids–XXV. Photoelectric photometry of asteroids obtained at ESO and Hoher List Observatory. *Astron. Astrophys. Supl. Ser.*, **95**, 461-470.

LAGERKVIST, C.-I e I.P. WILLIAMS (1987). Physical studies of asteroids XV. Determination of slope parameters and absolute magnitudes for 51 asteroids. *Astron. Astrophys. Suppl. Ser.* **68**, 295-315.

LANDOLT, A.U. (1983). UBVRI photometric standard stars around the celestial equator. *Astron. J.*, **88**, 439-460.

LASKER, B.M. *et. al* (1988). The guide star photometric catalog. *Astroph. J. Suppl. Ser.*, **68**, 1-90.

LAZZARIN, M., C. BARBIERI e M.A. BARUCCI (1995). Visible spectroscopy of dark, primitive asteroids. *The Astron. J.*, **110**, 3058-3072.

LEBOFSKY, L.A. (1978). Asteroid 1 Ceres: Evidence for water of hydration. *Mon. Not. R. Astron. Soc.*, **182**, 17-21.

LEBOFSKY, L.A. (1980). Infrared reflectance spectra of asteroids: a search for water of hydration. *Astron. J.*, **85**, 573-585.

LEVISON, H. e M. DUNCAM (1994). The long-term dynamical behavior of short-period comets. *Icarus*, **108**, 18-36.

LEWIS, J.S. e M.L. Hutson (1993). Asteroidal resource opportunities suggested by meteorite data. In *Resources of Near-Earth Space* (L. Lewis, M.S. Matthews e M.L. Guerrieri eds), Univ. of Arizona Press, Tucson, 523-542.

LISSAUER, J. (1993). Planet formation. *Annu. Rev. Astron. Astrophy.*, **31**, 129-174.

LUU, J. e D. JEWITT (1990a). Charge couple device of asteroids.1. Near-Earth and 3:1 resonance asteroids. *Astron. J.*, **99**, 1985-2011.

LUU, J. e D. JEWITT (1990b). Cometary activity in 2060 Chiron. *Astron. J.*, **100**, 913-931.

LUU, J. e D. JEWITT (1991). Observation of a rapid decrease in the brightness of the coma of 2060 Chiron in 1990 january. *The Astrophy. J.*, **366**, L47-L49.

MARCIALIS, R.L. e B.J. BURATTI (1993). CCD photometry of 2060 Chiron in 1985 and 1991. *Icarus*, **104**, 234-243.

MARZARI, F., D. DAVIS e V. VANZANI (1995). Collisional evolution of asteroid families. *Icarus*, **113**, 168-187.

MATSON D.L. (1986). IRAS asteroid and comet survey: preprint version No. 1. JPL internal document No. D-3698.

McCORD, T.B. e M.J. GAFFEY (1974). Asteroid: Surface composition from reflection spectroscopy. *Science*, **186**, 352-355.

McDOO, D.C. e J.A. BURNS (1973). Further evidence for collisions among asteroids. *Icarus*, **18**, 285-293.

McFADDEN, L.A. e M.J. GAFFEY (1978). Calibration of quantitative mineral abundances determined from meteorite reflection spectra and applications to solar system objects. *Meteoritics*, **13**, 556-557.

McSWEEN, H.Y. (1979). Are carbonaceous chondrites primitive or processed? A review. *Rev. Geophys. Space Phys.*, **17**, 1059-1078.

MEECH, K.J. e M.J.S. BELTON (1990). The atmosphere of 2060 Chiron. *Astron. J.*, **100**, 1323-1338.

MIGLIORINI, F., V. ZAPPALÀ, R. VIO e A. CELLINO (1995). Interlopers within asteroid families. *Icarus*, **118**, 271-291.

MILANI, A. e P. FARINELLA (1994). Age of the Veritas asteroid family deduced by chaotic chronology. *Nature*, **370**, 40-42.

MILANI, A. e Z. KNEZEVIC (1994). Asteroid proper elements and the dynamical structure of the asteroid main belt. *Icarus*, **107**, 219-254.

MORBIDELLI, A., V. ZAPPALÀ, M. MOONS, A. CELLINO e R. GONCZI (1995). Asteroid families close to mean motion resonances: dynamical effects and physical implications. *Icarus*, **118**, 132-154.

MOROZ, L.V. (1994). Asteroid Materials. *Solar System Research*, **28**, 195-210.

MOROZ, L.V., A.V. FISENKO, L.F. SEMJONOVA, C.M. PIETERS e N.N. KOROTAEVA (1996). Optical effects of regolith processes on S-asteroids as simulated by laser shots on ordinary chondrite and other mafic materials. *Icarus*, **122**, 366-382.

MOTTOLA, S. *et. al* (1995). The slow rotation of 253 Mathilde. *Planet. Space Sci.*, **43**, No. 12, 1609-1613.

OORT, J. (1950). Bull. Astron. Inst. Neth., **11**, 91-110.

PIETERS, C.M. e L.A. McFADDEN (1994). Meteorite and asteroid reflectance spectroscopy: clues to early Solar System process. *Annu. Rev. Earth. Planet. Sci.*, **22**, 457-497.

RIVKIN, A.S., E.S. HOWELL, D.T. BRITT, L.A. LEBOFSKY, M.S. NOLAN, e D.D. BRANSTON (1995). 3-μm spectrophotometric survey of M- and E-class asteroids. *Icarus*, **117**, 90-100.

SAFRONOV, V. (1969). Evolution of the protoplanetary cloud and formation of the Earth (Moscow: Nauka, eds).

SAWYER, S.R. (1991). A High Resolution CCD Spectroscopic Survey of Low Albedo Main Belt Asteroids. Ph.D. Thesis, Univ. of Texas.

SEARS, D.W.G. e R.T. DODD (1988). Overview and classification of meteorites. In *Meteorites and the Early Solar System* (J.F. Kerridge and M.S. Matthews, eds.), Univ. of Arizona Press, Tucson, 3-31.

SHAPLEY, H. e H.E. HOWARTH (1929). A source book in astronomy. McGraw-Hill Book Company.

SHER, D. (1971). On the variation in light of tumbling bodies. *Astrophys. and Space Science*, **11**, 222-231.

SHOEMAKER, E.M. J.G. WILLIAMS, E.F. HELIN e R.F. WOLF (1979). Earth-crossing asteroids; orbital classes, collision rates with Earth and origin. In *Asteroids II* (R.P. Binzel, T. Gehrels e M.S. Mattews eds), The University of Arizona Pres, Tucson, 253-282.

SPENCER, J.R. *et. al* (1995). The lightcurve of 4179 Toutatis: evidence for complex rotation. *Icarus* **117**, 71-89.

STERN, A. e H. CAMPINS (1996). Chiron and the centaurs: escapees from the Kuiper belt. *Nature*, **382**, 507-510.

THOLEN, D.J. (1984). Asteroid taxonomy from cluster analysis of photometry. PhD. Thesis, Univ. of Arizona.

THOLEN, D.J. (1998). Ephemeris program EPHEM Ver. 1.1, Copyright 1997 by Celestech, Honolulu, Hawaii.

THOLEN, D.J. e M.A. BARUCCI (1989). Asteroid taxonomy. In *Asteroids II* (R.P. Binzel, T. Gehrels e M.S. Mattews eds), The University of Arizona Pres, Tucson, 298-315.

VILAS, F. (1994). A cheaper, faster, better way to detect water of hydration in Solar System bodies. *Icarus*, **111**, 456-467.

VILAS, F. e M.J. GAFFEY (1989). Phyllosilicate absorption features in main-belt and outer-belt asteroid reflectance spectra. *Science*, **246**, 790-792.

VILAS, F., K.S. JARVIS e M.J. GAFFEY (1994). Iron alteration minerals in the visible and near-infrared spectra of low-albedo asteroids. *Icarus*, **109**, 274-283.

VILAS, F., S.M. LARSON, E.C. HATCH e K.S. JARVIS (1993). CCD reflectance spectra of selected asteroids. II. Low-albedo asteroid spectra and data extraction techniques. *Icarus*, **105**, 67-78.

VILAS, F. e M.V. SYKES (1996). Are low-albedo asteroids thermally metamorphosed? *Icarus*, **124**, 483-489.

WETHERILL, G.W. e C.R. CHAPMAN (1988). Asteroid and meteorites. In *Meteorites and the Early Solar System* (J. Kerridge and M. S. Matthews, eds.), Univ. of Arizona Press, Tucson, 35-67.

WILLIAMS, J.G. (1992). Asteroid families–An initial search. *Icarus*, **96**, 251-280.

XU, S., R.P. BINZEL, T.H. BURBINE e S.J. BUS (1995a). Small main-belt asteroid spectroscopic survey: Initial Results. *Icarus*, **115**, 1-35.

XU, S., R.P. BINZEL, T.H. BURBINE e S.J. BUS (1995b). "Small main-belt asteroid spectroscopic survey" Planetary Data System - Small Bodies Node (PDSSBN) (M.

A Hearn, University of Maryland, College Park, Maryland) http://pdssbn.astro.umd-.edu

ZAPPALÀ, V., A. CELLINO, P. FARINELLA e Z. KNEZEVIC (1990). Asteroid families. I. Identification by hierarchical clustering and reliability assessment. *Astron. J*, **100**, 2030-2046.

ZAPPALÀ, V., A. CELLINO, P. FARINELLA e A. MILANI (1994). Asteroid families: Extension to unnumbered multi-opposition asteroids. *Astron. J.*, **107**, 772-801.

ZAPPALÀ, V., P. BENDJOYA, A. CELLINO, P. FARINELLA e Cl. FROE-SCHLÉ (1995). Asteroid families: Search of a 12,487 asteroid sample using two different clustering techniques. *Icarus*, **116**, 291-314.

ZAPPALÀ, V. A. CELLINO, F. MIGLIORINI e M. DI MARTINO (1996). Eos fugitives: a plausible source of CV/CO chondrites. *Bull. American Astron. Soc.* **28**, 1100.

ZELLNER, B., M. LEAKE, D. MORRISON e J.G. WILLIAMS (1977). The E asteroids and the origin of the enstatite achondrites. *Geochim. Cosmochin. Acta*, **41**, 1759-1767.

ZELLNER, B., D.J. THOLEN e E.F. TEDESCO (1985). The eight-color asteroid survey: Results for 589 minor planets. *Icarus*, **61**, 355-416.